JAERI-Review
2003-042

ANNUAL REPORT OF KANSAI RESEARCH ESTABLISHMENT 2002

APRIL 1, 2002-MARCH 31, 2003

February 2004

Kansai Research Establishment

日本原子力研究所
Japan Atomic Energy Research Institute

本レポートは，日本原子力研究所が不定期に公刊している研究報告書です。
入手の問合わせは，日本原子力研究所研究情報部研究情報課（〒319-1195 茨城県那珂郡東海村）あて，お申し越しください。なお，このほかに財団法人原子力弘済会資料センター（〒319-1195 茨城県那珂郡東海村日本原子力研究所内）で複写による実費頒布をおこなっております。

This report is issued irregularly.
Inquiries about availability of the reports should be addressed to Research Information Division, Department of Intellectual Resources, Japan Atomic Energy Research Institute, Tokai-mura, Naka-gun, Ibarakiken 319-1195, Japan.

編集兼発行　日本原子力研究所

JAERI−Review 2003−042

Annual Report of Kansai Research Establishment 2002
April 1, 2002 − March 31, 2003

Kansai Research Establishment

Japan Atomic Energy Research Institute
Kizu-cho, Souraku-gun, Kyoto-fu

(Received December 2, 2003)

This report is the fourth issue of the annual report of Kansai Research Establishment, Japan Atomic Energy Research Institute. It covers status reports of R&D and results of experiments conducted at the Advanced Photon Research Center and the Synchrotron Radiation Research Center during the period from April 1, 2002 to March 31, 2003.

Keywords: Annual Report, Kansai Research Establishment, JAERI, R&D, Advanced Photon Research Center, Synchrotron Radiation Research Center, SPring-8

関西研究所年報 2002
2002 年 4 月 1 日－2003 年 3 月 31 日

日本原子力研究所
関西研究所

（2003 年 12 月 2 日受理）

本報告書は、日本原子力研究所関西研究所の第 4 号の年報であり、2002 年 4 月 1 日から 2003 年 3 月 31 日までの期間（平成 14 年度）に行われた光量子科学研究センター及び放射光科学研究センターの研究活動をまとめたものである。

関西研究所：〒619-0215　京都府相楽郡木津町梅美台８－１

Contents

This is a blank page.

Foreword

This is the fourth Annual Report of Kansai Research Establishment (KRE) covering the activities in FY2002. KRE carries out photon research relevant to energy research and consists of the Advanced Photon Research Center (APRC) in Kizu, Kyoto and the Synchrotron Radiation Research Center (SRRC) in Harima, Hyogo. FY2002 has left a mark on us, as we catapulted ourselves into an application phase from the facility-development phase of the past several years. Along with it a starting discussion on the new proposed merging of JAERI and JNC (Japan Nuclear Cycle) in FY2005 ensued.

At SRRC, not only all four beamlines(BL), including BL22XU in the RI (radio isotopic) Laboratory, have been put into full operation, but also all seven Groups (including the Simulation Group) have been in full activities (all but one Group Leaders have been appointed in fulltime by April 1, 2003). With this heightened activity level SRRC has produced a few earth-shaking discoveries along with many solid contributions in synchrotron radiation research in materials science. It has grown into a leading group as such in Japan and one of COEs in the world. Among the notable achievements in FY2002 the discovery of the catalytic property of noble metals in the perovskite compound is particularly memorable. In collaboration with the Daihatsu Motors Ltd. SRRC scientists have discovered the self-rejuvenating mechanism of the above catalyst through SR measurement. This remarkable catalyst for automobile exhaust would amount to hundreds of $M economic savings of noble metal consumption. The SR research also cast new insights into magnetic and superconducting properties of many strategic materials, including uranium/transuranium materials as well as materials such as perovskites.

The APRC with its new leadership in FY2002 started a number of new initiatives, both domestic and international. An increasing number of international scientists both at senior and junior levels now call APRC as their home. With the ongoing collaboration with the University of Michigan CUOS winding down, a new collaboration with SLAC has been negotiated on advanced accelerator research. The initiative on compact intense laser research at OECD has been led by JAERI Kansai. The laser research both on a compact Ti:sapph in the petawatt regime and on an FEL with the ERL (energy recovery linac) technology boasts the world-leading achievements in FY2002. We are happy that applications of these lasers at APRC have now in a swing, culminating in the studies of highly ionized noble gases and ferroelectric crystals among others.

One of the most notable developments of FY2002 is the renewed vigor in crossfertilization of the synchrotron light source (at SRRC) and lasers (at APRC). Contributions that push the envelop of the current photon research may be achievable through this intra-institutional crossing unique in the world. We now welcome your input and participation in this endeavor. We hope that we can entertain your engagements at our hub in this combined capability. In the past year a number of Government high officers have visited us in part to promote/listen to this initiative. We look forward to providing a playground for you in years to come in this vital field.

Since the July 2001 opening, a museum dedicated on photons, the Kids' (Kidu=Kizu) Museum of Photons in Kizu, has attracted more than 80K people, both kids and adults, encompassing many disciplines of photon applications in its exhibits. From the Government a fund to promote direct science mediation has been granted partially due to this public outreach.

We invite your participation to KRE whether in the collaborative lab work, in theoretical long-distance web work, or in science outreach activities. Happy photon research and welcome to Kansai!

Toshiki Tajima

This is a blank page.

1. Summary

JAERI(Japan Atomic Energy Research Institute) is the research institute complex of nuclear science and technology where broad-ranged top-of-the-line energy research facilities can be synthetically utilized that encompass from synchrotron radiation, X-ray laser, to high-intensity proton accelerator(under construction), accelerators of electron beam and ion beam, nuclear research reactors and advanced computer system. Kansai Research Establishment was established in 1995 to promote the research of laser and synchrotron radiation with the integrated theme of bright 'light'.

A new Long-Term Program for research, development and utilization of nuclear energy was drawn up in The Atomic Energy Commission of Japan in November 2000. This Program summarizes that nuclear science and technology has achieved remarkable developments in the 20th century and brought about substantial changes in lives and lifestyles. In the 21st century, the advance of nuclear science and technology is expected not only to form the basis for development of new energy technologies but also to serve to explore new frontiers. High brilliant synchrotron radiation and X-ray laser can contribute to the advance of life science and materials science related to nano-structure, environment and information technology. As JAERI is expected to join with JNC(Japan Nuclear Cycle Development Institute) in 2005 to become an integrated independent agency responsible for the over all atomic energy researcher in Japan our research will be pivotal in promoting the new direction in atomic energy research in Japan.

This Annual Report summarizes the research activities at both Synchrotron Radiation Research Center and Advanced Photon Research Center in the period from April 1, 2002 until March 31, 2003. Previous Annual Reports of Kansai Research Establishment of JAERI are shown in Table 1.

Table 1 Previous Annual Reports of Kansai Research Establishment of JAERI

JAERI-Review 2001-003	(March 2001)
JAERI-Review 2001-046	(February 2002)
JAERI-Review 2002-042	(February 2003)

2. Facilities of the Advanced Photon Research Center

The core competence of the Advanced Photon Research Center (APRC) is advanced lasers with high brilliance and high fluence. These lasers include a compact ultra short pulse peta watt laser, a fully spatially coherent X-ray laser, and high-power extremely efficient free-electron laser. These lasers are tools for the exploration of new nuclear energy science and technology and the development of novel radiation sources of X-rays, γ-rays, electrons and ions. In order to support this development, simulation research using supercomputers (Super Simulation Center for Photon-SSCP) and development of fundamental technologies of optical elements and devices like laser crystals, mirrors, gratings, etc. are also implemented in the APRC.

The APRC has engaged in the research and development of advanced lasers such as compact high power lasers with a peak power of petawatts (10^{15} watts), X-ray lasers with soft X-ray, and free electron lasers with high average power and high efficiency. Utilizing these lasers, the APRC also challenges generation and application of high-energy ion and X-ray, development of new particle sources, X-ray microscopes, etc.

These advanced lasers and their producing highly energetic ions and X-rays have distinctive characteristics such as high intensity, high coherency, or short pulse, which are different from conventional radiations. The APRC develops various techniques for utilizing these high quality radiations to various fields of science and technologies, along with JAERI's own knowledge of neutrons, synchrotron radiation, and ion beams research. The APRC also collaborates with industries and universities in research and development activities.

A bird's-eye view of the Advanced Photon Research Center is shown in Fig. 1. Research activities are mainly performed in the laboratory building where four big laboratories for development and applications of high power lasers are provided and the researchers' building where a super computer is equipped. There are the conference hall where we can hold symposiums and meetings to introduce research results of Kansai Research Establishment, and the guesthouse for accommodation.

The buildings with a dome at the right foot in the photograph is the "Kids' Science Museum of Photons", which was opened in July 2001, contributing to science educations for the younger generation in Keihanna Science City. The IT-based laboratory (ITBL) building shown at the left top was opened in March 2002.

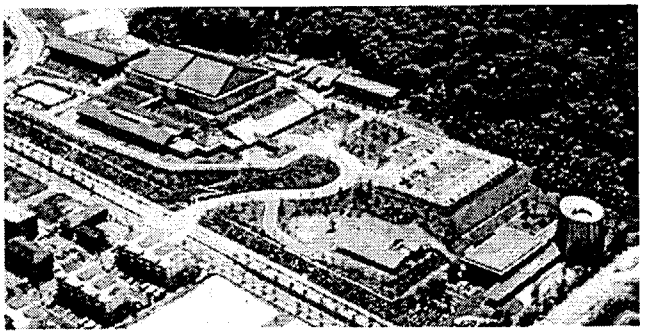

Fig. 1 The Advanced Photon Research Center

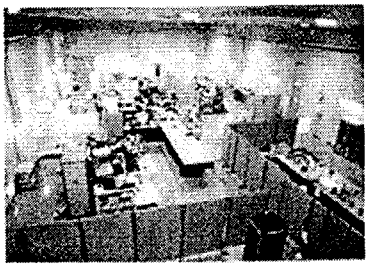

All-solid state, high average power laser laboratory

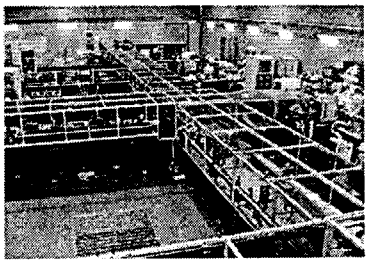

Ultrashort pulse, high peak power laser laboratory

Laser acceleration and high field science laboratory

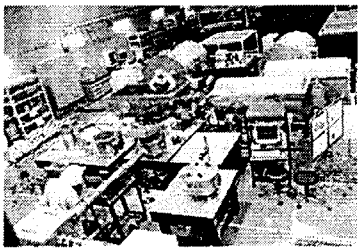

X-ray laser laboratory

Fig. 2 Four main laboratories of the Advanced Photon Research Center

3. Facilities of the Synchrotron Radiation Research Center

SPring-8 is a synchrotron radiation photon source, the highest and brightest third generation photon source in the world. Such a bright photon source can be employed to advance the materials science research, environmental research and nanoscience and biological research. SRRC of JAERI has contributed crucially to take a leadership in applications of this facility, in particular to materials science.

SPring-8 was operated in 2002 as scheduled. Three JAERI beamlines were operated as well as the new fourth line, BL22XU, has come into the commissioning. In the beamline BL23SU, surface chemistry, radiation effect on DNA and electronic structure of electronic materials were studied. In the beamline BL14B1, structure analysis under high pressure, correlation between structure and function of materials were investigated. In the beamline BL11XU, nuclear resonant scattering of materials, resonant inelastic scattering of colossal magnetoresistance manganites and surface structure during molecular beam epitaxy growth. The BL22XU beamline has the experimental equipments for high pressure studies and X-ray diffraction.

Uranium compounds started to be investigated by using the x-ray absorption magnetic circular dichroism(MCD)(Fig. 1) and the photoelectron spectroscopy in BL23SU in the radioisotope building. BL22XU is also ready to be used for studying the magnetic structure of uranium materials(Fig. 2).

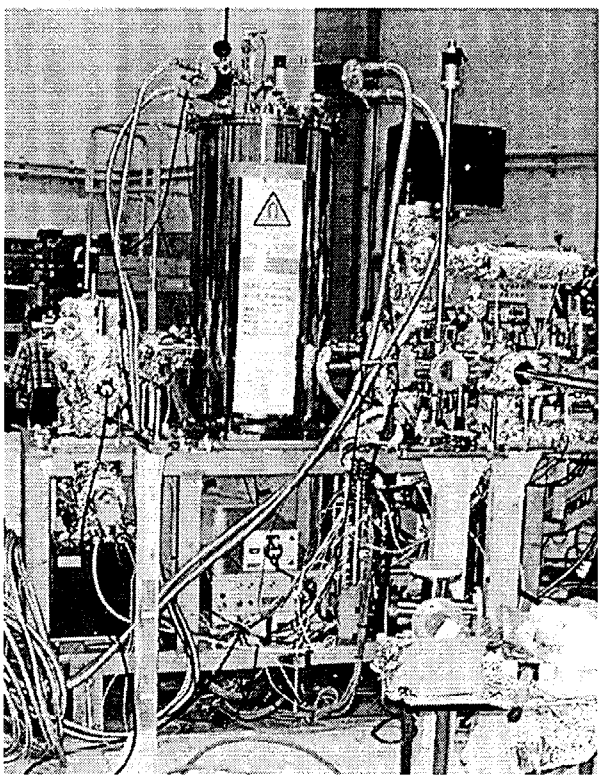

Fig. 1 MCD apparatus in BL23SU

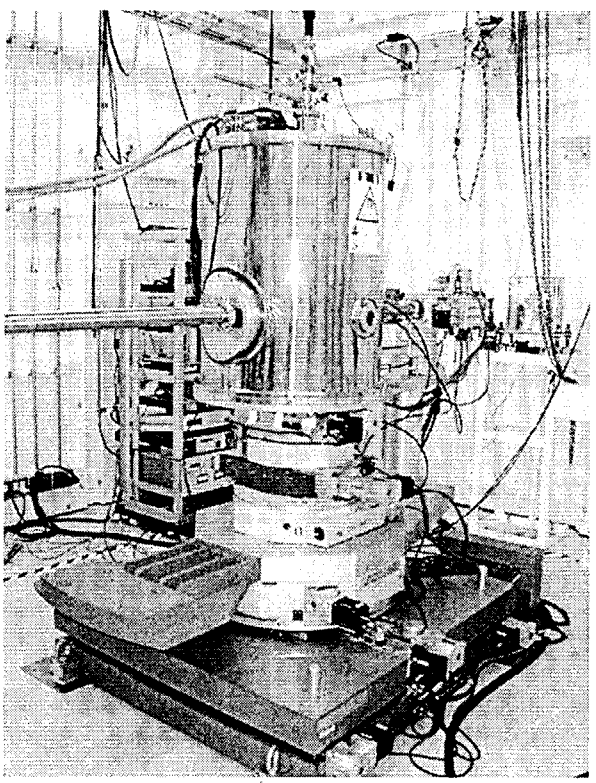

Fig. 2 Cryostat on diffactometer in BL22XU

4. Advanced Photon Science

Toyoaki KIMURA

The Advanced Photon Research Center (APRC) is pursuing the research and development of advanced photon sources such as a compact, ultra-short, high intensity laser, x-ray laser, and a superconducting linac-based free electron laser (FEL) and their applications.

In FY2002, the following remarkable advances have been made in the development of advanced photon sources. In the development of a compact, ultra-short, high intensity laser, a four-stage titanium-doped sapphire (Ti:sapphire) chirped pulse amplification (CPA) laser system achieved a peak power of 0.85 PW with a 33-fs pulse. We also developed a high average power LD pumped green laser in order to achieve better performance and compactness in a kHz, terawatt Ti:sapphire CPA laser system. Also, the construction of a compact diode-pumped Yb:YLF regenerative amplifier system has been completed. These compact laser systems with high average power will be applicable to various areas of physics and types of industries. In the R&D of the x-ray laser system using a double silver target, an x-ray beam was successfully obtained with a wavelength of 13.9 nm and an extremely low divergence of 0.2 mrad, which is more than ten times lower than that of x-ray lasers in other institutes. We also demonstrated that this x-ray laser beam has spatially full coherence in a Young's interference experiment with a double slit. In the research of a free-electron laser (FEL), full energy-recovery was demonstrated in a superconducting linac, and the first lasing in this energy-recovery type linac (ERL) -based FEL system was also successfully performed.

Remarkable progress was made in the studies where these advanced lasers are applied. In the research on high field science, we have obtained energetic electrons (>2 MeV) and protons (>1 MeV) produced by focusing 50 fs Ti:sapphire laser pulses at the intensity of $>10^{18}$W/cm^2. We have also completed installation of a target chamber system for the experiments with a 100 TW Ti:sapphire CPA laser. The study on the production of high energy protons is aimed at developing a compact laser-driven ion source which is applicable as an injector of an accelerator for cancer therapy. We have also observed emission of x-rays with an energy of 3.14 keV from plasma created by laser irradiation of Ar clusters at laser intensities over 10^{19} W/cm^2.

In the research on laser acceleration, we observed that energetic electrons with an energy above 0.5 MeV which were generated at an intensity of 8×10^{19} W/cm^2 by injecting 30 fs laser pulses with a peak power of 5 TW into a He gas jet. We also succeeded in the direct observation of coherent ultrahigh gradient wakefields of 20 GeV/m excited by a 2 TW, 50 fs laser pulse in a gas jet.

In the application research with x-ray lasers we successfully observed speckle patterns of x-rays from the surface of ferroelectric $BaTiO_3$ by using an x-ray laser beam with a wave length of 13.9 nm and clarified a change of the surface microstructure near the Curie temperature. This success leads to understanding the dynamic behavior of the surface microstructure of $BaTiO_3$ and its function.

Quantum control of chemical reactions has been studied by chirping a pulse of an ultra-short pulse laser. We have developed an acousto-optic programmable dispersive filter (AOPDF), which has high potential for controlling the time delay and phase difference between two pulses of the laser. We demonstrated that the excitation probability for both transitions from Cs $6S_{1/2}$ to two spin-orbit states, $7D_{5/2}$ and $7D_{3/2}$ can be satisfactorily controlled by changing the phase difference of two laser pulses.

In the developments of laser optical elements, we have improved the bonding technique for laser crystals with a good heat removal performance by a dry etching method to obtain high output power. In the research area of soft x-ray optical elements, we have started the study of multilayer development consisting of oxide and nitride as the multilayer mirror for use around the wavelengths of 4 nm. We also developed a laminar-type holographic grating with a high groove density for a flat-field spectrograph and a replica grating having good marketability.

In the research on computer simulation and analysis, a strong effect of radiation damping on the interaction of an ultra-intense laser pulse with an over-dense plasma slab has been found and studied via a relativistic particle-in-cell simulation including ionization. Hot electrons generated by the irradiation of a laser pulse with a radiance of $I\lambda^2 > 10^{22}$ Wμm^2/cm^2 and duration of 20 fs can convert more than 35% of the laser energy to radiation of incoherent x-rays. The radiation efficiency is shown to increase nonlinearly with laser intensity.

4.1 High Peak Power Laser Development

Laser System Development Group

Koichi YAMAKAWA

The research activities of the Laser System Development Group are focused on the following topics:

- Development of a petawatt Ti:sapphire laser system.
- Precision of a 100 TW, 20 fs Ti:sapphire laser system.
- Production of high-energy particle and x-ray sources of atomic clusters heated by the 100 TW, 20 fs laser.
- Development of compact diode pumped solid-state lasers.
- Quantum control of chemical reactions.

Recently, the technique of chirped pulse amplification (CPA) in conjunction with the advanced solid-state laser technologies has opened new avenues for the production of multiterawatt femtosecond pulses with ever increasing both peak and average powers. In this year, we have successfully produced laser pulses with peak power of 0.85 PW and pulse duration of 33 fs (see Fig. 1). To our knowledge, this result represents the highest peak power pulses yet produced used in any Ti:sapphire CPA system.

We developed a high average power LD pumped green laser in order to achieve better performance and compactness in kHz, terawatt Ti:sapphire CPA laser system. Also, a construction of a compact diode-pumped Yb:YLF regenerative amplifier system has been completed.

High field physics experiments are also carried out with the 100 TW, 10 Hz Ti:sapphire laser facility describe in more detail below address fundamental aspects of relativistic light-matter interaction for future studies. We have observed high-resolution x-ray emission spectra of plasma created by laser irradiation of Ar clusters at laser intensities over 10^{19} W/cm^2. The absolute number of x-ray photons for $He_{\alpha 1}$ resonant line of Ar (λ=3.9491 Å, 3.14 keV) is estimated as $N_{phot}=2\times10^8$ photons/pulse/pixel, which corresponds to the spectral power density of 2×10^8 W/Å. This could be ideal source s for ultrafast pump-probe type experiments. In finally, the adaptive pulse shaping was demonstrated for controlling quantum systems. The acousto-optic programmable dispersive filter (AOPDF) was shown to have high potential for controlling the time delay and phase difference between two pulses and exhibited an example of the completely destructive interference in the atomic wave function.

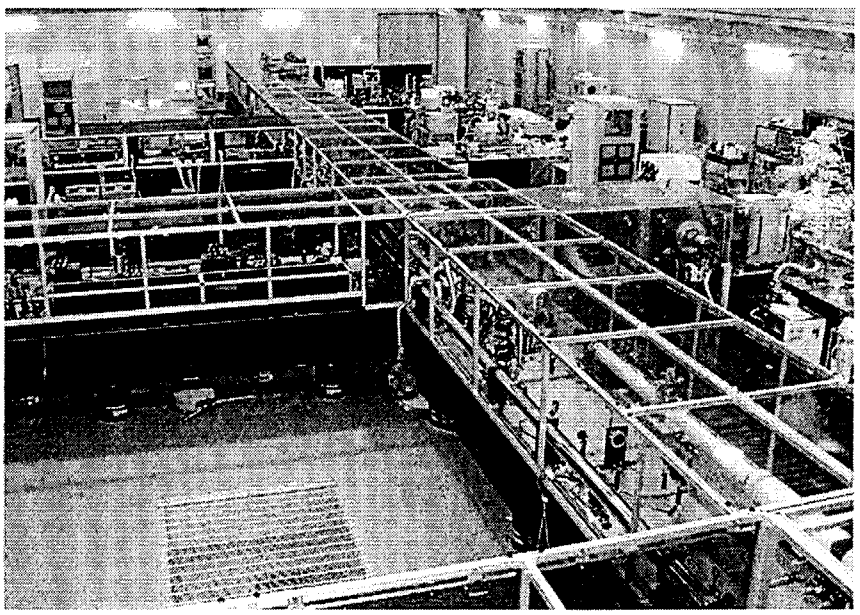

Fig. 1 Petawatt Ti:Sapphire Laser facility

4.1.1 Construction of the 100TW laser beam line for high field experiments

Yutaka AKAHANE, Hiromitsu KIRIYAMA, Norihiro INOUE, Hideki UEDA, Koichi TSUJI, Yoshiki NAKAI, Yoichi YAMAMOTO, Michiaki MORI, Yukio HAYASHI, Hideyuki KOTAKI, Shuji KONDO, Shuhei KANAZAWA,and Koichi YAMAKAWA

1. Introduction

It has been several years since the compact 100TW Ti:sapphire CPA laser system was developed at the Advanced Photon Research Center (APRC), whose focused intensity can be reached to 10^{20} W/cm^2. The pulse duration of the laser pulse is 20 fs, and the system operates at high repetition rate of 10 Hz. High repetition rate operation is very useful for various applications, such as the generation of high-energy electrons, ions, x-rays and even neutrons. To perform these high-field experiments, a completely-shielded room is required for the radiation safety. We dedicate to deliver the laser beam to the shielded room C101 and focus in the experiment chamber placed there. To deliver the ultrafast, high-peak power laser pulses to the room C101, a long length vacuum laser beam line over 50m is required. In this section we describe the construction of the laser beam transport line for the several high-field experimental campaigns and we will report its overview and performance.

2. Overview of the laser beam transport line

The schematic of our laser-beam line is shown in Fig.1 The 100TW Ti:sapphire laser system[1] placed in the room C103 is used as the laser beam source. An amplified laser pulse from the final power-amplifier of the laser system is up-collimated to 50mm diameter by the Gariren telescope, and introduced to the beam line, and compressed by the grating compressor in the next room C105. The energy of the output laser pulse from the final power-amplifier is routinely 1.6J, which is limited by the carbon-deposition threshold fluence on the compressor gratings at a 10 Hz operation. In the room C105 there are periscope consisted of two 8-inch diameter mirrors with a pair of laser beam monitoring cameras (CCD1, NearField (NF) and FarField (FF)) for the alignment of the pulse compressor. After the periscope, in order to avoid air-break-down or spectral and temporal distortion, all optical components are placed in vacuum (<10^{-4} Torr) tubes or chambers. The pulse compressor consists of two 1200-grooves/mm gold-coated ruled gratings and a pair of roof mirrors. The incident angle and the perpendicular separation between the two gratings in the compressor are 64.7 deg and 119 cm respectively, with considering the temporal dispersion by the extra material in the beam line. The alignment of the laser beam in the compressor chamber is confirmed by monitoring the FF image of the compressor output (CCD2, see Fig.1). The compressed, high peak-power laser pulse is then sent to the room C101, which is shielded by 1 m thick concrete wall and is specified as a controlled area for radiation. There are a NF monitor (CCD3) and a pair of monitors (CCD4, NF and FF) for the alignment of the laser beam in the room C101. By adjusting the position of the laser beam on the monitors from CCD1 to CCD4 in order, the laser-beam line successfully handles identical high-peak power, ultrashort laser pulses to the experiment chamber all the time. Just before the experiment chamber, a leakage from a 98% beamsplitter is down-collimated and introduced to the single-shot second-harmonics generation (SHG) autocorrelator for pulse width measurement. The leakage is also available for monitoring the laser energy and triggering the detector during the experiment. The laser pulse introduced to the experiment chamber is finally focused by a 45-degree off-axis parabolic mirror (Janos Technology;f=+177.8mm, 4inch) at the center of the chamber.

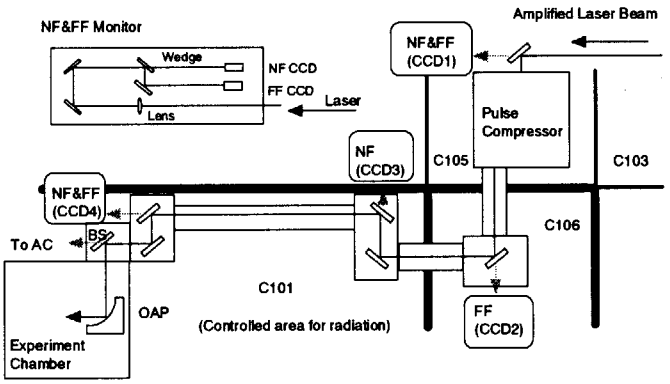

Fig. 1 Schematic of the laser beam transport line, NF; nearfield monitor, FF; farfield monitor, CCD; charge coupled device camera, BS; 98% beamsplitter, AC; SHG-autocorrelator, OAP; off-axis parabolic mirror

3. Performance of the laser beam transport line

We checked the pointing stability of the laser beam at the end of the beam line. The two figures in Fig.2

shows the shifts of pointing on the final laser beam monitor CCD4. Using the stable laser source (Tsunami laser), in Fig.2 (a), our laser system was confirmed to be stable up to 5 hours within 33 microradians. From the result in Fig. 2 (b), even in the operation of 100 TW laser system, the laser beam was found to be stable up to 1.5 hours. The unstability after 1.5 hours comes from the thermal misalignment of the Ti:sapphire amplifiers, which can be re-stabilized by aligning of the amplifier chain. In consequence, it was found that we supply the stable laser beam within 33 microradians by the re-alignment of the laser system at every 1.5 operating hours.

Next we measured the energy transmittance of the beam line. The compression efficiency of the pulse compressor was only 44%, which was found to be responsible for the degradation of the gratings. By changing the gratings to new ones, 54% compression efficiency is expected. The energy transmittance after compressor was 73%, which was limited by the reflectivity of the focal parabolic mirror (~90%) or Fresnel diffraction. The total energy transmittance of the beam line was only 29% at the moment. This could be simply improved by changing the gratings and focusing optics. The pulse width of the compressed ultashort laser was measured by a single-shot SHG autocorrelator placed just before the experiment chamber. The FWHM of the measured pulse width is 23.4 fs, which is near the Fourier transform-limited pulse width of 20.6 fs.

In the experiment chamber, we measured the spot size of the focused laser beam. By means of relay-imaging with the two lenses inside and outside the experiment chamber, the focus spot image of the attenuated laser beam was analyzed by a CCD camera with 100 times magnifications. Typical $1/e^2$ size of the spot was 9.21μm, which was 1.33 times as large as that of the diffraction limit. Approximately 52 % of the laser energy was contained in the focal spot. The peak intensity of the focusing laser pulse was thus estimated to be 3.2×10^{19} W/cm^2 from this optical measurement. In order to confirm the laser-focused peak intensity, we performed the tunneling ionization experiment of He using the attenuated laser beam. In the ionization experiment of He, the experimental ion yield of He^+ was reported to correspond to the Ammosov-Delone-Krainov (ADK) [2] calculation within 15% in the tunneling ionization region of laser intensity around 10^{15}W/cm^2 ,which is good reference for the focused laser intensity[3]. By applying the energy scaling of the laser pulse, we have obtained the "experimental" laser-focused peak intensity as 1.0×10^{19} W/cm^2. The reasons of the difference between the "ideal" focused peak intensity obtained by the optical measurement and the "real" one obtained by the He ionization experiment are not clear now, which are supposed to be such as the large scatters of the parabola mirror, relatively low vacuum environment of the chamber (base pressure; ~3×10^{-6}Torr), and so on. So far, we have succeeded to confirm experimentally that the laser focused peak intensity reached to over 10^{19} W/cm^2.

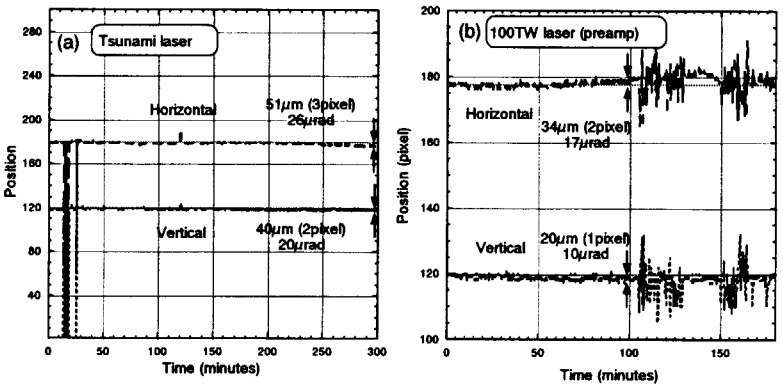

Fig. 2 Pointing stability of the laser transport beam line; (a) Tsunami laser (b)100TW laser

4. Conclusion

We have developed the laser transport beam line to deliver the 100TW laser pulse to the experiment area for the generation of high-energy radiations. The performance of the beam line, such as beam pointing stability, energy transmittance, and focusability was confirmed to sufficient for the high-field physics experiments at the intensity of over 10^{19} W/cm^2. As for the first experiment, a laser plasma cathode experiment is scheduled to be carried out soon, which will prove the high performance of our 100TW laser beam.

References

1) K. Yamakawa et al., Opt. Lett. 23, 1468 (1998).
2) M.V. Ammosov et al., Sov. Phys. JETP. 64, 1191 (1986).
3) B. Walker et al., Phys. Rev. Lett. 73, 1227 (1994)

4.1.2 Petawatt Ti:sapphire laser system

Makoto AOYAMA, Yutaka AKAHANE, Jinglong MA, Norihiro INOUE, Hideki UEDA, Hiromitsu KIRIYAMA, Koichi TSUJI, Yoshiki NAKAI and Koichi YAMAKAWA

1. Introduction

Since the advent of the chirped-pulse amplification (CPA) technique, there has been rapid progress in the development of high peak, ultrashort laser system. To date, pulses as short as 450-fs with 1.5 PW peak power have been generated by using a large scale, inertial-confinement-fusion, Nd:glass laser[1]. On the other hand, other major Ti:sapphire (Ti:S) CPA laser systems having broad bandwidth can accomplish extremely short pulse duration on the order of 10 fs. This is especially significant since it allows high repetition rate with a reasonable size system with average powers on the order of 20-30 W. To date, Ti:S CPA laser systems with peak powers of 100 TW and pulse durations of 20 fs operating at 10 Hz have been constructed [2]. In order to accomplish a higher peak power with a laboratory-scaled laser system, we have developed a petawatt (PW) Ti:S laser system that can produce 33 fs pulses with a peak power of 0.85 PW [3].

2. System configuration

For amplifying the laser pulses up to petawatt power level, a 3-pass booster amplifier with a 80 mm diameter, 33-mm-long Ti:S crystal (Crystal Systems Inc.) is added to our Ti:S CPA laser chain that produces 100 TW, sub-20 fs laser pulses at 10 Hz [2]. An inevitable concern in efficient amplification with such a large aperture amplifier is parasitic lasing (PL). We have developed a technique of PL suppression for a Ti:S which uses absorbative polymer thermoplastic claddings to lower disk-edge reflectivity. By this technique, the amplified energy has been expected to be as much as ~40-J for a ~70-J green pump.

The pulse stretcher and compressor for the petawatt laser system are considered to produce ~30 fs laser pulses. These components are the Offner triplet stretcher and the Tracy type compressor based on the mixed grating scheme. In order to compensate for the phase distortion of the materials up to fourth order in the laser chain, we have chosen a 1,200 groove/mm ruled grating in the stretcher and 1,480 groove/mm holographic gratings in the compressor.

3. Experimental results

We have produced laser pulses with energies of 37.4 J for 65 J pump laser and conversion efficiency of greater than 50 %. A measured autocorrelation trace of the laser pulse is shown in Fig. 1. The FWHM of the measured pulse duration was 32.9 fs. Therefore the peak power of the laser pulse was 0.85 PW. Spatial quality of the amplified laser pulses is 1.2 and 3.2 times diffraction limited in the horizontal and vertical planes, respectively. Such a Ti:S PW laser system has smaller beam sizes, compared with a Nd:glass-based PW laser. Therefore, the Ti:S PW system allows feasible experimental configurations of small f-number focusing optics in a realistic experimental setup, which assists in increasing the focused intensity. With an f/1 parabolic mirror, the laser pulses can be expected to realize a focused intensity of 3.8 x 10^{21} W/cm^2 with this beam quality. Recent advancements of adaptive optic devices, such as a deformable mirror, would push the diffraction limited focal spot into a higher focused intensity (> 10^{22} W/cm^2).

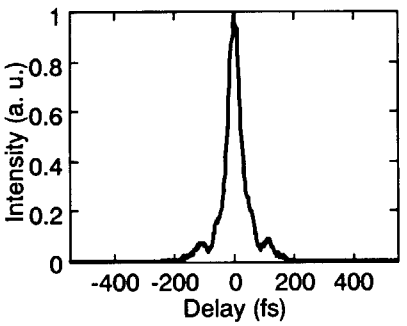

Fig. 1 Measured autocorrelation trace

References

1) M. D. Perry, D. Pennington, B. C. Stuart, G. Tietbohl, J. A. Britten, C. Brown, S. Herman, B. Golick, M. Kartz, J. Miller, H. T. Powell, M. Vergino, and V. Yanovsky, Opt. Lett. 24, 160, 1999.
2) K. Yamakawa, M. Aoyama, S. Matsuoka, T. Kase, Y. Akahane, and H.Takuma, Opt. Lett. 23, 1468, 1998.
3) M. Aoyama, K. Yamakawa Y. Akahane , J. Ma, N. Inoue, H. Ueda, and H. Kiriyama, Opt. Lett. 28, 1594, 2003.

4.1.3 High average power operation with a single-stage diode-pumped Nd:YAG amplifier with phase conjugation mirror

Hiromitsu KIRIYAMA, Toru NAGAI, Koichi YAMAKAWA, Nobuto KAGEYAMA[a)], Hirofumi MIYAJIMA[a)], Hirofumi KAN[a)], Hidetsugu YOSHIDA[b)], Masahiro NAKATSUKA[b)]
a) Central Research Laboratory, Hamamatsu Photonics K.K.
b) Institute of Laser Engineering, Osaka University

1. Introduction

In recent years there has been a rapid progress in the development of high-average-power and high-repetition-rate ultrashort-pulse (~20 fs) Ti:sapphire chirped-pulse-amplification (CPA) laser systems.[1)] These laser systems are commonly pumped by lamp-pumped Q-switched green lasers with relatively low average output powers of tens of watts, which limit their useful output to several watts. The solid-state laser system pumped by a laser diode (LD) is one of the most promising candidate pump sources for realizing high-average-power, high-repetition-rate Ti:sapphire CPA systems because of its high efficiency and correspondingly small system thermal load,; it is also extremely compact as compared to a lamp-pumped laser system.[2)] In order to achieve better performance and compactness in Ti:sapphire CPA laser system, we developed the novel LD pumped green laser system.[3)]

2. Results and conclusion

Our LD pumped green laser system consists of an oscillator, a multipass side-pumped slab amplifier, a stimulated-Brillouin-scattering (SBS) mirror, and a KTP crystal. An important feature of this architecture is the use of the same slab amplifier head for preamplification and main amplification of the laser pulses, the laser beam twice initially for preamplification and then again four-times for main amplification. The amplifier module consists of a water-cooled Nd:YAG zigzag slab side-pumped by a LD array on each side.

The infrared (IR) average output power as a function of average LD pump power is shown in Fig. 1. A maximum IR average output power of 362 W in a 29 ns (FWHM) pulse was achieved for an average LD pump power of 2.6 kW at 1 kHz.

The green average output power as a function of IR average input power is shown in Fig. 2. For 222 W IR average power incident on the KTP crystal we obtained a green average output power of 132 W, corresponding to a pulse energy of 0.13 J at 1 kHz, in a 28 ns pulse (FWHM) with a frequency conversion efficiency of 60 %. The reliability, efficiency, and compactness of LD pumped green laser systems have resulted in similarly reliable, efficient, and compact Ti:sapphire CPA laser systems and can not be attained with lamp pumped laser systems.

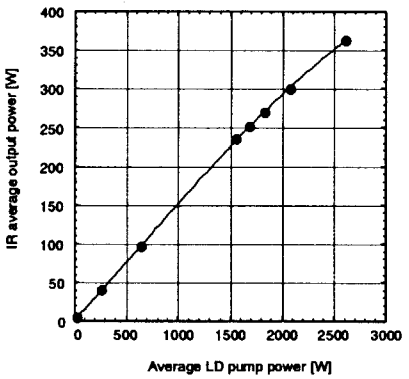

Fig. 1 IR average output power versus average LD pump power

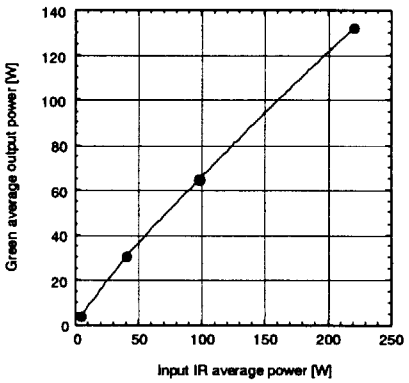

Fig. 2 Green average output power versus IR average input power

References

1) S. Backus et al., Opt. Lett. **22**, 1256 (1997).
2) J. J. Kasinski et al., IEEE J. Quantum Electron. **28**, 977 (1992).
3) H. Kiriyama et al., Opt. Lett., in press.

4.1.4 Multi-ten-milli-joule operation of chirped-pulse regenerative amplifier with a diode-pumped Yb:$LiYF_4$

Junji KAWANAKA, Hajime NISHIOKA[a)], Koichi YAMAKAWA and Ken-ichi UEDA[a)]

[a)]Institute for Laser Science, University of Electro-Communications

1. Introduction

Compact high-average-power femto-second lasers using a chirped pulse amplification technique that produce a moderate pulse energy are in high demand as one of the most useful tools for the recent high-field applications such as high-order harmonic generation[1-5]. Several milli-joule pulses with a pulse duration less than 30 fs has been generated at kilo-hertz repetition rate by use of a Ti:sapphire laser system with a single-stage amplifier.[6,7] Presently, second harmonic radiation of a diode-pumped Nd:YAG laser or of a cw lamp Q-switched Nd:YLF laser has been used in Ti:sapphire laser system as a pump source. Their energy conversion efficiencies defined as a ratio of the electrical input power and the green radiation are below 3% and their system sizes are large. If diode lasers are used to directly pump a Ti:sapphire laser, the energy conversion efficiency could be increased with more than one order of magnitude and the system could be downsized. Yb:$LiYF_4$(Yb:YLF) crystal is one of the promising laser materials in the diode-pumped femto-second lasers with high average power due to its high energy storage, wide spectral emission range, low nonliear refractive index and high thermal conductivity. Much reabsorption of lower levels in a laser transtion, however, is serious especially in diode-pump because of the quasi-three-level laser system. We are focusing on cooling of the laser material to reduce the absorption. The laser gain and the spectral gain width of a diode-pumped Yb:YLF were dramatically improved at low temperature.[8,9] In the present work, a diode-pumped regenerative amplifier with a cooled Yb:YLF crystal has been demonstrated at 20 Hz. In addition, high average power operation were discussed.

2. Regenerative amplifier

An x-type cavity was designed with two high reflectors and two dichroic mirror for a beam waist to be out of the cavity due to avoid optical damages of the Yb:YLF crystal and windows of a liquid-nitrogen cryostat in Fig. 1. A combination of a pre-bias-Pockels cell and a thin film polarizer was prepared for a seed pulse injection and a cavity damp. A 2 mm-thick, 20 at. % Yb:YLF crystal was cooled by our designed liquid-nitrogen cryostat. A 600 μm-core fiber-coupled laser diode was used as a pump source in a quasi-continuous-wave operation mode with no polarizations. The typical repetition rate and emission duration were 20 Hz and 4 ms, respectively. The pump beam was focused on the crystal with a circular spatial profile at about 600 μm diameter. Seed pulses with 85 fs FWHM from a mode-locked Ti:sapphire laser were stretched in time with about 1-ns by using a 1.2 km polarization-maintained single-mode fiber. The chirped pulse energy was about 20 pJ and the center wavelength was 1020 nm with 15 nm FWHM spectral width.

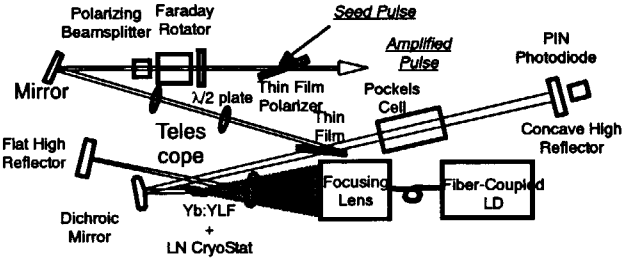

Fig. 1 Schematic diagram of Yb:YLF chirped-pulse regenerative amplifier

Figure 2 showed the amplified output pulse energy as a function of a peak pump power for different pump duration. The output pulse energy of 30.1 mJ was obtained at 92 W, 4 ms pump at the 12th round trip. Higher pump power leads to a surface damage of the quartz window of the cryostat. The output pulse energy was linearly increased with pump power and no effects due to the reabsorption with the crystal heating in pumping were found even at full power operation. To enlarge the pump cross section, therefore, would increase output power more. The observed optical-to-optical efficiency was as low as 8.1% because the half of the pump energy was wasted as partial reflection of s-polarized beam at the Brewster window and non-absorbed beam passed through the crystal. Evaluated initial gain values g_0 were 3.6 cm^{-1}, 5.3 cm^{-1} and 6.5 cm^{-1} for different pump durations of 1 ms, 2 ms and 4 ms, respectively, at a pump power of 100 W by fitting our numerical calculations to the experimental pulse energy with solid lines in fig. 2. The cavity loss was 0.05 for a round trip. An effective extraction efficiency, which was a ratio of an output pulse energy and a storage energy (E_{out}/g_0E_sV), was calculated to be 68% at 30 mJ output energy. The accumulated pulse energy fluence on the

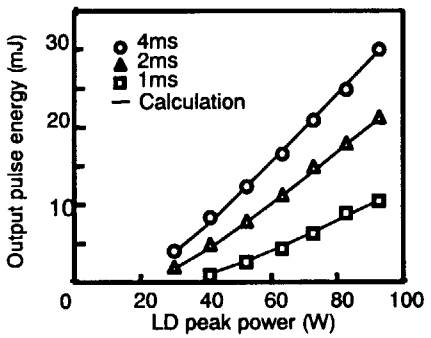

Fig. 2 Output pulse energy as a function of pump power

crystal during the regenerative amplification was higher than the saturation fluence E_s = 13 J/cm^2 of the crystal at liquid nitrogen temperature. A 10 mJ output power was obta ined for 1 ms pump duration. In a cw pump, therefore, an average power as high as 10 W could be obtained with 1 kHz repetition rate if thermal problems were out of c onsideration. Thermal effects such as thermal lensing and thermally induced birefringence become serious in a high average power operation. Thermal conductivity of the laser crystal is fortunately improved to 23 W/mK at liquid nitrogen temperature in our measurement, which is about twice as large as that of a YAG crystal at room temperature. Using a thin disk Yb:YLF crystal for an efficient thermal removal from the crystal such like a 60 W Yb:YAG thin disk laser [10], a high average power operation with ten milli-joule pulse energy would be realized with single stage amplifier.

A center wavelength of the output pulse was 1017 nm, which was the spectral peak wavelength of the measured emission cross section of an Yb:YLF crystal at liquid nitrogen temperature. A spectral width of the output pulse was reduced to 5 nm due to a spectral gain narrowing effect as shown in Fig. 3(a), which was one third of that of the seed pulse. This spectral narrowing effect induces the gradual decrease of a pulse duration of an amplified pulse as the number of a round trip increases, leading to lowering a damage threshold of optics. By reshaping a gain profile with a pellicle etalon in the regenerative cavity[11] and/or a spectral profile of a seed pulse with an acousto-optic dispersive filter[12], the damage threshold of optics in the cavity would be improved and a power density in the cavity would be allowed to increase with the increase of the pump peak power. The output chirped pulse was compressed in time with a grating pair compressor. The gold-coated gratings (1100 lines/mm) exhibited a diffraction efficiency of more than 95% at a 12.8° angle of incident. After pulse compression, the pulse energy was 18 mJ and the pulse duration was 795 fs (sech^2), producing 23 GW pulses. Figure 3(b) shows an autocorrelation waveform. A laser gain spectral range was measured by tuning an oscillation wavelength with a birefringent filter inside the cavity in Q-switch operation without a seed pulse. The pump intensity and the pump duration were 12 kW/cm^2 and 4 ms, respectively. The tuning range was obtained to be 30 nm. It should be noted that a sub-100 fs pulse duration after compression could be obtained due to the wide spectral gain width of a cooled Yb:YLF crystal by replacing the fiber stretcher to an antiparallel grating pair pulse stretcher and avoiding the spectral gain narrowing effect.

3. Summery

A diode-pumped regenerative amplifier has been demonstrated with a cooled Yb:YLF crystal. The obtained pulse energy was 30 mJ at 20 Hz repetition rate. The optical-to-optical efficiency was 8.1%. A sub-pico-second compressed pulse was generated with an output energy of 18 mJ. Improved laser gain at low temperature and low cavity loss enabled efficient regenerative amplification. A high effective extraction efficiency of 68% has been achieved due to the reduced saturation fluence of the crystal and the high effective pulse energy fluence in the regenerative amplifier. By adapting a thin disk laser crystal, kilo-hertz operation with milli-joule pulse energy would be realized.

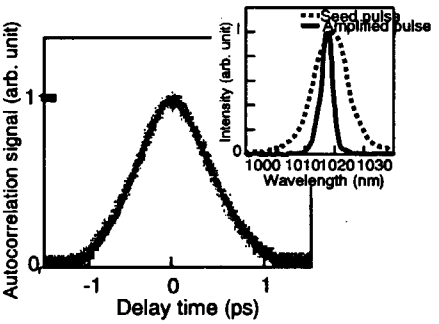

Fig. 3 (a) Power spectra and (b) autocorrelation signal of an amplified pulse

This research was partially supported by a grant-in-aid for scientific research of the Ministry of Education, Culture, Sports, Science and Technology of Japan.

References

1) J. Peatross, J. L. Chaloupka, and D. D. Meyerhofer, Opt. Lett. **19**, 942 (1994).
2) Y. Kobayashi, O. Yoshihara, Y. Nabekawa, K. Kondo, and S. Watanabe, Opt. Lett. **21**, 417 (1996).
3) T. Ditmire, J. W. G. Tisch, E. T. Gumbrell, R. A. Smith, D. D. Meyerhofer and M. H. R. Hutchinson, Appl. Phys. B **65**, 313 (1997).
4) D. Descamps, C. Lyngå, J. Norin, A. L'Huillier, C.-G. Wahlström, J.-F. Hergott, H. Merdji, P. Saliéres, M. Bellini and T. W. Hänsch, Opt. Lett. **25**, 135 (2000).
5) E. Takahashi, Y. Nabekawa and K. Midorikawa, Opt. Lett. **27**, 1920 (2002).
6) S. Backus, R. Bartels, S. Thompson, R. Dollinger, H. C. Kapteyn and M. M. Murnane, Opt. Lett. **26**, 465 (2001).
7) J. Z. H. Yang and B. C. Walker, Opt. Lett. **26**, 453 (2001).
8) J. Kawanaka, H. Nishioka, N. Inoue and K. Ueda, Appl. Opt. **40**, 3542 (2001).
9) J. Kawanaka, K. Yamakawa, H. Nishioka, and K. Ueda, Opt. Exp. **10**, 455 (2002).
10) E. Innerhofer, T. Südmeyer, F. Brunner, R. Häring, A. Aschwanden, R. Paschotta, C. Hönninger, M. Kumkar and U. Keller, Opt. Lett. **28**, 367 (2003).
11) K. Yamakawa and C. P. J. Barty, IEEE J. Selected Topics in Quantum Electronics **6**, 658 (2000).
12) F. Verluise, V. Laude, Z. Cheng, C. Spielmann and P. Tournois, Opt. Lett. **25**, 575 (2000).

4.1.5 X-ray radiation of clusters irradiated by ultrafast, high-intensity laser pulses

Y. FUKUDA, Y. AKAHANE, M. AOYAMA, N. INOUE, H. UEDA, Y. KISHIMOTO[a], K. YAMAKAWA, A. Ya. Faenov[b], A. I. MAGUNOV[b], T. A. PIKUZ[b], I. Y. SKOBELEV[b], J. ABDALLAH, Jr.[c], G. CSANAK[c], A. S. BOLDAREV[d], V. A. GASILOV[d]

[a]Naka Fusion Research Establishment, JAERI, Japan
[b]Multicharged Ions Spectra Data Center of VNIIFTRI, Russia
[c]Theoretical Division, Los Alamos National Laboratory, USA
[d]Institute of Mathematical Modeling, Russian Academy of Sciences, Russia

We have measured the high resolution x-ray emission spectra of plasma created by laser irradiation of Ar clusters at laser intensities over 10^{19} W/cm^2. To make these measurements possible, in addition to the effort to decrease a prepulse intensity using Pockels cell switches, micron-size clusters were produced using a specially designed conical nozzle.

Figure 1 shows the typical x-ray emission spectrum measured at the highest peak intensity of I=1.3×10^{19} W/cm^2 with 30-fs pulse duration, and the Ar gas pressure of p=60 bar. The mean cluster diameter at p=60 bar is estimated as ~1.5 μm by the 2D-hydrodinamic calculations of argon jet for the special nozzle. To decrease an effect of the prepulse, the contrast ratio was achieved on the level of K=5×10^{-6}. The resonant ($He_{\alpha 1}$) and its intercombination ($He_{\alpha 2}$) lines of the 1s2p-1s^2 transition in the He-like Ar (Ar^{16+}) were observed in the fourth reflection order as well as clearly resolved structure of the collisional and dielectronic satellite lines in the Li-like ion (Ar^{15+}). The radiation lines from the autoionizing states 1s2s^{l}2p^m of the multiply charged Be-like (Ar^{14+}) to F-like (Ar^{9+}) ions were also observed. Moreover, the Rydberg He-like lines of 1snp-1s^2 (n=3-6) transitions (He_β-He_ε) were observed in the fifth order at the same spectral record. No emission from 2p-1s line from H-like ion (Ar^{17+}) was observed. The absolute number of x-ray photons for He_α resonant line of Ar (λ=3.9491 Å, 3.14 keV) is estimated as N_{phot}=2×10^8 photons/pulse/pixel, which corresponds to the spectral power density of 2×10^8 W/Å. Figure 2 shows the cluster size dependence of x-ray emission spectra. Note that no x ray was observable at the Ar gas pressure of p=40 bar; at this pressure the cluster size is an order of magnitude smaller than that for p=60 bar. Thus, in the case of the p=40 bar experiment, even with K=4×10^{-4}, the prepulse could completely destroy the clusters. This result clearly demonstrates the important role of big clusters.

In order to explore the temporal dynamics of the cluster-plasma creation, the Boltzmann equation and a detailed collisional radiative model were solved simultaneously as a function of time. The calculations show that the emission from lower charged ion reaches the saturation level earlier. It is explained by a rapid shift of the ion composition towards higher charges as the result of impact ionization by hot electrons. The agreement with experimentally observed time-integrated spectra is quite good. It is suggested that the role of fs-laser pulse is the prompt generation of nonequilibrium cluster-plasma with high energy (~5 keV) free electrons.

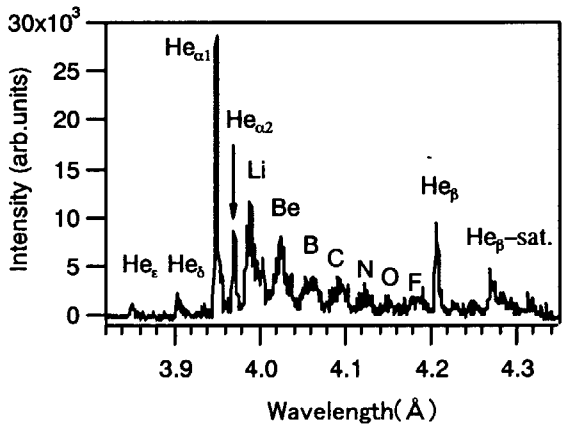

Fig. 1 X-ray emission spectrum from laser-irradiated Ar clusters measured at a laser intensity of I=1.3×10^{19} W/cm^2 with 30-fs pulse duration and a contrast ratio of K=5×10^{-6}

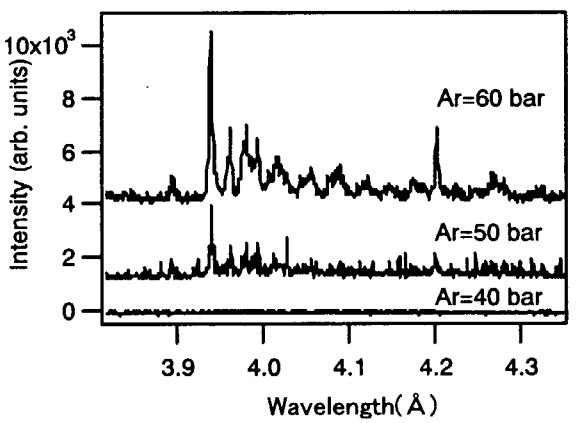

Fig. 2 The cluster size dependence of x-ray emission spectra measured at a laser intensity of I=2.5×10^{18} W/cm^2 with a contrast ratio of K=4×10^{-4}

4.1.6 Construction of a 'real' table-top terawatt Ti:sapphire laser for ultrafast laser applications

Fumiaki MATSUOKA, Etsuya YANASE, Masashi FUJINO[a)], Koichi YAMAKAWA
a) HOYA Photonics, Inc.

Recently, compact terawatt-class lasers have became to be able to construct in many laboratories by applying the technique of chirped-pulse amplification (CPA). Femtosecond laser pulses have two main features; 1) Short pulse duration and 2) High peak intensities. The first feature shows rapidity of interaction the laser pulse with materials. Many research activities of ultrafast material science or non-thermal processing etc. have been opened up. The second feature is effective in order to use the laser pulse as a driver of x-ray or high-energy particle sources. Based on these features, time resolved x-ray diffraction experiments were attempted at many laboratories [1].

We have recently constructed a TW Ti:sapphire laser system for such applications based on our ultrafast CPA technologies [2]. The laser system consists of an oscillator, a stretcher, a regenerative amplifier, a 4-pass amplifier and a compressor. The system occupies by 1.2 x 3.6 m^2 footprint on one optical table. We obtained output energy of 34 mJ and pulse duration of 38 fs (Fig. 1), which corresponds to the peak power of 0.9 TW at a repetition rate of 10Hz. The compressed laser pulse was focused in a vacuum chamber with an off-axis parabolic mirror (focal length of 76.2 mm, f-number:3). The focal spot size was 30 μm x 40 μm (Fig. 2), which corresponds to the peak intensity of $1x10^{17}$ W/cm^2. This is sufficient for several application experiments described below, which are currently in progress.

1) Processing
- Surface treatment of nuclear reactors' materials (stainless steel)
- Processing of electrical device materials (Si, Sapphire)

2) Material science
- Material dynamics with pump-probe technique
- Pulsed x-ray generation around 10keV for time resolved x-ray diffraction

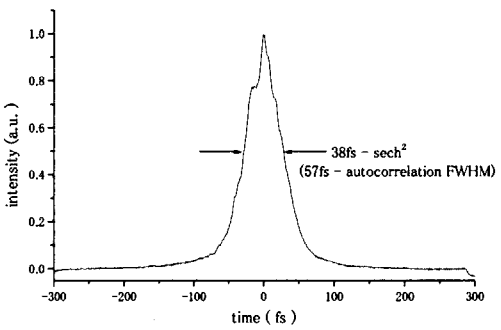

Fig. 1 Autocorrelation trace of compressed pulses

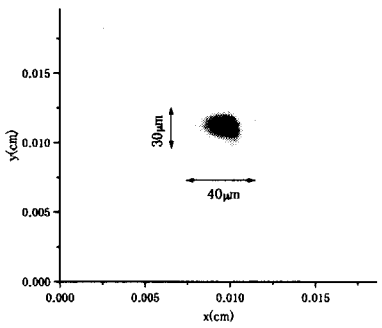

Fig. 2 Spot image profile at a focal position The output pulse was focused by a parabolic mirror (f=76.2mm).

Reference

1) A. Rousse, C. Rischel, J.Gautheir, Rev. of Mod. Phys., **73**, 17, 2001
2) K. Yamakawa et al., Opt. Lett. 23, 1468 (1998).

4.1.7 Phase control of excitation probability in the two-photon transition, Cs(6S) → Cs(7D), by the 767-nm light

Keiichi YOKOYAMA, Hidetaka YAMADA, Akihiro YABUSHITA, Yoshiaki TERANISHI, Yuji FUKUDA, Makoto AOYAMA, Yutaka AKAHANE, Norihiro INOUE, Hideki UEDA, Koichi YAMAKAWA, Atsushi YOKOYAMA[a)], Masahiro KAWASAKI[b)], Hiroki NAKAMURA[c)]

a) Department of Materials Science, JAERI

b) Department of Molecular Engineering, Faculty of Engineering, Kyoto University

c) Institute for Molecular Science

1. Introduction

Pulse shaping techniques developed for high-peak-power lasers are becoming necessary tools for controlling quantum systems. Of all the pulse shaping techniques, the spatial light modulator (SLM) combined with a liquid crystal array is most popularly used in the current quantum-control experiment. In comparison, the acousto-optic programmable dispersive filter (AOPDF), which is used this study, works with relatively new technique and different mechanisms and thus has potential advantages, such as, no dead area between liquid-crystal pixels or compactness compared to the SLM. However, the real performance to generate complex pulse shape so as to be required in quantum control has not been examined well. This report describes such an examination for the capability of the AOPDF.

Within the various experiments in quantum control, the phase control of excitation probability in atomic systems can be a good benchmark for the pulse shaper because of their simplicity, which can be regarded as a two-level system in most cases. The excitation probability of a two-level system can be controlled by the phase-related double pulse by adjusting the phase difference and time delay. This is owing to the fact that the phase of excited wave function is determined by both the phase of the ground state wave function and that of the electric field of the optical pulse. If the phase of the excited wave function produced by the first pulse differes by π from that by the second pulse, destructive interference occurs and the amplitude of the excited wave function becomes zero, at least in principle.

In the present study, we examine the performance of AOPDF for the atomic excitation of the cesium 6S -> 7D transition to see its potential and limitation. The Cs 7D state splits into two spin-orbit states, $7D_{5/2}$ and $7D_{3/2}$. The energy splitting is 21 cm^{-1}, so that usual ultrashort laser pulses excite the Cs atom into both states because of the broadness of the spectral band. Phase control of the shaped pulses also targets the selective excitation of these closely lying states.

2. Experiment

We measured the excitation probabilities for both the $6S_{1/2}\rightarrow 7D_{5/2}$ and $6S_{1/2}\rightarrow 7D_{3/2}$ transitions, scanning the phase difference and time delay between two transform-limited pulses. In reality, we observed the fluorescence from the two radiative decay processes, $7D_{5/2}\rightarrow 6P_{3/2}$ and $7D_{3/2}\rightarrow 6P_{1/2}$ as a measure of the excitation probability. Also, we measured the peak power and autocorrelation wave form of modulated pulses to obtain some characteristics of the AOPDF.

3. Results and discussion

The excitation probability was satisfactorily controlled with the phase difference at the time delay less than 500 fs. Figure 1 shows oscillation of the excitation probability (fluorescence intensity) as a function of the phase difference at two delays. The oscillation is caused by the interference between the wave function produced by the first pulse and that by the second pulse. At a certain phase, the probability is apparently suppressed to the noise level, indicating complete destruction of excited wave function due to the interference, and thus, an evidence for the good controllability of the excitation probability. However, at the longer time delay more than 800 fs, the probability does not go down to zero at any phase examined here and some portion of amplitude in the excited state seems to survive even at a completely destructive phase. The result implies that the pulse shape substantially deviates from the designed, at least, at the focus point in the gas cell. Several reasons can be infered for

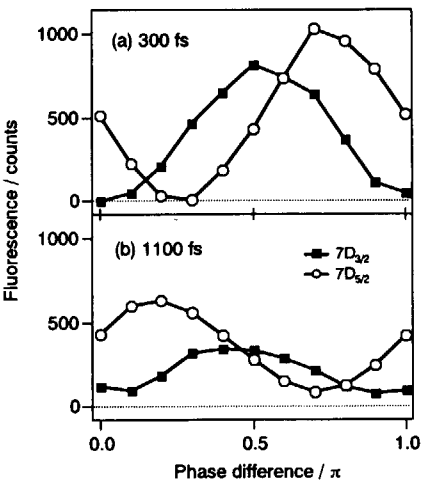

Fig. 1 Fluorescence intensity as a function of the phase difference measured at delay 300 fs (a) and 1100 fs (b)

the deviation: the character of the pulse shaper itself, modulation during beam delivery and focusing, and relaxation of excited wave function by some external perturbation. To collect more information potentially related to the observed degradation in the controllability, we measured the temporal profile of the peak power and autocorrelation wave form of the modulated pulse.

First, the peak power was found to exhibit peculiar temporal profile in some cases of the delayed double pulse as shown in Fig. 2. Because the AOPDF works as a chopper synchronized with the injection of an acoustic wave and the repetition rate is 20 kHz and duty cycle of ~ 0.5 in the present experiment, about two-thousand pulses emitted from the 82-MHz Ti:Sapphire oscillator can transmit the AOPDF by coupling with a single acoustic wave. According to the formula of diffraction efficiency, the peak power of those ~2000 pulses should be proportional to the power of acoustic wave existing in the crystal at that time. Provided that the acoustic wave has a form of well-separated two pulses, the acoustic power should have maximum when both pulses are in the crystal, i.e., in the correct timing for double pulse generation (referred to double-pulse period), and have a half of the maximum when one of two pulses is out of the crystal before and after the double-pulse period, i.e., single-pulse period. This situation is observed in the case of the double pulse with different center wavelength (760 and 780 nm) as shown by the dotted curve in Fig. 2. However, in the case of double pulse with the same center wavelength (770 nm) as shown by the solid curve in Fig. 2, the temporal profile of peak power shows a depletion in the double-pulse period compared to the peak power in the single-pulse period. This unexpected behavior is always seen at the delay larger than 800 fs, while the depletion is not clear at delay less than 800 fs probably because the acoustic wave is not clearly distinguished into two pulses. This behavior may be related to the degradation of pulse shape and to the incompleteness of the phase.

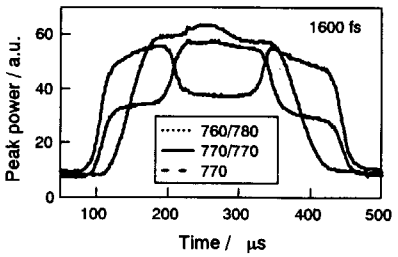

Fig. 2 Temporal profile of the peak power of the modulated pulses

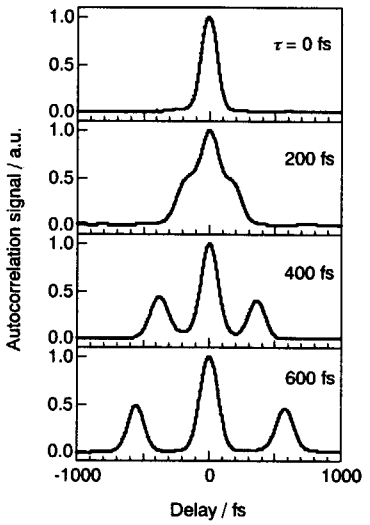

Fig. 3 Autocorrelation wave forms of the double pulse with various delays

Second, the autocorrelation wave forms of the modulated optical pulses show a triple peak as expected from the double pulse form (Fig. 3). The separation of those peaks is close to the given time delay in designing the pulse shape, indicating a faithful operation of the AOPDF with respect to the time delay. Furthermore, not only the time delay but also the phase difference has been successfully controlled by the AOPDF as follows. The phase shift between the two excitation probability curves for the different states (Fig. 1) must be proportional to the time delay with a proportional coefficient equal to a half of the energy splitting between the excited states (10.5 cm^{-1}). Figure 4 shows the phase shift measured at various time delays, showing that the proportional coefficient (10.7 cm^{-1}) is very close to the expected. It is concluded that the AOPDF seems to work as expected, at least, in terms of the time delay and phase difference.

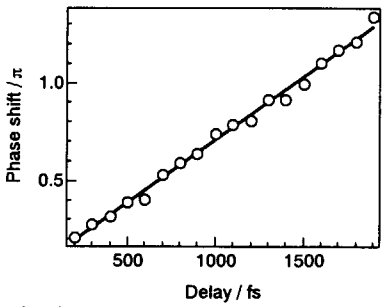

Fig. 4 Delay dependence of the phase shift

Although above two points are possible causes for the delay-dependent degradation of the controllability, some other possibilities remain to be considered, for example, potential modulation in the beam delivery or focusing and relaxation of the atomic wave function by some unexpected external perturbation. Currently, we have no information to support those possibility. Further experiments are needed, e.g. with different focusing spot size or different temperature of the gas cell.

4. Summary

The AOPDF was shown to have high potential for controlling the time delay and phase difference between two pulses and exhibited an example of the completely destructive interference in the atomic wave function. Delay-dependent degradation of the controllability was observed and the origin has to be figured out in the future work.

4.1.8 Ultrashort laser pulse ablations for nuclear grade SUS

Akihiko NISHIMURA, Fumiaki MATSUOKA, Hiroshi MURAKAMI and Eisuke MINEHARA

Ultrashort pulse lasers provide the precise machining generally characterized by the absence of heat diffusion and, consequently, molten layers. This is because of the ultrashort interaction time in comparison with thermal diffusion time. For ultrashort laser pulses, the heating process can be separated resulting in the two-temperature model which shows non-equilibrium temperature state in electrons and in lattices. The electron temperature is reached to the maximum value at the end of the ultrashort laser pulse. The lattice temperature is still cold as the absorbed energy has not transferred from the electron to the lattice. By introducing the optical penetration depth δ and the heat penetration depth $d=(D\tau)^{1/2}$, the ablation rate per a single laser pulse can lattice can be shown in the two different regimes which is dependent on the laser fluence F. The gentle ablation regime for lower laser fluence can be characterized by the optical penetration depth, while the strong ablation regime for higher laser fluence can be done by the heat penetration depth d. Especially, the gentle ablation regime shows the highest processing quality which is nearly free of molten layer because the thermal penetration depth is shorter than the optical penetration depth. All metal materials show the same behavior of the two different regimes. In case of copper, the laser fluence of ~ 0.7 J/cm^2 is the transient laser fluence of the two regimes for 150 fs ultrashort pulses[1,2].

When the laser fluence is determined by the optical penetration depth, no molten material can be observed by microscopy. On the other hand, when it is done by the electron penetration depth, ablation has a molten layer and a "corona" of re-solidification around an irradiated surface. Thus, ultrashort pulses cannot give considerable advantages for precise processing in the strong ablation regime. In addition, when ablation is done in air, the ultrashort laser pulse processing might lose the important advantage which is free from plasma generation near the ablation surface. Also, re-deposition of ablated metal and oxidization can occur after the ultrashort pulses which cause unfavorable debris around the surface.

To expand laser application fields, precise machining in air is very much expected. The in-core structural materials used in the BWRs are exposed to not only high-flux neutron and gamma radiation but also high temperature water environment[3]. In Japan, the welded BWR core shrouds have recently experienced the stress induced cracking. It is very serious because the cracking has occurred in austenitic stainless steels of SUS316L that is more resistant to the thermally induced stress corrosion cracking due to low carbon containment. Microscopic SEM observations for the BWR core shrouds are now giving us the important fact that a boundary of grains on the SUS316L surface thin layer is not an origin of cracking but a stress induced grain would be an origin of cracking. Figure 1 shows a plasma emission on a SUS sample by ultrashort laser pulse ablation. We will demonstrate the ultrashort laser material processing using ultrashort pulse lasers and clarify the keyhole formation on the stress induced stainless steels. To date, both of a Ti: sapphire CPA laser system and a vacuum chamber are under preparation for the abovementioned purpose to test ablation experiments in various gas conditions. Figure 2 shows the preliminary result of an ablation hole on nuclear grade SUS in air. This system can show us systematic data for the ablation experiments and will be used for the ablation demonstration by the JAERI-FEL which will be upgraded in future.

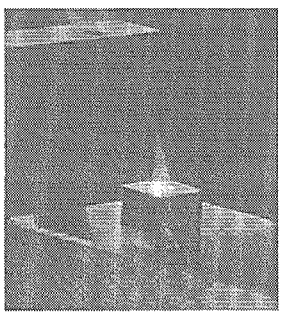

Fig. 1 Ablation in air

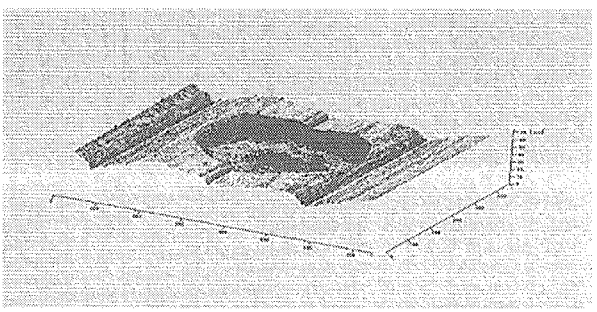

Fig. 2 An ablation hole on nuclear grade SUS

References

1) C. Momma *et al.*, Optics Comm. Chem. **129,** 134, 1996
2) S. Nolte *et al.*, J. Opt. Soc. Am. B. **14,** 2716, 1997
3) Y. Kaji *et a l.*, J. Nucl. Sci, Technol., **37,** 949,2000

4.2 X-ray Laser Development

Keisuke NAGASHIMA, Maki KISHIMOTO, Masataka KADO, Tetsuya KAWACHI, Noboru HASEGAWA, Momoko TANAKA, Yoshihiro OCHI, Kouta SUKEGAWA, Masaharu NISHIKINO, Renzhong TAI, Peixiang LU and Hiroyuki DAIDO

Outline of x-ray laser research

The x-ray laser research at Advanced Photon Research Center has started on April 1998. The main purpose is to develop compact and repetitive x-ray lasers with full spatial coherence and saturated intensity. The results in the first period, from 1998 to 2001, are 1) development of the compact CPA laser system for transient collisional excitation (TCE) x-ray laser experiments, 2) demonstration of lasing in the wavelength range of 8.8-46.9 nm by using various solid and gas targets, and 3) saturated amplification at 12.0 nm and 13.9 nm. The objectives in the second period, from 2002 to 2006, are 1) full spatial coherence with coherent length larger than beam size and 2) higher repetition rate up to ~ 0.1 Hz for practical applications.

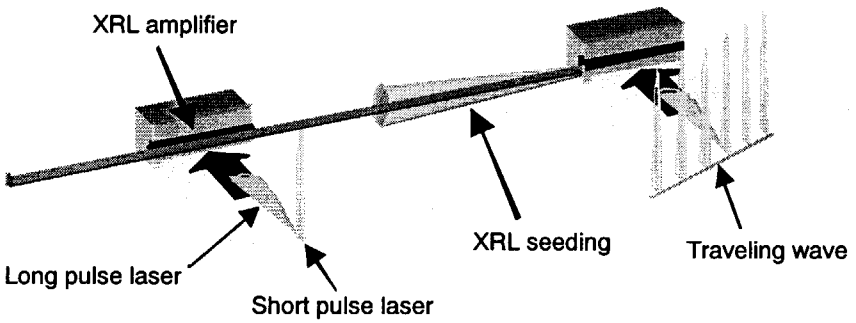

Fig. 1 Experimental configuration of the double target experiment

In 2002, we carried out a double target experiment for improving the spatial characteristics of TCE x-ray lasers and demonstrated a laser-pumped x-ray laser with full spatial coherence at 13.9 nm for the first time (**4.2.1**). In this double target experiment, an x-ray laser seeding light from the first target was amplified in an x-ray laser amplifier at the second target, as shown in Fig. 1. The observed divergence is 0.2 mrad and it is close to the diffraction limited value within a factor of two. The essential point of this experiment is that the seeding light is amplified in the second medium without refraction influence. From the Young's double slit experiment, it was found that the spatial coherent length is longer than the beam diameter and this x-ray laser beam is full spatial coherent (**4.2.2**). Temporal characteristics of TCE x-ray lasers were examined also (**4.2.3**). We tried an experiment for amplifying the other seeding light from higher order harmonics (**4.2.4**). The new devices for improving the experimental system are under construction, which are an OPCPA front-end laser system (**4.2.5**) and a full-auto target alignment system (**4.2.6**). The several applications have been started using this x-ray laser. We observed a surface microstructure of ferroelectric material, $BaTiO_3$ and clarified a change of the microstructure near the Curie temperature (**4.2.7**) and tried an observation using the x-ray microscope with schwarzschild optics (**4.2.8**).

4.2.1 Double target amplification of the nickel-like silver x-ray laser

Momoko TANAKA, Masaharu NISHIKINO, Tetsuya KAWACHI, Noboru HASEGAWA,
Masataka KADO, Maki KISHIMOTO, Keisuke NAGASHIMA

1. Introduction

The transient collisional excitation (TCE) scheme can achieve an x-ray laser with a high gain of a few tens per centimeter and picosecond pulse duration using a tabletop laser system. However, the beam divergence of the TCE x-ray laser is large (~10 mrad) and the spatial coherence is insufficient. There are two reasons for the large beam divergence of the TCE x-ray laser: Firstly, the gain of the TCE laser is so high that the amplification saturates with a gain medium length of several millimeters, and it obstructs to realize small Fresnel number. This difficulty can be overcome by use of two separated gain media, which is essentially equivalent to a long gain medium. The second reason is the refraction of the x-ray beam due to the large density gradient in the gain medium plasma. It can be overcome by use of gain medium with flat or calm density gradient. Recently, simulations[1] have shown that the peak of the gain region of the TCE laser is generated at first near the critical density region, and after that it moves away from the target surface, where the density gradient of plasma is calm. Injecting the seed x-ray at this timing, the x-ray laser will be amplified with little influence of the refraction. Here we report the demonstration of a nickel-like silver x-ray laser with diffraction limited beam divergence using two gain media.

2. Experiment and results

Two gain medium plasmas are generated by a picosecond glass laser system with two beam-lines[1]. Each beam consisted of two pulses; a pre-pulse with a pulse duration of 300 ps and a picosecond heating pulse with a temporal delay of 600 ps from the pre-pulse. The pulse duration of the heating pulse for the first target is 4 ps with the quasi-traveling wave arrangement[1] and that for the second target is 12 ps without the traveling wave. The energy ratio of the pre-pulse and the heating pulse is 1:8. The laser pulses are focused with line shape of 6.5 mm x 20 μm on flat silver targets with an irradiance of the heating pulse of ~10^{15} W/cm^2. The distance between the two targets is 20 cm. A part of the x-ray laser generated in the first medium is used as the seed x-ray laser, and it is injected into the successive second medium, which is used as an amplifier. The beam divergence of the seed x-ray laser is approximately 6 mrad in FWHM. The total energy of the seed x-ray laser is 270 nJ, which is two orders of magnitude smaller than that of saturated amplification[1].

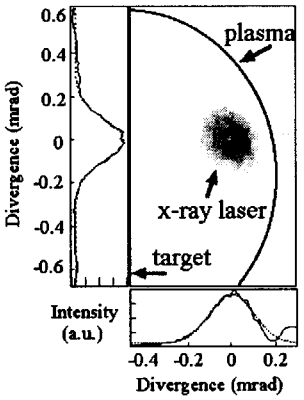

Fig. 1 Far field image of the x-ray laser
The line graphs are the intensity distributions; the solid line shows experimental result and the dashed line shows curve fit by a Gaussian.

Shown in Fig. 1 is the far field image of the x-ray laser generated by two gain media when the pumping time of the second medium is delayed from that of the first medium for 652 ps (15 ps earlier than the required time of the x-ray propagation for 20 cm). The solid line on the image implies an edge of a shadow of the gain medium plasma on the second target backlit by the seed x-ray. The narrow x-ray laser beam is seen inside the shadow of the plasma. It suggests that the x-ray laser is amplified in the second medium with little influence of refraction. The beam divergence is obtained to be a much reduced value of 0.20 mrad (FWHM). The beam pattern is fit well with a Gaussian profile. The total energy of this beam is 25 nJ. It will increase with increasing the energy of the seed x-ray and the second target length, because amplification in the second medium is not saturated. The gain coefficient of the amplifier plasma is estimated to be 7.9 cm^{-1}. This value is smaller than the gain coefficient of the single target, which is observed to be 35 cm^{-1} in a previous study[1]. The small gain coefficient and small beam divergence suggest that the gain region of this beam is located in a low density area, where the influence of refraction is negligible. The diffraction limited beam divergence for a coherent Gaussian beam with a beam west size of 50 μm is calculated to be 0.11 mrad. The observed divergence is only 1.8 times greater than this value. This implies that the obtained x-ray beam is quite close to the diffraction-limited condition.

References

1) T. Kawachi *et al.*, Phys. Rev. A **66**, 033815, 2002

4.2.2 Spatial coherence measurement of x-ray lasers generated by double-target amplification

Masaharu NISHIKINO, Momoko TANAKA, Maki KISHIMOTO, Masataka KADO
and Keisuke NAGASHIMA

1. Introduction

In the double-target configuration, a seed x-ray laser (XRL) beam from one target is injected into a plasma amplifier at another target. When the propagation of the x-ray laser beam is not affected by refraction in the amplifier, a highly directional XRL beam with the divergence of 0.2 mrad is generated.[1] The property of the spatial coherence is an important issue for application research, such as x-ray holography and interferometry. In this report, we show that the measurements of the spatial coherence of highly directional XRL beam by using Young's double slit interferometry.

2. Experimental

The spatial coherence of the XRL beam after amplification has been characterized via Young's double slit interferometry.[2] Double slits, consisting of a pair of 16-μm width slits separated by either 150, 200, 300, or 350 μm, were placed 2.3 m away from the second target where the beam diameter determined from observed divergence was 460 μm. The double slit was placed in either the horizontal or vertical direction to characterize the coherence along both directions. The fringe pattern was recorded in each XRL shot with a CCD camera placed 3.9 m away from the double slit.

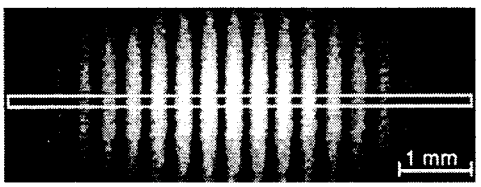

Fig. 1 An x-ray image of the fringe pattern

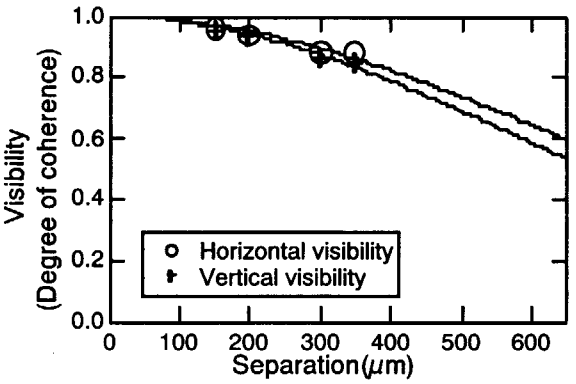

Fig. 2 The observed fringe visibility and the degree of coherence from the Gaussian shell-model

3. Result

Figure 1 shows the fringe pattern along the horizontal direction for the slit separation of 150 μm. Fringe visibility is defined as $V=(I_{max}-I_{min})/(I_{max}+I_{min})$, where I_{max} and I_{min} are the maximum and minimum intensities of the fringe pattern. The visibilities averaged over the horizontal and vertical directions are 0.96, 0.93, 0.88, and 0.86 for the slit separations of 150, 200, 300, and 350 μm, respectively. Dependences of the visibilities on the slit separations are plotted in Fig. 2. The spatial coherence of a quasimonochromatic light source is characterized by the normalized degree of coherence, which becomes equal to the fringe visibility in the case of an uniformly illuminated double slit. Assuming a Gaussian Shell-model for the source region, both the intensity distribution and the degree of coherence are given by Gaussian distributions.[3] From the comparison between the experimental result and the Gaussian Shell-model, the spatial coherence lengths L_c determined are 640 and 580 μm for the horizontal and vertical directions, respectively. Since these coherence lengths are greater than the beam size, the XRL beam has full spatial coherence[4]. Due to this high spatial coherence, we conclude the divergence of this XRL beam is very close to diffraction limit.

References

1) M. Tanaka *et al.*, Opt. Lett. (to be published); M. Tanaka *et al.*, in this report.
2) R. E. Burge *et al.*, J. Opt. SOC. Am B**14**,2742-2751(1997).
3) M. Born and E. Wolf, Principles of Optics. (pergamon, Oxford, 1986).
4) L. Mandel and E. Wolf, Optical coherence and quantum optics. (Cambridge University Press, New York, 1995).

4.2.3 Temporal durations of transient collisional excitation X-ray lasers

Yoshihiro OCHI, Tetsuya KAWACHI, Noboru HASEGAWA, Momoko TANAKA, and Keisuke NAGASHIMA

1. Introduction

Transient collisional excitation scheme has made great progress in X-ray laser (XRL) research using table-top lasers. The gain-saturation up to the wavelength of 12.0 nm and substantial gain at 8.8 nm have been demonstrated[1] in Advanced Photon Research Center. We have measured temporal durations of XRL in order to understand the gain generation in a plasma medium.

2. Experiment and Results

The experiment was performed with Nd:glass laser system with the charped pulse amplification at wavelength of 1.053 μm[2]. The laser system produced a low-intensity prepulse and a high-intensity main pulse. The prepulse was attached to produce a preformed plasma in adequate ionizing state and the main pulse to generate population inversions. The pulse duration was 400 ps and 4.8 ps for the prepulse and the main pulse respectively. Time separation between the pulses was set to be 500 ps. Typical laser energy on the target was 5-12 J. An energy ratio from the main pulse to the prepulse was set to be 8:1. A six-step mirror was employed in front of an off-axis prabolic focusing mirror in order to generate a quasi-traveling wave. The traveling wave velocity was measured to be 1.03c, where c represents the light speed, by use of a femtosecond streak camera with the time resolution of 2.15 ps.

The XRL outputs from three different materials, silver (Ag; Z = 47; $\lambda_{4d\text{-}4p}$ = 13.9 nm), palladium (Pd; Z = 46; $\lambda_{4d\text{-}4p}$ = 14.7 nm) and molybdenum (Mo; Z = 42; $\lambda_{4d\text{-}4p}$ = 18.9 nm), were recorded using a flat field grating spectrometer coupled with an x-ray streak camera with the time resolution (τ_{xsc}) of 1.68 ps. The flat field spectrometer consisted of a troidally bent gold mirror, an entrance slit of 200-μm width, and a holographic laminar grating with the average groove number of 1200 lines/mm. Time resolution of the flat field spectrometer (τ_{ffs}) depended on the XRL wavelength and they were calculated to be 2.58 ps, 2.73 ps, and 3.51 ps for Ag, Pd, and Mo respectively. The total time resolution of the instrument (τ_R) was represented by the root men square of τ_{xsc} and τ_{ffs}, i.e. $\tau_R = (\tau_{xsc}^2 + \tau_{ffs}^2)^{1/2}$.

Shown in Figs. 1 are the obtained streak images of the XRLs together with their temporal profiles. Temporal durations (FWHM) were obtained after de-convolving the instrumental time resolution τ_R using the formula $\tau_{XRL} = (\tau^2 - \tau_R^2)^{1/2}$. The measured pulse duration of the Ni-like Ag XRL agreed well with the value inferred from the intensity ratio of the XRL output with or without the traveling wave pumping in the previous work[1]. We can also see the trend that the temporal duration of the Ni-like XRL becomes shorter as the atomic number decreasing. Since the laser conditions for the several target materials were almost same, we can say that the electron temperature and density of the generated plasmas were comparable for these cases. Therefore over ionization may play an important role to shorten the gain duration for the lower atomic number material.

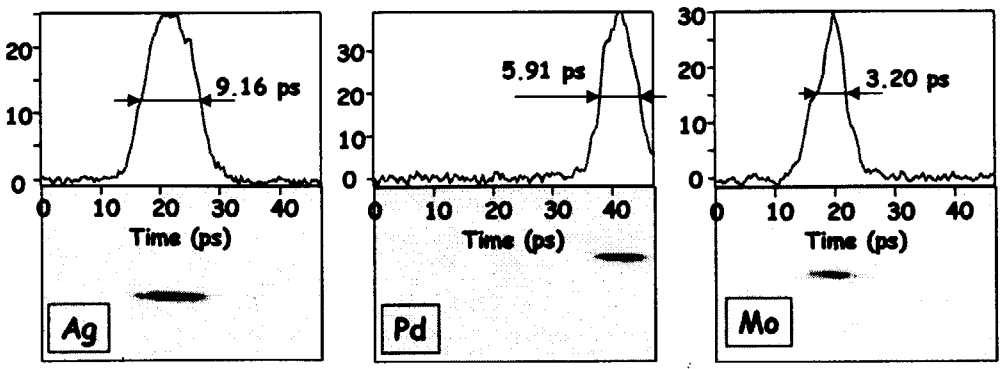

Fig. 1 Temporal durations of the Ag (Z = 47), Pd (Z = 46), and Mo (Z = 42) XRLs

References

1) T. Kawachi *et al.*, Phys. Rev. A **66**, 033815 (2002).
2) T. Kawachi, et al., Appl. Opt. **42**, 2198 (2003).

4.2.4 Amplified high order harmonic light for high coherent x-ray laser

Noboru HASEGAWA, Tetsuya KAWACHI, Maki KISHIMOTO, Kouta SUKEGAWA, Momoko TANAKA, Masataka KADO, Tai RENZHONG, Yoshihiro OCHI, Masaharu NISHIKINO and Keisuke NAGASHIMA

1. Introduction

We proposed a method to generate high spatial and temporal coherent x-ray laser, in which high order harmonic light is used as a seed light of a laser-produced x-ray amplifier[1]. The high order harmonic light is very suitable for this purpose because it has high spatial and temporal coherence [2,3].

In this report, we conducted an experiment for the amplification of the 29th order harmonic light of the Ti;Sapphire laser with the neon-like manganese x-ray laser medium (λ=26.9nm) pumped by the Nd:Glass laser.

2. Experiment and results

The experimental setup is shown in Fig. 1. The high order (29th) harmonic light was required for the seed light for Ne-like Mn x-ray laser with the wavelength of 26.9 nm. It was generated by irradiating Ar gas jet target with the Ti;Sapphire laser under the conditions that central wavelength of fundamental light was 780.1 nm, spectrum band width was 15nm, pulse duration was 80 fs, incident laser intensity was $4x10^{14}$ W/cm^2, neutral gas density was less 10^{17} cm^{-3}. The generated harmonic light was injected into the x-ray laser medium as the seed light for the x-ray laser. The Ne-like Mn x-ray laser medium was generated by irradiating Mn slab target with the Nd:Glass laser under the conditions that the energy ratio of the pre-pulse to the main pulse was 1:7, the total input energy was 8 J, the pulse duration was 7 ps each, the width and the length of the line-focus were 20 μm and 6 mm, respectively. The intensity of the pre-pulse and the main pulse was $4x10^{14}$W/cm^2 and $3x10^{15}$W/cm^2, respectively. Each driver lasers were synchronized by the 'Lock-to-Clock' synchronizer (Spectra-Physics) and the timing jitter measured by the streak camera was less than 5ps. Fundamental and scattered laser light were cut with 0.8μm thickness Al filter and the generated x-rays were detected by grazing incidence spectrometer with CCD detector.

The spatial profiles of the seeded x-ray laser (solid line) and no seeded x-ray laser (dashed line) were shown in Fig. 2. The seeded x-ray laser had narrow divergence (2mrad) compared to the no seeded one (6mrad). The amplification of the seed light was obtained, because the divergence of the seeded x-ray laser was equal to the 29th harmonic light (2mrad).

3. Summary and future plan

We obtained the 26.9nm amplified harmonic light for the purpose of high coherent x-ray laser. The divergence of amplified harmonic light was preserved form the seed light. In future, we are planning the high coherent Ni-like silver x-ray laser with this method, this wavelength (λ=13.9nm) is expected for the several applications.

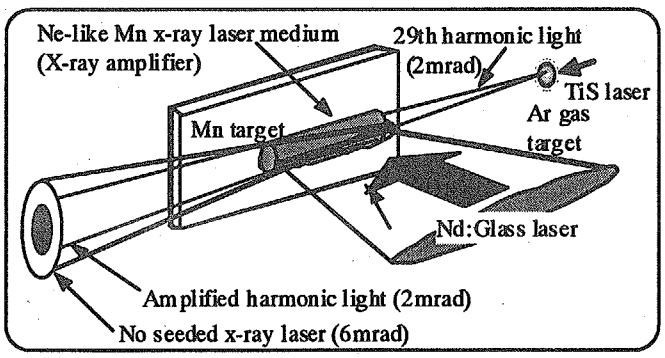

Fig. 1 Experimental setup
The generated harmonic light was injected into the x-ray laser medium as the seed light for x-ray laser.

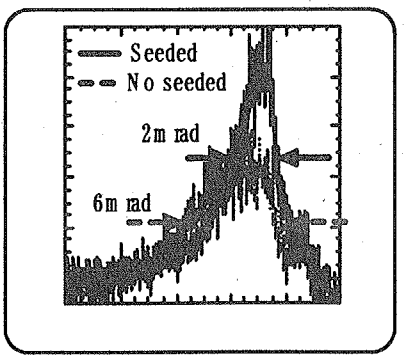

Fig. 2 Seeded x-ray laser spatial profile
The seeded x-ray laser had narrow beam divergence compared to the no seeded one.

References

1) N. Hasegawa *et al.*, SPIE Proceedings 4505, 204, 2001
2) R. A. Bartels *et al.*, Science Vol.297, 19, 376, 2002.
3) C. Lynga *et al.*, Phy. Rev. A Vol.60, 4823, 1999

4.2.5 Basic design of optical parametric charped pulse amplification (OPCPA) system for X-ray laser driver

Maki KISHIMOTO and Kouta SUKEGAWA

1. Introductuion

We have been developing a compact x-ray laser system and its application facility for studying nano-structure material and biological researches since 1998 and it has been demonstrated that high gain coefficients in soft x-ray amplification can be achieved using the compact CPA (chirped pulse amplification) tabletop sized Nd:glass laser system with a few 10J energy and several picoseconds pump laser pulse duration as a x-ray laser driver in TCE scheme. Moreover, we have succeeded in observing a dynamically changing domain structure with ps order lifetime on the surface of a ferroelectrics BaTiO3 crystal by measuring ps x-ray speckles by means of the TCE x-ray laser in the last year. To widen the field of application of the x-ray laser, upgrading and modification of the present x-ray laser driver, such as high repitation rate, pump laser pulse optimization, are needed. Especially, it is very important for the effective generation of x-ray laser to control the pump laser pulse. Therefore we are planning to introduce optical parametric charped pulse amplification (OPCPA) in the front end system of the x-ray laser driver.

2. Design of front end system using OPCPA

We are using an intense charped pulse amplification (CPA) Nd: glass laser at the wavelength of 1053nm for x-ray laser driver. In the front end of the present Nd:glass laser system, a 1053nm seed pulse from Tsunami pumped with Millennia is stretched and amplified with the stretcher and the regenerative amplifier, respectively. However the regenerative amplifier is very difficult to align the optics and suppress a pre-pulse and an amplified spontaneous emission (ASE). Therefore we planned to replace the regenerative amplifier with an OPCPA system. In OPCPA, an intense pump laser is made to interact with a nonlinear crystal to produce amplification of a seed light with a broad bandwidth. Features of the OPCPA system include (1) simple and compact optical arrangement and (2) low pre-pulse and ASE. Figure 1 shows a basic design of the OPCPA front end system for x-ray laser driver. In order to obtain high gain, the OPCPA system uses two amplifiers in series: A 15mm-long BBO crystal (Type I) followed by a 15mm-long LBO crystal (Type I). A 532nm Nd:YAG laser (Hoya Continuum, Powerlight 8000) is used for the pump laser and delivers up to 800mJ with a pulse duration of 7ns. When the pump laser is phase-matched with the seed pulse in the nonlinear crystal, part of the pump laser energy transfers to the seed light, leads to amplification of it.

3. New triggering system for Nd:glass laser control

The elimination of the timing jitter between the seed pulse from the stretcher and the pump laser pulse is needed for effective optical parametric amplification. A precision trigger signal generator (HP DG2040) was used for the master clock generator of the glass laser system and all the equipments of the glass laser controller were synchronized with it. As a result, we achieved the timing jitter between the seed pulse and the pump laser pulse of less than 1ns.

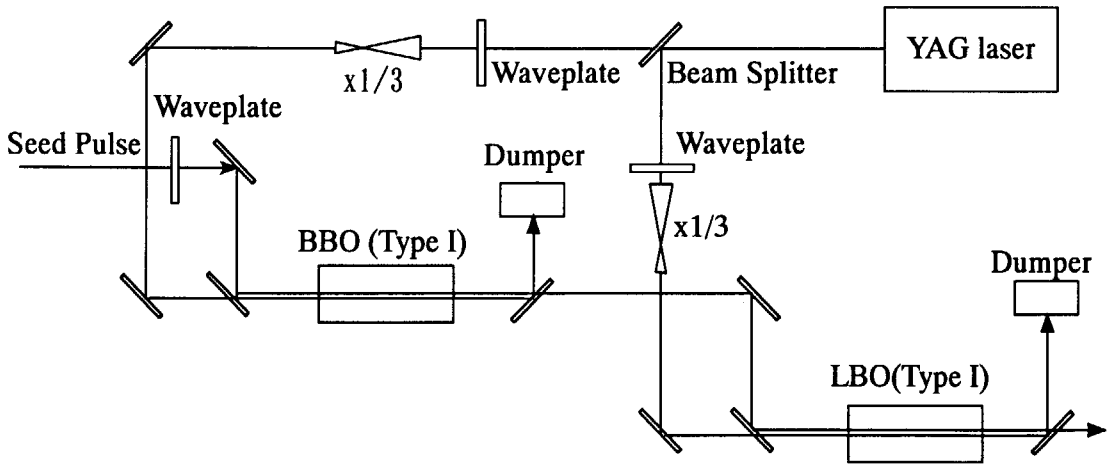

Fig. 1 Basic design of the front end system using OPCPA for the x-ray laser driver

4.2.6 Development of target auto-alignment system for high repetition x-ray laser

Kouta SUKEGAWA, Maki KISHIMOTO, Masataka KADO, and Keisuke NAGASHIMA

1. Introduction

Spatially full coherent x-ray lasers have been recently demonstrated by double target method at JAERI.[1] The beam divergence of 0.2 mrad is achieved with the full coherent x-ray lasers, which is one order better than ordinary x-ray lasers. The problem that is unstable beam pointing occurred by the beam divergence. Beam pointing stability is very important for application research. Because it must align a target in every 1 shot in case as a solid target, it is difficult to generate an x-ray laser at high repetition rate. Low repetition rate limits the application of x-ray laser. To solve these problems, a high precision target alignment system is needed. Therefore, we have been developing an auto-alignment system for high repetition rate.

2. Alignment system

Shown in Fig. 1 is a schematic drawing of our auto-alignment system. This system consists of a vacuum chamber, two targets, motor stages(SIGMA-TECH, 10-nano-Feedback-Stage) to fix target, four He-Ne lasers (Melles Griot, 5 mW, 632.8 nm), four position sensors (HAMAMATSHU,Position Sensitive Detector, PSD) and 1 inch aluminum mirrors. Two He-Ne laser irradiate one target and the reflected laser light is detected with the PSD. The first laser is used to decide a position in the straight direction, and irradiates the target with grazing incident. Another one decides rotating direction. The PSD signal is digitized with an AD converter and is taken by a computer. The optimum target position is calculated from the PSD output data, and the target is moved there with motor stages. The target is aligned to a fixed position by driving the stage for straight and rotating direction.

When the target drives for straight direction x [mm] or rotating direction y [degree], we express the PSD output values as $F_{he}(x,y)$[V] and $F_{ka}(x,y)$ [V],respectively. $F_{he}(x,y)$ and $F_{ka}(x,y)$ are expressed with the following equations.

$$\begin{pmatrix} F_{he}(x,y) \\ F_{ka}(x,y) \end{pmatrix} = \begin{pmatrix} a_1 & b_1 \\ a_2 & b_2 \end{pmatrix} \begin{pmatrix} x \\ y \end{pmatrix} + \begin{pmatrix} c_1 \\ c_2 \end{pmatrix} \qquad (1)$$

Where, the parameter a_1~c_2 are real numbers. Solving the equation (1), we obtain the target shift amounts. Based on the equation (1), we tested this system performance. We found out that the error of this system is ± 28 μm for straight direction , ± 8 μrad for rotating direction.

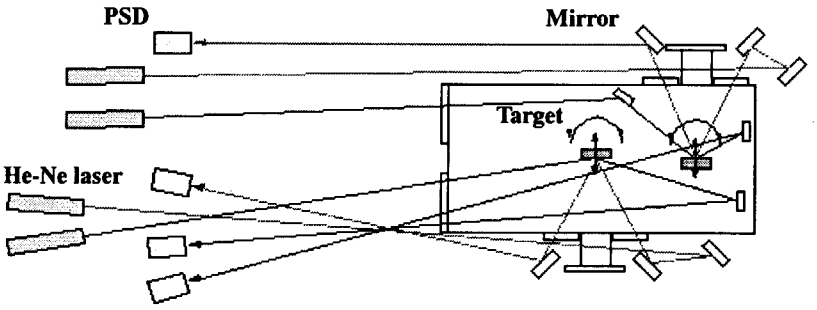

Fig. 1 Schematic drawing of an auto-alignment system

3. Summary

We have been developing the auto-alignment system for high repetition rate. We found out that the error of this system is ± 28 μm for straight direction, ± 8 μrad for rotating direction as a result of test performance. This system is practical as a conclusion as target alignment system from beam divergence of the x-rays laser 0.2 mrad at present.

Referrence

1) M.Tanaka et al.,Opt Lett.(to be published)

4.2.7 Instantaneous View of local Polarization Clusters in Cubic $BaTiO_3$

Renzhong TAI, Kazumichi NAMIKAWA[a)], Maki KISHIMOTO, Momoko TANAKA, Akikatsu SAWADA[b)], Kouta SUKEGAWA, Masataka KADO and Keisuke NAGASHIMA

a) The department of physics, Tokyo Gakugei University

b) The department of physics, Okayama Univeristy

1. Introduction

By a technique of picosecond soft x-ray laser (13.9 nm) speckle, the instantaneous surface structure was observed and reported for a single crystal of $BaTiO_3$ with ferroelectric multi-domain structure (90° *a/c* domains), as heating toward the Curie temperature T_c [1)2)]. The critical behavior near T_c shows an existence of strong polarization fluctuations during domain annihilation process.

Here, we mainly report the fluctuation behavior in paraelectric phase of $BaTiO_3$ by using the same experimental technique, which is relevant closely to the complex phase transition mechanism of this prototype ferroelectric material.

2. Results

Several improvements were made this time to enhance the performance[3)]. The results are shown in Fig. 1. The external DC electric field E was injected normal to the specimen surface. The scattering looks stronger vertically due to the relatively higher spatial resolution in this direction for our grazing -incidence setup. The speckles generally exhibit a diffuse-like feature, indicating the existence of some microscopic-scale structures in the cubic phase. Particularly, the sensibility of the speckles to the E suggests that these microscopic structures be the type of dipole-related, as that so-called polarization clusters.

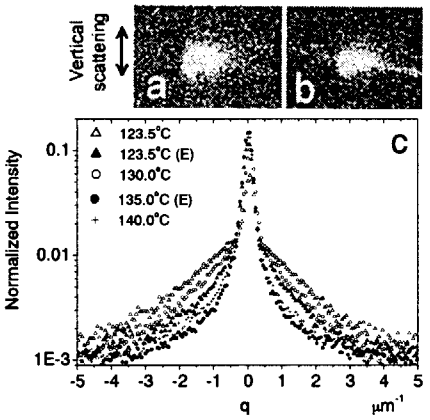

Fig. 1 Experiment data
E denotes external electric field (2KV/cm); a and b are an example of speckles patterns with and without E respectively, c is vertical intensity distribution.

3. Discussions

The matter correlation function has been calculated, from which, those characteristic parameters as shown in Fig. 2 for the clusters have been extracted[3)]. It is found that, within the measured temperature region ($T_c^- \sim T_c$ +20 °C), the size of the polarization clusters doesn't change significantly (with a value of around 0.8 μm), the distance of adjacent clusters decreases approximately linearly as cooling toward T_c, the cluster's polarization increases monotonically as cooling and reaches its maximum at T_c + 5 °C, and then decreases continuously until over across T_c.

The macroscopically averaged polarization <|P|> within the specimen has its maximum just at T_c and decreases dramatically in the part of T_c^-. From microscopic consideration, the <|P|> represents the interaction strength of adjacent two clusters, and has been shown to exhibit a critical behavior near T_c[3)].

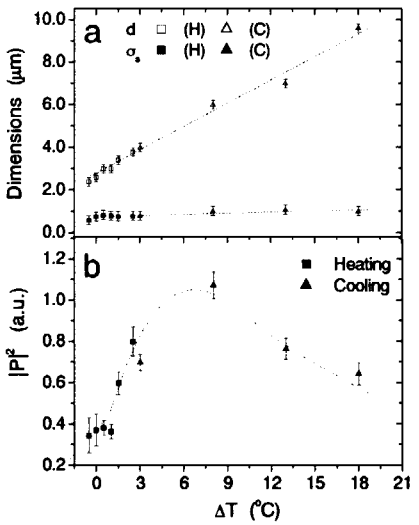

Fig. 2 Characteristic parameters of the local polarization clusters estimated from Fig. 1

References

1) R.Z. Tai *et al.*, Phys. Rev. Lett. **89**, 257602 (2002).
2) R.Z. Tai *et al.*, AIP series of conference proceeding (Eighth International Conference on Synchrotron Radiation Instrumentation, 2003).
3) R.Z. Tai *et al.*, submitted to Phys. Rev. Lett.(2003).

4.2.8 Observation of biological cell with ultra-short pulsed x-ray lasers

Masataka KADO, Maki KISHIMOTO, Momoko TANAKA, Yasuhito KINJO, Masaharu NISHIKINO, Kouta SUKEGAWA, Keisuke NAGASHIMA, Teysuya KAWACHI, Yoshihiro OCHI, Noboru HASEGAWA, Peixan LU, RenZhong TAI, and Kunio SHINOHARA

a) Radiation Laboratories, Tokyo Metropolitan Industrial Technology Research Institute
b) Radiation Research Institute, Faculty of Medicine, The University of Tokyo

1. Introduction

X-ray microscope is able to observe small structure inside biological cells with greater spatial resolution than optical microscopes without any artificial treatments. Laser plasma x rays have an advantage on short pulse duration, which makes possible to obtain images faster than any movement of specimens or chemical affection due to radiation damage [1]. Phase differential interference microscope with x-ray lasers are even powerful tools, which use phase differential to produce images instead of using absorption or phase shift. High contrast images will be obtained with the phase differential interference microscope because the microscope uses differential phase shift instead of absolute phase shift.

2. Phase differential interference microscope with x-ray lasers

The phase differential interference microscope is consisted with a Schwarzchild x-ray microscope as a condenser lens, a sample mount to hold specimens, a Fresnel zone plate as an objective lens, an interference system, and a back illuminated soft x-ray CCD camera. Ni-like Ag x-ray lasers [2] with wavelength 13.9nm were focused with the Schwarzchild type x-ray microscope onto specimens and the image of the specimens were magnified with the Fresnel zone plate onto the x-ray CCD camera with magnification of 200. The spatial resolution of the microscope was measured with a knife edge and was 0.36 μm from 25 – 75 % rise. An interference system, which is consisted with a pair of transmission grating and will be installed between the Fresnel zone plate and the x-ray CCD camera, is now being designed. The first grating divides an x-ray laser into two beams using the different diffraction angle of the 0^{th} and 1^{st} orders of the incident x-ray laser. The second grating makes the diffracted x-ray lasers parallel and the x-ray lasers overlap at the x-ray CCD camera to create interference images.

3. Observation of human chromosomes

Biological cells were expanded by interfacial unfolding method and chromosomes were extracted. The extracted chromosomes were picked up and placed on a silicon nitride membrane with the thickness 100 nm and dried. The chromosomes were observed under an optical microscope. A couple of chromosomes were selected and the position was marked. Shown in figure 1 (a) is an optical microscope image of the selected chromosomes and shown in figure 1 (b) is an x-ray image of a chromosome in the selected area.

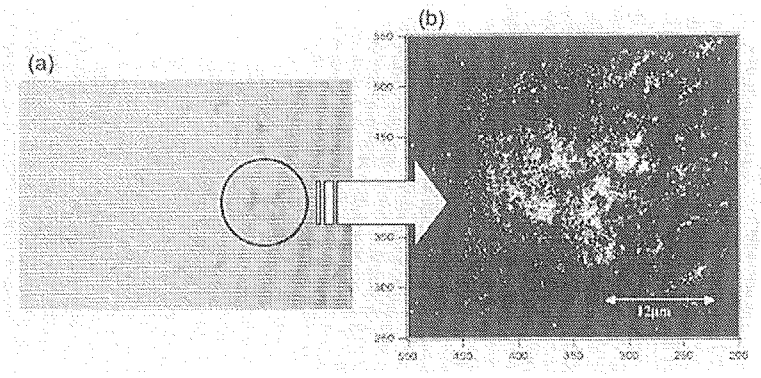

Fig. 1 An optical microscope image (a) and an x-ray image (b) of human chromosomes

4. Summary

The dried human chromosomes have been observed with the differential interference microscope. Interference system, which will be installed into the microscope, is now being designed and is expected to enhance the contrast of the x-ray images.

References

1) M. Kado, M. C. Richardson, et al., Proc. of Experimental Biology and Medicine **220**, 21, 1999.
2) T. Kawachi, M. Kado, M. Tanaka, et al., Phys. Rev. A **66**, 033815, 2002.

4.3 Free-Electron Laser Development

Eisuke J. MINEHARA

Since a vacuum tube oscillator which was thought to be an ancestor of the free-electron laser device (FEL) was invented as the first coherent electromagnetic waves generator, we have tried to realize a powerful and efficient electromagnetic generator, i.e., free-electron laser (FEL) for industrial uses, for examples, pharmacy, medical, civil engineering, shipbuilding, semiconductor industry, chemical industries, environmental sciences, space-debris orbit control, power beaming and so on[1] over 100 years. In order to realize such a tunable, highly-efficient, high average power, high peak power and ultra-short pulse FEL, the JAERI FEL group have successfully demonstrated the efficient and powerful FEL driven by a compact, stand-alone and zero-boil off super-conducting rf linac with and without an energy-recovery geometry[2]. Because the JAERI FEL successfully produced the world-shortest FEL pulse length of 250 fs , the highest efficiency of 6-9%, the highest peak power of 1GW and the highest average power of >2kW, we first opened and originated the novel researches and applications using the femtosecond ultrashort, highly-efficient and high average power FELs[3]. Recently, we successfully demonstrated to recover electron beam energy for the next acceleration with stable acceleration and stable FEL oscillation April 2002 and August 2002, respectively.

Our reports and discussions on the FELs in the subsections will cover the industrial high power FELs, the JAERI compact, stand-alone and zero-boil off cryostat and operational experiences over these years[4], our discovery of the new, highly-efficient, high-power, and ultra-short pulse lasing mode, some conceptual design works of the energy-recovery linac based light source and so on. Applications of the FEL and nuclear isomer studies will be included as a possible and future extension in the JAERI FEL research activities. We could succeed to run the system continuously with a few short stops and a few minor troubles for two years in 2001 and 2002 Japanese fiscal years and without warming up because the original tools and technique was successfully adopted to exchange quickly 4K and 10K/50K He refrigerators for 15 minutes each without any damage and any bad effects to the heat exchange and absorber agents in a He gas atmosphere. After we have repeated to exchange the refrigerators many times, a continuous low-temperature operation interval was estimated to be very long, longer than 10 or 20 years or more. No warm-up operation of the superconducting rf linacs looks very nice to realize maintenance-free and easy-operation linacs.

The FEL research group's achievement was recognized as the distinguished contribution and merits in the science and technology by Minister of Education, Culture, Sports, Science, and Technology during the fiscal year 2002 science and technology week. The satellite meeting of the FEL-SUT IRFEL international conference was held to discuss about the recent progresses in high power IR FELs in the FEL laboratory at Tokai just after the conference. Free-electron laser Franco-Japan workshop which was hosted by INRS, French Embassy at Tokyo was co-chaired by Dr. Perret-Gallix, director of INRS Tokyo office, and Dr. E. J. Minehara, JAERI FEL research group leader from 11th to 13th November, 2002.

References

1) J. Hecht and D. Teresi, " Laser, Supertool of the 1980s" 1982, Ticker & Fields, 383 Orange Street, New Heaven, Connecticut 06511, U.S.A.
2) E.J.Minehara et al., Nucl. Instrum. Methods Phys. Res. Sect.A445, 183 (2000).
3) N.Nishimori et al., Phys.Rev. Lett. 86, 5707 (2001).
4) E.J.Minehara et al., pp159-161, in the proceedings of Particle Accelerator Conference, 1995, Dallas. E.J.Minehara et al., Free Electron Laser Challenge 2(SPIE) Vol.3614, pp.62-71, 1999.

4.3.1 Generation of a Chirped FEL Pulse

Ryoichi HAJIMA and Ryoji NAGAI

1. Superradiant pulse in a perfectly synchronized FEL oscillator

In a short bunch FEL oscillator, a superradiant pulse is generated in slippage region. An analytical study shows this superradiant FEL pulse has a nonlinear frequency chirp [1]. This frequency chirp, that is time-frequency correlation, evolves continuously through a number of round trips, if the FEL oscillator is operated at perfectly synchronized cavity length. We have investigated the evolution of the chirped FEL pulse by a simulation code based on slowly-evolving-wave-approximation (SEWA), which is applicable to a few-cycle optical pulse. Figure 1 shows calculated FEL pulse evolution for the JAERI-FEL parameters. We see the frequency chirp increases as the FEL approaches to the saturation [2].

2. Experimental result

Temporal structure of an optical pulse from the JAERI-FEL has been measured by autocorrelation of second-harmonic-generation signal from a Te crystal [3]. An experimentally obtained fringe-resolved autocorrelation signal is used for pulse form retreaval with the assumption of a chirped-sech^2 pulse. Figure 2 shows the autocorrelation signal with a fitted curve, which gives the FWHM of the intensity envelope of 319fs (4.09λ) and frequency chirp inside the FWHM, 14.3% [2].

An infrared laser pulse with such large frequency chirp is useful for quantum controll of chemical reaction: the resonant excitation of atomic or molecular systems, which have an anharmonic potential ladder [4].

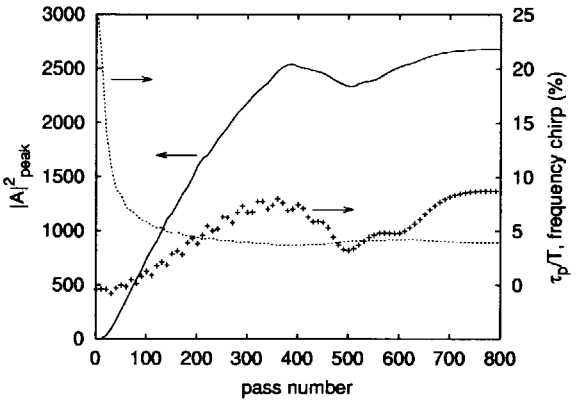

Fig. 1 Numerically calculated FEL pulse evolution for the JAERI-FEL parameters; Peak intensity (solid line), FWHM duration as optical cycles (dotted line), and frequency chirp inside FWHM duration (+)

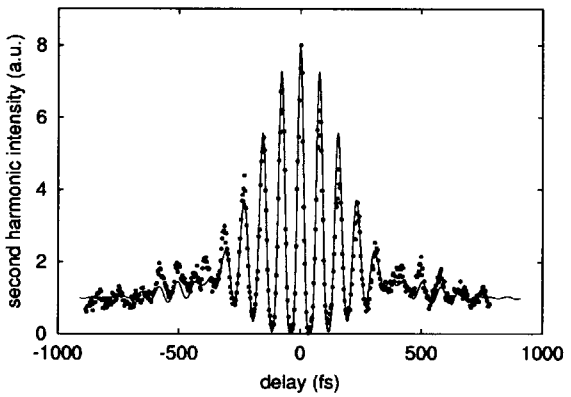

Fig. 2 A fringe-resolved SHG signal from the JAERI-FEL (dots)
The solid line is a fitted curve by chirped-sech^2 pulse.

References

1) R. Bonifacio et al., Rivista del Nuovo Cimento 13, 1 (1990).
2) R. Hajima and R. Nagai, Phys. Rev. Lett. 91 (2003) 024801.
3) R. Nagai, R. Hajima et al, Nucl. Instr. Meth. A.483 (2002) 129.
4) S. Chelkowski et al., Phys. Rev. Lett. 65 (1990) 2355.

4.3.2 HOM Instability for the JAERI ERL-FEL

Masaru SAWAMURA, Ryoichi HAJIMA, Ryoji NAGAI, Nobuhiro KIKUZAWA,
Nobuyuki NISHIMORI, Eisuke MINEHARA

1. Introduction

JAERI has been developing a high-power FEL with a superconducting linac. After the initial goal of kilowatt FEL lasing was achieved in 2000, the linac has been modified into an energy-recovery linac (ERL). Energy recovery is the process by which the energy invested in accelerating a beam is returned to the rf cavities by decelerating the beam. Energy recovery of an FEL beam driven by a superconducting linac is a possible way of greatly increasing the efficiency of the laser since most of the beam energy remains after lasing occurs. This energy-recovery technology with a superconducting linac is the most promising for the next stage of 10kW FEL lasing owing to increasing the beam current without additional rf power sources.

Transverse beam displacement on successive recirculations can excite HOMs that further deflect the initial beam. The effect is worse in superconducting rf cavities because of higher Q values of HOMs. The threshold current depends on the various parameters of cavity and beam optics such as Q values, frequencies and R/Q of the HOMs, beam energy, beta functions and phase advance in the paths and recirculation path length.

2. HOM Instability Simulation

A simulation code, named BBU-R, has been developed to calculate the threshold current at an actual machine configuration. Analytic model for simulation is impulse approximation, where the transverse position of the bunch is treated as one point and the transverse deflection through the cavity as single deflecting force [1].

This simulation code requires the transfer matrices between the adjacent cavities and the HOM parameters such as frequency, R/Q and loaded Q value. The HOM frequencies and R/Q of the JAERI superconducting cavity was calculated with the 2.5-D rf cavity code PISCES II, which can evaluate all the eigenfrequencies and fields for arbitrarily shaped axially symmetric rf cavity [2]. The loaded Q values and frequencies of the HOMs were measured with a network analyzer connected to the HOM coupler, from which reflection power was measured. The transfer matrices were calculated with the code TRANSPORT.

The threshold current is defined as the current where the beam can be transported within 5 times of diameter of the initial. The initial beam has 1mm diameter and 0.5mm offset from the axis. The beam diameter increases with the current. Table 1 lists the threshold currents when one of 10 HOMs is excited and all of 10 HOMs are excited and Fig.1 shows the beam position as a function of the time near and above the threshold current.

Table 1 Threshold current

No.	Mode	Threshold Current(A)
#1	TE111 π/5	666.40
#2	TE111 2π/5	487.31
#3	TE111 3π/5	34.36
#4	TE111 4π/5	10.74
#5	TE111 π/5	578.94
#6	TM110 π	32520.32
#7	TM110 4π/5	16.79
#8	TM110 3π/5	5.47
#9	TM110 2π/5	7.03
#10	TM110 π/5	1482.74
#1-#10	All modes	3.42

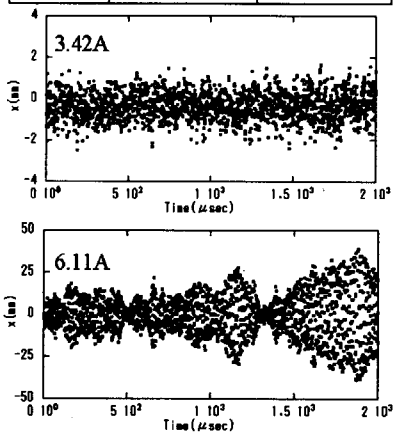

Fig. 1 Bunch position vs. time for 3.42A beam current, approximately threshold (top), and for 6.11A beam current, above threshold (bottom)

3. Results

The threshold current of the JAERI ERL-FEL limited by the HOM instability is calculated to 3.42A, which is large enough to increase the beam current from 5mA to 40mA of our next stage.

References

1) J.Bisognano, *et al.* CEBAF-PR-87-007 (1987)
2) Y.Iwashita, Computational Accelerator Physics, Williamsburg, VA, AIP conference proceedings No.361 Sept. 1996, 119-124

4.3.3 Linac Optics Optimization for Energy Recovery Linacs

Ryoji NAGAI, Ryoichi HAJIMA, Masaru SAWAMURA, Nobuyuki NISHIMORI,
Nobuhiro KIKUZAWA and Eisuke MINEHARA

1. Introduction

A superconducting linac based ERL is an extremely efficient accelerator for synchrotron light sources and free-electron lasers. The performance of the ERL light sources is improved as the beam average current is increased. The average current, however, is limited by instabilities such as multi-pass transverse BBU. It was shown by an analytical solution[1] that the BBU threshold current is inversely proportional to the Q factor of the higher-order-mode (HOM) and transfer matrix elements of divergence to transverse position (R12 and R34). To suppress the BBU instability, the HOM should be damped sufficiently. The HOM damping should be incorporated into the superconducting cavity design. To achieve high BBU threshold current, transport optics along the superconducting linacs should be optimized to minimize R12 and R34. This optimization can be performed through a numerical design of the linac optics.

Result of local optimization method such as Newton method strongly depends on starting parameters. A set of initial parameters to start the optimization cannot be fixed a priori for a system with a lot of free parameters such as linac optics design of the ERL. The linac optics has many free parameters because of the lengthy structure of the linac. The local optimization method is therefore not suitable to find directly the optimum parameters of the linac optics. Genetic algorithm is well known as an optimum parameter global search method. In the case of many free parameters, however genetic algorithm spends a lot of computation time. Hence we employ two-step optimization utilizing the local and global optimization methods. Genetic algorithm is only used to find the starting parameters of the local optimization, and the parameters are refined by the following local optimization. The optimum parameters of the linac optics for a simple one-pass configuration ERL are easily found using the two-step optimization method.

2. Linac optics optimization

In this optimization, we assume a conceptual ERL with a simple one-pass configuration, external quadrupole triplets between cryomodules. Each cryomodules includes eight cavities, which are 9-cell 1.3 GHz TESLA cavities[2]. The main linac accelerates the beam to 6 GeV.

The linac optics is numerically optimized based on Bazarov's guideline[3]. The optimization code takes the two-step optimization method to find quickly and globally optimum parameters. At first step, proper starting parameters for the local optimization are found by genetic algorithm. The parameters are then refined in the local optimization step by BFGS method.

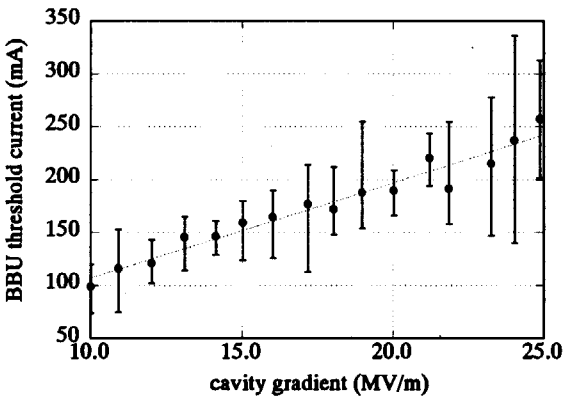

Fig. 1 BBU threshold current vs. cavity

In the linac optics optimization of the ERL, the cavity gradient is a principal parameter. The linac optics is optimized with various cavity gradients and the threshold current is estimated with 1 MHz HOM frequency spread. As shown in Fig. 1, the threshold current is increasing with the cavity gradient. It is found that it is possible the threshold current of more than 100 mA even if the cavity gradient is less than 15 MV/m.

3. Conclusion

The optimum parameters of the linac optics for a simple one-pass configuration ERL have easily found utilizing genetic algorithm. As a result of the optimization, the BBU threshold current more than 100 mA is reasonably available with cavity gradient of 15 MV/m. The cavity gradient of 15 MV/m is the most economical so far as 10-year running cost is concerned.

References

1) J.J. Bisognano, G.A. Krafft, Proc. of the 1986 Linear Accel. Conf. (1986) 452-454.
2) B. Aune, et al., Proc. of the 1999 Part. Accel. Conf. (1999) 245-249.
3) I. Bazarov, et al., CHESS Technical Memo 01-003 (2001).

4.3.4 A doubling of the repetition rate of a thermionic electron gun at JAERI-FEL

Nobuyuki NISHIMORI, Ryoji NAGAI, Eisuke J. MINEHARA, Nobuhiro KIKUZAWA,
Ryoichi HAJIMA, Masaru SAWAMURA

1. Introduction

A high power FEL with an energy recovery linac (ERL) has been used for many applications in J-lab IR demo [1]. An ERL is an intrinsic device to realize not only a high power FEL, but also the forth generation light source in x-ray region. The first lasing in JAERI-FEL with an ERL was achieved in August 2002[2]. At that time, the distance between electron micro-pulses was 28.8 m corresponding to 10.4 MHz repetition, while the distance between optical cavity mirrors was 7.2 m. In order to further increase FEL power and effectively decrease the optical cavity loss, the repetition frequency of the electron pulses has been doubled. Since the FEL performance strongly depends on the incident electron beam, the doubling has to be done without degrading the gun performance such as peak current, pulse length, charge per pulse and stability between pulses. Here the electron beam performance in 20.8 MHz operation is reported.

2. Performance of the gun

The grid-pulser for 20.8 MHz operation has been designed and made by Kuper and Ovchar in BINP[3]. A step recovery diode (SRD) with two pulse switches and an energy accumulation line are used to form short pulses. When the first switch is switched on, the SRD as a capacitor is charged for 5 ns. Then the first switch is switched off and the second switch is switched on. The SRD is discharged, while a magnetic energy is accumulated in the accumulation line. When a sharp restoration of the resistance of SRD occurs, the energy accumulated in the line is sent to a load as a fast current. This is different from the principle of the grid-pulser[4,5] previously used for 10.4 MHz operation, in which a high voltage pulse with a short duration is applied to a load. Figure 1 shows an electron macro-pulse shape at 20.8 MHz repetition rate of micro-pulses measured with a current transformer positioned 1m downstream from the gun. The time jitter and amplitude fluctuation measured are 12 ps rms and 0.6%, respectively. The peak current and pulse length measured are 0.8 A and 0.8 ns FWHM, respectively. These performances of the electron beam at 20.8 MHz are comparable with those realized at 10.4 MHz [4].

3. Summary

The repetition rate of electron micro-pulses of the electron gun has been doubled from 10.4 MHz to 20.8 MHz without degrading the beam performance. Our final goal is to increase the repetition rate up to 83.3 MHz. The BINP grid-pulser used for 20.8 MHz might be used for 41.6 MHz. However an electron pulse with the same peak current and pulse length as that realized at 20.8 MHz would not be produced. An operation of the BINP pulser at 83.3 MHz is impossible, because it takes more than 20 ns for charging and discharging SRD. We have a plan to develop a grid-pulser using two SRD switches which can produce high voltage pulses with short pulse durations at 100 MHz repetition rates in principle [6].

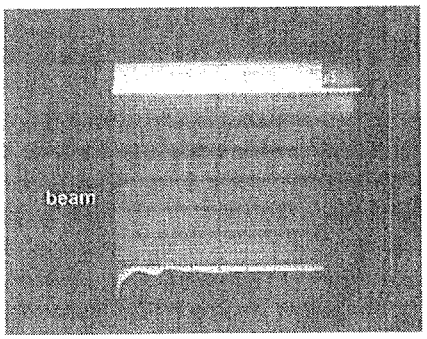

Fig. 1 An electron beam signal measured with a current transformer positioned 1m downstream from the gun
The macro-pulse length is 150 μs and the peak current is 0.8A. A ringing is observed for the first 50 μs.

References

1) G.R. Neil et al., Phys. Rev. Lett. **84**, 662 (2000).
2) R. Hajima, et al., NIM A **507** 115 (2003).
3) E.A. Kuper and V.K. Ovchar, in Proceedings of the Third Symposium on APR, Kyoto, 2001.
4) N. Nishimori et al., NIM A **445** 436 (2000); in Proceedings of 7th EPAC, Vienna, 2000.
5) R.F. Koontz, IEEE Trans. Nuclear Scien. **26** 4129 (1979).
6) S. Talmadge et al., NIM A **285** 333 (1989).

4.3.5 Proposal of a new nuclear cosmochronomter of the p-process

Takehito HAYAKAWA[a,b], Toshiyuki SHIZUMA[a] and Toshitaka KAJINO[a,b]
a) Japan Atmoic Energy Research Institute, Tokai Ibaraki, Japan
b) National Astronomical Observatory, Mitaka Tokyo, Japan

Nuclear cosmochronometers provide an advance of the chronology of the Solar System and chemical evolutions of the Galaxy[1]. It is considered that the p-process nuclides were synthesized by photodisintegration reactions in supernova explosions[2,3]. A few p-process cosmic clocks whose half-lives are as long as the age of the Solar System are known[4]. We here propose a new chronometer of the p-process and present a calculated result of the mean age of the p-process which occured before the Solar-System formation using the Solar-System abundance. Since it is considered that the p-nuclei were produced from the progenitor s-nuclei rich seed in supernova explosions, there may be correlations in the abundances between p- and s-process isotopes. We calculated the ratio of the p-nuclei to the s-nuclei, which are two neutron-rich isotopes to the p-nuclei, for three isotopes of Os, Pt and Hg, and thereby we found that these ratios show good systematic values. The ground state of the ^{190}Pt nucleus, which is pure p-nucleus, is unstable against alpha decay to ^{186}Os (half-life of 650 Gyr). With calculating the initial abundance of ^{190}Pt by using the systematic ratios of the p-nuclei to s-nuclei in thses heavy mass region, we can use the ^{190}Pt-^{192}Pt system as a new cosmic clock of the p-process. Figure 1 shows the calculation result using the average value of systematic ratios.

Taking the abundance of 0.01 %, which is a Solar abundance, we obtained the result of 49 Gyr as the mean duration time of the p-process, which is much longer than the age of the Universe. We would like to stress that the age highly depends on the present abundance of ^{190}Pt. Replacing the abundance of 0.01 % with 0.0104 %, we obtained an age of 12 Gyr, which is shorter than the Galaxy age. This result indicates an importance of the measurement of the Solar abundance with high accuracy. Finally, we note that the ratio in the Solar System abundance depend highly on the evolution of the metallicity in the Galaxy, and thus the advance of the chemical evolution of the Galaxy is required. This new tool is useful for the study of the pre-solar grain in primitive meteorites.

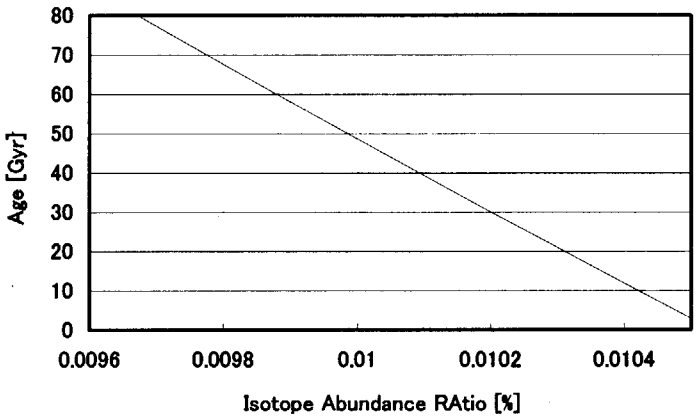

Fig. 1 The mean age of the p-process calculated by the clock of ^{190}Pt-^{192}Pt

References

1) E.M.Burbidge, et al., Rev. Mod. Phys. 55 (1957) 149.
2) M.Arnould, Astron. Astrophys. 46 (1976) 117.
3) S.E.Woosley and W.M.Howard, Astrophys. J. Suppl. 36 (1978) 285.
4) J.Audouze and D.N.Schramm, Nature 237 (1972) 447.

4.3.6 A new isomer in ^{187}Re produced by inelastic excitation

Toshiyuki SHIZUMA, Yosuke TOH, Masumi OSHIMA, Masahiko SUGAWARA[a], Makoto MATSUDA, Takehito HAYAKAWA, Mitsuo KOIZUMI, AKIHIKO Osa, Y.H. Zhang[b] and Z. Liu[b]
a) Chiba Institute of Technology, Narashino, Chiba 275-8588, Japan
b) Institute of Modern Physics, Chinese Academy of Sciences, Lanzhou 730000, China

1. Introduction

Nuclear structure studies of high-spin states in ^{187}Re have been limited because this nucleus resides at the line of β-stability, and few heavy-ion fusion-evaporation reaction would populate those states. To date only low-spin levels have therefore been known from studies on β decay of ^{187}W, ^{186}W (α,t), ^{186}W (^{3}He,d), and ^{187}Re (d,d') reactions. In order to investigate higher-spin states, we employed an inelastic scattering reaction with a heavy-ion beam. This type of reaction has been proven to be useful for population of levels of medium to high spins in heavier stable isotopes [1].

The nucleus ^{187}Re lies in the region where many high-Ω orbitals are close to both the proton and neutron Fermi surfaces. High-K(=ΣΩ) multi-quasiparticle states formed by stretched coupling of these high-Ω quasiparticles therefore can compete with collectively excited states nearby a yrast line [2]. (K is defined as a projected component of the total angular momentum on the nuclear symmetry axis). Transitions depopulating such states often involve large spin/K changes, low transition energies, parity change, or combination of these, making the initial state to be an isomer with a comparatively long half-life.

In this paper, we present results of the inelastic scattering experiment on ^{187}Re, which include identification of a new isomer based on a three-quasiparticle excitation.

2. Experiment

A 500 MeV ^{82}Se beam derived from the tandem and booster accelerator at Japan Atomic Energy Research Institute was used to bombard a thick target (26 mg/cm^2) of natural Re. The beam energy was selected as about 15 % higher than the Coulomb energy for the ^{82}Se + ^{187}Re system. Emitted γ rays were detected by the GEMINI Ge-detector array consisting of twelve Compton-suppressed HP-Ge detectors, placed at 32°(2 detectors), 58°(2), 90°(4), 122°(2) and 148°(2) with respect to the beam axis. Events were recorded on magnetic tapes when two or more Ge detectors were detected in coincidence. Relative Ge times between coincident g rays were also measured. The time window was set to 200 ns so that half-lives less than about 100 ns could be extracted. A total of 1.5x10^8 coincidence events were collected. The energy calibration was made by using ^{133}Ba and ^{152}Eu standard sources. Two-dimensional E_γ-E_γ matrices of both the prompt-prompt and prompt-delayed coincidence were created to construct the level scheme.

3. Results and Discussion

From γ-ray correlation analysis, a new isomer was found at an excitation energy of 1682 keV with $I^\pi=(19/2^+)$. From comparison of measured and predicted alignments, g-factors, Nilsson configuration of $\pi 9/2^-[514]\nu\{1/2^-[510]11/2^+[615]\}$ was assigned for the isomeric state. In addition, as shown in Fig. 1, the half-life of the isomer was extracted as 114(23) ns. The isomer decays to the $K^\pi=19/2^-$ level at 1474 keV via a K-allowed E1 transition. The hindrance factor for this transition is obtained as F=5x10^6. This value is consistent with F=1.1x10^6 for a 115 keV, E1 decay of the 123 ns isomer in ^{185}Re [3], as well as the systematic value of F=10^3 ~10^7 expected for K-allowed E1 transition in the region [4]. The present result has been published [5].

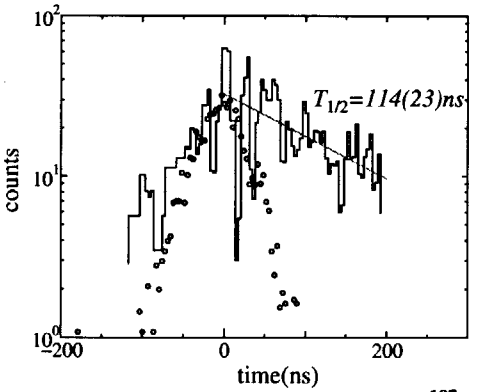

Fig. 1 A proposed level scheme in ^{187}Re

References

1) C. Wheldon *et al.*, Phys. Lett. B **425**, 239, 1998
2) P.M. Walker and G.D. Dracoulis, Nature **399**, 35, 1999
3) T. Shizuma *et al.*, Z. Phys. A 359, 229, 1997
4) K.E.G. Lobner, The Electromagnetic Interaction in Nuclear Spectroscopy, 1975
5) T. Shizuma *et al.*, Euro. Phys. J. A 17, 159, 2003

4.4 Optics research and development

The Novel Optics Research Group

Masato KOIKE, Osamu YODA, Akira SUGIYAMA, Masahiko ISHINO, Kengo WADA, Kazuo SANO[a)], Hideki KUMATA[b)]

a) Shimadzu Scientific Research Inc., b) Shin Seiki Corporation

1. Introduction

In the developments of laser optical elements, we have improved the bonding technique for laser crystals to obtain high output power. In the research area of soft x-ray optical elements, we have started a study of multilayer development consisting of oxide and nitride as the multilayer mirror for use around the wavelengths of 4 nm. Also we developed a laminor-type holographic grating with a high groove density for a flat-field spectrograph and a replica grating having good marketability.

2. Achievements

In the developments of laser optical elements, we have improved the laser crystal integration which can bring a good heat elimination performance by bonding YVO_4 host crystals to a Nd:YVO_4 laser crystal to obtain the high output power. The invented new method (Patent pending) by the dry etching procedure in the bonding technique shown in Fig. 1, can be also applied to the other crystals such as hygroscopic and fluoride crystals. The bonded crystal was evaluated in optical properties and laser oscillation characteristics, further observed by a transmission electron microscope (TEM). As the results, we have found that the Nd:YVO_4 crystal integration has a good heat conduction property and the output power has increased approximately twice without giving rise to the heat destruction that are occurred in usual crystals.

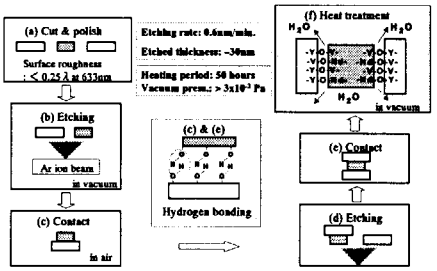

Fig. 1 Schematic of new dry etching procedure

In the developments of soft x-ray optical elements, we have started to fabricate the multilayer mirrors with short periodic lengths for use in the carbon K-absorption edge region (? = 4.4 nm). We have found that the Co_3O_4, SiO_2 and BN are suitable for multilayer components. The calculated soft x-ray reflectivities of the Co_3O_4/SiO_2 and Co_3O_4/BN multilayers are shown in Fig. 2. We have fabricated the Co_3O_4/SiO_2 and Co_3O_4/BN multilayers and evaluated the multilayer structure by x-ray scatterings and TEM observation. It is found that the Co_3O_4/SiO_2 multilayer has uniform layer structure whereas in the Co_3O_4/BN multilayer the aggregated Co_3O_4 layers are observed. Furthermore, we have developed a flat field holographic grating with a high groove density (2400 lines/mm) in the wavelength region of 0.7-6.0 nm. The intensity of the higher order lights was approximately one order magnitude lower than that of the mechanically ruled grating. We have obviously observed Si K emission line (0.713-nm), as shown in Fig. 3, that is difficult to measure using a mechanically ruled grating. Including the diffraction efficiency, all the characteristics of the newly developed holographic grating were superior to those of the mechanically ruled grating. In addition we have developed a marketable flat field grating (1200 lines/mm) replicated from the original holographic grating and it showed almost same performance to the original grating.

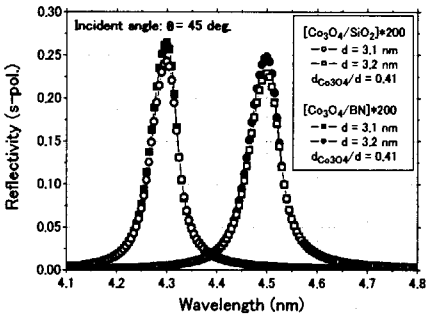

Fig. 2 Calculated soft x-ray reflectivities of multilayers

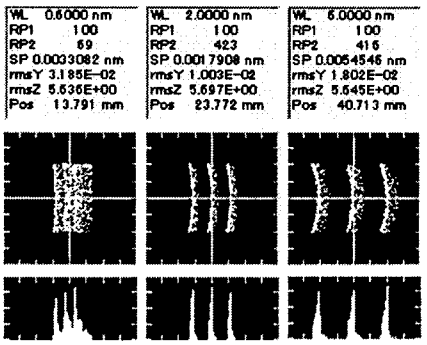

Fig. 3 Spot diagrams and line profiles of the flat field spectrograph with the 2400 lines/mm holographic grating

4.4.1 Fabrication for integrated laser crystal of $Nd:YVO_4$

Akira SUGIYAMA

1. Introduction

In our previous studies, we succeeded in bonding Ti:sapphire laser crystals. [1,2] In this case, the bonding surfaces of a stable oxide crystal were treated with chemical processes to clean up and to create a hydrophilic (-OH) thin layer for hydrogen bonding. However, in applications for different crystal bonding, the chemical processes require the selection of suitable chemical etchants for each crystal to be bonded and optimization in the handling of the etching period and temperature. In most of the cases, hazardous strong acid and alkaline water are used for the etchant in a time consuming procedure. In addition, these etchants cannot be applied for hygroscopic crystals and fluoride crystals. From the viewpoint of these problems, we have developed a dry etching process using ion beam irradiation instead of the conventional chemical processes.

2. Experimental results

In our bonding method, it is not necessary to use any adhesives and high pressure, which may lead to optical damage or distortion in the crystal. Our bonding process was composed of six successive treatments. [3] In newly developed dry etching process, the polished surfaces were etched around 30 nm by an ion beam with the accelerated voltage of 200 V and current of 10 mA for 50 min. By this treatment, the hydrophilic properties of the etched surfaces are improved.

To evaluate laser oscillation performance of the integrated crystal, we measured laser output power with the test bench, as shown in Fig. 2. The specimen was located in short cavity of length 30 mm, and pumped by a fiber coupled CW laser diode array. For the heat reduction of laser crystal, the specimen was cooled by chiller water at 293 K.

Figure 2 shows the result of laser power measurements. From this figure, we cannot find a significant difference in both output curves of the bonded crystal and the single one till the pump power reaches 10 W. However, in excess of 10 W, the usual single crystal was broken by the strong thermal load caused by CW laser pumping. On the other hand, the output power of integrated one still increased, then saturated at the pump power of around 16 W. To evaluate the thermal load in these specimens, we calculated the thermal distribution and the highest temperature at the hot spot in each crystal by using a finite element method. From the calculation, we found that the difference of the highest temperature reaches 162 K at 10 W pumping level and the heat reduction capacity of the integrated crystal has twice that of the single one. As a result, the integrated crystal could increase the laser output power in high power pumping.

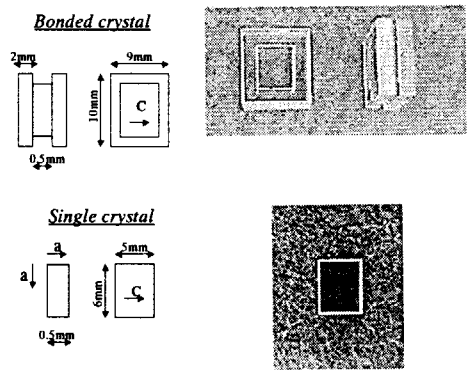

Fig. 1 Integrated $Nd:YVO_4$ laser crystal

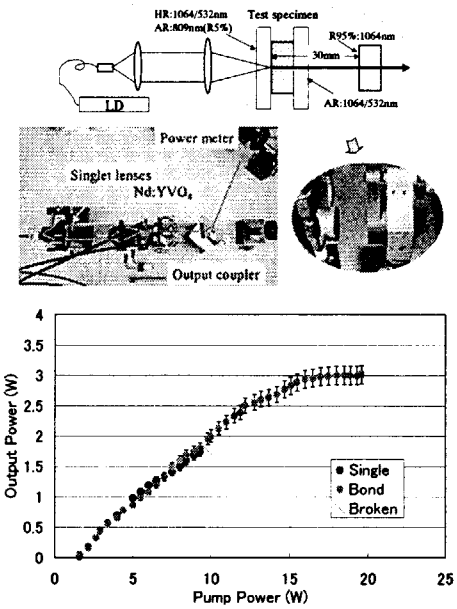

Fig. 2 Laser Output as a function of LD power

References

1) A. Sugiyama, H. Fukuyama, T. Sasuga, T. Arisawa and H. Takuma, Appl. Opt., **37**, 2407, 1998
2) A. Sugiyama, H. Fukuyama, Y. Kataoka, A. Nishimura and Y. Okada, Proc. of SPIE., **4231**, 261, 2000
3) A. Sugiyama, H. Fukuyama, M. Katsumata and Y. Okada, Proc. of SPIE., **4944**, 361, 2003

4.4.2 Fabrication of multilayer mirrors for use in the carbon K-absorption edge region

Masahiko ISHINO and Osamu YODA

1. Introduction

The multilayers consisting of alternating periodic layer structures of absorber and spacer materials have been utilized for soft x-ray optical elements. Up to now, soft x-ray lasers operated around the carbon K-absorption edge region have been reported: soft x-ray lasers using Ni-like tantalum (Ta^{45+}) and Ni-like tungsten (W^{46+}) are operated at the wavelengths of 4.5 nm[1] and 4.3 nm[2], respectively. The multilayer mirror containing carbon layers has high soft x-ray reflectivity in the longer wavelength region of the carbon K-absorption edge (λ = 4.4 nm)[3]. However, the reflectivity in the shorter wavelength region of the absorption edge is quite small due to x-ray absorption by carbon. We have then started to develop the soft x-ray multilayer mirrors for use in the carbon K-absorption edge region.

2. Experimental

As the result of theoretical calculation[4], we have found that cobalt oxide (Co_3O_4) is a candidate for the absorber material, and that silicon oxide (SiO_2) and boron nitride (BN) are suitable for the spacer materials. We fabricated Co_3O_4/SiO_2 and Co_3O_4/BN multilayers by the ion beam sputtering method. To evaluate the structure of the fabricated multilayers, small angle x-ray scatterings with CuKa_1 x rays were measured. In addition, high-resolution cross-section transmission electron microscopy (TEM) images of the multilayers were observed.

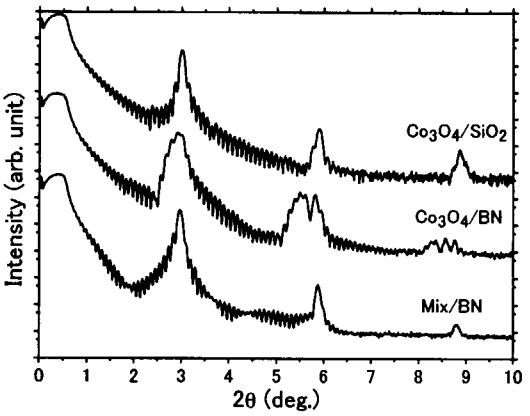

Fig. 1 X-ray reflectivity curves derived for the fabricated multilayers

3. Results

Figure 1 shows the x-ray reflectivity curves of the fabricated multilayers derived from x-ray scattering measurements. The x-ray reflectivity curve of the Co_3O_4/SiO_2 multilayer contains as many as three definite Bragg peaks in the measured 2θ region due to uniform layer structure. On the other hand, Bragg peaks of the Co_3O_4/BN multilayer are broad and the higher order peaks split into two or three. Figure 2 shows the TEM image of the Co_3O_4/BN multilayer. The Co_3O_4 and the BN layers are in dark and in light contrast, respectively. The aggregated Co_3O_4 layers are observed and each layer thickness is irregular. The aggregation of Co_3O_4 may cause the irregular layer thickness and large roughness, and result in split of the Bragg peaks. The combination of Co_3O_4 and BN is inappropriate as a multilayer mirror. To improve the Co_3O_4 layer structure in the Co_3O_4/BN multilayer, we adopted a mixed oxide compound (Mix), which was a mixture of chromium oxide (Cr_2O_3) and Co_3O_4, instead of Co_3O_4 alone. In the x-ray reflectivity curve of the Mix/BN multilayer, the higher order Bragg peaks do not split (see Fig. 1). We confirmed that the Co_3O_4/SiO_2 and the Mix/BN multilayers are promising candidates for the soft x-ray mirrors for use in the carbon K-absorption edge region.

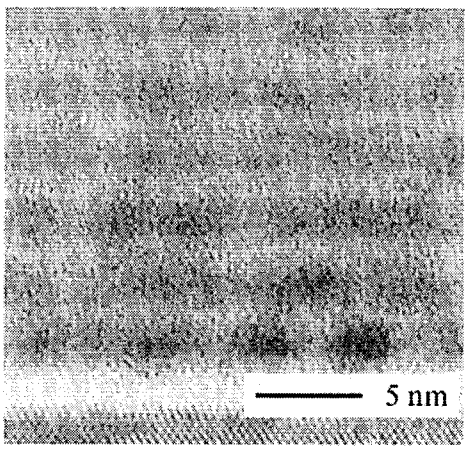

Fig. 2 High-resolution cross-section TEM image of the Co_3O_4/BN multilayer

References

1) H. Daido et al., J. Opt. Soc. Am. B **16**, 2295, 1999.
2) B. J. MacGowan et al., Phys. Rev. Lett. **65**, 420, 1990.
3) F. Schäfers, Physica B **283**, 119, 2000.
4) M. Yamamoto and T. Namioka, Appl. Opt. **31**, 1622, 1992.

4.4.3 Laminar-type holographic grating for a soft X-ray flat field spectrograph in the 0.7-6 nm region

Masato KOIKE, Kazuo SANO[a)], Eric GULLIKSON[b)], Yoshihisa HARADA[c)], Hideki KUMATA[d)]
a)Shimadzu Scientific Research Inc., b) Lawrence Berkeley National Laboratory,
c) Shimadzu Corporation, d) Shin Seiki Corporation

1. Introduction

Taking advantages of the significant progress of soft x-ray imaging detectors, such as a charge-coupled detector, streak camera, and microchannel plate, soft X-ray flat field grazing spectrographs have been widely used for plasma diagnostics, emission spectroscopy,[1)] and soft X-ray laser development.[2)] Recently we developed a laminar-type holographic (LTH) grating compatible with the VLS grating of 1200 lines/mm. To generate the grating pattern that the local grating constant varies from 1000 to 1400 lines/mm we employed a recording method called aspheric wave-fronts recording.[3)] The advantages of laminar-type holographic gratings we have found were the excellent suppression of higher orders light and stray light compared with the VLS grating.[4,5)] To extend these merits of the LTH grating into ~1 keV region we designed and fabricated a LTH grating of 2400 lines/mm compatible with the VLS grating.[6)]

2. Design and fabrication

The soft X-ray flat field spectrograph which Kita et al. developed[7)] and we have assumed for designing the LTH grating is shown in Fig. 1. It consists of the entrance slit E, a spherical grating G, and an image plane S. The image plane is parallel to the grating normal at its center.

The parameters we have assumed for the designing LTH grating are as follows: the radius of curvature of the grating R = 15920 mm; effective grating constant σ = 1/ 2400 mm; ruled width W = 50 mm; ruled height L = 30 mm; slit height H = 1 mm; wavelength of the recording laser λ_0 = 441.6nm; spectral order m = +1; distance from slit to the grating center r = 237.0 mm; incidence angle α = 88.65°; distance from the focal plane perpendicular to the y-axis to the grating center D = -235 mm; and wavelength range of 0.6-6 nm.

We used an aspheric wave-front resulting from the reflection of a spherical wave-front from a spherical mirror to record a holographic grating. The following recording parameters were determined by means of the analytical design method[8)] : distance CO r_C = 2057.09 mm, radius of curvature of M1 R1= 400.00 mm, distance DO_1 p_D = 830.91mm, distance O_1O q_C = 300.00 mm, angle of $\angle$ COx γ = -60.000°, angle of $\angle$ O_1Ox δ=11.175°, angle of $\angle DO_1x_1$ η_D = 40.687°. For the definition of the parameters refer to Fig. 2.

The substrate of the master holographic grating was fused quartz with a RMS roughness of 0.5 nm as measured by an interference microscope with a 40x objective. The photoresist, OFPR5000, was used as an etching mask. The sinusoidal grooves of the holographic grating thus recorded were processed into 10 nm laminar grooves by reactive ion beam etching in CHF_3. After this then Au coating was performed. The duty ratio (ratio of land-width to period) is 0.28. The local grating constant varies from 2064.48 lines/mm at the point of (y = +20mm, z = 0mm) to 2830.07 lines/mm (y = -20mm, z = 0mm).

As a reference, we also measured a replica grating of the blazed-type mechanically ruled VLS grating,[7)] The radius of curvature R and groove parameters n_{20}, n_{30}, and n_{40} for this grating are: R=15920 mm, n_{20} = -7.08090 $\times 10^{-3}$mm^{-1}, n_{30} = 2.85666 $\times 10^{-5}$mm^{-2}, n_{40} = -5.25446 $\times 10^{-7}$mm^{-3}.

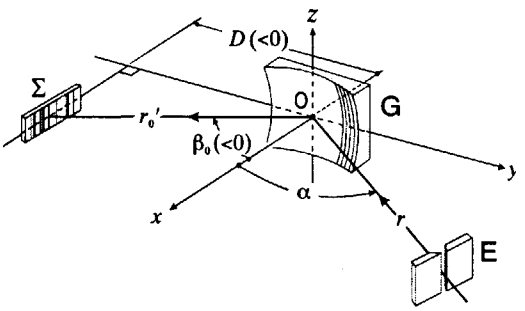

Fig. 1 Schematic diagram of the soft X-ray flat field spectrograph

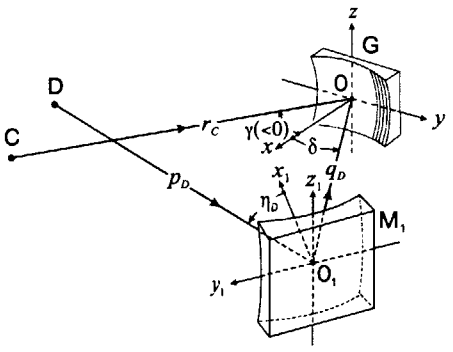

Fig. 2 Schematic diagram of the recording system of the holographic grating

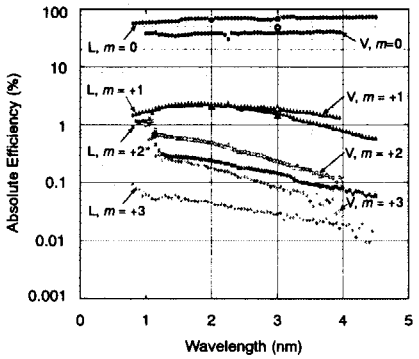

Fig. 3 Absolute efficiency for the fix incident angle α = 88.65°

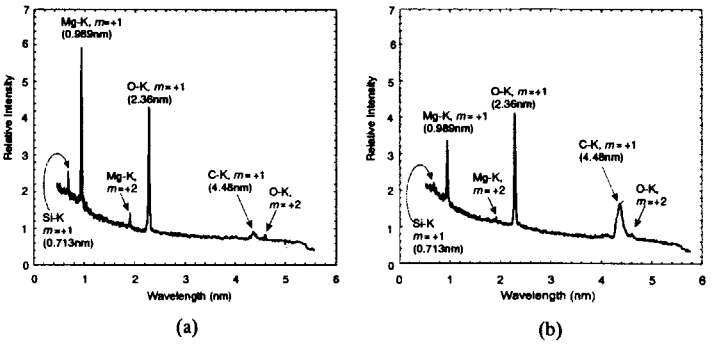

Fig. 4 Emission spectra of Si-K, Mg-K, O-K, and C-K taken with the LTH grating (a) and VLS grating (b)

3. Performance

The absolute efficiency of the two gratings was measured at the reflectometers installed at the BL-11 of the AURORA,[9] a compact superconducting storage ring, at the SR Center of Ritsumeikan University, and the beamline 6.3.2, built and operated by Center for X-ray Optics, at the Advanced Light Source (ALS), Lawrence Berkeley National Laboratory.[10] The test gratings employed were the master LTH grating and a commercial Au-coated replica of the standard VLS grating with a blaze angle of 1.9°, which gives a blaze wavelength of 1.5 nm at an angle of incidence of 88.65°. The measurements were performed at a fixed incident angle of 88.65°, the same condition as the case of the standard spectrograph.[7]

Figure 3 shows the absolute efficiency of the LTH grating, L, and the VLS grating, V, *m* being the spectral order. The data indicated by large symbols at 2 and 3 nm were measured at the ALS and the others were at the AURORA. For the *m* = +1 order, the LTH grating had a efficiency comparable with the replica VLS grating except for wavelengths longer than ~3nm. An essential difference can be seen in the higher orders, between the two gratings. The LTH grating maintained lower higher order light than those of the VLS grating regardless of wavelength. Considering the 0th order light of the LHG grating was higher than that of the VLS grating. It is concluded that the reflected and diffracted light are concentrated to lower order lights of *m*=0,+1 for the LHG grating. The VLS grating distributes the power to more various orders.

A measurement of the spectral resolution was performed using a spectrograph with a laboratory X-ray source at the Advanced Photon Research Center of the Japan Atomic Energy Research Institute, Japan.

Figure 4 shows the emission spectra of Si-K (0.713 nm), Mg-K (0.989 nm), O-K (2.36 nm), and C-K (4.48 nm) obtained with the LTH grating (a) and VLS grating (b). The soft X-ray generator with a molybdenum anode was driven by a power of 4.1 kV and 0.04 mA. The cathode current was 5.5A. A back-illuminated CCD detector was used having an imaging array (pixels) of 1340 × 400, and pixel size of 20 μm × 20 μm. The exposure time was 1 min.

It is noted that the Si-K band (0.713nm) was clearly observed by the LTH grating and also this grating showed a higher intensity for the Mg-K line (0.989 nm) and O-K line (2.36 nm) than the VLS grating with comparable resolution. On the other hand, the C-K line (4.48 nm) was not observed to be more intense with the LTH grating than the VLS grating consistent with the results obtained from the absolute efficiency measurement (refer to Fig. 3).

References

1) T. A. Sasaki et.al., Nucl. Instrum. Methods Phys Res. **A467/468**, 1489, 2001.
2) T. Kawachi et al., J. Opt. Soc. Am. **B14**, 1863, 1997.
3) M. Koike, T. Yamazaki, and Y. Harada, J. Electron Spectroscopy and Related Phenomena, **101-103**, 913 1999.
4) T. Yamazaki et al., Appl. Opt., **38**, 4001, 1999.
5) M. Koike et al., Proc. SPIE, **4146**,163, 2000.
6) M. Koike, K. Sano, E. Gullikson, Y. Harada, H. Kumata, Rev. Sci. Instrum., **74**,1156, 2003.
7) T. Kita, T. Harada, N. Nakano, H. Kuroda, Appl. Opt., **22**, 512, 1983.
8) T. Namioka and M. Koike, Nucl. Instrum. Methods, **A319**, 219, 1992.
9) H. Iwasaki et al., J. Synchrotron Rad. **5**, 1162, 1998.
10) J. H. Underwood, E. M. Gullikson, M. Koike, and P. C. Batson, Proc. SPIE, **3113**, 214, 1997.

4.5 Laser Driven Particle Acceleration Development

Kazuhisa NAKAJIMA, Masaki KANDO, Hideyuki KOTAKI, Shinichi MASUDA, Shuji KONDOH, Shuhei KANAZAWA, Takayuki HONMA, Igor V. SMETANIN

Laser Acceleration Research Group

1. Introduction

In the past decade great advances of ultraintense ultrashort pulse lasers have brought about tremendous experimental and theoretical progress in development of laser-driven particle accelerator concepts. In particular recent world-wide experiments have successfully demonstrated that the laser-plasma acceleration experiments is capable of generating ultrahigh accelerating gradient of the order of 100 GeV/m and of accelerating electrons up to the high energy exceeding 200 MeV in a few mm-scale interaction length [1]. These capabilities make it possible to realize a table-top accelerator and high energy frontier accelerators in a reasonable size and cost. We report our research activities on the laser acceleration experiments as well as the outlook for developments of laser-driven particle injectors, accelerators and radiation sources.

2. Laser particle acceleration experiments

The first high energy gain acceleration attaining 300 MeV has been opened with the injection of an electron beam at an energy matched to a wakefield phase velocity in a tenuous plasma by our group [2]. Our research has been focused on the laser acceleration experiments for high energy electron acceleration achieving more than 1 GeV with channel-guided scheme as well as on high quality beam generation with both conventional and advanced technologies in the use of 100 TW laser pulses. In order to accomplish these experiments, we have completed the Laser Acceleration Test Facility (LATF) consisting of the photocathode RF gun, the 150 MeV microtron accelerator, the electron beam line and the laser transport line. The official permission of their utilities has been allowed as a result of tests of radiation doses produced by LATF for the radiation safety clearance [3].

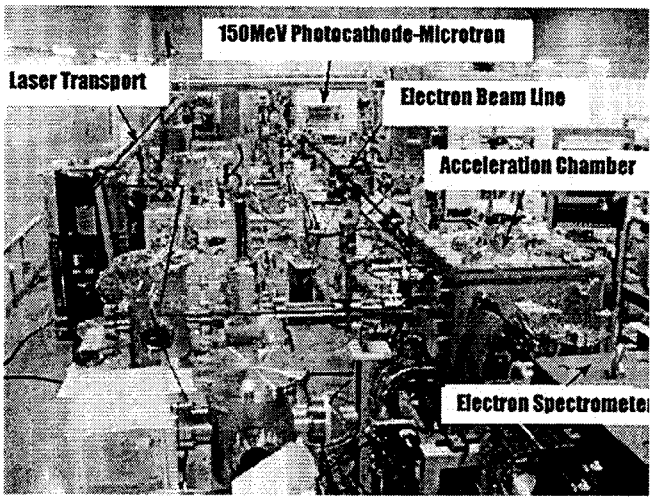

Fig. 1 An outlook of the Laser Acceleration Test Facility consisting of 150 MeV electron accelerator and 100 TW laser transport system

The preliminary experiment in LATF was conducted to demonstrate electron acceleration by ultraintense laser pulses. As shown in Fig. 1, the peak power of 5 TW, 30 fs laser pulses guided into the acceleration chamber through the laser transport was focused on the He gas jet to produce laser-plasma interactions at the laser intensity of the order of 10^{19} W/cm^2. Energetic electrons with a large energy spread up to several tens MeV were generated due to the wave-breaking of laser wakes and the direct laser field acceleration. In the relativistic intensity regime, nonlinear plasma dynamics evolves complex particle acceleration mechanisms. One of the purposes of laser particle acceleration experiments is to elucidate relativistic particle generation and acceleration mechanisms in plasma.

3. Plasma cathode developments for a high quality electron beam generation

Novel optical electron injectors that use laser-triggered injection of plasma electrons into the wakefield have been proposed as a plasma cathode to promise generation of high quality electron beams. There are three major schemes referred to as a transverse optical injection [4], a colliding pulse optical injection [5], and a nonlinear wavebreaking injection [6]. None of the proof-of-principle experiments for these schemes has

been succeeded so far because of experimental difficulties on a spatial and temporal control of laser pulses and plasmas. We propose a new scheme of the colliding pulse injection different from the beat wave injection [5] that uses three short laser pulses, one high-intensity pump pulse and two counterpropagating injection pulses with different frequencies generating a laser beat wave with a slow phase velocity to pump background plasma electrons into a fast wakefield. A new colliding pulse injection takes place at the collision of a pump pulse with one counterpropagating injection pulse with the same frequency as the pump pulse when the ponderomotive force exerted by the standing wave laser field can inject plasma electrons into the wakefield excited by the pump pulse. The particle-in-cell simulations reveals a remarkable beam quality with a few femtosecond electron bunch and a small energy spread less than 1%. As a first step of this plasma cathode development, we present the direct observation of 20 GeV/m of coherent ultrahigh gradient wakefields excited by a 2 TW, 50 fs laser pulse in a gas jet as well as precise measurements of its time-resolved gas density distribution [7].

4. Ponderomotive acceleration by relativistic laser fields

As a focused laser intensity increases to more than the laser strength parameter a_0 =1, given by the amplitude of the vector potential normalized with the electron rest mass, the electron quiver motion in the laser field reveals relativistic nonlinear effects. This nonlinear electron motion results from the ponderomotive force proportional to a_0^2. The resultant energy of electrons can be obtained from the relativistic Lorentz equation to become nonzero energy gain after interaction with a focused laser pulse in vacuum free space [8], contrary to the Lawson-Woodward theorem [9]. This particle acceleration mechanism is known as the relativistic ponderomotive acceleration.

We used the paraxial approximation for a set of solution of Maxwell equations to represent focused electromagnetic fields of a laser pulse propagating in vacuum. Our thorough investigations about the ponderomotive acceleration show that the longitudinal electromagnetic fields exert a damping force on an electron motion to prevent a particle from scattering off the pulse propagation axis. This effect makes extreme spatial and temporal properties of an electron beam with nanometer size and attosecond duration. A simulation result of the ponderomotive acceleration of electrons by a temporally Gaussian laser pulse of the Hermite-Gauusian TEM_{00} mode shows that the accelerated electron bunch length leads to the attosecond range shorter than the laser wavelength.

5. Applications of laser particle acceleration

It is well known that the relativistic laser-plasma interactions can produce a large variety of energetic photon radiations and particles through particle acceleration mechanism by strong laser fields. Particularly the electron acceleration mechanism plays a important basic role in the relativistic plasma dynamics and interactions. The relativistic ultrashort electron bunch generated by laser-plasma acceleration mechanisms can radiate an intense ultrashort pulse of X-rays and gamma rays with a narrow band spectrum via Thomson or Compton scattering of counter propagating intense laser pulses. These X-ray pulses are useful for material and biological applications to investigate ultrafast phenomena. In addition the laser-driven electron beam can create relativistic positrons via electron-positron pair creation process in a solid density plasma. These phenomena will beget a positron beam source in a table top.

We pursue technologies of laser particle acceleration that realize unprecedented acceleration gradients and extreme properties of accelerated beams. These basic technologies will be reorganized to create a new instrumentation for a wide range of sciences from atomic and molecular science to high energy frontier science.

References

1) V. Malka et al., Science **298**, 1596 (2002).
2) H.Dewa et al., Nucl. Instr. and Meth. in Phys. Res. **A410**, 357 (1998); M. Kando et al., Jpn. J. Appl. Phys. **38**, L967 (1999).
3) M. Kando et al., JAERI-Conf 2000-006, 218 (2000).
4) D. Umstadter et al., Phy. Rev. Lett. **76**, 2073 (1996).
5) E. Esarey et al., Phy. Rev. Lett. **79**, 2682 (1997).
6) S. Bulanov et al., Phys. Rev. **E58**, R5257 (1998).
7) H. Kotaki et al., Phys. Plasamas **9**, 1392 (2002).
8) F. V. Hartemann et al., Phy. Rev. E **51**, 4833 (1995).
9) J. D. Lawson, IEEE Trans. NS-**26**, 4217 (1979).

4.5.1 Laser Electron Acceleration Experiments

Masaki KANDO, Hideyuki KOTAKI, Shin-ichi MASUDA, Shuji Kondo,
Shuhei KANAZAWA, Takayuki HOMMA, and Kazuhisa NAKAJIMA[a)]

a) JAERI Kansai and High Energy Accelerator Research Organization (KEK)

1. Introduction

Recent progress of high-peak power lasers enables to produce high energy electrons by irradiation of the lasers into an underdense plasma. Energy of the electrons accelerated in a plasma by the laser reaches to 200 MeV [1)], and the smallerst emittace is 0.1 π mm-mrad [2)], that is better than that of obtained by conventional RF accelerators technologies [3)]. Many electron generation experiments have been done [1,2,4)], however, the underlying acceleration mechanisms are still open to argument. The acceleration mechanisms are classified to two major schemes: electrostatic plasma wave induced acceleration and laser field (both electric and magnetic) induced acceleration. A plasma cathode experiments using a 100 TW Ti:Sa laser system has been initiated at JAERI-APRC. Using this high peak power laser, the expected focused intensity is 10^{20} W/cm^2. The maximum electron energy of our experiment is over 200 MeV predicted by one-dimensional particle-in-cell simulations [5)]. Here we report the preliminary results of the plasma cathode experiment.

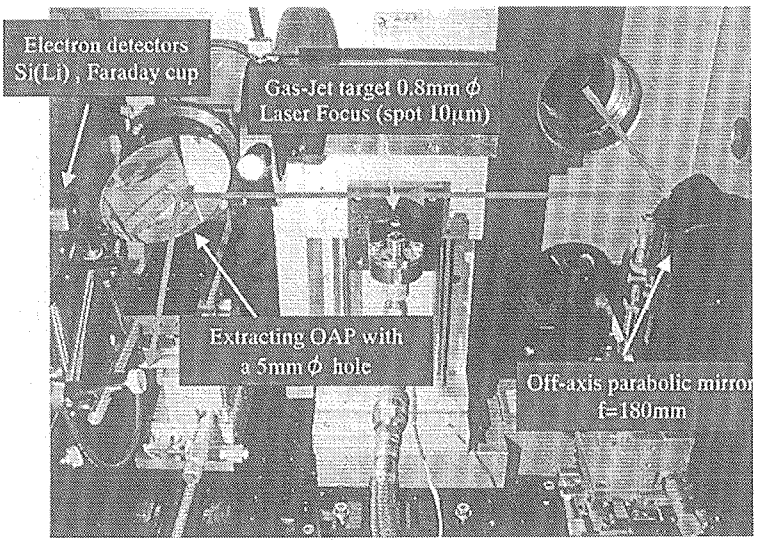

Fig. 1 Experimental setup of the plasma cathode

2. Experimental setup of single-pulse plasma cathode

The 100 TW laser system developed by JAERI laser group [6)] is used as a driver for particle generation. The laser beam is compressed in a grating pair located next to the laser room and then delivered to the experimental room through a 30 m long vacuum duct. The laser beam is focused by an off-axis parabolic mirror (OAP) with the focal length of 177 mm (f/3.5). The setup in the interaction chamber is shown in Fig. 1. The focused laser beam is then collimated by another OAP with the same focal length which has a through-hole of 5 mm and delivered to the outside of the chamber to measure the laser pulse energy. The generation of fast electrons are monitored by a Si(Li) semiconductor detector biased to 400 V. The surface of the Si(Li) detector is covered by an aluminum foil and a black tape to avoid irradiation of the strong laser and plasma radiations. The energy distribution of the electrons is measured by a dipole magnet spectrometer, which has the maximum field strength of 1.1 T and has 32 channel plastic scintillation detectors with photomultipliers. The spectrometer covers up to 600 MeV with the 10 % resolution. The charge of the electrons are measured by three Faraday cups. Two OAPs are insulated and used as Faraday cups and the other is placed after the extracting OAP.

3. Preliminary results

The transmission efficiency from the entrance of the pulse compressor to the interaction point was 17 % at the experiment. The expected efficiency was 52 %. This poor transmission efficiency limited the focused intensity achieved at the interaction chamber. The pulse duration of the compressed laser was measured and was 30 fs at full width half maximum. The spot radii of the focused laser were 5.3 × 3.5 μm containing 50 % of the total energy. The maximum intensity at the experiment was 7.3×10^{18} W/cm^2.

The electron signals were successfully measured by the Si(Li) detector. The measured and analyzed signals of the accelerated electrons were shown in Fig. 2. Since the high sensitivity of the detector, electrons were detected even at the low intensity of 4.6×10^{18} W/cm^2. The measured signals were sum of the energy deposition in the Si(Li) of the electrons that could reach to the Si(Li) after the shielding foils. Exact energy spectrum was difficult to deduce from Fig. 2, however, this high sensitivity is useful to monitor the electrons and optimize electron acceleration. At the spectrometer, no electrons were detected. This was because the accelerated electrons were few and their energy was low and could not reach to the spectrometer detectors that was placed 1 m downstream from the interaction point.

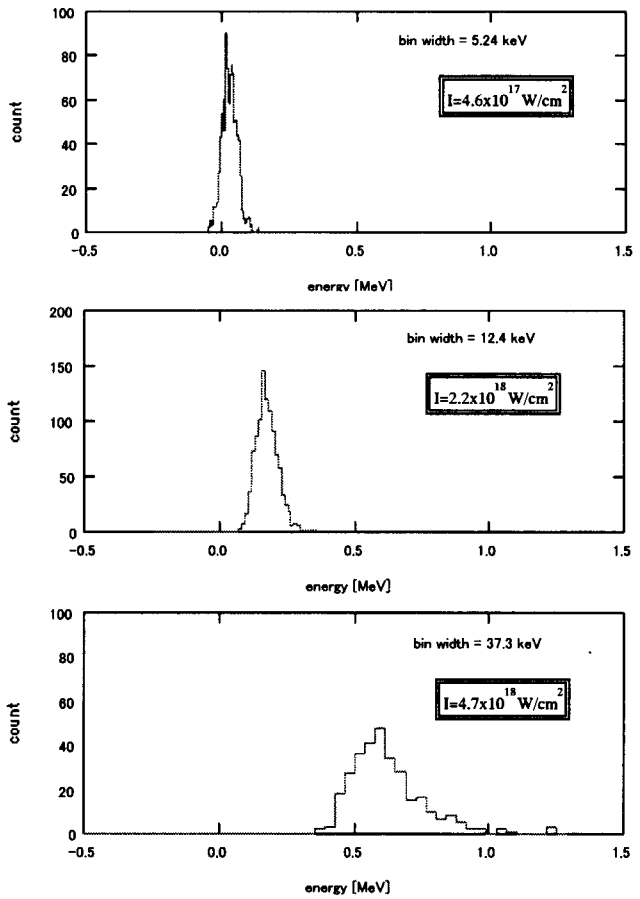

Fig. 2 Electron signals measured by the Si(Li) detector at various laser intensities

4. Summary

We have started the experiments of plasma cathode to generate high energy, high quality electrons beam. The energy of 200 MeV will be achieved just focusing the 100 TW Ti:Sa laser pulse into an underdense plasma. We have verified that the Si(Li) semiconductor detector works well to monitor an accelerated electrons. Improvements of the transmission efficiency through the laser transport is the key problem to achieve high energy electron acceleration.

References

1) V. Malka et al. : Science **298**, 1596, 2002.
2) S.-Y. Chen et al., Phys. Plasmas **6**, 4739,1999.
3) X. J. Wang et al. : Nuclear Instruments and Methods **A 375**, p.82, 1996.
4) T. Hosokai et al., Phys. Rev. E **67**, 036407, 2003.
5) S. Masuda et al., Proc.of Quantum Aspects in Beam Physics, 2003 (in print).
6) K. Yamakawa et al., Opt. Lett., **23**, p.1468, 1998.

4.5.2 Generation of a high quality electron beam by the colliding two laser pulses

Hideyuki KOTAKI, Masaki KANDO, Shin-ichi MASUDA, Shuji KONDO,
Shuhei KANAZAWA, Takayuki HOMMA, and Kazuhisa NAKAJIMA

1. Introduction

Electron beam injection triggered by an intense ultrashort laser has been proposed as an injector of ultrashort electron beams referred to as "optical injection". Presently there are three major schemes: nonlinear wave-breaking injection[1], transverse optical injection[2], and colliding pulse optical injection[3)4)5)]. Three laser pulses consisting of a pump pulse for wakefield excitation and two injection pulses for trapping the electrons from the plasma make up the colliding pulse optical injector. The colliding pulse optical injection is a high quality optical injector. The optical injection, however, is the most difficult.

The counter-propagate laser pulses inject electrons from the plasma into a wakefield excited by one of the laser pulses. One of the laser pulses injects and accelerates electrons. We call the mechanism "colliding pulse optical acceleration". The experiment of the colliding pulse optical acceleration is easier than the colliding pulse optical injection, and has the possibility to become a high quality electron injector similar to colliding pulse optical injection. We present optical injection and acceleration schemes that utilize two counter-propagating laser pulses.

2. Colliding pulse optical acceleration by 2 laser pulses

Two counter-propagating laser pulses each produce plasma waves. The interaction of pulse 0 and pulse 1 generates a standing wave. We assume the electric field **E** is

$$\mathbf{E} = \mathbf{E}_0\cos(k_0z-\omega_0t)+\mathbf{E}_1\cos(k_0z+\omega_0t),$$

where ω_0 and k_0 are the frequency and the wave number of the laser, and E_0 and E_1 are electric field of the laser pulses. The momentum p_{inj} of the injection is obtained

$$p_{inj} = \gamma_{inj}m_ec = CE_0E_1[\sin(2\omega_0t)-2\omega_0t\cos(2k_0z)],$$

where γ_{inj} is the normalized energy of injection and C is $e^2/2m_e\omega_0^3$. This equation shows that electrons in the plasma are accelerated from oscillations generated by the colliding laser pulses. Electrons in the plasma are injected into the wakefield, when the laser pulses collide and the laser strength parameter is above the trapping threshold. For the laser strength parameters a_0 of 1.0 and a_1 of 0.4, the rms electron pulse duration τ_e(rms) is written by

$$\tau_e(\text{rms}) = \quad 0.10\,\tau_L(\text{FWHM}),$$

where τ_L(FWHM) is the full width at half maximum pulse width of the laser pulse. The electron bunch compression effect is included in the pulse duration.

3. Simulation results of the optical injection

In order to estimate the quality of the generated electron beam, we performed 1-D Particle-in-Cell (PIC) simulations[6] for the colliding pulse optical acceleration in the linear regime. The length of the simulations is 1 mm, and the colliding point of two laser pulses is at the center. A portion of the electrons in the plasma is trapped and accelerated to high energy by the wakefield excited by the pump pulse. The accelerated electron beam is clearly separated from electrons in the plasma.

The electron beam at $n_e=7\times10^{17}\text{cm}^{-3}$ for $a_0=1.0$ and $a_1=0.4$ has a pulse duration of 7.4 fs (rms) and a charge of 31 pC corresponding to the peak current of 1.5 kA. It would be difficult to generate such an ultrashort intense electron beam with conventional RF accelerators. Figure 1 shows the pulse duration of the injected and accelerated electron beam. The dotted lines show the theoretical value at $\lambda_p[\mu\text{m}]=0.8\tau_L(\text{FWHM})[\text{fs}]$. The simulation results are consistent with the theoretical values. The electron bunch injected into the wakefield excited by the pulse 0 is also compressed and stretched in the field before becoming relativistic. The pulse duration of the accelerated electron beam changes after trapping into the wakefield which works as a compressor and a stretcher not only an accelerator.

Figure 2 shows the accelerated electrons energy at $n_e=7\times10^{17}\text{cm}^{-3}$ for $a_0=1$ and $a_1=0.4$. The accelerated energies are consistent with linear theory and the energy spread is very small. The energy and the energy spread are 9.5 MeV and 1.42%, respectively.

For the quality of the electron beam, the emittance is one important parameter. Figure 3 shows the distribution of the transverse normalized velocities β_t of the accelerated electrons at $n_e=7\times10^{17}\text{cm}^{-3}$ for $a_0=1.0$ and $a_1=0.4$. We can obtain an emittance of the electron beam from $\beta_t = 0.0029$. The normalized emittance ε_{nx} of the electron beam is approximately,

$$\varepsilon_{nx} = r_e\gamma\beta\beta_t,$$

where r_e is the electron beam radius, γ is the normalized energy, and β is the longitudinal normalized velocity of the electron. For the electron energy of 9.5 MeV, γ and β are approximately equal to 18.6 and 1, respectively. Assuming the electron beam radius, r_e=15μm, the normalized emittance of the accelerated electrons is 0.3 π mm mrad (rms). This emittance is smaller than the best quality beam produced by conventional RF accelerator technology such as a photocathode RF-gun[7)8)].

These results show that the colliding pulse optical acceleration by two laser pulses has a possibility of small energy spread and low emittance electron injection.

4. Conclusions

We have explored the generation of a high quality electron bunch by using colliding pulse optical acceleration by two counter-propagating laser pulses that are a realistic method for experiments of high quality electron generation. The mechanism is a new one for electron injection and acceleration. We have made a numerical simulation of the optical injection scheme and compared it to the calculation of the optical acceleration. In particular, we have studied the pulse duration of the injected and accelerated electron bunches. The wakefield compressed the electron bunch and the space charge stretched the electron bunch. The colliding pulse acceleration scheme investigated has the ability to produce relativistic electron bunches with low energy spread; low normalized transverse emittance, and short bunch length.

References

1) S. Bulanov, N. Naumova, F. Pegoraro, and J. Sakai, Phys. Rev. E **58**, R5257, 1998
2) D. Umstadter, J. K. Kim, and E. Dodd, Phy. Rev. Lett. **76**, 2073, 1996
3) E. Esarey, R. F. Hubbard, W. P. Leemans, A. Ting, and P. Sprangle, Phy. Rev. Lett. **79**, 2682, 1997
4) C. B. Schroeder, P. B. Lee, J. S. Wurtela, E. Esarey, and W. P. Leemans, Phy. Rev. E **59**, 6037, 1999
5) E. Esarey, C. B. Schroeder, W. P. Leemans, and B. Hafizi, Phys. Plasmas **6**, 2262, 1999
6) S. Masuda, T. Katsouleas, and A. Ogata, Nucl. Inst. and Meth. A **455**, 172, 2000
7) K. Nakajima, Nucl. Instr. and Meth. in Phys. Res. A **455**, 140, 2000
8) X. J. Wang, M. Babzien, K. Batchelor, I. Ben-Zvi, R. Malone, I. Pogorelsky, X. Qui, J. Sheehan, J. Sharitka, and T. Srinivasan-Rao, Nucl. Instr. and Meth. A **375**, 82, 1996; X. J. Wang, X. Qiu, and I. Ben-Zvi, Phys. Rev. E **54**, 3121, 1996

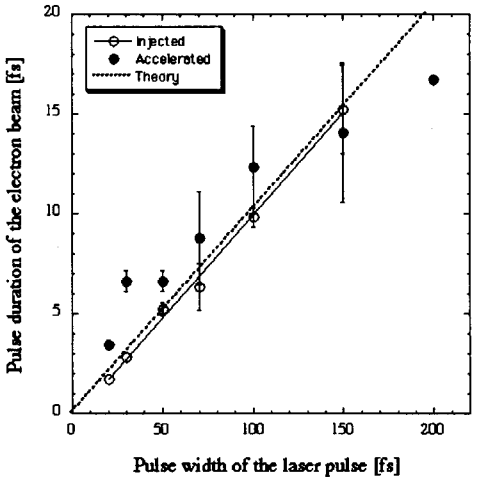

Fig. 1 The pulse duration of the electron beam for a_0=1.0 and a_1=0.4

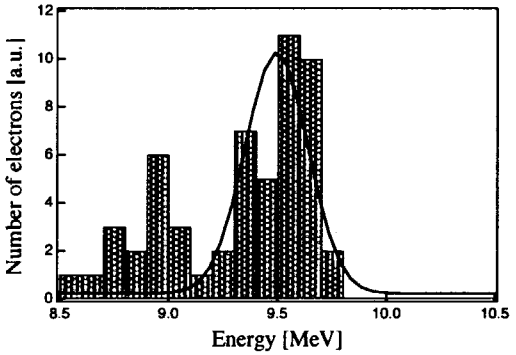

Fig. 2 The energy spectrum of accelerated electrons at n_e=7×10^{17}cm^{-3} for a_0=1 and a_1=0.4

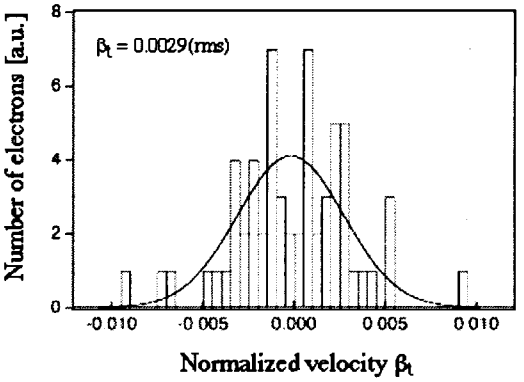

Fig. 3 The distribution of the transverse normalized velocity β_t of the accelerated electrons for a_0=1.0 and a_1=0.4 at n_e=7×10^{17}cm^{-3} and a laser pulse width of 50 fs.

4.5.3 Generation of Femtosecond Electron Bunches by Lowest order Eermite-Gaussian mode (TEM_{00}) via Relativistic Laser Ponderomotive Acceleration in Vacuum

Shinichi MASUDA, Masaki KANDO, Hideyuki KOTAKI, Shuji KONDO,
Shuhei KANAZAWA, Takayuki HONMA, Igor Smetanin and Kazuhisa NAKAJIMA[a)]
a) JAERI Kansai and High Energy Accelerator Research Organization (KEK)

1. Introduction

The relativistic laser ponderomotive acceleration (LPA) in vacuum [1)] is one of a way to generate the high energy electrons. When the laser beam focused on the electrons in vacuum, laser electric field accelerates the electrons in its polarization direction and then the electrons are pushed in the laser propagation direction by **vxB** force. As a results, the electrons are accelerated to the laser propagation direction oscillating in the polarization direction. However, the electrons are scattered by the transverse ponderomotive force because the electron quiver amplitude exceeds the laser spot size. To avoid the scattering, using the higher order Hermite-Gaussian mode is supposed [2)]. The electrons are focused by the TEM_{10} and TEM_{01} modes. However, it is difficult to adopt the higher order mode experimentally because the dominant mode of the most laser is the TEM_{00} (lowest order Hermite-Gaussian) mode.

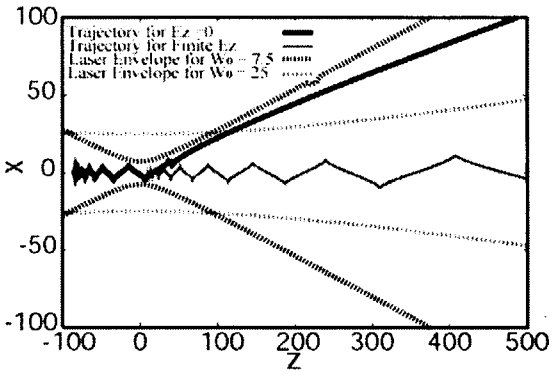

Fig. 1 Electron trajectories in laser beam
When the longitudinal electric and magnetic field is zero, the electron is scattered. The electron is confined around the laser propagation axis for the case of finite longitudinal field. Solid lines are electron trajectories and dashed lines are laser envelope. The laser is linearly polarized in the *x*-direction propagating along the *z*-axis. The position is normalized by the laser wave length λ/2π.

We found a focusing effect of TEM_{00} mode by taking an effect of the longitudinal electric and magnetic field into account. Figure 1 shows the electron trajectory in (x, z) plane. The electron is scattered when the laser has no longitudinal field. On the contrary, the electron in the laser beam with longitudinal field is confined around the z-axis. We will report the optimal parameters for LPA with longitudinal field and the possibility of generation of femtosecond electron bunches.

2. Optimum Condition of LPA

In this section, we will report the energy gain of the electron acceleration and the optimum condition of LPA. We solved numerically Lorentz force equation with Boris push algorithm [3,4)] to track the electron trajectories in the laser field. The laser electric and magnetic fields are modeled in our calculation as follows. The laser envelope of transverse electric field linearly polarized in the x-direction is given by the paraxial approximation:

$$E_x = E_0 \frac{w_0}{w(z)} \exp\left(-\frac{x^2+y^2}{w^2(z)}\right)\sin\Psi, \qquad \Psi = \omega t - kz - k\frac{x^2+y^2}{2R(z)} + \tan^{-1}\frac{z}{z_R}, \qquad (1)$$

where E_0 is the peak amplitude of the laser electric field, k is wave number equal to ω/c, w_0 is the spot size at the focus, $w(z)$ and $R(z)$ are the spot size and radius of curvature at z-position defined by

$$w(z) = w_0\sqrt{1+\frac{z_R^2}{z^2}} \quad \text{and} \quad R = z\left(1+\frac{z_R^2}{z^2}\right),$$

respectively. A constant z_R, Rayleigh length, is given by $z_R = kw_0^2/2$. The transverse magnetic field is $B_y = E_x$ from Faraday's low. The longitudinal electric field is obtained from the condition that the divergence of E is equal to zero. An approximation is

$$E_z = \mathrm{Re}\left\{-\frac{i}{k}\frac{\partial E_x}{\partial x}\right\} = E_0\frac{w_0}{w(z)}\left[\frac{2x}{kw^2(z)}\cos\Psi - \frac{x}{R(z)}\sin\Psi\right]\exp\left(-\frac{x^2+y^2}{w^2(z)}\right). \qquad (2)$$

The longitudinal magnetic field, B_z, is also calculated from $\nabla\cdot\mathbf{B} = 0$. In addition, a time envelope function, $\exp\left[-(t-z/c)^2/4\tau^2\right]$, is multiplied above electromagnetic fields to express the laser pulse so that the laser

pulse reaches the focal point at $z = 0$ at time $t = 0$.

Theoretical analyses [1,2] predict the energy gain is proportional to γa_0^2, where γ is Lorentz factor of electrons. Here a_0 is normalized vector potential defined as $a_0 = \sqrt{eE/mc\omega}$, where e is magnitude of electron charge, m is electron mass, c is speed of light in vacuum, ω is angular frequency of laser. An optimum acceleration length to obtain the maximum energy gain determined by Rayleigh length, z_R given by $z_R = kw_0^2/2$, where w_0 is laser spot size and k is laser wave number. Scaling lows for the energy gain and the optimum laser spot size are expressed by $\Delta\gamma = k_\gamma \gamma a_0^2/4$ and $kw_0 = k_w \gamma a_0$, respectively. The coefficients, k_γ and k_w, are depend on the laser pulse length. We found k_γ and k_w are 1.5 and 5.5 for the laser pulse length $\tau = 20\ \omega/2\pi$, respectively. A relationship between the energy gain and the laser power is $\Delta\gamma = \left(k_\gamma / 4k_w\right)\sqrt{P[\mathrm{W}]/\left(5.5\times10^8\right)}$ with the help of $P = 5.5\mathrm{x}10^8 (k\ w_0)^2 a_0^2$ [W]. When the laser power, for instance, P = 100 TW, the maximum energy gain is 15 MeV.

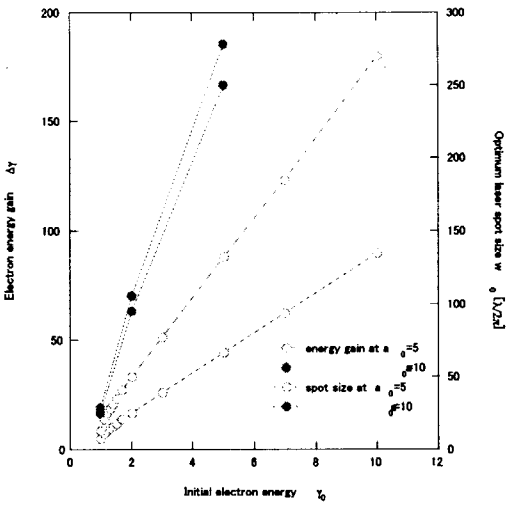

Fig. 2 Electron energy after the interaction with the laser pulse as a function of the laser spot size

The maximum energy of the electrons are plotted, which are initially lined up on z-axis around the laser focus. the laser pulse length $\tau = 20\ \omega/2\pi$.

3. Femtosecond Electron Bunch Generation

It is pointed out that LPA can generate short electron bunches of the order of 100 attosecond [2]. We also observed a femtosecond electron bunch generation. The electron bunch length is estimated from Fig. 3 that shows the electron distribution after the interaction with the laser pulse. The electron density distribution is the bunch is shown in Fig. 4. The bunch length is 2 fs for the laser with wave length λ=800 nm.

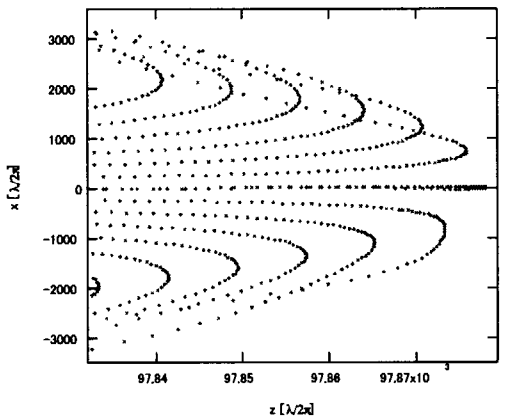

Fig. 3 Electron distribution in (x,z) plain at ωt = 99000

The initial electron energy γ = 1, a_0=10 and laser spot size is $w_0 = 25\ \lambda/2\pi$. Laser pulse length is $\tau = 20\ \omega/2\pi$.

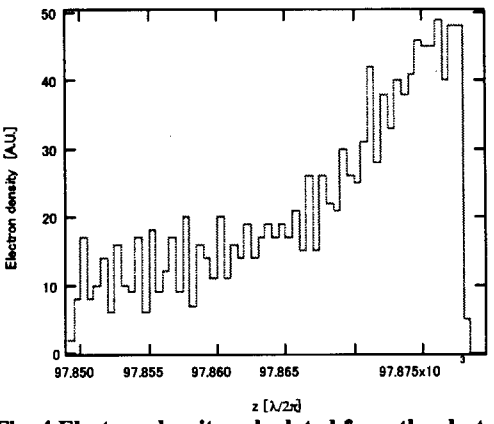

Fig. 4 Electron density calculated from the electron distribution in Fig. 3

The electron bunch length is 5 $\lambda/2\pi$ (FWHM).

4. Summary

We studied the LPA scheme in vacuum. The longitudinal electric and magnetic field has focusing effect on the electrons. A scaling low between the energy gain and the laser power is obtained. The maximum energy gain is proportional to the square root of laser power. The femtosecond electron bunch is generated.

References

1) F.V. Heartmann, *et. al.*, Phys. Rev. E, **51**, 4833 (1995)
2) G. V. Stupakov, *et. al.*, Phys. Rev. Lett., **86**, 5274 (2001)
3) C. K. Birdsal and A. B. Langdon, Plasma Physics via Computer Simulation, McGrow-Hill, 1985
4) R. W. Hockney and J. W. Eastwood, Computer Simulation Using Particles, Inst of Physics Pub Inc. 1988

4.5.4 Stimulated annihilation and generation of coherent gamma-ray radiation in the strong laser field

Igor V. SMETANIN and Kazuhisa NAKAJIMA

1. Introduction

Recent progress of high-power femtosecond laser technologies [1] has renewed interest in the annihilation of electron-positron pairs in the strong field. Propagation in electron-positron vacuum is accompanied by self-action of intense electromagnetic wave [2]. Coherent pair creation due to nonlinear Compton scattering restricts luminosity of γ-γ colliders [3]. QED vacuum decay via spontaneous pair production can be studied with high-power x-ray free-electron lasers [4]. Amplification of γ - radiation and lasing is possible in the electron-positron plasma [5].

We propose here a new concept of coherent generation of γ-ray radiation, the mechanism of which is the stimulated nonlinear coherent annihilation of electron-positron pairs in the strong laser field. In our concept, relativistic ($\gamma_0 mc^2$ the energy) beam of electrons and positrons interacts with the counter-propagating high-power laser radiation. If the energy of laser photon in the beam (center-of-mass) reference frame exceeds mc^2, coherent stimulated generation of γ-ray photons becomes possible. The energy of photon emitted is $\hbar\omega_\gamma \approx 4\gamma_0^2\hbar\omega_i \approx (mc^2)^2/\hbar\omega_i$, $\hbar\omega_i$ is the laser quantum. Annihilation of an electron- positron pair in the strong laser field can be considered as the resonant two-photon transition in an inverted two-level quantum system. In the nonlinear oscillation regime, inversion can be removed in one pass and the π-pulse of coherent γ-ray radiation is generated. Estimates show the scheme proposed is a promising high-brightness source of coherent γ-radiation.

2. Electron-positron pair as an inverted two-level system

We consider the case of non-polarized electrons and positrons, which allows to use the Klein-Gordon field approach to describe particle's dynamics in the strong laser field [6]. The deep analogy between annihilation and Compton processes allows to construct the theory of the proposed scheme by analogy with that of the two-level Compton x-ray FEL [7].

Let the vector potential of the γ-ray mode is $A_\gamma \exp(i[k_\gamma z - \omega_\gamma t])$, and that of the laser pulse is $A_i \exp(i[k_i z + \omega_i t])$, no depletion of laser mode is assumed. Stimulated annihilation of the electron-positron pair is accompanied by the emission of two photons in laser and γ-ray modes and obeys the energy and momentum conservation laws, $p + p' = k_\gamma - k_i = q$ and $\varepsilon_p + \varepsilon_{p'} = \omega_\gamma + \omega_i$. The interaction Hamiltonian can be reduced to the diagonal form by conventional Bogolubov's transformation. Annihilation and pair creation then can be treated as two-photon resonance transitions between correspondent quantum levels of the efficient two-level system, the upper state of which consists in the electron-positron pair and N pair of photons, and the lower state is (N+1) photon pairs.

To describe the nonlinear evolution of the electron-positron pair in the interaction region and coherent generation of coherent γ-rays, we solve the system of coupled Klein - Gordon and Maxwell equations. Seeking the pair's wavefunction in the form of superposition of upper and lower states of the effective two-level oscillator, we get the closed self-consistent system of equations which are analogous to the Maxwell - Bloch system in the conventional nonlinear optics, and admits a solution in the form of coherent π-pulses.

3. Coherent oscillations in the two-level electron-positron system

We find that the amplitudes of the upper (u_p) and lower (v_p) energy levels oscillates in the interaction region

$$u_p = \cos(\chi/2), \qquad v_p = -i\sin(\chi/2)$$

with the γ-ray pulse area

$$\chi(z) = (\mu/c\hbar)\int_0^z E_\gamma(z)dz$$

where $\mu = e^2c^2E_i/(2\omega_\gamma\omega_i\sqrt{\varepsilon_p\varepsilon_{q-p}})$ is the characteristic dipole moment of the electron-positron two-level system, $E_{\gamma,i}$ are the wave's electric field amplitudes, and the boundary conditions (z=0) $u_p = 1$, $v_p = 0$ are assumed . Evolution of the pulse area for the amplified γ-ray signal is guided by the pendulum equation

$$\partial^2\chi/\partial z^2 = \alpha^2 \sin\chi$$

with the linear gain coefficient

$$\alpha = \left(\frac{\pi e^4 E_i^2 nc^2}{\hbar\omega_\gamma\omega_i^2\varepsilon_p\varepsilon_{q-p}}\right)^{1/2},$$

n is the pair's density in the beam of electrons and positrons.

3. π-pulses of coherent γ-ray radiation

Intensity of the coherently generated γ-ray field in the process of stimulated annihilation oscillates with the interaction distance z as follows

$$I_\gamma(z) = dn^{-2}\left(\frac{\alpha z}{\kappa},\kappa\right)I_\gamma(0)$$

Here $dn(x,\kappa)$ is the elliptic Jacobi function, $\kappa = \sqrt{1+I_\gamma(0)/I_m}$, $I_\gamma(0)$ is the initial intensity of the γ-ray photon flux, determined by spontaneous pair annihilation. The parmeter $I_m = \hbar\omega_\gamma nc$ is the maximum intensity of the amplified wave which can be attained as a result of annihilation of positrons and electrons having the equal beam densities n.

The maximum intensity can be achieved for the interaction distance $L_{max} = \alpha^{-1}\kappa K(\kappa)$, $K(x)$ is the complete elliptic integral of the first kind,

$$I_\gamma(L_{max}) = I_m + I_s(0),$$

which corresponds to the formation of the coherent π-pulse of the amplified wave, that is the pulse area becomes $\chi(L_{max}) = \pi$. At this optimum interaction condition, all the inversion is removed in one pass, i.e., all the electron-positron pairs annihilate coherently [7].

For estimates, the interaction conditions are optimal when in the center-of-mass reference frame both photons have equal energies $\hbar\omega_i' \approx \hbar\omega_\gamma' \approx mc^2$. The electron-positron beam gamma factor scales with the laser frequency as $\gamma_0 \approx mc^2/\hbar\omega_i$ and for $\hbar\omega_i = 1eV$ reaches the value $\gamma_0 \approx 2.5\times10^5$, which corresponds to the energy of co-propagating electron and positron beams ~125 GeV. The linear gain coefficient scales as $\alpha[cm^{-1}] \approx 0.53\times10^{-2}\times\left[a_0\times(n/10^{24}cm^{-3})^{1/2}\times(\gamma_0/2.5\times10^5)^{-3/2}\right]$, and the output maximum γ-ray intensity as $I_m = 1.2\times10^{27}W/cm^2\times\left[(n/10^{24}cm^{-3})\times(\gamma_0/2.5\times10^5)\right]$. Here a_0 is the normalized vector potential of the laser field. As the laser radiation spectral width is restricted by the electron-positron beam energy spread $\Delta\gamma/\gamma$, coherent annihilation can be stimulated by radiation of an x-ray FEL and even the Thomson source. The corresponding parameters are collected in the Table

$\hbar\omega_i$	γ_0	$\hbar\omega_\gamma$	n[cm^{-3}]	α[cm^{-1}]	$I_m[W/cm^2]$
$1eV$	2.5×10^5	250GeV	10^{24}	$0.0053a_0$	$\sim1.2\times10^{27}$
125eV	2×10^3	2GeV	10^{24}	$7.4\,a_0$	$\sim10^{25}$
1.25keV	200	200MeV	10^{24}	$7.4\times10^3 a_0$	$\sim10^{24}$
1.25keV	200	200MeV	10^{18}	$7.4a_0$	$\sim10^{18}$

References

1) M.D. Perry et al., Opt. Lett. **24**, 160, 1999
2) N. Rozanov, JETP **86**, 284, 1998; G. Brodin et al., PRL **87**, 171801, 2001
3) P. Chen, V. Telnov, PRL **63**, 1796, 1989
4) C.D. Roberts, S.M. Shmidt, D. V. Vinnik, PRL **89**, 153901, 2002
5) L. Rivlin, Sov. J. Quantum Electron. **3**, 2413 , 1976 (in Russian)
6) A.I. Nikishov. In.: Proc. P.N. Lebedev Physics Inst. (Ed. N.G. Bassov), vol. 111, 152-278, Moscow, 1976.
7)I.V. Smetanin, Laser Phys. **7** , 318, 1997; E.M. Belenov et al., JETP **105,** 808, 1994.

4.5.5 Evolution of an intense elliptically polarized electromagnetic wave in underdense plasmas

I. V. SMETANIN, D. FARINA[a)], J. KOGA, K. NAKAJIMA[b)], S. V. BULANOV[c)]
a) Institute of Plasma Physics, CNR, Milan Italy
b) High Energy Accelerator Research Organization (KEK), Tsukuba
c) General Physics Institute, Russian Ac. Sci., Moscow, Russia

1. Introduction

Propagation of electromagnetic radiation in a plasma has been studied intensively for decades. Evolution of the structure and propagation characteristics of intense electromagnetic waves are of crucial importance for laser wakefield acceleration, for high-harmonic generation, and for many other aspects of the laser-plasma interaction[1-3].

In theoretical studies, the laser-plasma interaction is usually considered in the specific limiting cases of linear or circular wave polarization, which can lead to discrepancies between the idealized case and real experimental situations. Consideration in the general case of elliptic polarization shows[4,5] that an intense electromagnetic wave propagates under self-induced birefringence, which is analogous to the conventional Faraday rotation, even if the ellipticity in its polarization is very small and no static magnetic field exists in the plasma. To the lowest order of perturbation theory, this effect can be described in terms of the nonlinear shift between refractive indices of the left- and right-circular polarization components

In the present paper, we study the structure and the oscillation regimes in the evolution of an intense elliptically polarized electromagnetic wave propagating in an underdense plasma. We show that the wave electric field has two transverse components, which contain odd harmonics of the principal mode, and in the longitudinal component with even harmonics. As a result of the longitudinal plasma oscillation excitation, a phase shift between the electric field components arises. In addition, a nonlinear oscillations seen in the electromagnetic wave amplitude occur. We show that the phase shifts between the transverse components of the first and third harmonics are equal to each other. Evidently, in the case of a circularly polarized wave the longitudinal electric field and the higher harmonic terms vanish.

2. Propagation of an elliptically polarized wave in plasma

To describe the relativistically strong plane electromagnetic wave evolution in a plasma we use a system consisting of Maxwell equations and the electron hydrodynamics equation. We seek solution to this self-consistent system of equations using the standard multi-scale perturbation procedure[6]. The parameter of a smallness ε is the typical value of the wave amplitude, which is assumed to be small but finite.

To the first order in the smallness parameter, there is no perturbation in plasma density, and we have a linear wave equation for the plane electromagnetic wave which admits a sultion of the form

$$a(x,t) = e_y A_y \sin\Theta_y + e_z A_z \cos\Theta_z$$

where $e_{y,z}$ are the unit polarization vectors of y- and z- field components, the phases are $\Theta_{y,z} = \omega_0 t - k_0 x + \varphi_{y,z}$, and the amplitudes $A_{y,z}$ and phases $\varphi_{y,z}$ are the slowly varying functions. The wavenumber and frequency of the electromagnetic wave are normalized to the plasma parameters by conventional manner.

To the third order of multiscale perturbation theory, we find that for both the wave components, the common propagation characteristics are the total wave intensity $A_y^2 + A_z^2$ and the net phase shift $\varphi = (\varphi_y + \varphi_z)/2$. The total wave intensity is a function of the intrinsic wave coordinate $A_y^2 + A_z^2 = F(\varsigma)$, $\varsigma = x - k_0 t/\omega_0$, and the net nonlinear shift in frequency of the electromagnetic wave is

$$\partial_t \varphi = -\frac{1}{8\omega_0} F(\varsigma)\left[1 + \frac{3}{2}\frac{\sin^2 \delta\varphi}{4\omega_0^2 - 1}\right]$$

The negative sign of the right hand side is a consequence of the nonlinear frequency down shifting.

Difference in the propagation of y- and z-components depends on the temporal evolution of the phase shift $\delta\varphi = \varphi_y - \varphi_z$ and function $G(\varsigma,t) = (A_y^2 - A_z^2)/(A_y^2 + A_z^2)$, which characterizes the difference in component's amplitudes and at the initial moment of time coincides with the wave polarization ratio G_0, i.e., the eccentricity of the polarization ellipse, normalized to the total wave intensity. It varies from the value

$G_0 = 1$ for the wave polarized along the y-axis to $G_0 = -1$ for the wave polarized along the z-axis, and vanishes $G_0 = 0$ for the circular polarization. Assuming zero initial phase difference $\delta\varphi = 0$, we find the functions $\delta\varphi$ and G exhibit nonlinear oscillations

$$G = G_0 \cos\left(\sqrt{1-G_0^2}\,\tau\right),$$

$$\tan\delta\varphi = -\left(\frac{G_0^2}{1-G_0^2}\right)^{1/2} \sin\left(\sqrt{1-G_0^2}\,\tau\right)$$

where the new time variable is introduced

$$d\tau = \frac{3}{8\omega_0}\frac{F(\varsigma)}{4\omega_0^2 - 1}dt\,.$$

Propagation of an elliptically polarized wave is illustrated in the Figure 1, where the spatio-temporal evolution is shown in two limiting cases, when the initial polarization is close to the circular with $G_0 = 0.1$ and to the linear polarization with $G_0 = 0.99$.

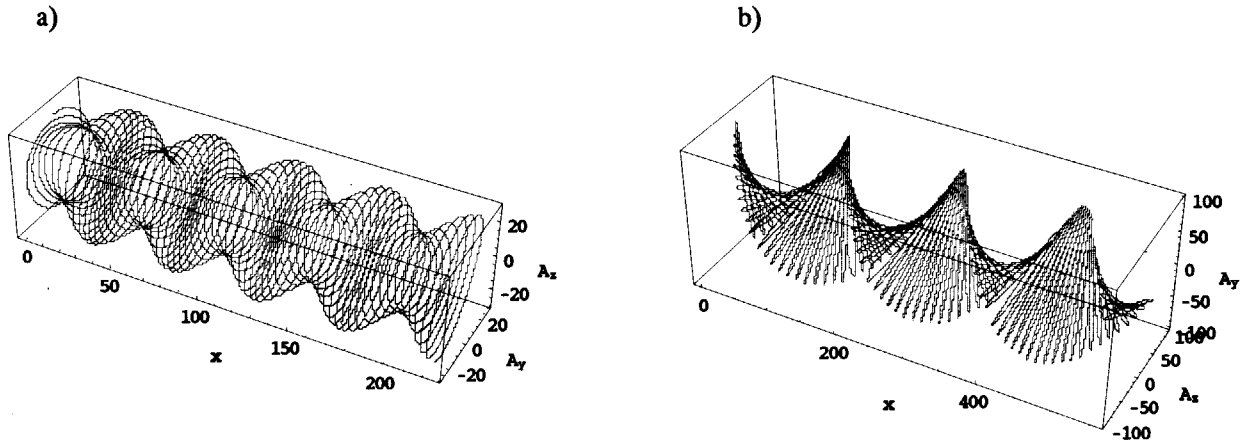

Fig. 1 The characteristic spatio-temporal evolution of the elliptically polarized waves in a plasma for different initialpolarization ratios: a) $G_0 = 0.1$, where the wave polarization is close to circular, b) $G_0 = 0.99$, where the wave is almost linearly polarized

References

1) E. Esarey et al., IEEE Trans. Plasma Sci., **24**, 252, 1996
2) A.I. Akhiezer, R. V. Polovin, Sov. Phys. JETP, **30**, 915, 1956
3) S. V. Bulanov et al., in: Rev. Plasma Phys. (ed. V.D. Shafranov), vol. 22, 227, 2001
4) J. Arons, C. E. Max, Phys. Fluids, **17**, 1983, 1974
5) B. Chakraborty et al.,Phys. Rev. A **28**, 1047, 1983
6) A. H. Nayfeh, "Perturbation Methods", Wiley, New York, 1982.

4.6 Advanced Photon Simulation Research

The simulation group for advanced photon science

Mitsuru YAMAGIWA, Akira SASAKI, James KOGA, Kengo MORIBAYASHI, Yutaka UESHIMA, Takayuki UTSUMI, Takao KONDOU, Timur ESIRKEPOV, Sergei BULANOV [a)], Toshiki TAJIMA

a) General Physics Institute of Russian Academy of Sciences

Some of recent activities of the simulation group for advanced photon science are reported, in conjunction with high field science (radiation damping effect and light intensification by two laser pulses), computational science (data and task management system for large-scale simulation), and atomic process and x-ray generation (basis set approach in the CIP method for accurate solutions of the Schrodinger equation, opacity of the Xe plasma, and x-ray emission from inner-shell ionization).

A strong effect of radiation damping on the interaction of an ultraintense laser pulse with an overdense plasma slab has been found and studied via a relativistic particle-in-cell simulation including ionization. Hot electrons generated by the irradiation of a laser pulse with a radiance of $I\lambda^2 > 10^{22}$ $W\mu m^2/cm^2$ and duration of 20 fs can convert more than 35% of the laser energy to radiation. This incoherent x-ray emission lasts for only the pulse duration and can be intense. The radiation efficiency is shown to increase nonlinearly with laser intensity. Similar to cyclotron radiation, the radiation damping may restrain the maximal energy of relativistic electrons in ultraintense-laser-produced plasmas.

A method to generate ultrahigh intense electromagnetic fields has been suggested, based on the laser pulse compression, carrier frequency upshift, and focusing by a counterpropagating breaking plasma wave, relativistic flying parabolic mirror. This method allows us to achieve the quantum electrodynamics critical field (Schwinger limit) with present-day laser systems.

A prototype of the data and task management system for advanced photon simulation has been developed. This system named as Distributed Discovery Director (D-cube), controlling a file sever, a backup server, a visualization/analysis server, a database server, a Web server, is expected to promote executing large-scale simulation.

A simple polynomial basis-set that is easily extendable to any desired higher-order accuracy to solve the Schrodinger equation has been proposed. This method, i.e. the CIP-BS method, is based on the Constrained Interpolation Profile (CIP) method and straightforwardly extended for solving various linear and nonlinear partial differential equations in the study of the dynamics of a broad spectrum of complex physical processes.

The atomic code and database originally developed for the X-ray laser research has been found to be useful for the development of extreme-ultra violet light (EUVL) source. The opacity of Xe plasma, which determines the maximum radiation flux from the plasma, has been investigated through detailed analysis of the atomic structure. Comparison with experimental emission spectrum has been found to useful to improve the accuracy of the atomic calculations, which will also improve the reliability of modeling x-ray lasers.

The x-ray emission from the inner-shell states of S and Fe ions excited by black-body radiation has been studied. At a low temperature, the x-ray intensities from inner-shell excited states are smaller than that of He α. However, at high temperature, both are almost the same. From this feature, we may understand the temperature of the black-body radiation. This may be applied to the analysis of the x-ray emission from x-ray binary stars. Namely, the atomic data along with the inner-shell ionization processes may be useful for astrophysics as well as inner-shell ionization x-ray lasers.

4.6.1 Radiation damping and the effects on the interaction of ultra-intense laser pulses with an overdense plasma

Alexei ZHIDKOV [a)], James KOGA, Akira SASAKI, Mitsuru UESAKA [a)]

a) Nuclear Engineering Research Laboratory, Graduate School of Engineering, The University of Tokyo

1. Introduction

The recent advance of the high-power, short pulse laser technique allowing laser intensities over 10^{20} W/cm^2 [1)] makes the study of relativistic effects in the interaction of such laser pulses with high-Z matter interesting for various applications[1)]. With a laser pulse energy of about 1 kJ[1)] and a pulse duration of 20 fs, the laser intensity can exceed 10^{22} W/cm^2 which is critical for well known relativistic effects such as radiation damping[2)]. We have observed the strong effect of radiation damping on the interaction of an ultra-relativistic laser pulse with overdense plasmas via a fully relativistic particle-in-cell simulation.[3)]

2. Theory

The electron self-interaction problem, radiation damping (RD), is central to both classical and quantum electrodynamics[2)]. In ordinary plasmas, the effect of RD is negligible because the plasma field usually is not strong enough for radiation to dominate the particle motion. However in overdense plasmas, the RD can become important due to Thomson scattering. Roughly, the RD force and the Lorentz force are comparable at the normalized laser amplitude of $a_0=((3/\pi)\lambda/r_e)^{1/5}$ where $a_0=eE_0/mc\omega$, E_0 is the amplitude of the electromagnetic wave and ω is the laser frequency, r_e is the classical electron radius and λ is the laser wavelength[3)]. This corresponds to an intensity of 10^{22} W/cm^2 for a 1μm laser.

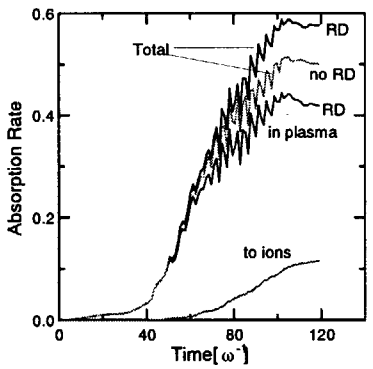

Fig. 1 Evolution of the absorption rate with (RD) and without (no RD) radiation damping. I=5x10^{22} W/cm^2, the plasma corona gradient is 1.7 μm.

3. Results

We performed fully relativistic 1D particle-in-cell simulations with mobile ions for a Cu slab irradiated by a normally incident laser pulse including plasma ionization and the radiation damping in the form of Dirac-Lorentz equation3). The laser intensity is varied from 10^{22} –10^{23} W/cm^2, λ=0.8 μm, and the pulse duration is 20 fs. The prepulse effect is included through the initial condition for the plasma density. The thickness of the plasma slab is 3 μm with a maximal ion density N_i=9x10^{21} cm^{-3}. The density profile of the plasma corona is an exponential profile with gradients of 1.7μm. For I< 10^{22} W/cm^2 we observe no radiation damping effect during the laser irradiation. For I=10^{22} W/cm^2, the plasma energy loss to radiation is only 0.2%. The effect of radiation becomes strong at I=5x10^{22} W/cm^2. Absorption rates of the Cu plasma are shown in Fig. 1. The total absorption rate is the total pulse energy minus the current electromagnetic pulse energy normalized to the total pulse energy. 55% of the laser energy is absorbed with 40% of the laser energy remaining in the plasma in the form of kinetic and electrostatic field energy after reflection of the laser pulse (indicated by 'in plasma' in the figure). The total absorption rate is 7% higher in the presence of RD than that without. The effect of radiation damping considerably increases with the laser intensity. At I=10^{23} W/cm^2, 35% of the absorbed laser energy is converted to plasma radiation. In conclusion, we have found that more than 35% of the laser energy can be converted to a X-ray burst at a laser irradiance of $I\lambda^2$=5x10^{22} W μm^2/cm^2 during the laser irradiation. Such a short pulse intense X-ray burst source can have many uses.

References

1) S. P. Hatchett, C.G. Brown, T.E. Cowan *et al.*, Phys. Plasmas **7**, 2076 (2000).
2) L.D. Landau, E.M. Lifshits, The Classical Theory of Fields (Pergamon, NY,1994).
3) A. Zhidkov, J. Koga, A. Sasaki, and M. Uesaka, Phys. Rev. Lett. **88**, 185002 (2002).

4.6.2 Light intensification towards the Schwinger limit

Sergei V. BULANOV [a)], Timur ESIRKEPOV and Toshiki TAJIMA
a) General Physics Institute of Russian Academy of Sciences

1. Introduction

We present the first method, which allows us to achieve the quantum electrodynamics critical field in the laboratory frame with present-day technology. Possible experiments based on our scheme can lead to new great achievements in the high-energy physics.

We examine the following scenario. A short intense laser pulse (the "*driver* pulse") induces wakefield in a plasma. As it is well known, the wakefield phase velocity $v_{ph}=\beta_{ph}c$ equals the laser pulse group velocity, which is close to the speed of light in a vacuum when the laser pulse propagates in the underdense plasma. The corresponding Lorentz factor is $\gamma=(1-v_{ph})^{-1/2}\sim\omega_d/\omega_{pe}$, where ω_d is the *driver* pulse frequency, ω_{pe} is the Langmuir frequency. The nonlinearity of strong wakefield causes a nonlinear wave profile, including a steepening of the wave and formation of localized maximums in the electron density — the spikes. This amounts to **wavebreaking regime** (see Ref. 1 and references therein). Theoretically the electron density in the spike tends to infinity, but remains integrable[1)]. Sufficiently weak counter-propagating laser pulse (the "*source* pulse") will be partially reflected from the density maximum. The reflection coefficient scales as γ_{ph} and the reflected wave vector-potential scales as γ_{ph}^{-3}, as it is shown in[1),2)]. As we see, the electron density maximum acts as a mirror flying with the relativistic velocity $v_{ph}\sim c$. The frequency of the reflected radiation is up-shifted by factor $(1+\beta_{ph})/(1-\beta_{ph})\sim 4\gamma_{ph}^2$, in accordance with the Einstein formula. It is important that the relativistic dependence of the Langmuir frequency on the *driver* pulse amplitude causes parabolic bending of constant phase surface of the plasma wave, since the *driver* pulse has a finite transverse size[1)]. As a result, the surface where the electron density is maximal has a shape close to a paraboloid. Because we have a curved mirror, the frequency $\tilde{\omega}_s$ of the reflected radiation depends on the angle: $\tilde{\omega}_s\sim\omega_s(1+\beta_{ph})/(1-\beta_{ph}\cos\theta)$, where ω_s is the *source* pulse frequency, and θ is the angle between the reflected wave vector and the direction of the driver pulse propagation in the laboratory frame. The curved mirror focuses the reflected light. The focal spot size is of the order of the diffraction limited size. In the reference frame of the wakefield it is $\lambda?_s=\lambda_s\times((1-\beta_{ph})/(1+\beta_{ph}))^{1/2}\sim\lambda_s/2\gamma_{ph}$, where λ_s is the wavelength of the *source* pulse. In the laboratory frame the focal spot size is approximately $\lambda_s/4\gamma_{ph}^2$ along the paraboloid axis, and $\sim\lambda_s/2\gamma_{ph}$ in the transverse direction. In the focal spot the resulting intensity gain factor scales with γ_{ph} as $\gamma_{ph}^{-3}\times(\tilde{\omega}_s/\omega_s)^2\times(D_s/\lambda?_s)^2=64(D_s/\lambda_s)^2\times\gamma_{ph}^3$, where D_s is the diameter of the efficiently reflected portion of the *source* pulse beam. Theoretically, the actual gain can be even greater, because (a) this estimation corresponds to one-dimensinal case, whereas the density modulation in the 3D breaking wakewave is stronger, (b) the reflectance of the 3D paraboloidal mirror is greater at the periphery. Thus the intensity of the reflected light in the focus can be huge, even up to the QED critical electric field.

We consider the following example. A one-micron laser pulse (*driver*) generates wakefield in a plasma with density $n_e=10^{17}\mathrm{cm}^{-3}$. The corresponding plasma wavelength is $\lambda_p\sim100$ μm. The Lorentz factor, associated with the phase velocity of the wakefield, is estimated as $\gamma_{ph}\sim\omega_d/\omega_{pe}\sim100$. The counter-propagating one-micron laser pulse with intensity $I_s=10^{17}\,\mathrm{W/cm}^2$ (*source*) is partially reflected and focused by the wakefield cusp. If the efficiently reflected beam diameter is $D_s=200$ μm, then the final intensity in the focal spot is $\tilde{I}_s=1.3\times10^{29}\,\mathrm{W/cm}^2$. The *driver* pulse intensity should be sufficiently high and its beam diameter should be enough to give such a wide mirror, assume $I_d=10^{18}\,\mathrm{W/cm}^2$ and $D_s=800$ μm. Thus, if both the *driver* and *source* are one-wavelength pulses, they carry 17 J and 0.1 J, respectively. We see that in an optimistic scenario the QED critical electric field may be achieved with the present-day laser technology!

2. Simulation

To demonstrate the feasibility of the effect of the light reflection and focusing by the breaking wakewave, we performed three-dimensional particle-in-cell (PIC) simulations using the code REMP. In the simulations the *driver* pulse propagates in the direction of the x-axis. Its dimensionless amplitude is $a_d=1.7$ corresponding to peak intensity $I_d=4\times10^{18}\,\mathrm{W/cm}^2\times(1\mu\mathrm{m}/\lambda_d)^2$, where λ_d is the *driver* wavelength. The *driver* is linearly polarized along the z-axis, it has the gaussian shape, its FWHM size is $3\lambda_d\times6\lambda_d\times6\lambda_d$. The *source* pulse propagates in the opposite direction. Its wavelength $\lambda_s=2\lambda_d$. The *source* pulse amplitude is chosen to be small, $a_s=0.05$, to reduce the distortion of the wakewave. The pulse shape is rectangular in the x-direction and Gaussian in the transverse direction, its size is $6\lambda_d\times6\lambda_d\times6\lambda_d$. To distinguish the

electromagnetic radiation of the *driver* from the *source* pulses, we set the *source* pulse to be linearly polarized in the direction perpendicular to the *driver* polarization, i. e. along the *y*-axis. The laser pulses propagate in the underdense plasma slab with the electron density $n_e=0.09n_{cr}$, so the Langmuir frequency $\omega_{pe}=0.3\omega_d$. The plasma slab is localized at $2\lambda_d<x<13\lambda_d$ in the simulation box with size $22\lambda_d \times 19.5\lambda_d \times 19.2\lambda_d$. The simulations were carried out on 720 processors of the supercomputer HP Alpha Server SC ES40 at JAERI Kansai. The mesh size is $dx=\lambda_d/100$, total number of quasiparticles is 10^{10} (ten billion). The boundary conditions are absorbing on the *x*-axis and periodic in the transverse directon, both for the electromagnetic fields and quasi-particles. We emphasize that the simulation grid must be and in fact was chosen to be fine enough to resolve the huge frequency up-shift, exhausting all the supercomputer resources.

Figure 1a shows the plasma wakewave induced by the *driver* laser pulse as modulations in the electron density. We see the electron density cusps in the form of paraboloids. They move with velocity $v_{ph}\approx 0.87c$, the corresponding gamma-factor is $\gamma_{ph}\approx 2$. It is important that the wakewave dynamics is close to wave-beaking regime. Each electron density maximum forms a semi-transparent parabolic mirror, which reflects a part of the *source* pulse radiation.

Figure 1b shows the electric field components. The *driver* pulse is seen in the cross-section of the *z*-component of the electric field in the $(x,y,z=0)$-plane. The *source* pulse and its reflection is seen in the cross-section of the *y*-component of the electric field in the $(x,y=0,z)$-plane. The part of the *source* pulse radiation is reflected from the flying paraboloidal mirrors, then it focuses yielding the peak intensity in the focal spot, and finally it defocuses and propagates as a spherical short wave train, whose frequency depend on the wave vector direction, in agreement with mentioned formula. The main part of the reflected light power is concentrated whithin the angle $\sim 1/\gamma_{ph}$, hence this coherent high-frequency beam resembles a searchlight. The wavelength and duration of the reflected pulse are approximately 14 times less than the wavelength and duration of the *source* pulse, in agreement with the Einstein formula since $(1+\beta_{ph})/(1-\beta_{ph}) \approx 14.4$. The intensity increases 256 times in agreement with our estimation.

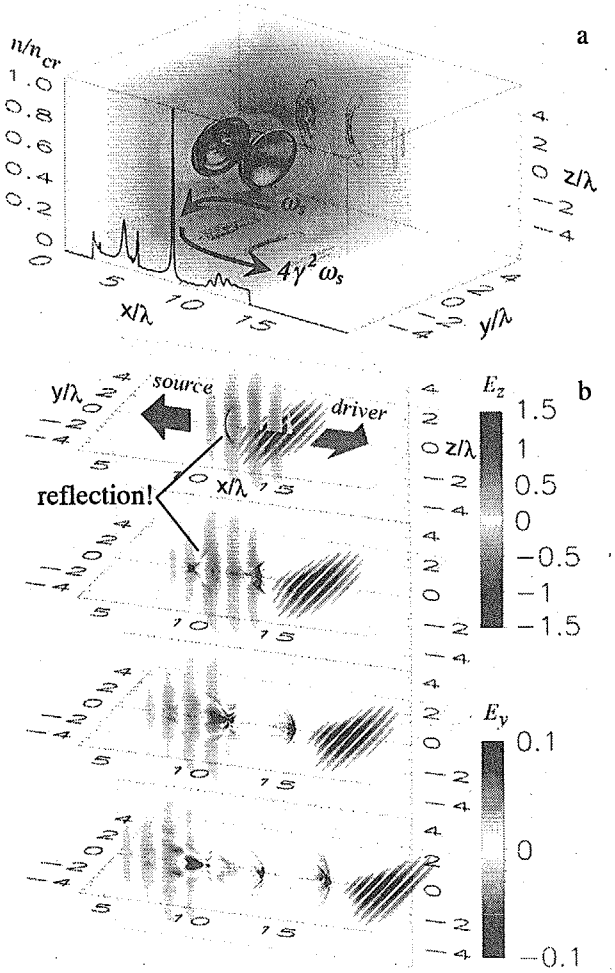

Fig. 1 a) The electron density in the wake of the *driver* laser pulse at $t=14\times 2\pi/\omega_d$
b) The cross-sections of the electric field components
The $(x,y,z=0)$-plane: $E_z(x,y,z=0)$, the plane $(x,y=0,z)$: $E_y(x,y=0,z)$ at t = 16, 18, 20, $22\times 2\pi/\omega_d$ (top-down)

Similar processes may occur in laser-plasma interation spontaneously, e.g. when a short laser pulse exciting plasma wakewave is a subject of the stimulated backward Raman scattering or a portion of the pulse is reflected back from the plasma inhomogeneity. Then the backward scattered electromagnetic wave interacts with plasma density modulations in the wakewave moving with relativistic velocity. According to scenario described above, the electromagnetic radiation, reflected by the wakewave, propagates in the forward direction as a high-frequency strongly collimated (within the angle $\sim 1/\gamma_{ph}$) electromagnetic beam.

References

1) S. V. Bulanov, et. al. in: Reviews of Plasma Physics. Vol. 22, ed. by V.D. Shafranov (Kluwer Academic / Plenum Publishers, NY, 2001), p. 227.
2) S. V. Bulanov, T. Esirkepov,T. Tajima, Phys. Rev. Lett. **91**, 085001 (2003).

4.6.3 Data and Task Management System for Large-Scale Simulation

Yutaka UESHIMA, Takao KONDOU, Daisuke WAKABAYASHI[a)] and Toshiki TAJIMA
a) Research Organization for Information Science and Technology

1. Data and Task Management for Large-Scale Simulation

It is difficult for heuristic research via computer simulation to specify an important output before the simulation. The tendency is that the variety, amount, and size of the output data grow rapidly when heuristic research via large-scale simulation is performed. A lot of processing is needed in order for a researcher to understand the many kinds, large amount, and large size of data. It becomes difficult to manage, since these data must be stored in a dispersed manner.

The output of such a large-scale simulation needs processing with distributed resources, and forces complicated monotonous work on a researcher. On the other hand, distributed resources can be operated now in a single system image with Web technology, which developed quickly after the IT revolution. If the data can be accessed from the Web, it becomes possible for many remote researchers to participate in the research. Consequently, the sharing of large-scale simulation data, which has not been realized so far, will be possible.

In order to construct such an environment, the problems of analysis, data movement, format conversion, and the upload to the Web, etc. must be solved. When these tasks are done one by one after a large-scale simulation is completed, the time to be spent will be about 10 times as long as the time spent on the simulation itself. A large-scale simulation has other problems in the trial-and-error analysis. Since the amount of data becomes immense, it is very difficult to grasp "which file is for what data" and "what analysis / visualization processing has been performed".

Therefore, we have developed the data and task management system which uses Web technology as a base, in order to conquer the difficulty accompanying heuristic large-scale simulation research.

2. Distributed Discovery Director

A large-scale data management system, D-cube (Distributed Discovery Director), is under development to overcome the difficulty of heuristic large-scale simulation. D-cube was named with the meaning of managing distributed data and resources and directing discovery.

D-cube is described by "SHELL" and "PERL". Now, the server groups currently controlled have eight kinds of functional servers, i.e., a massively parallel computer, a parallel computer for testing, a file server, a backup server, a visualization / analysis server, a database server, a Web server, and a control server. Consequently, all research processes, such as planning of a simulation, trial-analysis, and past information retrieval, can be now performed asynchronously in parallel and at high speed. In addition, the procesess can now also be reproduced by database management.

D-cube is mounted in the progressive parallel plasma code(P-cube) which is used in advanced photon simulation research of the Japan Atomic Energy Research Institute, and the following functions can be operated from the Web browser.

1) The environment (execution computer, visualization servers, database server, and file storage directory, etc.) for executing the simulation can be set.

2) The system parameters concerning the JOB queuing of the simulation (Queue class etc.) can be set.

3) The input parameter of the code can be set.

4) It is possible to call the input data of a finished simulation from a database, and re-perform the simulation.

5) The simulation JOB can be queued with a restart function. There are three modes of queuing. These are

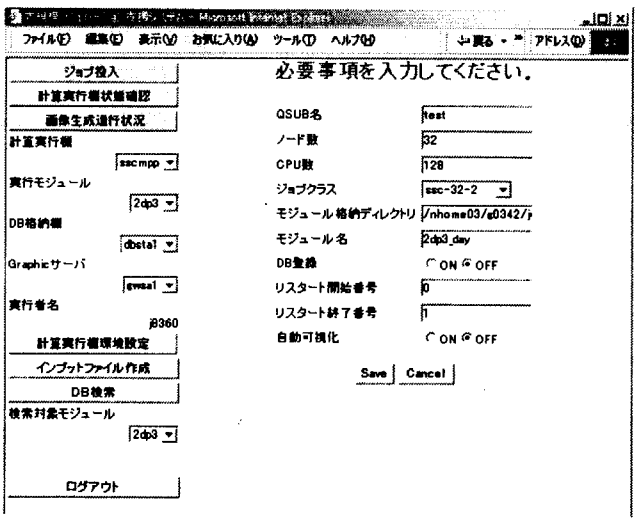

Fig. 1 Setting screen of the environment and JOB control

fulyl-automatic mode (simulation, visualization and all of other needed processes), simulation mode (simulation and other needed processes), and re-visualization mode (visualization and other needed processes).

6) Making of necessary directories and file copying are done automatically.

7) Up-loading to the Web and making of the html are done automatically.

8) The format conversion of the visualized data and making of thumbnails are done automatically.

9) The parameter for the visualization and the analysis can be done.

10) The process of the simulation JOB and the automatic execution task can be followed and confirmed.

11) Standard output and error output of the simulation can be displayed on the Web browser.

12) The log of the automatic execution task can be displayed.

13) Backup and restore of all data not only including analysis data but also the execution environment etc. is possible.

14) The login and logout functions are provided.

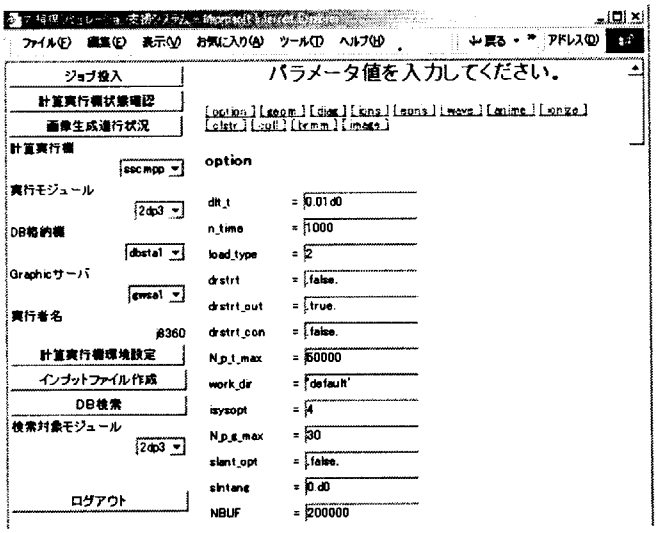

Fig. 2 Setting screen of the input of the simulation

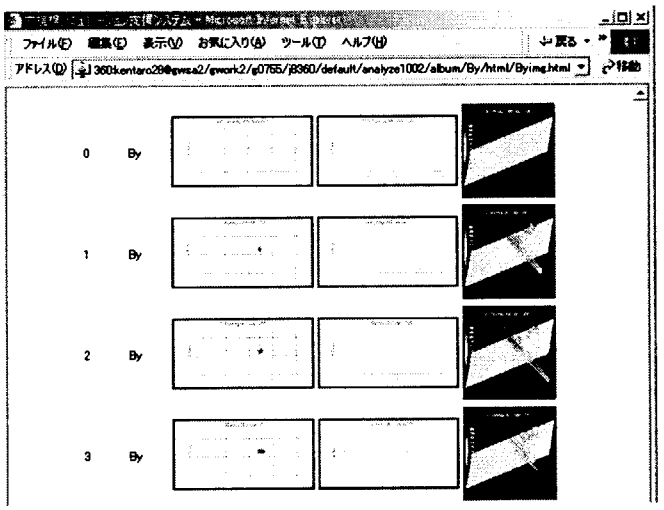

Fig. 3 View screen of the visualization data

3. Future work

The D-cube is mounted only in P-cube now. Moreover, generality and maintainability are not at a high level, and it is difficult to transplant the present version to other systems and functions. Therefore, it will be divided into a general part and a special part and redesigned to restructure all components with JAVA. The main functions to restructure are as follows.

1) Although commands are sent to the remote computer by "RPC" in the present version, it is becoming impossible to use "RPC" with the present security. Therefore, more secure communication such as SSH, SCP, and SOAP will be used.

2) Although control of servers is static in the present version, a function of procedure control based workflow table will be added and control of the servers will be dynamic.

3) Distributed processing of database and visualization processing etc. will be performed and improvement in the speed and a failover function will be added.

4) The present interface is only a Graphical User Interface, GUI. With the VT emulator in the Web browser the Command Line Interface, CLI will be used.

Moreover, the points which should be taken into consideration in these system configurations are as follows. Since improvement in the speed and massive parallelization should be done with the highest priority, the D-cube system must be made so that a simulation program can be managed with the minimum correction. Moreover, modification of a simulation program must be a rapid process in heuristic research and the system must follow the program changes easily.

4.6.4 Accurate solutions of the Schrodinger equation by the basis set approach in the Constrained Interpolation Profile Method

Takayuki UTSUMI, James KOGA, Takashi YABE[a)], Takayuki AOKI[a)], Masatoshi SEKINE[b)]

a) Tokyo Institute of Technology
b) Tokyo University of Agriculture and Technology

1. Introduction

There is a growing interest in the accurate solutions of the excited states of atoms and their time dependent solutions for computational design of material properties, catalysis, medical drugs, and so on, or for elucidating non-linear phenomena in strong interactions.

We have proposed[1)] a simple polynomial basis-set that is easily extendable to any desired higher-order accuracy to solve the Schrodinger equation. This method, i.e. the CIP-BS method, is based on the Constrained Interpolation Profile (CIP) method[2)] and the profile is chosen so that the subgrid scale solution approaches the real solution with the constraints from the spatial derivative of the original equation. Thus the solution even on the subgrid scale becomes consistent with the master equation. By increasing the order of the polynomial, this solution quickly converges. The Schrodinger equation is transformed into the discretized form by taking scalar products with each basis function. In this formulation, the singularities due to the kinetic operator or the Coulomb potential at the origin are eliminated in the Hamiltonian, and the boundary conditions are imposed with a one-to-one correspondence to the analytical ones. 3rd and 5th order polynomials are tested on the one-dimensional Schrodinger equation and are proved to give solutions a few orders of magnitude higher in accuracy than conventional methods for lower-lying eigenstates.

2. Numerical solutions

We consider the eigenvalue spectrum for the radial Schrodinger equation of the hydrogen atom. The system size is set to 1000.0 a.u. in order to obtain sufficient precision for states with a high principal quantum number n. In Table I, we present the results of energy levels for s-, p-, and d-orbitals. Here the grid interval is 1.0 a.u. and the boundary condition $\varphi(0)=\varphi(r_N)=0$ is imposed for this eigenvalue problem. We can see from samples of the calculated orbitals shown in figure 1 that the derivatives contained in the eigenvectors are solved consistent with the eigenfunctions. The results show excellent agreement with the analytical spectrum. It should be emphasized that the singularities due to the kinetic operator and the Coulomb potential at r=0 are eliminated in the Hamiltonian by taking the scalar product.

Table I Relative errors of energy levels of bound states of the hydrogen atom with the CIP-BS[2] method

no.	analytical	l =0	l =1	l =2
1	-0.5	8.21E-09		
2	-0.125	2.77E-10	8.16E-11	
3	-0.05556	7.34E-11	3.10E-11	1.40E-12
4	-0.03125	3.88E-11	1.48E-11	3.63E-13
5	-0.02	2.37E-11	3.12E-11	6.25E-12
10	-0.005	2.17E-12	3.14E-12	7.90E-12
15	-0.00222	1.11E-11	1.49E-11	5.34E-12

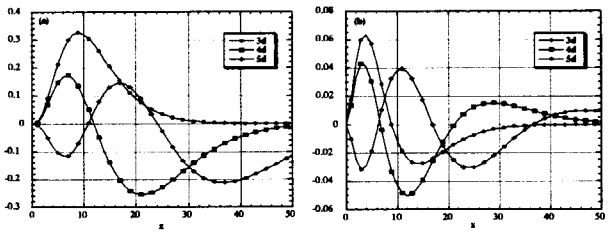

Fig. 1 The calculated (a) eigen functions and (b) their first derivatives for the *3d,4d,5d* orbitals of the hydrogen atom They are not normalized nor interpolated.

3. Conclusions

The CIP method has provided accurate solutions for various differential equations, especially for hydrodynamics, and the CIP-BS method is more attractive for the analysis of quantum mechanical processes. It is straightforwardly extended for solving various linear and nonlinear partial differential equations in the study of the dynamics of a broad spectrum of complex physical processes.

References

1) T. Utsumi, J. Koga, T. Yabe[a)], T. Aoki[a)], M. Sekine, submitted to Computer Phys. Comm..
2) T. Yabe and T. Aoki, Computer Phys. Comm., **66**, 219, 1991.

4.6.5. Theoretical investigation of the opacity of the Xe plasma

Akira SASAKI

1. Introduction

The spectral characteristics of Xe is reported, which is interesting for the extreme ultra-violet light (EUVL) source for the semiconductor technology. The atomic structure of near Pd-like Xe (Xe^{8+}) is investigated using the HULLAC code to show the high density Xe plasma has a large opacity in the 13.5nm band. The atomic process calculations are shown to be useful for developing an efficient EUV source.

2. Model

The energy level and radiative rate of Xe^{6+} and Xe^{12+} are calculated using the HULLAC code[1]. The emissivity, opacity and radiation flux from the surface of the plasma are calculated assuming a uniform plasma sphere in the local thermodynamic equilibrium (LTE). Population distribution of the Xe ion is calculated using the Saha-Boltzman relation. Figure 1 shows the energy level diagram of Xe^{9+}. Xe^{9-17+} ions have similar level structure[2] so that strong emission occurs through 4d-4f and 4d-5p resonance lines. On the other hand, as in high density plasmas ($n_e>10^{20}/cm^3$), the emission and photo absorption through satellite lines become significant. The effect of every possible absorption channel is investigated.

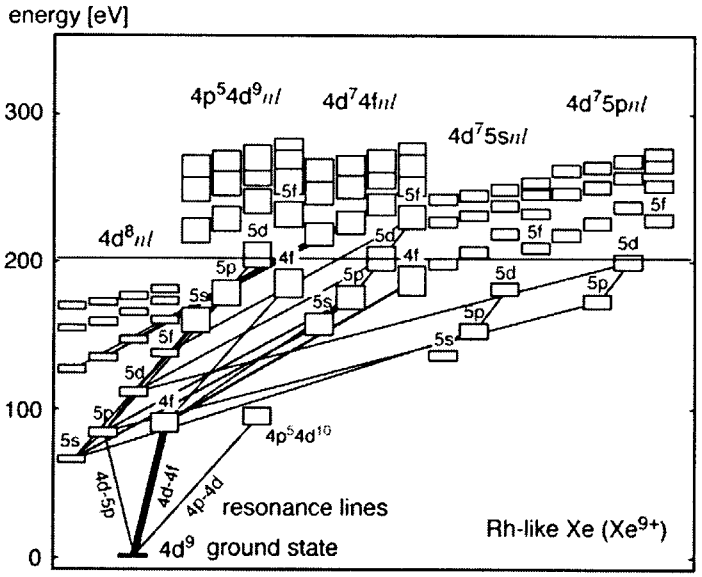

Fig. 1 The energy level diagram of Xe^{9+}

3. Result and discussion

It is found that the 4d-4f satellites between $4d^8nl$ to $4d^74fnl$ configurations determine the opacity and emission of the 11nm band, whereas the 4d-5p satellite lines originating from $4d^75pnl$ configurations and the 4p-4d satellite lines originating from $4p^54d^9nl$ determine the opacity of the 13.5nm band.

Figure 2 shows the emissivity and opacity of the Xe plasma. The maximum opacity in the 13.5nm band appears to be 10^3/cm. Although the emission at 13.5nm band is previously attributed to 4d-5p transition of Xe^{10+} [3], 4p-4d and 4d-5p satellites are found to produce the observed red wing structure of the 4d-4f transition array. This result also implies the maximum radiation flux determined by the Planck radiation can be obtained from laser produced Xe plasmas with moderate thickness.

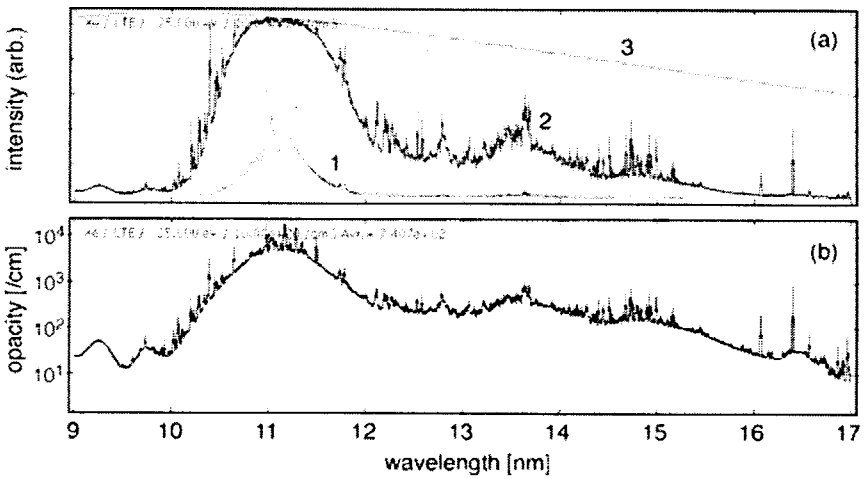

Fig. 2 (a) (1)Emissivity, (2)radiation flux at the surface of the plasma relative to the (3)Planck radiation, and (b) opacity of the Xe plasma, for $n_e=10^{21}/cm^3$, $T_e=25eV$, $r=10\mu m$

References

1) M.Klapisch et al., J. Quant. Spectrosc. Radiat. Transf. **58**, 687 (1997).
2) A.Sasaki, J. Plasma Fusion Res. **79**, 315 (2003).
3) J. Blackburn et al., J. Opt. Soc. Am. **73**,1325 (1983).

4.6.6 X-ray emission from inner-shell ionization of Ne-like ions

Kengo MORIBAYASHI, Takashi KAGAWA[a)] and Dong Eon KIM[b)]

a) Department of Physics, Nara Women's University
b) POSTECH, Korea

1. Introduction

The inner-shell ionization processes, which are produced by high intensity x-ray sources, have been considered to be useful methods for x-ray laser emission.[1-5] The x-ray sources also play an important role in x-ray astrophysics. Recently, the 'photo-ionized plasmas' have been paid attention to in x-ray binary star system such as CygmusX-3,[6,7] where a normal star is located near a neutron star (NS) or a black hole (BH) and a lot of atoms or ions are transferred from the star to the NS (BH) via accretion due to gravitation. On the other hand, high intensity x-rays are emitted from the NS (BH). After ions are inner-shell photo-ionized by x-rays, the characteristic x-rays may be emitted from inner-shell excited states (IES) of ions. From these x-rays, we may understand the ionized states of stars and the temperature of the x-rays emitted from the NS (BH). Until now, only the Lyα, Heα, and Kα x-rays from heavy ions such as Si, S and Fe have been discussed because the x-ray detector has only a low resolution in the satellites 'Chandra' or 'Asca'.[6,7] The x-ray emission from IES is expected to become important for the analysis of the x-ray sources in the x-ray binary stars because the satellite 'Astro-E2' will be launched in future, which has an x-ray detector with a higher resolution.[8] In this paper, we calculate the x-ray spectra emitted from IES of S and Fe ions in black-body radiation.

2. Atomic processes

The initial state of ions is assumed to be the ground state of Ne-like ion. We consider photo-ionization, radiative transition, and auto-ionization processes. We have calculated atomic data of theses processes for Ne-like ions using Cowan's code.[9] For other ions, we employ the empirical formula[4,10] in order to simplify the model. By using these atomic data, we solve the following equation for the rate of change of concentration of various atomic states:

$$\frac{dN_k}{dt} = -\alpha_k N_k + \sum_{m(>k)} \beta_{mk} N_m , \qquad (1)$$

where N_k, α_k and β_{mk} are the population, decay constant in the k state, and the transition rate from the m state to k state, respectively. The photon number is given by

$$P_k = \int_0^\infty N_k Ar dt , \qquad (2)$$

where Ar is the radiative transition probability from the IES.

3. Results and discussions

The x-ray intensities emitted from the IES may give important information to astrophysics as mentioned above. Here we show our results of the x-ray intensities emitted from inner-shell states excited by black-body radiation.

Figures 1(a) and (b) show x-ray intensities as functions of the averaged x-ray energies emitted from IES and He-like ions of S and Fe, respectively. The symbols are for cases of various temperatures (T_B) of the black body radiation. In Fig.1(a), the x-ray intensities from IES of Ne-like ions are much smaller than that from the He-like ion (the largest photon energy) for T_B<3 keV. On the other hand, for T_B≥3keV, both intensities are almost the same. This comes from the fact that as T_B increases, the inner-shell-photo-ionization rates become larger that is, they are comparable to or larger than other rates such as auto-ionization, radiative transition, outer-shell ionization for T_B≥3keV.[4] In Fig.1(b), almost the same feature as Fig.1(a) is found. Namely, the x-ray emission from the He-like ions dominates at low T_B, while that from the IES is comparable to that from the He-like ion at high T_B. At high T_B, the x-ray intensities from IES of Ne-like Fe ions (see Fig.1(b)) are larger than those of Ne-like S ions (Fig.1(a)), which is due to the fact that branching ratio between the radiative transition probability and autoionization rate (Aa) from the IES, that is, $Ar/(Aa+Ar)$, becomes larger. Figure 1 indicates that the x-ray spectra from

the IES inform us of the temperature of the black-body radiation. This may be useful for astrophysics because the satellite 'Astro-E2' will be able to measure these x-rays emitted from x-ray binary stars. In this paper, we have used the atomic data derived from the empirical formula and the averaged photon energies. For comparison with the real spectra, more detailed atomic data are required.

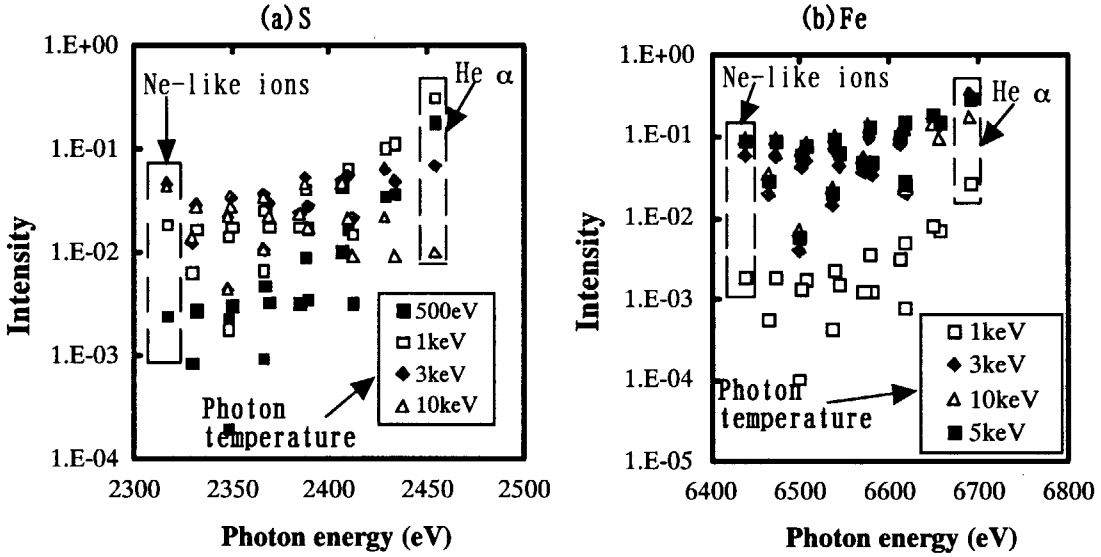

Fig. 1 X-ray intensity vs. photon energy (eV) emitted from the inner-shell excited states for various photon temperatures of the black body radiation; (a) S ions, (b)Fe ions Enclosed by dashed lines are the x-ray emissions from inner-shell excited states of Ne-like (left side) and Heα (right side).

4. Conclusions

We have studied the x-ray emission from Ne-like S and Fe ions to apply for astrophysics. We have calculated the x-ray intensities from the inner-shell excited states of Ne-like to Li-like ions and He α. The intensity of He α is much larger than those of the inner-shell excited states of Ne-like ions for a low temperature of less than 3 keV. On the other hand, for temperature of more than 3keV, they are almost the same. This feature may inform us of the temperature of x-rays emitted from x-ray binary stars. For the analysis of the x-ray binary stars, more detailed atomic data may be required.

Acknowledgements

We wish to thank to Profs. T. Tajima, H. Takabe, N. Kawai, and Drs. T. Dohtani, M. Nishiuchi, J. Koga, and M. Yamagiwa for their useful discussions.

References

1) M.A.Duguay and M.Rentzepis, Appl.Phys.Lett.**10**, 350, 1967
2) H.C.Kapteyn, Applied Optics **31**, 4391, 1992
3) S.J.Moon, D.C.Eder, and G.L. Strobel, AIP Conference Proceedings **332**, 262, 1994
4) K. Moribayashi, A.Sasaki, and T.Tajima, Phys.Rev.A **58**, 2007, 1998
5) K. Moribayashi, A.Sasaki, and T.Tajima, Phys.Rev.A **59**, 2732, 1999
6) F. Paerels, *et al.,* Astrophysical J. **553,** L135, 2000
7) D.A, Liedahl and F. Paerels, Astrophysical J. **468**, L33, 1996
8) Private communication to N. Kawai.
9) R.D. Cowan, J.Opt.Soc.Am. **58**, 808, 1968
10) K. Suto and T. Kagawa, Phys. Rev. A **58**, 5004, 1998

4.7 High power laser applications

Hiroyuki DAIDO

We are investigating the ultra-high intensity laser-matter interaction physics especially for the relativistic plasma phenomena such as a few MeV x-ray and particle generation and their applications. During this fiscal year, we have obtained energetic electrons and protons (>1MeV) produced by focusing a 50fs high intensity Ti Sapphire laser pulse at the intensity of $>10^{18}$W/cm^2. Ultra-high intensity short pulse lasers also contribute to the various fields such as pump probe measurement for ultra-fast phenomena in crystalline or non-crystalline materials and coherent control of chemical reactions both of which have been performed theoretically and experimentally in the Advanced Photon Research Center. In this section, we will introduce the present status of the projects on the high intensity physics applications of the ultra-short high intensity lasers. One of the most attractive applications of this project is schematically shown in Fig.1. We hope to obtain a few tens of MeV protons using such a small and safe installation which can be applicable to the injector of a cancer therapy accelerator and a small table top accelerator for material engineering and so on. We can also make a plan to build a laser driven cancer therapy machine which can deliver a few hundred MeV protons without conventional accelerator devices.

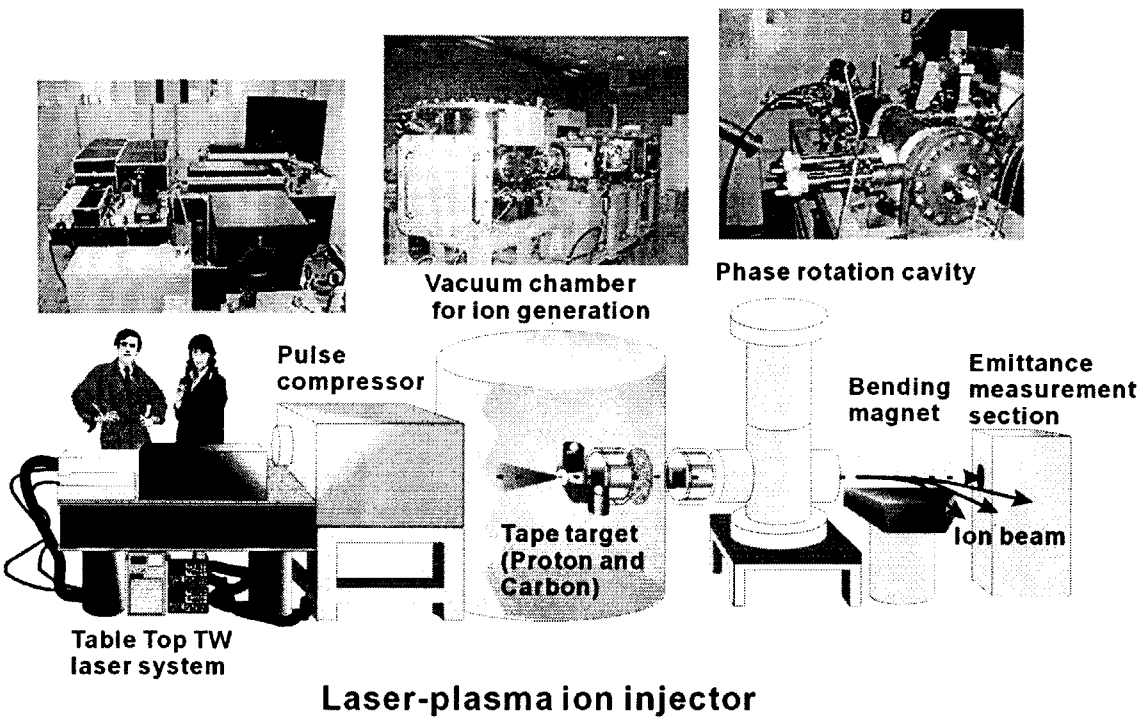

Fig. 1 Schematic drawing of the table-top laser driven ion generator

4.7.1 Development of laser-driven ion source for compact cancer therapy accelerator

Atsushi FUKUMI[a)], Hiroyuki DAIDO, Koji MATSUKADO[a)], Zhong LI[a)], Yukio HAYASHI, Mamiko NISHIUCHI, Satoshi ORIMO, Takayuki UTSUMI, Sergei BULANOV, Timur ESIRKEPOV, Toshiki TAJIMA, Mitsuru UESAKA[b)], Koji YOSHII[b)], Takahiro WATANABE[b)], Tomonao HOSOKAI[b)], Ken-ichi KINOSHITA[a,b)], Alexei ZHIDKOV[a,b)], Akira NODA[c)], Yoshihisa IWASHITA[c)], Toshiyuki SHIRAI[c)], Shu NAKAMURA[c)], Atsushi YAMAZAKI[c)], Atsushi OGATA[d)], Yoshio WADA[d)], Tetsuo KUBOTA[d)] and Akio MORITA[e)]

a) National Institute of Radiological Sciences
b) Nuclear Engineering Research Laboratory School of Engineering, University of Tokyo
c) Institute for Chemical Research, Kyoto University
d) Graduate School of Advanced Sciences of Matter, Hiroshima University
e) High Energy Accelerator Research Organization

1. Introduction

Protons or heavy ions can provide a prospective means for cancer therapy owing to their characteristic depth dose distribution in body, so called Bragg peak. Many medical facilities using proton or heavy ion accelerators have been working all over the world. A laser-driven ion source can play a role of compact ion injector and enables to reduce the size of the accelerator[1)]. This would contribute to the wider spread of cancer therapy facilities. We have then started a project for developing a compact ion accelerator for cancer therapy.

It is well known that energetic ions are emitted from a target irradiated by an ultra-intense laser pulse. Several studies have been reported in the last decade[2-4)]. As the injector, the accelerator requires 10^9-10^{11} ions per second with the energies of 2 MeV/nucleon for cancer therapy. This will be achieved by using a T^3-laser system, which is rather compact and can deliver intense pulses. However, when the ultra-intense laser irradiates the foil target, suppression of a pre-pulse becomes serious. One of the ways for solving this problem is to make positive use of the pre-pulse[5)]. The pre-pulse forms a layer of underdense plasma (preformed plasma) near the irradiated region of the foil before the arrival of the main pulse. The main pulse consequently interacts with this preformed plasma. In this regime, the relativistic self-focusing would make focusing size of the laser beam smaller and increase the laser intensity in the plasma. The electrons are accelerated inside the channel. Fast electrons then yield a large and long-living charge separation, which causes the effective ion acceleration. In order to test the scheme, we have performed the experiments at Nuclear Engineering Research Laboratory in the University of Tokyo.

2. Experimental setup

Figure 1 shows the experimental setup. The experiments were performed with Ti:sapphire laser system providing laser pulses of 800-nm wavelength and 50-fs duration. Peak power was about 3 TW. A laser pulse was focused onto the targets with normal incidence angle. The targets were 3-μm-thick Ti and 5-μm-thick Ta foils. The focal spot diameter was 18 μm (FWHM) with peak irradiance of 6×10^{18} W/cm^2. The contrast ratio of pre-pulse to main pulse was obtained to be 10^{-5} with the third order autocorrelator.

In order to obtain the ion energy spectra and to resolve the ion spices, a Thomson parabola ion analyzer (B=0.16 T, E=4×10^5 V/m) was placed along the target normal direction. The angular distribution of ions was measured with CR-39 track detectors with a 0.8-μm-thick Al range filter, which stops the protons with the energies smaller than 100 keV. The CR-39 track detectors surrounded the laser-target interaction point at the distance of 80 mm. The degree of vacuum was kept about 10^{-4} Torr during the measurements.

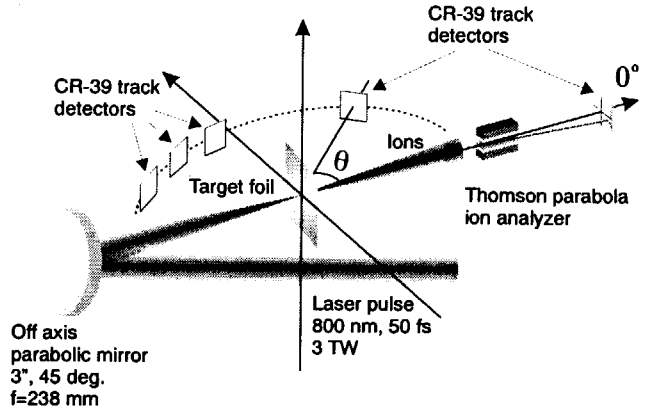

Fig. 1 Experimental setup

3. Results and discussion

The experimental results for 5-μm-thick Ta foils are shown in Figs. 2-3. The proton energy spectrum obtained with the Thomson parabola ion analyzer is shown in Fig. 2 (a). The protons with energies up to 1 MeV are found. These protons are attributed to contaminations of hydrogen layer on the target. Figure 3 shows the angular distribution of protons. The propagation direction of the laser pulse is defined as an angle of 0°. A collimated proton beam is obtained in the forward direction.

These results are examined by the simulations based on the underdense plasma regime. A profile of the preformed plasma caused by the pre-pulse is determined by using a two-dimensional (2D) hydrodynamics (HD) simulation code. Subsequently, multi-parametric particle-in cell (PIC) simulation code analyzes the interaction of the main laser pulse with the preformed plasma. The energy spectrum computed in the simulations is presented in Fig. 2 (b). One can find that the simulation results are in good agreement with the experimental results. By contrast, the results of simulations assuming the solid density plasma sheet (overdense plasma regime) are also shown in Fig. 2 (c). In this case, the results of simulations are far from that of experiments. Simulated angular distribution of protons is given in Fig. 3. Highly collimated proton beams in both the forward and backward directions are predicted.

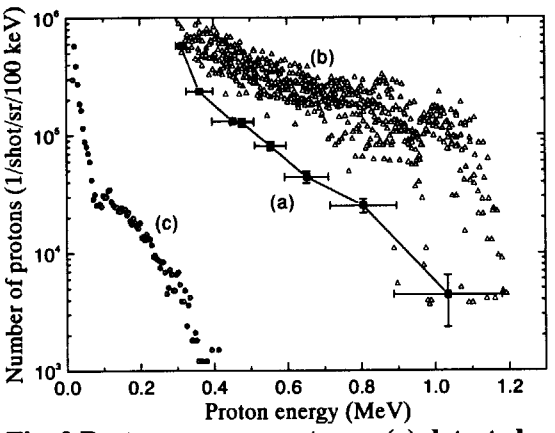

Fig. 2 Proton energy spectrum: (a) detected with Thomson parabola ion analyzer (Ta 5 μm); (b) obtained in the multi-parametric PIC simulation; (c) result of PIC simulation for the 3-μm fully ionized highly overdense Hydrogen plasma slab

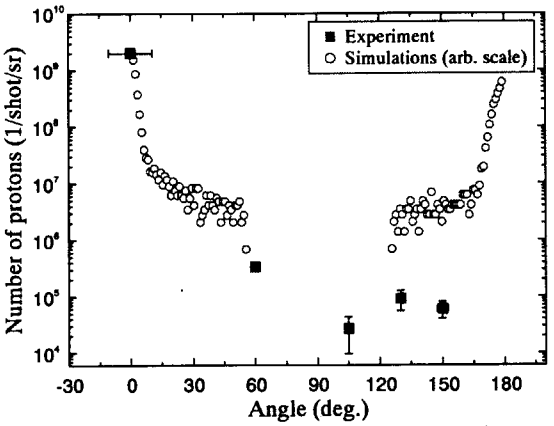

Fig. 3 Angular distribution of protons with energies greater than 100 keV

4. Conclusion and prospects

We have carried out the experiments for generating the energetic ions as the laser-driven ion source. Using 5-μm-thick Ta foil, we could obtain the collimated proton beam with the energies up to 1 MeV. The experimental results are compared with the simulations based on the underdense plasma regime in which the pre-pulse yields the layer of underdense plasma before the arrival of the main pulse. The simulations show the consistent results with experiments. Further studies, for instance optimizing the laser-shooting condition or increasing the protons in the target, would provide the sufficient energy and number of protons required by the cancer therapy.

5. Acknowledgements

This work was partly supported by Ministry of Education, Culture, Sports, Science and Technology of JAPAN (Advanced Compact Accelerator Development project).

References

1) S. V. Bulanov and V. S. Khoroshkov, Plasma Phys. Rep. **28**, 453, 2002.
2) E. L. Clark *et al.*, Phys. Rev. Lett. **85**, 1654, 2000.
3) A. Maksimchuk *et al.*, Phys. Rev. Lett. **84**, 4108, 2000.
4) M. Hegelich *et al.*, Phys. Rev. Lett. **89**, 085002, 2002.
5) K. Matsukado *et al.*, submitted to Phys. Rev. Lett.

4.7.2 Energy spectrum of electrons from a solid foil irradiated by a short intense laser pulse

Zhong LI[a)], Hiroyuki DAIDO, Koji MATSUKADO[a)], Atsushi FUKUMI[a)], Timur ESIRKEPOV[b)]
Yukio HAYASHI, Satoshi ORIMO, Akito SAGISAKA, Koichi OGURA, Etsuya YANASE
Kenichi TAKAGAKI, Mamiko NISHIUCHI, Michiaki MORI, Takayuki UTSUMI, Shu NAKAMURA[c)]
Akira NODA[c)], Yoshihisa IWASHITA[c)], Toshiyuki SHIRAI[c)], Atsushi YAMAZKI[c)]
a) National Institute of Radiological Sciences
b) Moscow Institute of Physics and Technology, Moscow, Russia
c) Institute for Chemical Research, Kyoto University

1. Introduction

Laser driven ion generation is paid attention recently because of its potential applications[1)]. The electron is a key medium in this process. The energy of the laser pulse is coupled into that of electrons firstly via multiple heating mechanisms. The heated electrons transfer the energy onto atoms which cause the excitation and ionization of the atoms, bring on X-ray and ion emission consequently. The charge separation due to the movement of the electrons produces electrostatic field in a target directly and accelerates the ions up to a few tens of MeV.

A project is being taken to develop a compact ion injector for a medical therapy accelerator with a laser driven ion source. The study on the measurement of electron energy spectrum for ion generation driven by laser pulse is reported here.

2. Experimental setup

The experiment was performed at the Advanced Photon Research Center. The laser pulse, generated from a Ti:sapphire laser working at a wavelength of 800 nm, with an energy of 200 mJ per pulse in a pulse duration of 50 fs was focused on the solid foil target perpendicularly with a 3-inch off-axis parabolic mirror with a focal length of 327 mm. The contrast ratio of the main pulse to the ASE background was $1:10^{-6}$ after the compressor. The FWHM diameter of the focus spot was 15 μm which induced a focused peak intensity of 2×10^{18} W/cm^2 on the target. The target is 3 μm thick Ta foil. The energy spectrum of the electrons was determined with a magnetic energy spectrometer[1)]. The measurable energy is up to 3.5 MeV with a magnetic intensity of 7 mT induced by a pair of permanent magnets. The energy scale and the intensity conversion rate from the electron number to the photo-stimulated luminescence (PSL) given by the imaging plate were calibrated with a ^{90}Sr-^{90}Y ß source. The uncertainty is less than 10% for the energy determination and 5% for electron number determination.

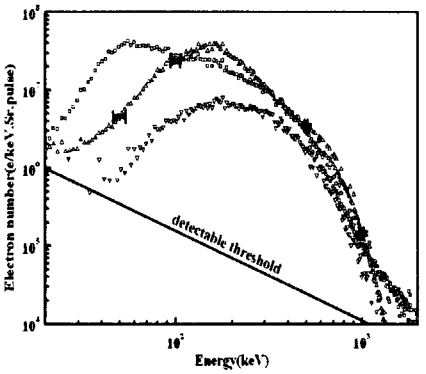

Fig. 1 Energy spectra of electrons at 0° (□), 22.5° (△) and 45° (▽)

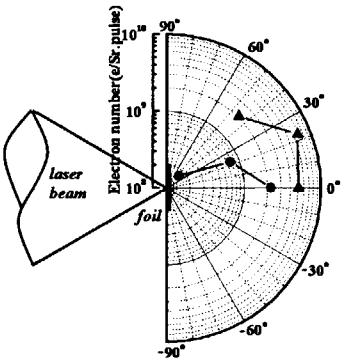

Fig. 2 Angular distribution of electron in 0.1-1MeV (▲) and <100keV (●) electrons.

3. Results and analysis

The energy spectra of the electrons emitted from the 3 μm thick Ta foil at 0°, 22.5° and 45° off the laser axis were determined as shown in the Fig. 1. A high energy electron (>1 MeV) tail appeared at 0°. The angular distribution of electrons in 0.1-1 MeV and <100 keV are given in Fig. 2. It was found that the electron under 100keV flowed out along the laser axis but the electron in 0.1-1MeV spurted out with an angle of 22.5° approximately off the laser axis[2)]. The obtained electron energy spectra together with the experimental data of the ion are now compared with those of the PIC computer simulation.

References

1) H. Daido *et al*, Annual report of Kansai Research Establishment 2001, 56.
2) W. Yu *et al*, Phys. Rev. E 61, R2220(2000). J.J.Santos *et al*, Phys. Rev. Letts. 89, 025001(2002).

4.7.3 Ion beam control from a laser plasma source

Shu NAKAMURA[a)], Yoshihisa IWASHITA[a)], Toshiyuki SHIRAI[a)], Akira NODA[a)],
Koji MATSUKADO[b)] and Hiroyuki DAIDO
a) Nuclear Science Research Facility, Institute for Chemical Research, Kyoto University
b) National Institute of Radiological Science

1. Introduction

Studies on interactions between a short-pulse intense laser pulse and a solid or dense plasma have recently been reported[1, 2]. These reports indicate emission of high energy ions whose kinetic energy reaches some MeV/u. While attained high energy has a great advantage as an ion source, although the number of ions decreases exponentially with its energy. In order to make better use of such high energy ions, we plan to gather them around an energy about 2 MeV/u and maximize the number of ions with narrow energy spread[3].

2. Phase rotation (Energy compression) Scheme

To use the laser produced ion beam as an ion source, it has to be generated at high repetition rate(10Hz or more). So we are investigating this scheme using a high repetition(~10Hz) high power(~10TW) ultra-short-pulse(~50fs) laser. As the energy of this laser per pulse is less than a few J, we will use thin(~a few μm) foil target for generation of MeV ion jets[4]. Because of the very short pulse width of this laser, we estimate that the initial time spread of ions is less than the order of 1ps. After passage of some distance, i.e. a few tens of cm from the target, the time spread of whole ions becomes broad, although the time spread of ions with the same energy does not change. Applying decelerating RF electric field, which is synchronized with the laser shooting, for the earlier arrived ions and the accelerating field for the later arrived ions, we can compress the energy spread. By application of this phase rotation scheme, the ion beams in the energy range of ±5 % is expected to be compressed into the range within ±1 % of our goal(Fig. 1). The ions with the same energy are applied the same electric field because the time spread of them is small enough than a period of the RF. As a result, the energy spread after the phase rotation is almost determined by a linearity of RF electric field. In a simple calculation, the phase rotation technique can attain the energy spread within ±0.3%.

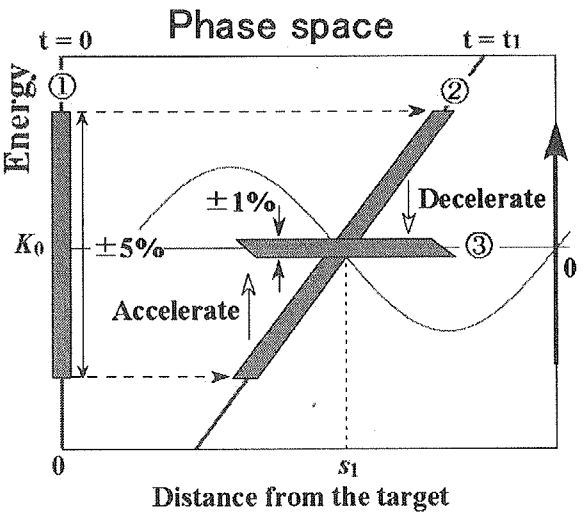

Fig. 1 Schematic view of a phase rotation scheme
1) The initial(t=0) distribution
2) The ion bunch with the energy spread is lengthened during its flight ($t=t_1$).
3) Distribution after phase rotation

3. Conclusion

We aim at an achievement of phase rotation scheme for protons at first. The energy spread of ±5 % around the central value of 0.5 MeV/u is expected to be reduced to less than ±1 %.

Reference

1) E. L. Clark *et al.*, Phys. Rev. Lett. **85**, 1654, 2000.
2) Stephen P. Hatchett *et al.*, Phys. Plasmas **7**, 2076, 2000.
3) A. Noda *et al.* Beam Science and Technology, **6**, 21, 2001.
4) M. Hegelich *et al*, Phys. Rev. Lett. **89**, 085002, 2002.

4.7.4 The 10TW Table Top Laser System

Koji MATSUKADO[a)], Yukio HAYASHI, Satoshi ORIMO, Mamiko NISHIUCHI,
Akito SAGISAKA, Michiaki MORI, Atsushi FUKUMI[a)] and Hiroyuki DAIDO
a) National Institute of Radiological Sciences

A 10TW Table Top Laser system was constructed as a complementary system for basic and preparation experiments of the 100TW laser experiments. The 10TW laser system is composed of 3 parts: the 1TW module, the 10TW module and the pulse compressor. At the moment, the last one is shared with the 100TW laser system. The optical layout of the 10TW laser system is shown in the Fig. 1. The photograph 1 shows the actual configuration of the auxiliary laser system placed in the room of C105. Specifications of the 10TW laser system are the wave length of 800nm, peak power of 10TW(=300mJ/30fs), and repetition rate of 10Hz.

We have performed two experiments using the 10TW laser system. The 10TW laser system was operated routinely five days in a week, during the experimental period. Through the experiments, output energy of the laser system was kept around 700mJ/pulse, and its fluctuation was about 1%. The pulse duration was 50fs after the compression. The transfer efficiency from the output of the laser system to the target chamber was 30%, which should be improved by the beam alignment technique, resulting in peak power of 4TW power on targets. The temporal structure of output pulse was measured by the cross-correlator.

We are planning to make many experiments using the 10TW laser system at present.

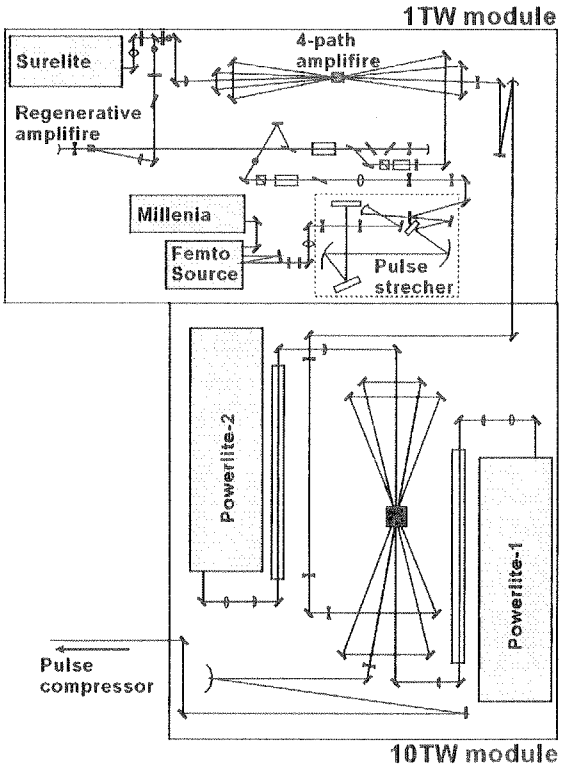

Fig. 1 The optical layout of the 10TW laser system

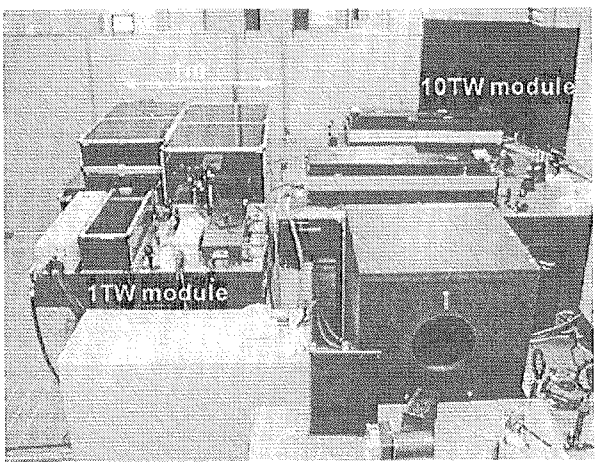

Photograph 1 The 10TW laser system in the room of C105

Acknowledgement

This work is supported by the fund of Advanced Compact Accelerator Development Project from the Ministry of Education, culture, sports, science and technology of Japan. The authors thank Dr. K. Yamakawa of JAERI-APRC for giving us many useful information and suggestions.

4. 7. 5 Third order cross-correlation at 10TW Ti: Sapphire laser system

Satoshi ORIMO, Koji MATSUKADO, Michiaki MORI and Hiroyuki DAIDO

1. Introduction

For a high-field plasma experiment, it is very important to characterize the parameters of a pumping laser. Our Ti: Sapphire laser system delivers 300mJ energy, 10Hz repetition rate, 30 fs pulse- width, giving an out put power of 10TW. Using high power femto-second lasers for high field physics, we need a strict control of temporal pulse shape. Using a third order cross-correlation technique, we measure the temporal profile of the pulse between a –100ps and +100ps from the main peak which given the contrasts ratio.

2. Experimental setup

A Ti: Sapphire laser light is attenuated by a λ/2 wave plate and a thin film polarizer. A third order cross-correlator is called "SEQUOIA" system (The SEQUOIA system is the 10^8 dynamic range third order femtosecond cross-correlator). A laser pulse is separated into two lines. One is fed into the frequency doubled crystal and the other simply propagates through the delay line. The two beams are recombined into a third harmonic crystal. The signal is proportional to the temporal overlap between the two pulses. The delay line is controllable driven by the computer. A laser contrast ratio is measured using a personal computer. A third order cross-correlaor requires a 10Hz TTL synchronization trigger from the Ti: Sapphire laser system. The third order signal is detected by a photo-multiplier (PM tube). The computer properly controls the gain of the PM tube in order to adjust the measurement level between the noise and the saturation effect. The dynamic range of the measurement is also strongly increased by the use of neutral filters which are set at the input the cross-correlator.

3. Results

Measured contrast ratios as a function of time are shown in Fig. 2 (a), (b). The pre-pulse is composed of weak nano-second pulse which comes from amplified spontaneous emission (ASE), a few pico-second prepulse due to misalignment of the compressor and leakage of the switch out at the regenerative amplifier which cannot be measured in the cross-correlator. In Fig. 2 (b), the contrast ratio of the nano-second pulse is 10^{-6} and the contrast of the pico-second pre-pulse adjacent to the main pulse is 10^{-3} as shown in Fig. 2 (b). The contrast ratio of the longer time period is also shown in Fig. 2(a) where the pre-pulse level is almost constant. Note that the level is 10^{-5} in this case because the sampling point of the laser pulse cannot be adjust at the peak but little weaker place in the main pulse due to the resolution limit. Any way, we can measure the contrast ratios accurately using combination of the fine with a narrow range and wide-range detections.

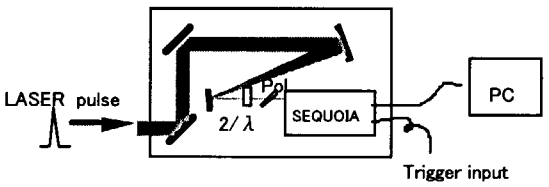

Fig. 1 Setup of the 3rd order cross-correlator

Table 1 System performance of the 3rd order cross-correlator

Dynamic range	>10^8
Delay range	270ps
Temporal resolution	<120fs
Wavelength	760-840nm
Delay precision	<20fs
Acquisition	>1000kHz

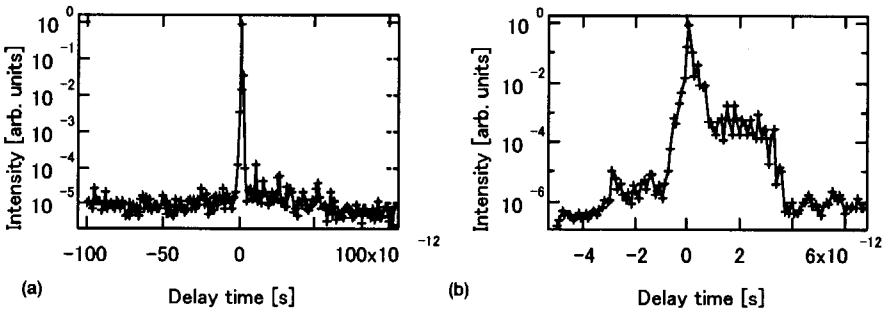

Fig. 2 Third order cross correlation (-100ps to +100ps) at 10TW 3rd order cross-correlator laser system
(a) temporal resolution is rough with a wide temporal range.
(b) temporal resolution is fine with a narrow temporal range.

4.7.6 Observation of preformed plasmas for laser-plasma interactions

Akito SAGISAKA[a)], Hiroyuki DAIDO[a)], Koichi OGURA[a)], Satoshi ORIMO[a)], Yukio HAYASHI[a)], Mamiko NISHIUCHI[a)], Michiaki MORI[a)], Koji MATSUKADO[a,b)], Atsushi FUKUMI[a,b)], Zhong LI[a,b)], Shu NAKAMURA[a,c)], Kenichi TAKAGAKI[a)], Hisanao HAZAMA[a)], Takayuki UTSUMI[a)], Sergei BULANOV[d)] and Timur ESIRKEPOV[a,e)],

a) Advanced Photon Research Center, Kansai Research Establishment, Japan Atomic Energy Research Institute
b) National Institute of Radiological Science, Japan
c) Institute for Chemical Research, Kyoto University
d) General Physics Institute, Russian Academy of Sciences
e) Moscow Institute of Physics and Technology, Russia

1. Introduction

High-intensity laser-matter interactions have been investigated extensively. High-energy x-ray, electrons, and ions from a high-intensity laser-produced plasma have been observed and the results have been compared with the simulations. Matsukado *et al.* reported the production of high-energy protons with Ta plasma by using the high-intensity Ti:sapphire laser[1]. To interpret the experimental results, they proposed the ion generation in the preformed plasma slab created by a prepulse. The experimental results indicated that the characterization of preformed plasma was essentially important.

In this experiment, we measured the preformed plasmas of metal targets produced by a high-intensity Ti:sapphire laser.

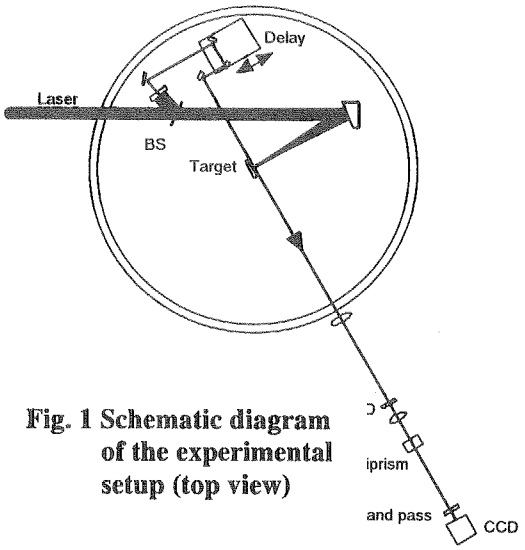

Fig. 1 Schematic diagram of the experimental setup (top view)

2. Experiment

A linearly polarized commercial 10 TW Ti:sapphire laser was used at the wavelength of 800 nm. The pulse duration of 50 fs (FWHM) was measured by an auto-correlator. However, the temporal shape of the laser pulse was composed of prepulses such as the leakage of the switch out from the regenerative amplifier, continuous nano-second duration pulse came from the amplified spontaneous emission (ASE), pico-second pedestal component. In this laser system, the contrast ratio of prepulse at ~12 ns before the main pulse was $\sim 10^{-4}$. The ASE level of $\sim 10^{-6}$ was measured by the third-order cross-correlator. Figure 1 shows the schematic of the experimental setup. The laser beam was divided into pump and probe beams. The pump beam was focused by an off-axis parabolic mirror with an f number of 6.5, giving estimated peak intensity of up to $\sim 10^{18}$ W/cm^2 at the target surface. On the other hand, the probe beam was used for interferogram. The interference fringes were produced by using a Fresnel biprism and detected by a CCD camera[2].

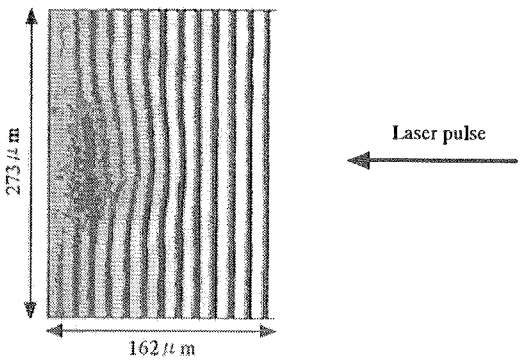

Fig. 2 Interferogram of the preformed plasma for an Al target

3. Results

Figure 2 shows the interferogram with a preformed plasma of an Al slab target. It was taken at the time of ~10 ps before the main laser pulse arrived. The arrow shows the direction of the laser pulse propagation and the target surface corresponds to the left-side edge of the figure. In this case, the intensity of the main pulse is $\sim 5 \times 10^{16}$ W/cm^2 and the prepulse intensity is $\sim 5 \times 10^{12}$ W/cm^2. The preformed plasma size is larger than the laser spot size. The preformed plasmas definitely play an important role for laser-matter interactions such as x-ray and particle generations. We will systematically investigate the effect of prepulse for high intensity laser-plasma interaction using interferometers.

References

1) K. Matsukado, T. Esirkepov, H. Daido, T. Utsumi, Z. Li, A. Fukumi, *et al.*, submitted to Phys. Rev. Lett.
2) B. Rus, P. Zeitoun, T. Mocek, S. Sebban, M. Kalal, A. Demir, *et al.*, Phys. Rev. A **56**, 4229 (1997).

4.7.7 Radiation dose from laser plasma sources

Yukio HAYASHI, Atsushi FUKUMI, Koji MATSUKADO, Shu NAKAMURA, Zhong LI,
Koichi OGURA, Akihito SAGISAKA, Mamiko NISHIUCHI, Michiaki MORI,
Kenichi TAKAGAKI, Satoshi ORIMO, Hiroyuki DAIDO

1. Introduction

The technology to make the short pulse high power laser systems has been studied for long time. Recently, using chirped pulse amplification technique, we can make compact ultra-short high power laser for various applications, such as compact radiation sources, because high-energy particles can be made by the interaction between high power laser pulse and a plasma[1].

Here we will show radiation dose data from the laser plasma interaction experiment.

2. Radiation dose data from laser plasmas experiment

We used Ta and Ti targets, which were placed in a vacuum chamber as shown schematically in Fig. 1. The chamber had cylindrical shape with a radius of 50cm. The laser pulse width and laser energy were 50fs and 200mJ, respectively. The laser pulse was focused with off-axis parabolic mirror having f number of 6.5, giving peak laser intensity of 10^{18}W/cm^2 on the target. Peak-to-pedestal ratio was about 10^{-6} measured by a cross correlator.

Ion Chamber and the glass dosimeter were used to measure the radiation doses. The Ion Chamber was located at an angle of 67.5 degrees from the target normal, and a window was set between the Ion Chamber and the target (Port #D in Fig. 1).

The glass dosimeter was placed on the chamber wall at 180deg from laser incident direction as shown in Fig. 1.

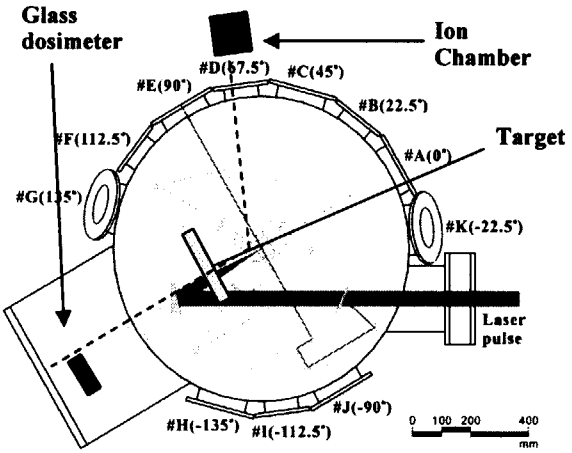

Fig. 1 Geometry of the target and detectors

3. Results

3.1 Dependence of X-ray dose on target material

Next we have systematically measured the target material and thickness dependence of the dose with Ion Chamber placed at the 1.26m from the port #D. Three different thickness of Ta targets (1,3,5μm) and Ti 3μm target were used in the experiments. The results are listed in the Table 1.

Table 1 Dose rate at R=1.26 (m)

Target	Integration time (sec)	Number of shots	Total Dose including background (n Sv)	Dose per shot without background (nSv/shot)
Ta 1μm	2326	75	80. ±10.	0.53±0.13
Ta 3μm	2702	375	280. ±10.	0.61±0.03
Ta 5μm	2695	300	220. ±10.	0.56±0.03
Ti 3μm	3938	375	210. ±10.	0.37±0.03

The dose per shot for the Ta targets with various thicknesses is almost identical, and about 0.6 (nSv/shot) at the detector. In the case of Ti target, the dose per shot was lower than that of Ta target, and 0.37 (nSv/shot) at the detector.

Energetic electrons produced the laser-plasma directly interact with the vacuum chamber wall in which play an important role to convert electron energy into x-ray energy. Details are now investigated.

3.2 Backward dose detected with the glass dosimeter

We put on the glass dosimeter at the vacuum chamber wall as shown in Fig. 1. We did about 2300 laser shots at this experiment, and found 20μSv of the X-ray dose, which was generated by the interaction between the high-energy electrons and the parabolic mirror.

If we carry out the laser-plasma experiment in similar laser and target condition at 1Hz 40hours/week, the dose at the backside chamber wall will exceed the allowed dose limit of 1mSv/week.

Acknowledgements

The authors wish to thank Mr.Kondo, Mr.Kanazawa, Mr.Manabe and Mr.Ueno of JAERI for their encouragement and supports.

Reference

1) G.Malka *et al.*, Phys.Rev.E.**66**, 066402,(2002)

4.7.8 Characterization of water window x-ray generation from laser plasma using double-stream gas-puff target irradiated by a nano-second laser pulse

Masayuki SUZUKI [a)]*, Kensuke MURAI [b)], Etsuya YANASE, Mamiko NISHIUCHI, Zhong LI, Takatsugu OKETA, Ken-ichi TAKAGAKI, Kunioki MIMA [a)], Henryk FIEDOROWICZ [c)] and Hiroyuki DAIDO

a) Institute of Laser Engineering, Osaka University
b) National Institute of Advanced Industrial Science and Technology
c) Institute of Optoelectronics, MUT
*Present address: The Institute for Solid State Physics, the University of Tokyo

1. Introduction

We have investigated the interaction process between a nano-second pulse and a gas-puff target[1)]. In this report, we present results on the absorbed laser energy and water window (2.2-4.4 nm) x-ray emission from a double-stream gas-puff target irradiated by a nano-second laser pulse. The double-stream gas-puff target provides a good x-ray source in the water window spectral range driven by a nano-second laser pulse.

2. Experimental setup

A commercial Nd:YAG laser that delivered laser energy of 540 mJ in 8 ns at 1064 nm was used. The laser was focused with a plano-convex lens of 100 mm focal length, giving a total intensity of about 10^{12} W/cm^2. The laser irradiated the double-stream gas-puff target perpendicularly with respect to the flow of the gas. The double-stream gas-puff target consisted of two nozzles on concentric circle nozzles. The details of the double nozzle gas-puff target have been described elsewhere[2)]. The focused position was about 1 mm from the nozzle exit. Nitrogen, Argon, Krypton, and Xenon were used as target gases. The valves were backed with gases having a pressure of 10 atm. The density of the gas at the place of 1 mm above the nozzle exit was about 10^{20} cm^{-3} under the backing pressure of 10 atm. The water window x-ray emission from a laser produced plasma have been measured using a grazing incidence spectrometer with a varied spacing grating of 2400 grooves/mm. The spectra were recorded on a back illumination type CCD camera with a pixel size of 24 μm x24 μm (Princeton Instruments Inc., model SX-TE/524-TKB/1). The absorbed laser energy was estimated by measuring the transmitted laser energy through the gas-puff target with collection lens of a 113 mm focal length with a diameter of 50 mm coupled with a power meter. Instead of power meter, we used bi-planar photo tube as a detector for the time-resolved transmission measurement.

3. Experimental Results and discussions

Figure 1 shows the fractions of absorbed laser energy measured with a colorimeter. Absorption of a laser pulse was ~43 % for Nitrogen, ~65 % for Argon, ~84 % for Krypton, and ~93 % for Xenon for the double-nozzle setup. On the other hands, absorption of the laser pulse was ~13 % for Nitrogen, ~33 % for Argon, ~73 % for Krypton, and ~92 % for Xenon for the single-nozzle setup (without using the outer nozzle). Absorption of the laser pulse for the double-stream gas-puff targets are over 2 times higher than the single-stream targets by using the low atomic number targets. The absorption of laser pulse in the double nozzle gas-puff target increases because of increasing the gas density. The water window x-ray emission at 2-4 nm wavelength region from Nitrogen and Argon double-stream gas-puff target and solid carbon target are shown in Fig. 2. Using the Nitrogen double-stream gas-puff target, the water window x-ray emission from He-like ($1s^2$-$1s2p$, $1s^2$-$1s3p$, $1s^2$-$1s4p$, and $1s^2$-$1s5p$) lines are obtained between 2 nm and 3nm wavelength region. On the other hands, He-like lines could not be observed in the wavelength region using the single-stream gas-puff target. Using the Argon double-stream gas-puff target, strong x-ray emission from Ne-like ($2s^22p^6$-$2s^22p^5(2P^{3/2})3s$) line is obtained at 4.9 nm wavelength. The intensity of Ne-like line using the double-stream gas-puff target is about 7 times higher than that using the single-stream gas-puff target.

According to the gas density from the double-stream gas-puff target, the electron density of the double-stream gas-puff plasma is about $10^{20\text{-}21}$ cm^{-3}. It is possible to estimate Collisional-Radiative equilibrium (CRE) model in this plasma electron density region[3)]. An approximate relationship between the ionic charge state of the CRE model and the plasma electron temperature can be found by neglecting the three-body recombination term in comparison to the radiative recombination in the stationary state. We

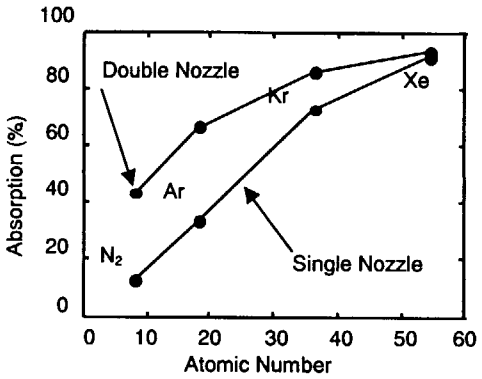

Fig. 1 Absorption of the laser light obtained from transmitted laser energy through Nitrogen, Argon, Krypton, and Xenon double and single nozzle gas-puff target

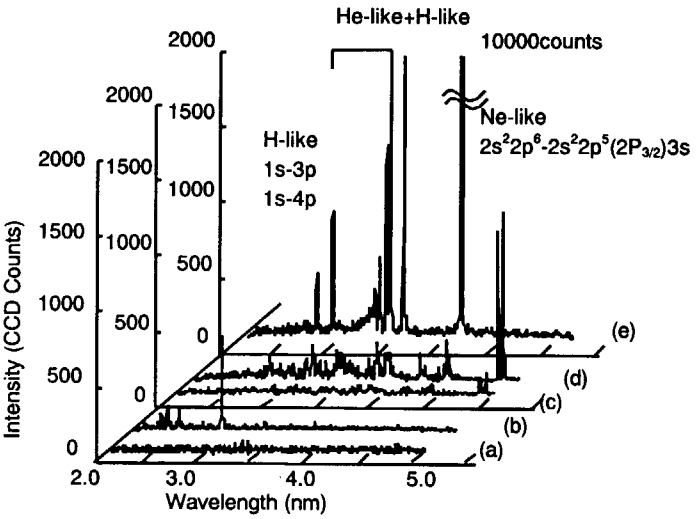

Fig. 2 X-ray spectra in the wavelength range between 2 and 5 nm
The target gas was used Nitrogen in (a) and (b), and Argon in (d) and (e), and the solid Carbon in (e). The single nozzle was (a) and (c), and the double nozzle for (b) and (d).

have estimated the plasma electron temperature using the following equation described by D. Colombant[4]. The equation for ion charge Z is following;

$$Z = \frac{2}{3}\left[AT_e(eV)\right]^{\frac{1}{3}}, \tag{1}$$

where Z is atomic number, A is the atomic number of the element, and T_e is the electron temperature. As the estimated plasma temperature, we estimated the plasma electron density using the following equation.

$$\alpha_{\lambda_0} = \frac{13.49}{\lambda_0^2} Z^* \left(\frac{n_e}{n_c}\right)^2 \frac{1}{\sqrt{1-n_e/n_c}} \frac{1}{T_e^{3/2}}, \tag{2}$$

where λ_0 is the laser wavelength, Z* is the average plasma ion charge, n_e is the plasma electron density, n_c is the critical density, and T_e is the plasma electron temperature. The Coulomb logarithm is assumed, ie., ln Λ=5 for the plasma conditions considered in this experiment. As the results of our estimations, the plasma temperature is ~90 eV and the plasma electron density is about ~10^{20} cm^{-3}.

4. Conclusion

The double-stream gas-puff target provides a good x-ray source in the water window spectral range driven by a nano-second laser pulse.

References

1) M. Suzuki *et al.*, Phys. Plasmas. **10**, 227, 2003, and reference is therein.
2) H. Fiedorowicz *et al.*, Appl. Phys. B **70**, 305, 2000
3) See, for example, I. C. E. Turcu and J. B. Dance, X-RAY FROM LASER PLASMA: Generation and Applications, John Wiley & Sons Ltd, England, 1999
4) D. Colombant and G. F. Tonon, J. Appl. Phys. **44**, 3524, 1973

4.7.9 Expansion of soft x-ray source plasma in a gas-puff target

Koichi OGURA

1. Introduction

When a high-power pulsed laser is focused on to a target, a plasma is generated. It is interesting as a source of extreme ultraviolet radiation and X-rays, because the plasma emits photons in a broad spectrum from visible rays to X-rays. The laser plasma X-ray sources are an almost ideal X-ray probe for the study of time-dependent processes and an X-ray source for lithography. When a solid target is irradiated, the debris particles are generated. The debris causes the degradation of the reflectivity of the X-ray optical elements and the reduction of the efficiency of focusing optics. Therefore it is necessary to develop a target which will not generate any debris. A gas puff target dose not generates any debris inherently. But a collision between a plasma which produced in the gas puff and a nozzle lead to sputtering of a material of the nozzle. The sputtered material degrades the reflectivity of the X-ray optical elements. In order to design the nozzle that generate no debris, we should characterize the plasma expansion.

Here, the angular distribution of the expansion velocity of a plasma at a distance of 100 mm from the laser focus point are measured with an electric probe to characterize the plasma expansion.

2. Experimental

The gas puff target was made by gas expanding through a nozzle, which was installed in a vacuum chamber. The throat of the nozzle was 800 μm in diameter, and the jet expansion half-angle was 45°. Gas flow through the nozzle was initiated by a fast solenoid valve. The backing pressure of the valve was 2 MPa. The pressure in the vacuum chamber was maintained at 10^{-3} Pa before opening the valve. The laser plasma was produced by focusing the laser beam (λ=532 nm) produced with an Nd:YAG laser system. The laser beam irradiated the gas jet transversely with respect to the flow of the gas and the laser focus was placed 1.0 mm above the nozzle tip causing a plasma. The laser pulse energy was 100 ~ 400 mJ. The angular distribution of expansion velocity of a plasma in the plane which includes the axis of the nozzle and was perpendicular to the laser beam was measured with the electric probe. The probe was made of tungsten wire with a diameter of 0.7 mm and a length of 3 mm. The negative potential was applied to the probe externally. The probes were installed round the circumference with a center at the focal point and a radius of 100 mm. The probes were set at 0°, 60°, and 90° with axis of the nozzle, respectively. The velocity was obtained from the time it took the plasma to travel the distance between the focus position and the probe.

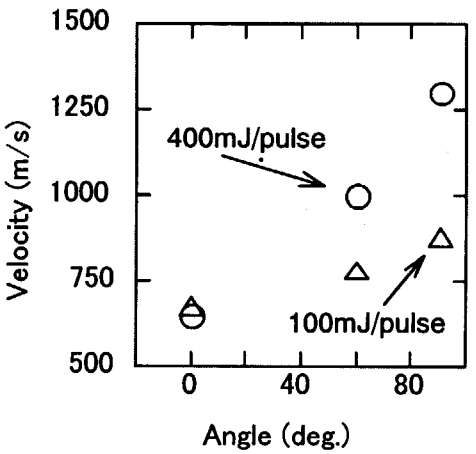

Fig. 1 The expansion velocity of plasma

3. Results

The velocity of plasma as a function of the angle at the backing pressure of 2 MPa are shown in Fig. 1. The velocity for the laser energy of 400mJ at the angle of 0° is the same as that for 100mJ. The velocity at the angle of 90°(low gas density region) is higher than that of 0°(high gas density region). It is found that at the angle of 0° the plasma expansion is small and the plasma drift with the velocity of the gas flow. The lower the gas density is, the higher the velocity of the plasma expansion is. To increase the gas density between the plasma and the nozzle tip can prevent the collision between the plasma and the nozzle tip.

4.7.10 Direct Ab Initio Molecular Dynamics Study of Photodissociation of Formic Acid

Yuzuru KUROSAKI, Keiichi YOKOYAMA, Yoshiaki TERANISHI

1. Introduction

Formic acid is an important molecule in the combustion of unsaturated hydrocarbons, in the interstellar cloud, and in atmospheric chemistry. The following two channels that lead to molecular products are widely known:

$$HCOOH \rightarrow H_2O + CO \quad (1)$$
$$\rightarrow CO_2 + H_2, \quad (2)$$

which are referred to as dehydration and decarboxylation, respectively. When formic acid in the ground singlet state (S_0) absorbs a photon in the UV region, it is excited to the first-excited singlet state (S_1) through the n-π^* transition. Formic acid in the S_1 state can switch to a highly vibrationally excited state of S_0 through the internal conversion (IC) and undergo dehydration or decarboxylation on the S_0 surface.

In this report we theoretically examine reactions 1 and 2 of formic acid photodissociation using the direct ab initio molecular dynamics method.

2. Methods of calculation

Trajectories were started at the transition states (TS) of reactions 1 and 2 in the direction of the imaginary vibrational mode. Initial conditions were generated by distributing the energy that corresponds to the difference between the photolysis energy and barrier height into the normal modes on the basis of microcanonical sampling. The initial phases of the normal modes were selected randomly. The rotational energy was set to zero. The numerical integration of the equation of motion was carried out using the 4-th order Runge-Kutta method and 6-th order Adams-Bashforth-Moulton predictor-corrector method. The required values for the force was obtained at the RMP2(full)/cc-pVDZ level of theory using the MOLPRO program. In the present calculation about 300 trajectories were numerically integrated for each reaction 1 and 2 using 248 and 193 nm light, thus a total of about 1200 trajectories were calculated.

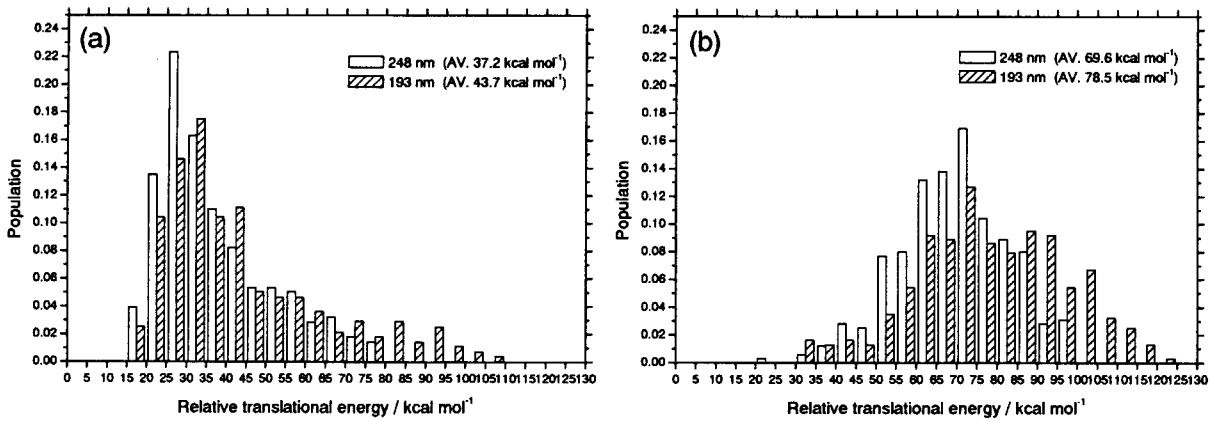

Fig. 1 Population of relative translational energy for (a) reaction 1 and (b) reaction 2

3. Results and discussion

In Fig.1 are shown the populations of the relative translational energy for reactions 1 and 2. It is seen from the figure that the population for reaction 2 concentrates on higher energies than that for reaction 1. This difference in the population comes from the geometries of TS's for reactions 1 and 2; it was calculated that the geometry of H_2O in the TS of reaction 1 is quite different from that of H_2O at equilibrium, while the geometries of CO_2 and H_2 in the TS of reaction 2 are similar to those at equilibrium. It was found that in reaction 1 the available energy is mostly distributed to the internal energy of H_2O and that in reaction 2 to the relative translational energy.

4.7.11 Theoretical study on highly efficient and selective excitation by coherence control

Yoshiaki TERANISHI

1. Introduction

Recently, there has been a growing interest, both experimental and theoretical, in controlling atomic and molecular processes by laser fields. This is basically due to the fact that the recent remarkable progress in laser technology has opened new possibilities of realizing it. In this study, we discuss excitation processes of atoms by a quadratically chirped laser pulse. Not only one-photon excitation, but also multi-photon excitation can be achieved with unit probability, even when the final state has quasi degenerate states. By taking Cs and K atoms as examples, the usefulness and efficiency of our control scheme are discussed.

2. Theory

The basic theory is given in Refs. 1) - 3). All the conditions for controlling are given analytically according to the formulae given in Ref. 3), and the validity of the analytical theory is checked by solving time-dependent coupled channel equations numerically. In the numerical calculation, we include 18 states from 6S to 9S for Cs atom target, and 10 states from 4S to 4D(3/2) for K atom target.

3. Results

Figure 1 shows the results of one photon excitation of K atom from 4S to 4P. There are two 4P states, 4P(3/2) and 4P(1/2). Complete and selective excitation to 4P(1/2) is achieved (see Fig. 1(A)) under the quadratic chirping shown in the lower figure of Fig. 1(A), while the complete transition to 4P(3/2) takes place by changing the shape of chirping (Fig. 1(B)). The energy splitting between 4P(3/2) and 4P(1/2) is about 57.7 cm^{-1} which is about one order of magnitude smaller than the band width of the laser pulse.

It should be noted that the transition time for both cases is the same order of the uncertainty limit. This means that our control scheme provide almost fastest selective excitation.

We also discussed two-photon excitation of Cs atom from 6S to 7D. In this case, complete and selective excitation is possible but, the transition time is several times larger than the uncertainty limit because of one photon excitation from 6S to 6P.

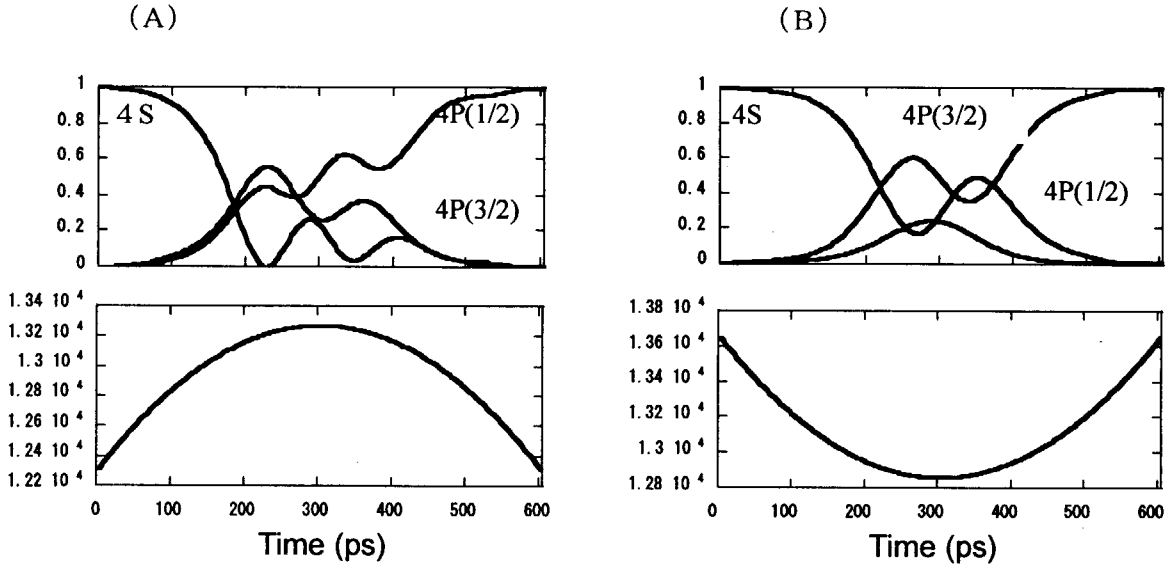

Fig. 1 The time dependence of the population of K atom (upper) and the frequency of the laser pulse (lower).

References

1) Y. Teranishi and H. Nakamura, Phys. Rev. Lett. **81** (1998) 2032-2036.
2) Y. Teranishi and H. Nakamura, J. Chem. Phys. **111** (1999) 1415-1424.
3) K. Nagaya, Y. Teranishi, and H. Nakamura, in *Laser control and manipulation of molecules*, edited by A. D. Bandrauk, R. J. Gordon, and Y. Fujimura (American Chemical Society, Washington, 2001).

4.7.12 Temperature dependence of the ultrafast energy relaxation of a molecule in alcohol : a result inconsistent with the multimode Brownian oscillator model

Hiroshi MURAKAMI

The structural dynamics of complex systems such as liquid and protein have been an issue of the condensed matter physics for several decades[1]. The structural dynamics (relaxation) on an ultrafast time scale can be probed in real time only by means of femtosecond time-resolved spectroscopies, such as a fluorescence up-conversion technique[2]. Although the studies have demonstrated the existence of several relaxation components, a problem is that most of the measurements have been made only at room temperature. It is necessary to perform the spectroscopy as a function of temperature in order to clarify the mechanism of the relaxation in detail, because the relaxation process shows some temperature dependence according to its origin. Thus, we have developed a femtosecond time-resolved fluorescence (FTRF) spectroscopy system combined with a vibrating cryostat using liquid nitrogen for the preceding years[3]. Further, we have reconstructed a streak camera system to allow us to measure the fluorescence dynamics under excitation using a pulse laser with a high repetition rate of ~96 MHz. It is possible at present to obtain FTRF spectra up to 10 ns at an arbitrary temperature above 100 K. At this report, we describe the experimental result of FTRF spectra of a coumarin dye in an ethanol/methanol mixture (voluminal ratio 4:1). The FTRF spectra from the dye molecule were obtained at 296, 230, and 170 K. It was found that the peak-energy shift of the spectrum occurs to the low-energy side with time owing to the relaxation process, and the temporal profile of the peak shift is dependent of temperature. Fitting of a sum of exponentials to the temporal profile of the peak shift reveals that there are three components at each temperature. The first component has a time constant of a few hundred fs, the second one a few ps, and the last one changes from tens ps at 296 K to a few ns at 170K. The first and second ones seem to correspond to the vibrational motions and the ß-fast process of the matrix. On the other hand, it is considered from the temperature dependence of the time constant that the last one is attributed to the diffusion process of the solvent molecule. In addition, the dynamic range of the components changes drastically at 170 K, that is, that of the two fast components decreases at 170 K, while that of the slow component increases.

The multimode Brownian oscillator (MBO) model has been applied successfully to explaining the results obtained from various femtosecond spectroscopies for a molecule in condensed materials[4]. In the MBO model, the electronic state of the molecule interacts with only a few localized harmonic modes, called as a Brownian oscillator (BO). Those modes are independent of one mode another and damped by the bath oscillators, like a Brownian motion. An exponential behavior in the correlation functions obtained from such spectroscopies is reasonably derived for the case that the BO is overdamped, while an oscillatory one for the case that it is underdamped. The interaction of the electronic state of the molecule with the BO is represented as two harmonic potentials with the positions of the minima displaced, which are depicted schematically for one BO mode in the figure(Fig. 1). If this model is applied to our result, the three relaxation components are regarded to be three overdamped BO modes. This model, however, leads to that the dynamic range of the energy relaxation of each component is independent of temperature as long as the excitation energy is not varied. This is not consistent with the experimental result. It should be noted that this inconsistency has been never revealed through the measurement only at room temperature. Motions of atoms in the medium are regarded to be an ensemble of harmonic oscillators in the MBO model. At high temperature, the system fluctuates apart from the minimum of the potential curve and it seems doubtful that the interaction between atoms can be assumed to be harmonic, so anharmonicity in the interaction should be taken into account. The anharmonicity will not come to an ensemble of independent relaxation modes. We note that a model of hierarchically constrained dynamics in which the relaxation processes with different spatial/temporal scales does not occur independently explains the relaxation process of the electronic state of a molecule in (bio)polymers[5]. In progress is data analysis with taking account of anharmonic terms in the interaction energy between atoms.

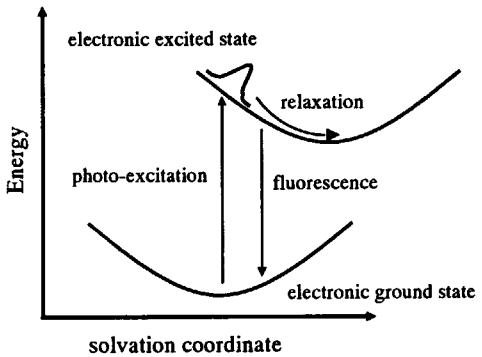

Fig. 1 Energy diagram of a molecule interacting with a BO mode

References

1) See for a review, J. Non-Cryst. Solids, **307-310**, 2002
2) M. L. Horng *et al.*, J. Phys. Chem. **99** (1995) 17311
3) H. Murakami, J. Mol. Liq. **89**, 33, 2000 ; J. Lumin. **102**, 295, 2003
4) Y. J. Yan and S. Mukamel, Phys. Rev. **A41**, 6485, 1990
5) H. Murakami and T. Kushida, Phys. Rev. **B54**, 978, 1994 ; J. Chem. Phys. **108**, 10309, 1998

5. Synchrotron Radiation Science

Osamu SHIMOMURA

The following 6 research fields and an experimental facility development field were studied in FY2002 in the Synchrotron Radiation Research Center.

In the experimental facility development field, we carried out the commissioning and optical adjustments at the quantum structure physics beamline, BL22XU. We installed a cryogenically cooling system for the monochromator at BL11XU. In the beamline BL23SU, an electron beam distortion caused by the APPLE-2 type undulator was successfully corrected by steering magnets using the high accuracy correction table. In the beamline BL14B1, two-dimensional focusing was realized by combining sagittally focusing double-crystal monochromator and vertical focusing.

In the materials science at high pressure, in-situ X-ray diffraction study, conducted on the graphite-diamond conversion with H_2O fluids as solvent, showed that the diamond growth was described by an interface-controlled or diffusion-controlled process depending on the growth temperature. Liquid selenium, exhibiting semiconductor-metal transition at high temperature and high pressure, showed that the electronic transition was accompanied by a structural change and characterized as a weak first-order transition. The electron density of $C_6H_4H_{12}$ was determined. The electron surrounding hydrogen atom was clearly displayed as lobes.

In the field of the interface structure analysis of materials, the surface structure of GaAs(001) under MBE crystal growth condition and the structure evolution of Bi on Au(001) under electrochemical condition were studied. The local structure of Pd-containing perovskite catalyst was investigated to know the structure changes with reduction and oxidation in the atmosphere. The phonon properties of high temperature superconducting copper oxides were studied as a function of hole doping level in $La_{2-x}Sr_xCuO_4$.

In the research field of surface chemical reaction the oxide-layers formation in the O_2/Si(001) system was found to be controlled by the incident energy of O_2 molecules although the coexistence of the oxide-layers formation and the SiO desorption has been discussed in the gas oxidation. The photo-fragmentation processes of condensed C_6H_5F and HCOOH grown on the Si ,and the desorped ions from sulfur-containing amino acids followed by sulfur K-edge excitation were studied. Guanine radical was investigated by K-resonance photoexcitation at oxygen and nitrogen.

In the field of heavy element materials, the resonantly enhanced peak at 2 eV was observed in the inelastic X-ray scattering spectra of $La_{0.8}Sr_{0.2}MnO_3$. The temperature dependence of the intensity at 2 eV may show the anisotropic ferromagnetic exchange interaction in the material. The scanning type synchrotron radiation Moessbauer microscope was developed to detect the distribution of the magnetic hyperfine in the iron foil with step of 60 μm.

In the research field of electronic materials science, the electronic structure of uranium monochalcogenides (US,USe,and UTe), $SrFe_{1-x}Co_xO_3$, and dysprosium iron garnet was investigated by the x-ray absorption magnetic circular dichroism(MCD) to evaluate experimentally the orbital moment and the spin moment separately. $UTGa_5$(T=Rh,Ir) and Fe_xNbS_2 was studied to investigate the electronic structure by using the photoelectron spectroscopy. The smoked Japanese roof tile "Ibushi-Kawara" was characterized so that half of the carbon atoms in Kawara forms layer-structured clusters and the rest half of the carbon atoms forms random-structured clusters.

In the field of synchrotron radiation simulation research, the full-potential linealized aurumented plane wave method was used to show both orbital and magnetic orders and to clarify the mechanism of the resonant x-ray scattering on orbital and magnetic superlattice spots in $KCuF_3$.

5.1 Beamline and Experimental Facilities Development

5.1.1 Installation of the multi-crystal switching system and introduction of the cryogenically cooling system for the monochromator on BL11XU at SPring-8

Hideaki SHIWAKU, Takaya MITSUI, Kazukiyo TOAZAWA, Kouji KIRIYAMA, Taikan HARAMI

1. Introduction

We introduced a cryogenically cooling system for a monochromator and developed a multi-crystal switching system on a cryogenically cooled monochromator of the JAERI materials science beamline, BL11XU at SPring-8[1-2]. In order to make progress in our science, it is necessary to ensure at least the energy range of 6 ~ 70 keV which is achieved by employing Si(111) and Si(311) crystals.

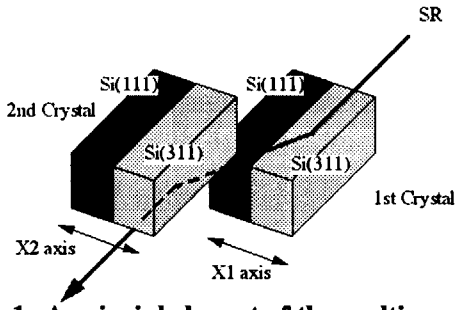

Fig. 1 A principle layout of the multi-crystal switching system

2. Multi-crystal switching system and cryogenically cooling system

The principle of the crystal switching is shown in Fig. 1. Two crystals are arranged side by side, and they are translated in the horizontal direction for exchanging the crystals. Indium sheets were inserted between the crystals in order to improve the thermal contact, as shown in Fig. 2. Four adjustment stages of the SPring-8 standard type monochromator[3] were removed to avoid the crystal vibration. A sheet heater was installed on the α-axis stage to prevent the over-cooling of the residual adjustment stages.

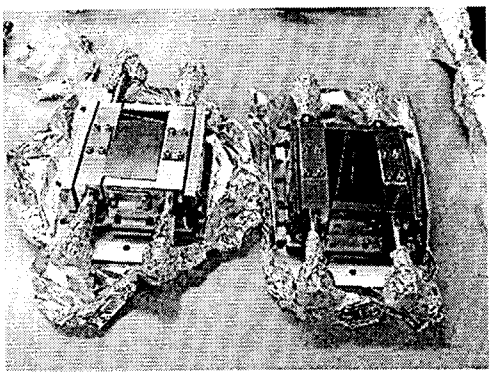

Fig. 2 A photograph of the crystal holders Si(111) and Si(311) crystals are set in the crystal holders, respectively.

Figure 3 shows the liquid nitrogen cooling system for BL11XU[4]. In order to introduce cryogenically cooling system, an X-ray shielding hutch and hutch utilities were modified.

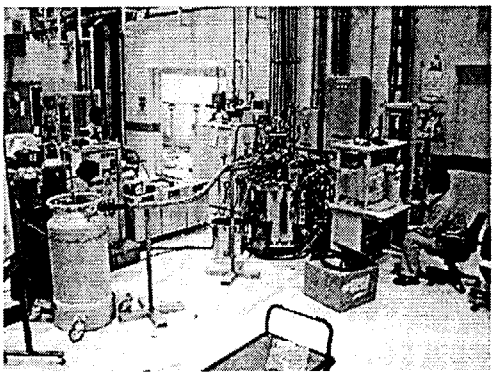

Fig. 3 A photograph of the cryogenically cooling system for the monochromator

3. Results

We checked that there was no distortion of the crystal by this crystal fixed method in the off-line experiment. Performance evaluation experiments of the monochromator are performed now. The stabilization of the x-ray from the monochromator is expected. It takes only 5 minutes to exchange the crystal from Si(111) to Si(311) and adjust crystals geometry in vacuum and at liquid nitrogen temperature. This mechanism will be easily applied to other crystals, for example asymmetrical-cut crystals or more pair of the crystals.

References

1) H. Shiwaku, T. Mitsui *et al.*, Proc. SRI2003, in press
2) K. Tozawa, H. Shiwaku *et al.*, Proc. SRI2003, in press
3) M. Yabashi *et al.*, Proc. of SPIE, 3773 (1999) 2
4) T. Mochizuki, Y. Kohmura *et al.*, Nucl. Instr. and Meth. A, 467-468 (2001) 647

5.1.2 Commissioning of New JAERI Beamline BL22XU in SPring-8

Hiroyuki KONISHI, Takahisa SHOBU, Kazukiyo TOZAWA

The construction of a new JAERI Beamline in SPring-8, a quantum physics structure beamline BL22XU, has been finished at the end of FY2001. Next, we carried out the beamline commissioning and optical adjustments in FY2002.

The preliminary operation of an insertion device ID22 and the optical adjustment of a front-end started at the 5th cycle in 2002A operation schedule. An offline performance examination of a liquid nitrogen circulation system, including the temperature measurements on the inside parts of monochromator chambers, was also made at that time.

As a check on an interlock system had already finished at the end of FY2001, we could introduce the synchrotron radiation beam to an optical hutch for the first time after the irradiation baking of front-end on May 22.

BL22XU has four hutches and a lot of optical elements, two monochromators and four reflection mirrors. Therefore, the condition of radiation survey of shielding hutches on the setting of beamline components was very complex as shown in Table 1. We accomplished radiation survey on the optical hutch on the condition A-F till the end of May. But because some accidents, a vacuum leakage at the insertion device or a breakdown of the liquid nitrogen circulation system on an electrical system, happened, radiation survey on other hutches was completed at the beginning of October.

An adjustment of monochromators was given the highest priority in optical elements. Running conditions of liquid nitrogen circulator system were found out with to decrease the vibration of monochromator crystals by liquid nitrogen flow. As shown in Fig. 2, monochromators make nearly full use of their ability.

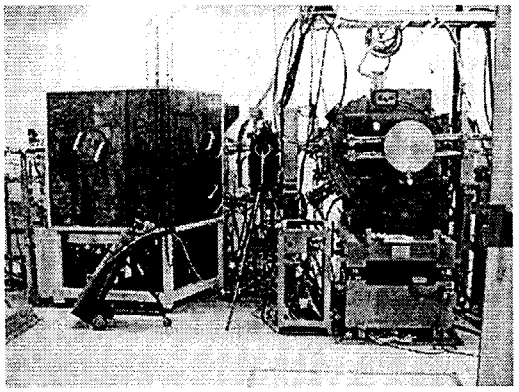

Fig. 1 Photograph of Monochromators in the optical hutch
The left is for high-energy, and the right is for low energy.

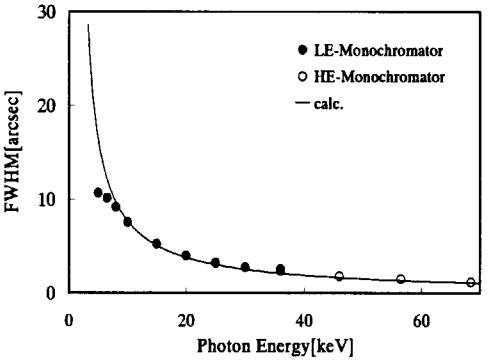

Fig. 2 Energy dependence of diffractive width of monochromators

Table 1 The conditions on radiation survey of shielding hutches

	Hutch	Insertion Device	Beamline Components
A	Optical	Min. Gap	Filter IN
B	Optical	Min. Gap	Filter OUT, BeW IN, HE-Mono IN
C	Optical	Min. Gap	Filter OUT, BeW IN, HE-Mono OUT, BC IN
D	Optical	Min. Gap	Filter OUT, BeW OUT, LE-Mono IN
E	Optical	70keV Setting	Filter OUT, BeW IN, HE-Mono IN, DSS IN
F	Optical	9keV Setting	Filter OUT, BeW OUT, LE-Mono IN, DSS IN
G	Experimental1-3	70keV Setting	Filter OUT, BeW IN, HE-Mono IN, DSS OUT
H	Experimental1-3	9keV Setting	Filter OUT, BeW OUT, LE-Mono IN, DSS OUT

BeW: Beryllium Window, HE-Mono: High Energy Monochromator, LE-Mono: Low Energy Monochromator, DSS: Down Stream Shutter, BC: Beam Catcher

References

1) H.Konishi, H.Shiwaku, T.Shobu, K.Tozawa *et al.*, SPring-8 Information. **7**, 309, 2002

5.2 High Pressure Science

Katsutoshi AOKI

The group has been engaged in investigation on the behavior of substances at high pressure up to 100 GPa for a wide temperature span from 4 to 2700 K using brilliant x-ray light at SPring-8, a third-generation synchrotron-radiation facility. The substances extremely densified under such high pressure often undergo structural or electronic phase transition, creating physical and chemical properties quite different from those at ambient pressure. Soft material graphite, for example, transforms into the hardest material diamond at pressures around 8 GPa and temperatures above 2000 K. The electronic property changes from semi-metallic to insulator in association with the structural transformation. High pressure study of structural and electronic phase transition allows deeply understanding the nature of substances and further provides innovative idea for developing new materials.

A multi-purpose diffractometer was newly constructed to investigate high-pressure structure precisely by x-ray diffraction with a diamond-anvil type high-pressure cell. The system is effectively used for both single crystal and powder x-ray diffraction measurements over a wide pressure and temperature range of 0-100 GPa and 4-273 K, respectively. Two types of detectors are equipped: an area detector of imaging plate and a fast detector of CCD camera. The former is employed for collecting accurate diffraction data to determine precise crystal structure including atomic positions and electronic density, and the latter for monitoring real time change in diffraction pattern to investigate transition kinetics. The system can be combined with a beryllium compound refractive lens, which allows focusing of incident x-ray beam by a factor of several tens in magnitude. We have started high pressure measurements on electron density in typical molecular crystals and order-disorder transition in quasi-crystal.

Graphite-diamond conversion process has successfully investigated by in situ x-ray diffraction measurement and a new model for the conversion mechanism was proposed on the basis of kinetic analysis. The conversion reaction was initiated in a supercritical aqueous fluid formed at high pressure and high temperature, and its process was monitored using energy-dispersive powder-diffraction technique with white light from a synchrotron radiation source. Diffraction patterns were collected every ten seconds. Data collection with such a short time interval enabled us to follow the conversion process in good time resolution and hence to analyze the conversion mechanism from the diffraction peak intensities measured as a function of time. The diamond growth process was described initially as an interface-controlled one and became diffusion-controlled as the temperature approached the "nose" in a time-temperature-transformation diagram. With further increase in temperature toward a graphite-diamond equilibrium temperature, interface-controlled growth became dominant again. The time-dependent measurement first revealed reentrant behavior in the graphite-diamond conversion path.

Selenium forms eight-membered ring or spiral chain in the molecular structure, exhibiting semiconductor-metal transition in its liquid phase at high pressure and high temperature. The relation between the structural change and the semiconductor-metal transition has intensively been investigated by EXAFS, x-ray diffraction and density measurement, but still remains unclear. We carried in-situ energy-dispersive x-ray diffraction and density measurements with a multi-anvil type high-pressure apparatus. The peak shift in radial distribution function observed for liquid selenium at various pressures and temperatures indicated that the electronic transition was accompanied by a structural change and hence characterizes as a weak first-order phase transition.

The electron density of $C_6N_4H_{12}$ (HMT) was determined for a pressure range of 0-4 GPa at room temperature. High quality diffraction data were collected using monochromatized x-ray light from a synchrotron radiation source and an area detector of imaging plate. Precise analysis of the diffraction date by Maximum-Entropy-Method (MEM) reproduced successfully the electronic density of the constituted HMT molecules. The electron surrounding hydrogen atom, which could hardly be seen for ambient pressure crystal, was clearly displayed as lobes in the density map of the pressurized crystal. The dramatic change was likely interpreted in terms of depression of vibrational motions. The synchrotron-radiation powder diffraction combined with MEM was thus demonstrated as a promising tool for investigating electron density or bonding state in molecular solids significantly densified at high pressure.

5.2.1 Kinetics of the graphite-diamond transition with aqueous fluids under high pressures and temperatures

Wataru UTSUMI, Taku OKADA and Nozomu HAMAYA

1. Introduction

Aqueous fluid is an important candidate as a catalyst for forming natural diamonds. Diamond synthesis under high pressures and temperatures with aqueous fluid is a good experimental simulation that may bring us much information on the formation mechanism of natural diamond in the earth interior. Although water in a supercritical state and fluids composed of carbon, oxygen, and hydrogen have been experimentally confirmed to have a catalytic effect on diamond formation, no kinetic studies have been reported due to the technical difficulties. We have conducted an in situ x-ray diffraction study on the graphite-diamond conversion with aqueous fluids and made a kinetic analisys for this transformation.

2. Experimental

Experiments were carried out using a DIA type high-pressure apparatus (SMAP2) installed on beamline BL14B1 (JAERI beamline) at the SPring-8. A mixture of brucite ($Mg(OH)_2$) and graphite (C) was used as the starting material and the graphite to diamond conversion process was observed in a supercritical aqueous fluid formed by dehydrating brucite under high-pressure and temperature. For the *in situ* observations, we performed the energy dispersive powder diffraction using white x-rays. Data collections were made every 10 seconds to observe the time-dependence of the transition. Experiments were repeated at various P-T conditions (1700, 1835 °C at 7.7 GPa, and 1400, 1450, 1500, 1630 °C at 8.8 GPa) and the obtained data were kinetically analyzed by using the Avrami rate equation.

3. Results

Figure 1 plots the required times for diamond transformations under various P-T conditions in a Time-Temperature-Transformation (TTT) diagram, which describes the progress of a transformation in a graph of temperature against the logarithm of the time. Here, the times required to achieve 10% completion of the transformation. The present experimental data indicates that as the temperature increased, the transformation time decreased, which means that they are located on the low-temperature side of the TTT curve that should have a "C-shape." Our previous experimental data using Fe-Al metal alloy were located on its high-temperature side, which shows the contrast to the present study with aqueous fluid as a diamond forming catalyst.

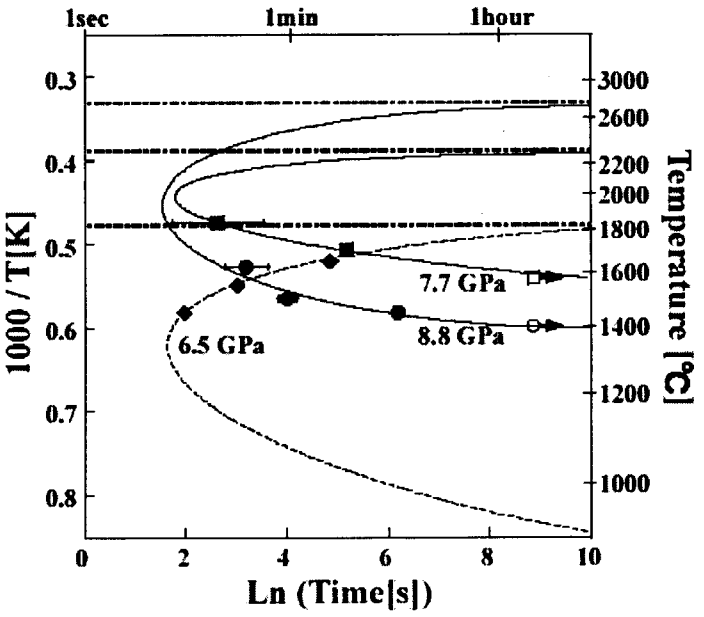

Fig. 1 Time-Temperature-Transformation (TTT) diagram of graphite-diamond transformation

The kinetic analysis clarified a general tendency of the variations in the nucleation and growth process of diamond formation. At low temperatures, the diamond growth process is interface-controlled, but diffusion-controlled growth becomes dominant as temperature approaches the "nose" of the TTT curve. As the temperature approaches the graphite-diamond equilibrium temperature, interface-controlled growth is dominant again.

5.2.2 Structural change of liquid selenium under high pressure

Yoshinori KATAYAMA, Yasuhiro INAMURA, Kazutaka NAKANO*, Takeshi MIZUTANI† and Masaaki YAMAKATA[a)‡]

a) Japan Synchrotron Radiation Research Institute
Present addresses: *Himeji Institute of Technology, †Spring-8 Service, ‡ Rigaku corporation

1. Introduction

At ambient pressure, liquid selenium (l-Se) is a semiconductor. It consists of long chain molecules in which each atom is covalently bonded to two neighbors. Previous X-ray diffraction studies have revealed that the structure of l-Se under pressure differs from that at atmospheric pressure: structure factor of l-Se at 8.4 GPa is similar to that of liquid tellurium (l-Te) at atmospheric pressure[1]. This result suggests that l-Se exhibits semiconductor-to-metal (SC-M) transition under pressure because l-Te is metallic. In fact, Brazhkin *et al.* have found that electrical conductivity of l-Se increased abruptly at a boundary in the pressure-temperature phase diagram[2]. The boundary has a negative slope ($dT/dP < 0$) and the triple equilibrium point is located at P=3.6±0.5 GPa and T=527±20 °C. To study a relation between the structural change and the SC-M transition we have measured EXAFS[3], x-ray diffraction[4] and density for l-Se along a path that crossed the reported boundary.

2. Experimental

EXAFS measurements on l-Se were performed on BL01B1 and BL14B1 at the SPring-8. In-situ energy dispersive X-ray diffraction experiments were carried out using a multi-anvil apparatus installed on JAERI materials science bemaline I (BL14B1) at the Spring-8. Density measurements were carried out at a high-pressure station on BL10XU and JAERI materials science beamline II (BL11XU) at the SPring-8. In the density measurements, the sample was put in a sapphire ring and the x-ray absorption was measured as a function of sample position. From a curve fit analysis of the absorption profile, the density was obtained.

3. Results

From EXAFS measurements, it was found that the two-fold covalent bonds are preserved in the semiconductor region. In contrast, a significant decrease of EXAFS oscillation was observed in the metallic region. The decrease indicates that the covalent bonds weaken and/or break. Diffraction data were obtained just above the melting temperature in a pressure range from 2.5 GPa to 8.3 GPa. The structure factor at 2.5 GPa is similar to that at ambient pressure. Above 3.5 GPa, however, the shape of the structure factor starts to change. Figure 1 shows the radial distribution function. The first peak, which corresponds to the covalent bonds, shifts to large-r side and the overlap between the first peak and the second peak increases with increasing pressure. The density of l-Se at about 3GPa increases with increasing temperature and has a maximum around 830 °C. These results indicate that the SC-M transition is accompanied by a structural change, which has a weak first-order character.

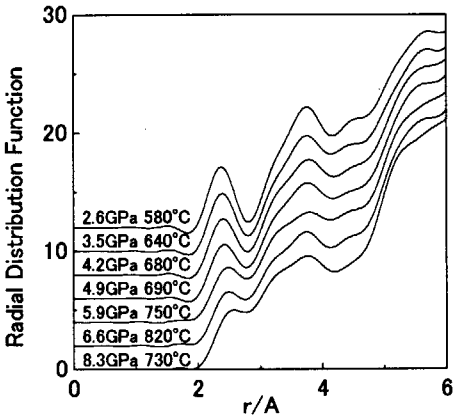

Fig. 1 Radial distribution function of liquid selenium at various pressures

References

1) K. Tsuji, O. Shimomura, K. Tamura, H.Endo, Z. Phys. Chem. Neue Folge **156,** 495, 1988.
2) V. V. Brazhkin, R. N. Voloshin, S.V. Popova, JETP Lett. **50,** 424, 1989.
3) Y. Katayama, *J. Synchrotron Rad. Res.* **8,** 182, 2001.
4) Y.Katayama, T.Mizutani, W.Utsumi, O.Shimomura, K.Tsuji:, phys.stat.sol. (b) **223,** 401, 2001.

5.2.3 Construction of multi-purpose diffractometer for DAC at SPring-8

Tetsu WATANUKI, Akihiko MACHIDA, Tomohiro IKEDA, Hiroshi KANEKO[b], Yasuo OHISHI[c], Nozomu HAMAYA[d], Osamu SHIMOMURA[a], Yutaka YOKOZAWA[e], Masatsugu KANAYAMA[f], Shoichi YASUKAWA[e], Ryosuke SHIMIDZU[g]

[b]SPring-8 Service Co. Ltd.,
[c]Japan Synchrotron Radiation Research Institute,
[d]Department of Physics Ochanomizu University,
[e]Rigaku Co. Ltd., [f]Rigaku Aihara Seiki Co. Ltd.,
[g]Photon Design Co. Ltd.

In order to perform high pressure experiments, a diffractometer for a diamond anvil cell (DAC) was installed (Fig. 1) at new undulator beamline BL22XU at SPring-8. This system is designed for both single crystal and powder X-ray diffraction measurements at room temperature and also at low temperatures. The system mainly consists of three parts; optics and sample positioning stages, detectors, and a microscope. On the basic setup of sample stages including an ω-axis, translations and an arc-stage, various components can be easily mounted with high reproducibility; a χ–ϕ circle goniometer, a 4K He closed cycle cryostat with another arc-stage, and a simple DAC holder. Two types of detectors, an imaging plate (IP); the detection area size of 400 x 400mm^2, and a CCD camera; the size of 70 x 70mm^2, are equipped. The sample, mounted on the diffractometer, can be monitored by the microscope. With use of the microscope, the sample pressure can be also measured by ruby luminescence method. The incident X-ray beam is ordinarily monochromatized at 20-30 keV, which can be focused by a beryllium compound refractive lens.

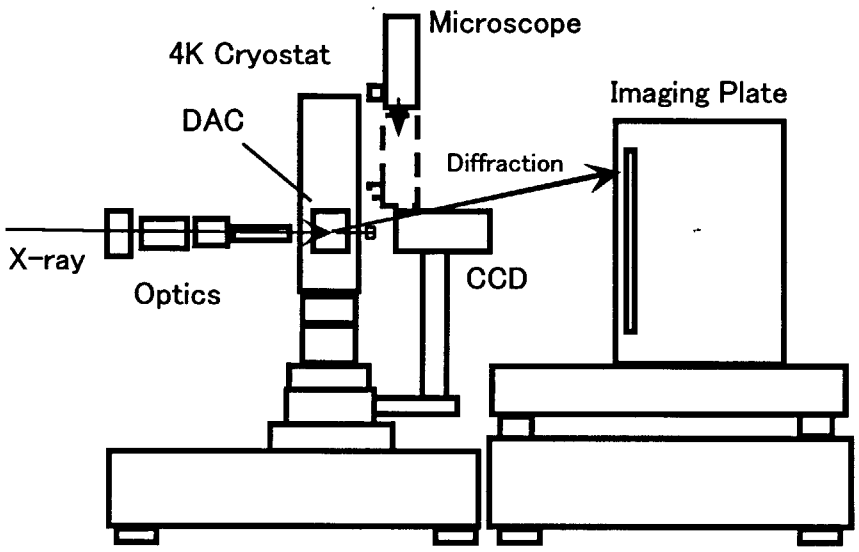

Fig. 1 Schematic view of the multi-purpose diffractometer for DAC

5.2.4 Electron density analysis of hexamethylenetetramine under high pressure

Tomohiro IKEDA, Tetsu WATANUKI, Yasuo OHISHI[a)]
a)Japan Synchrotron Radiation Research Institute

1. Introduction

Hexamethylenetetramine (HMT; $C_6N_4H_{12}$) is well known as a simple organic compound that has very high symmetric crystal structure (cubic, $I\bar{4}3m$). For the specific symmetrical structure, the detailed crystal structure analyses have been reported by X-ray diffraction and Neutron diffraction under ambient pressure. In previous study, we had obtained the electron density distributions of HMT under ambient pressure at 18 K and R.T. In order to investigate the possibility of electron density study about organic compound under high pressure, the electron densities of HMT under high pressure were analyzed by Maximum Entropy Method (MEM)[1)] using Synchrotron Radiation powder data in this study.

2. Experimental

The high pressure X-ray diffraction experiments were performed at SPring-8 BL10XU using diamond anvil cell (DAC) at R.T. The powdered samples were loaded into a hole of Rhenium gasket with small ruby crystals. The diameter of the flat parts of diamonds was 0.45 mm. As pressure transmitting medium Helium was used. The X-ray diffraction patterns were detected using Imaging Plate at 0.7, 1.4, and 3.4 GPa. The wavelength of X-ray was 0.496 Å. Each exposure time of X-ray was 40 minutes. In order to compare with data under high pressure, the diffraction experiment under ambient pressure was also performed.

3. Results

There were no significant differences in obtained diffraction patterns. The crystal structure of ambient pressure was maintained up to 3.4 GPa. The MEM/Rietveld analysis[2)] was performed for obtaining electron densities. Observed and calculated data showed good fitting in Rietveld analysis. The lattice constant of 3.4 GPa was smaller than that of ambient pressure 6 %. However, the bond length between C and N of 3.4 GPa was smaller than that of ambient pressure only 0.7 %. This fact means that the molecular of HMT is fairy rigid and the intermolecular region is mainly compressed.

Figure 1 shows MEM electron densities of HMT (110) plane at ambient pressure and 3.4 GPa. Electrons belonging to hydrogen atom can be hardly seen in Fig. 1(a). On the other hand, those can be seen as lobes which are shown by arrows in Fig. 1(b). Electron density distributions of hydrogen in Fig. 1(b) are similar to those at 18 K under ambient pressure. It is considered that changes of hydrogen electron densities by high pressure are due to the decreasing of thermal vibration of carbon and hydrogen atoms.

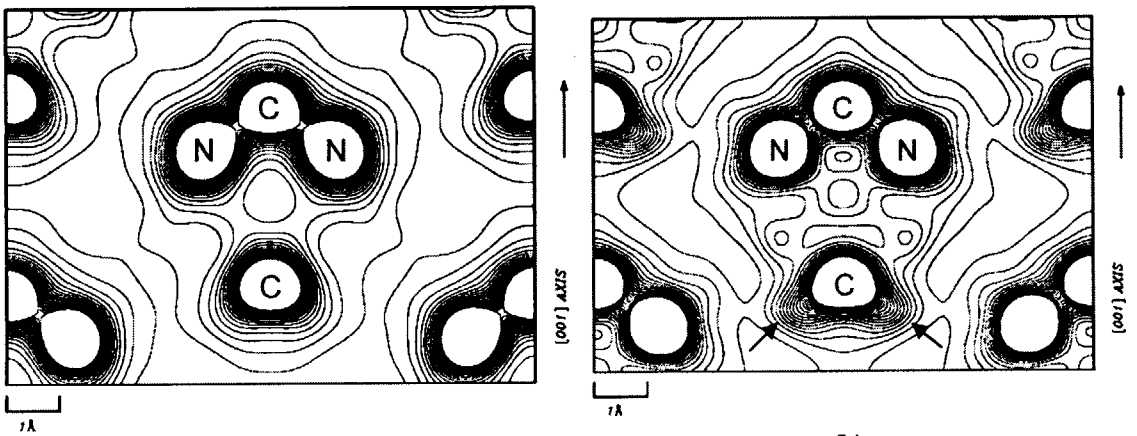

Fig. 1 MEM densities of HMT (110) plane at (a) ambient pressure and (b) 3.4 GPa Contour lines are drawn from 0.1 to 2.1 with 0.1[e/A^3] step width.

References

1) M. Sakata and M. Sato, Acta Cryst. **A46**, 263, 1990
2) M. Takata, E. Nishibori and M. Sakata, Z. Kristallogr. **216**, 71, 2001

5.3 Structural Physics Research

Structural Physics Group

Group leader
Jun'ichiro MIZUKI

The major research purpose of the structural Physics Group is to investigate (1)structural aspects of relevant surfaces and interfaces, where one encounters crystal growth of compound semiconductors by MBE, and electrochemistry, (2)close relation between structures and catalytic activities, (3)dynamics of transition metal oxides, in which the interplay between spin, charge and orbital degrees of freedom is the key ingredient underlying the physics, (4)micro-domain structures in ferroelectronic materials, (5)syntheses of new materials which expect to show superconductivity, magneto-resistant effect, and new functions related to magnetism. Also, since exploiting the full potential of the SPring-8 remains a permanent challenge for the experimentalist, we have been working on the focusing monochrometer crystal/system for the bending magnet beamline. Thus, a final goal of our group is to make the rational design of new materials with specific properties by investigating the relationship between the static and dynamical structure of the materials and their properties.

In this chapter, we will show the recent results regarding to (1) ~ (5). As surface and interface researches, two studies will be presented. One is concerning to the surface structure of GaAs(001) under MBE crystal growth condition, and another to the structure evolution of Bi on Au(111) under electrochemical condition. As the study of the structure- catalytic activity relationship, the local structure of $LaFe_{0.57}Co_{0.38}Pd_{0.05}O_3$, which is a Pd-containing perovskite catalyst, was investigated carefully with Fe, Co, and Pd K-edge by a XAFS technique to know how the structure changes with reduction and oxidation fluctuation. As an example of (3), inelastic X-ray scattering was carried out to study the phonon properties of high TC superconducting copper oxides. The evolution of phonon anomaly as a function of hole doping level in $La_{2-X}Sr_XCuO_4$ will be presented, and discuss this with relation to the superconductivity. And as a beamline deveploment, new focusing optics will be presented.

5.3.1 Kinetics study on phase transition of ultra thin Bi layer formed on Au(111)

Kazuhisa TAMURA and Jun'ichiro MIZUKI

1. Introduction

In the last two decades, electrode surface structures have been energetically investigated using *in situ* scanning probe microscopy (SPM) and surface x-ray diffraction (SXRD). Due to such considerable efforts, it has been recognized that reactivity of electrochemical reactions strongly depends on electrode surface structure. On the other hand, details of surface process during electrochemical reactions are still uncovered especially from the kinetic point of view, due to many technical limitations. Investigating electrode surface structure is not only an essential problem in electrochemistry, but also quite important to make a whole picture of electrochemical reactions. To monitor electrode surface processes, techniques, which possess features of "millisecond time resolution", "nano-scale spatial resolution", and "*in situ*", must be employed. Among several *in situ* nano-scale techniques, only SXRD has three features. In this report, phase transition process of electrochemically formed ultra Bi thin layer on Au(111) was studied using time-resolved SXRD and electrochemical techniques.

2. Experimental

Au(111) electrode was annealed with hydrogen flame and cooled to room temperature before experiment. Electrode surface was protected by an electrolyte drop after cooling. Electrolyte was 1.0 M $HClO_4$ containing 2.5 mM Bi_2O_3. A "drop cell" was used as an electrochemical cell[1]. SXRD measurements were carried out at SPring-8 BL14B1. Energy of x-ray was 30 keV. Coordinate system was hexagonal, a = b = 2.885 Å and c = 7.063 Å. X-ray intensity was measured by NaI detector and time-resolved measurements were achieved using multi channel analyzer (MCA)

3. Results

Ultra thin Bi layer formed on Au(111) is known to have three structures, i.e., disorder, (2×2)-Bi, and $(p \times \sqrt{3})$-2Bi structure, depending on its coverage. Figure 1 shows transition curves of (a) current and (b) x-ray intensity observed at (1/2,1/2) in phase formation of (2×2) from $(p \times \sqrt{3})$ structure. X-ray intensity in this figure reflects area of (2×2) structure under several assumptions.

Current transients show huge jumps and exponential decrease at t=0 and t > 0 sec, respectively. In this phase formation current value mainly reflects kinetics of desorption process of Bi atoms, thus these electrochemical results show that Bi atoms desorb randomly (so called, Langmuir type) from $(p \times \sqrt{3})$ phase. Further, ΔE dependence of Bi desorption was not observed, indicating that surface diffusion of Bi atoms or electrotransfer is slow and both/one of them dominate this desorption process. On the contrary, transient curves of x-ray intensity show sigmoid curve and dependency on ΔE. These results show that (2×2) phase formation proceeds with nucleation-growth and ΔE affects kinetics very strongly.

For many decades, kinetics of electrochemical reaction have been analyzed and discussed in terms of electron transfer process. Our results clearly revealed that structural change of electrode surface have to be independently monitored to make a whole picture of electrochemical reaction.

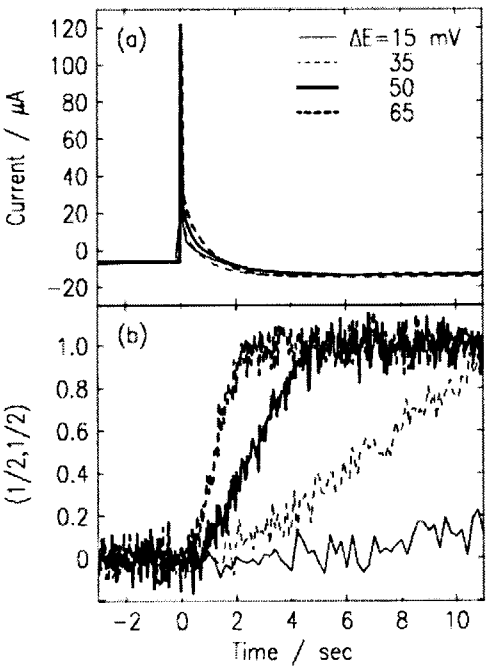

Fig. 1 Transient curves of (a) current and (b) x-ray intensity observed at (1/2,1/2,0.2); electrode potential was stepped at t = 0 sec ΔE corresponds to overpotential for (2 × 2) structure formation.

Reference

1) K. Tamura, B.M. Ocko, J.X. Wang, and R.R. Ad ic, J. Phys. Chem. B, **106,** 3896, 2002.

5.3.2 Crystal structure of Pd-perovskite catalyst in redox fluctuating atmosphere IV

Yasuo NISHIHATA, Jun'ichiro MIZUKI, Hirohisa TANAKA[a)], Mari UENISHI[a)]
a) Materials R&D Div., Technical Center, Daihatsu Motor Co., Ltd.

1. Introduction

Catalytic converters are widely used to reduce the amount of NOx, CO and unburned hydrogen carbons in automotive emissions. In conventional catalysts, precious metals initially have nanometer-order dispersions, but the catalytic activity deteriorates through the particle growth of metals during the vehicle use. It is important to control the catalytic active site not only to maintain high efficiency, but also to economize on precious metals. Perovskite crystals including the precious metal retain its high metal dispersion owing to structural responses to the reduction-oxidation (redox) fluctuations in exhaust-gas composition that occur in state-of-the-art gasoline engines[1].

2. Experiments

Pd-containing perovskite catalysts were prepared by the alkoxide method. The powdered catalyst, $LaFe_{0.57}Co_{0.38}Pd_{0.05}O_3$, was subjected to thermal ageings under oxidation, reduction, re-oxidation atmospheres in due order at 800°C for 1 hour on each ageing step. We employed x-ray absorption fine structure (XAFS) techniques near the Pd K-edge (24.35 keV) at BL14B1, and near the Co (7.71 keV) and Fe (7.11 keV) K-edges at BL01B1 of SPring-8.

3. Results

The valence state of Pd can be estimated from the XANES spectrum (Fig. 1(a)). Compared to the PdO spectrum, the oxidized catalyst shows chemical shift of about 1.7 eV, indicating that the valence of the Pd in the catalyst is higher than the normal bivalence seen in PdO. The theoretical calculation suggested that Pd could exist in such an unusual oxidation state at the B-site: it is trivalent as Co is[1)]. The edge position of the reduced catalyst is identical to that of Pd-foil, suggesting that Pd is in a metallic state. After the re-oxidation treatment, the edge position shifted back to higher energy.

The spectrum of the oxidized catalyst represents trivalent Co occupying the B-site in the perovskite structure (Fig. 1(b)). The spectrum of the reduced catalyst shows a large edge shift to the lower energy side. It can be reproduced from the spectrum of the oxidized catalyst and that of Co-foil at a ratio of 0.49 to 0.51. This implies that about half the Co was transformed into metallic state. The spectrum of the re-oxidized catalyst was completely restored to that of the oxidized. On the other hand, a drastic change in the spectra near the Fe K-edge was not observed (Fig. 1(c)).

The elements occupying the B-site of the perovskite structure could be reduced in a reductive atmosphere at 800°C. They were reduced easily in due order: Pd > Co > Fe. In total, about 30% of the elements occupying the B-site of $LaFe_{0.57}Co_{0.38}Pd_{0.05}O_3$ was transformed into metallic state. Then, all metals occupied the B-site again by the re-oxidation treatment.

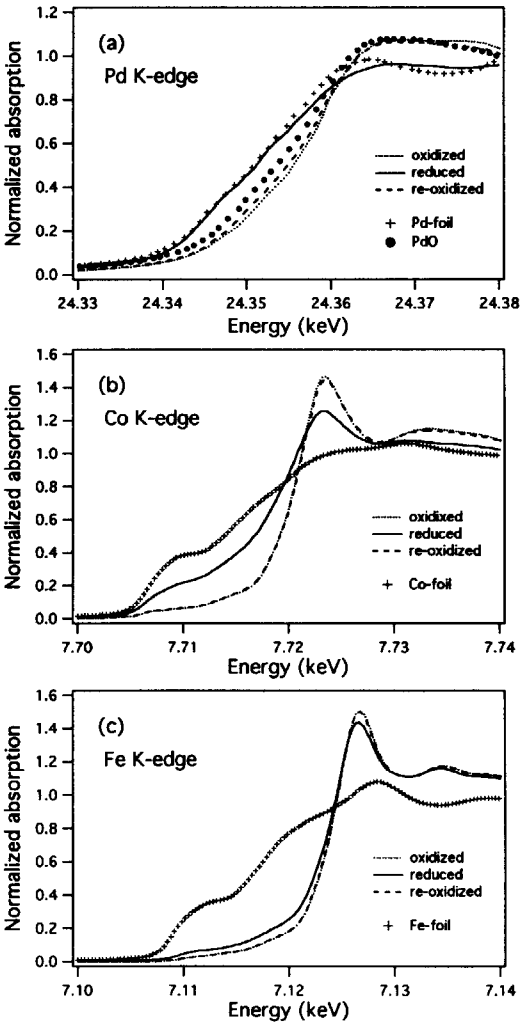

Fig. 1 XANES spectra of $LaFe_{0.57}Co_{0.38}Pd_{0.05}O_3$ near the Pd, Co and Fe K-edges

References

1) Nishihata, Y. *et al. Nature* **418**, 164-167 (2002).

5.3.3 Domain boundaries in the GaAs(001)-(2x4) surface

Masamitsu TAKAHASI, Yasuhiro YONEDA, N. YAMAMOTO[a)] and Jun'ichiro MIZUKI

a) Faculty of Science, Himeji Institute of Technology

The GaAs(001)-2x4 reconstructed surface is the growth surface in the standard molecular-beam epitaxy (MBE) condition. For this surface, the β2(2x4) model is well established by diverse surface techniques such as scanning tunneling microscopy (STM), reflection-high energy electron diffraction (RHEED) and surface X-ray diffraction (SXD). Its unit cell contains two As dimers in the topmost layer and one As dimer in the third layer. However, most of these experimental studies were carried out by transferring the samples from the growth chamber to another analysis chamber. High As overpressure needed for MBE growth has been a barrier to in situ studies of GaAs in practical MBE conditions. In the present work, we have applied in situ SXD technique to GaAs(001)-2x4 surface at substrate temperatures ranging from 480℃ to 610℃ in an As flux of $5x10^{-7}$ Torr.

The experiments were performed with a X-ray diffractometer directly coupled with a MBE chamber which is placed at a synchrotron radiation facility, SPring-8 [1]. Using this instrument, the sample can be subjected to SXD measurements at the same position as prepared. With variation of the substrate temperature and As overpressure, the GaAs(001)-2x4 surface is subdevided into the α, β and γ phases on the basis of relative intensities of fractional-order streaks in a RHEED pattern. These RHEED patterns were interpreted in terms of different atomic arrangements in the 2x4 unit cell. However, we have shown that the α and γ phases result from disordering of the surface 2x4 periodicity by in situ SXD [2]. In the α and γ phases, X-ray diffraction peaks originating from the fourfold symmetry show shift in [110] direction as well as significant broadening of the peaks (Fig.1). This behavior is explained by a simple model where the formation of the antiphase domain boundaries characteristic to each phase is taken into consideration. In the γ phase, a local structure reminiscent of the c(4x4) structure causes a separation of 7a between neighboring 2x4 unit cells, where a is the lattice constant of the 1x1 surface unit cell. On the other hand, domain boundaries with a separation of 5a are dominant in the α phase. This separation can be accounted for by local formation of the α and α2 structures whose stability in Ga-rich conditions is predicted by first-principles calculations.

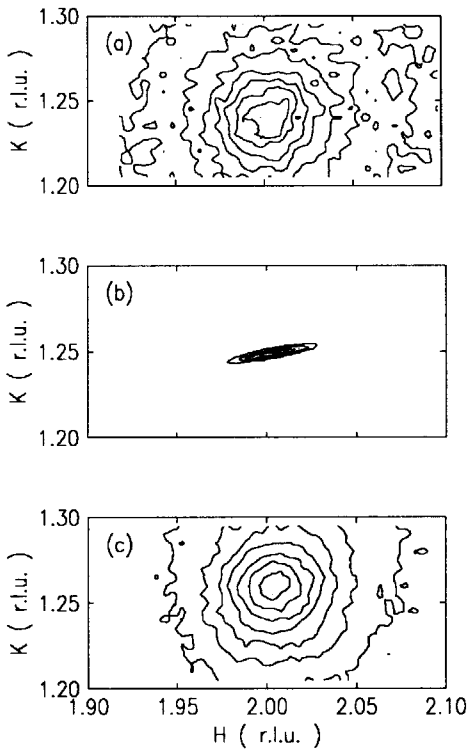

Fig. 1 X-ray peaks profiles at (2, 1.25, 0.04) (a) the α phase at 610℃, (b) the β phase at 520℃ and (c) the γ phase at 480℃

References

1) M. Takahasi , Y. Yoneda, H. Inoue, N. Yamamoto and J. Mizuki, Jpn. J. Appl. Phys. 41 (2002) 6247.
2) M. Takahasi , Y. Yoneda and J. Mizuki, Phys. Rev. B 68 (2003) 085321.

5.3.4 Magnetic and X-ray diffraction study of the Gd/Fe amorphous multilayered thin films fabricated by magnetron sputtering

Kenji YOSHII, Masaichiro MIZUMAKI,[a] Jun'ichiro MIZUKI, Masafumi TAKAGAKI,[b]
Akihisa KOIZUMI [b] and Nobuhiko SAKAI [b]
a) Japan Synchrotron Radiation Research Institute, Mikazuki, Hyogo 679-5149, Japan
b) Himeji Institute of Technology, Kamigouri, Hyogo 678-1297, Japan

Magnetic thin films consisting of transition metals and rare earth metals have attracted much attention because of the possibility of application as magneto-optical devices. Among such systems, Gd/Fe multilayers show a variety of magnetic phases arising from a competition between the exchange and Zeeman interactions [1,2]. Magnetic behavior of some Gd/Fe multilayered systems has been explained on the basis of the Camley's model [3]. However, no systematic studies have been reported for the magnetic properties with changing a thickness ratio of Gd to that of Fe. In this work, we investigated the properties of such a system to examine the theoretical model.

The samples were prepared by alternately depositing Gd (x Å) and Fe (100-x Å) layers on a polyimide film in a dc-magnetron sputtering system. The total number of Fe(100-x Å)/Gd(x Å) layers is 30. The x values are 20, 30, 50, 70, and 80. Magnetization measurements were performed by use of a SQUID magnetometer (Quantum Design MPMS). To evaluate the quality of the films, we also performed X-ray diffraction using synchrotron radiation at the BL46XU beamline of SPring-8.

Figure 1 shows the temperature dependence of the magnetization of [Fe(100-x Å) /Gd(x Å)]x30 multilayers with an applied field of 100 Oe. The monotonic decrease in magnetization at low temperatures for x=20 and 30 implies the presence of antiferromagnetic interaction between the Gd and Fe layers. The samples with x = 50 and 70 Å exhibit the compensation temperatures ($T_{comp.}$) of ~100 K and ~200K, respectively. The higher value of T_{comp} for x = 70 Å is qualitatively explained in connection with a phase stability predicted by the Camley's model [4]. A further analysis has been carried out on the assumption that the moment of Fe is constant (=2.2μ_B) below 300K, and the magnetization of Gd is composed of that in the interfacial and bulk-like regions[5]. It was found that the magnetic behavior of the present system exhibits a two-dimensional effect even at the Gd thickness of 70 Å, while such an effect was reported only for much thinner films in the other magnetic systems [4].

The synchrotron X-ray diffraction showed both the periodicity of the layers and the flatness of the interfaces for the [Fe(10 Å) /Gd(10 Å)]x50 film. From a preliminary analysis, the interdiffusion area between the Fe and Gd layers was found to be ~2Å. The same quality is plausibly expected also for the [Fe(100-x Å) /Gd(x Å)]x30 series. Further results will be published in the near future.

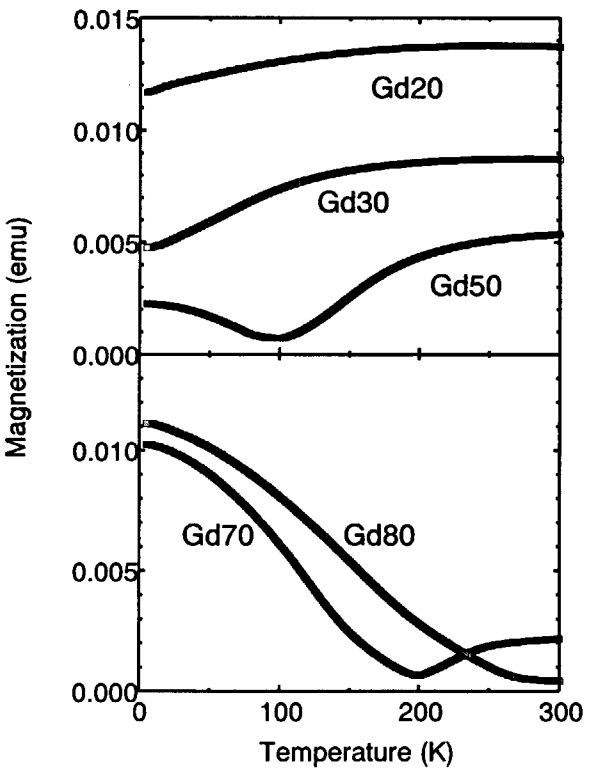

Fig. 1 Temperature dependence of magnetization of [Fe(100-x Å) /Gd(x Å)]x30 multilayers 'Gd20' means [Fe(80 Å) /Gd(20 Å)]x30 multilayers.

References

1) A. Koizumi *et al.*, Phys. Rev. **B61**, R14909-14912, 2000.
2) M. Takagaki *et al.*, J. Phys. Soc. Jpn. **72**, 245-248, 2003, and references therein.
3) R. E. Camley and D. R. Tilley, Phys. Rev. **B37**, 3413-3421, 1988.
4) M. Mizumaki *et al.*, submitted to J. Mag. Mag. Mater.
5) D. Haskel *et al.*, Phys. Rev. Lett. **87**, 207201, 2001.

5.3.5 Inelastic x-ray scattering studies of phonons in $La_{2-x}Sr_xCuO_4$

Tatsuo FUKUDA, Jun'ichiro MIZUKI, Kazuhiko IKEUCHI[a)], Kazuyoshi YAMADA[a)], Alfred Q.R. BARON[b)], Yoshikazu TANAKA[c)], Satoshi TSUTSUI[b)], Yasuo ENDOH[d)]
a) Inst. Chem., Kyoto Univ. b) JASRI, SPring-8 c) RIKEN, SPring-8 d) Inst. Mat. Res., Tohoku Univ.

1. Introduction

The significance of electron-phonon interaction in high-T_c superconductors (HTcS) have been recognized again for two types of recent experiments. First one is the angle-resolved photoemission (ARPES) studies, which shows a 'kink' structure in the dispersion of electron quasiparticles [1)], and one explanation of this kink structure is interactions with electron quasiparticles with the highest energy longitudinal optical (LO) phonon mode. Second one is the inelastic neutron scattering (INS) measurements, which shows anomalous softening in the highest energy LO phonon mode along <100> direction with doping holes[2)]. However, samples only below optimum hole concentration have been investigated so far by INS studies, because the crystal growth becomes difficult as hole concentration increases. Therefore, we carried out phonon measurements on one of typical high-T_c superconductors, $La_{2-x}Sr_xCuO_4$ (LSCO), by inelastic x-ray scattering (IXS) measurements. We used x=0.12 (optimum doped) and x=0.29 (over-doped) samples.

2. Experiments

The single crystals of LSCO was grown at Kyoto University using the traveling-solvent floating-zone (TSFZ) method. The experiments were performed at BL35XU of SPring-8. The incident x-rays from an undulator source were monochromated using a Si(111) double-crystal monochromator, followed by a Si(888) high-energy-resolution backscattering monochromator, operating at 15.816keV. Then, the x-ray beam was led to the sample position, and the scattered photons were energy analyzed by 4 spherical silicon crystal analyzers, which are settled at 10 m apart from the sample. The momentum and energy resolutions were about 0.076 $Å^{-1}$ and 6.0~6.2 meV. The measurements were done mainly with a reflection mode (Bragg geometry) at low temperature to reduce diffuse elastic scattering and tails of low energy phonons.

3. Results

We mainly measured the highest energy LO phonon mode along <100> direction, which reveals strong anomaly with doping. Fig. 1 shows the dispersion relation of the LO phonon peak. The INS results of a non-doped and x=0.15 samples[2)] are also shown. While the x=0.12 and 0.15 samples reveal a strong softening, the dispersion of x=0.29 sample is almost the same as that of non-doped sample. In other words, the softening becomes large with increasing x from 0 to around optimum doped (x ~0.15) concentration, beyond which it becomes small again following the change of T_c. This result implies that the electron-phonon interaction which causes the LO phonon softening seems to be important for the formation of Cooper-pairs.

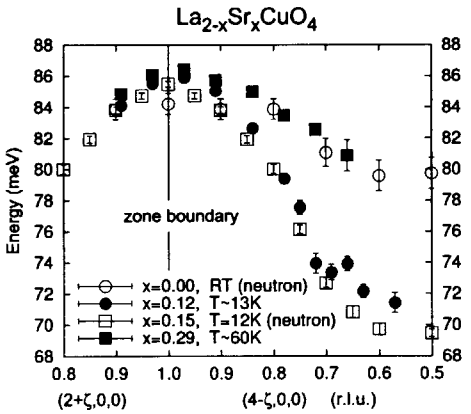

Fig. 1 the dispersion relation of the highest energy LO branches along <100>

References

1) A. Lanzara *et al.*, Nature **412** 510, 2001.
2) L. Pintschovius *et al.*, Physica B **174**, 323, 1991.; R.J. McQueeney *et al.*, Phys. Rev. Lett. **82**, 628, 1999; L. Pintschovius *et al.*, Phys. Rev. B **60**, R15039, 1999.

5.3.6 Two-dimensional X-ray focusing by crystal bender and mirrors

Yasuhiro YONEDA, Norimasa MATSUMOTO, Yokito FURUKAWA[a)],
Tetsuya ISHIKAWA[a,b)] and Jun'ichirou MIZUKI
a) Japan Snchrotron Radiation Research Institute (JASRI),
b) Institute of Physical and Chemical Research (RIKEN)

1. Introduction

One of the best method of focus monochromatic x-rays without losing energy resolution is two-mirrors and two-crystals optics. By combining sagittally focusing double-crystal monochromator (DCM) and vertical focusing mirror, two-dimensional focusing can be realized. Considering a given energy resolution, this focusing system gives ideally the highest intensity possible on a point sample from a divergent beam emitted by a point source. The energy resolution is not dependent on the incoming beam divergence when the mirror curvature is adjusted. Its minimum value is determined by the Darwin width of the monochromator crystals. The intensity is at its highest because the full divergence of the incoming beam can be used. In addition, higher harmonics are rejected without detuning the two crystals of the monochromator.

In this article, we will describe test results of sub-millimeter 2D focusing by using a newly developed crystal. A reasonably good focusing of 0.5 mm was achieved using both Si 311 and 111 reflections with the inclined geometry.

2. Crystal design

The design of the sagittal crystal on the DCM, illustrated in Fig. 1 was first proposed by Kushnir *et al.*[1)] After final etching, the crystal shape is W = 62.7 mm and L = 90 mm (γ = 1.435). Thickness of diffracting plane and thicker legs are 0.5 mm and 2.0mm, respectively.

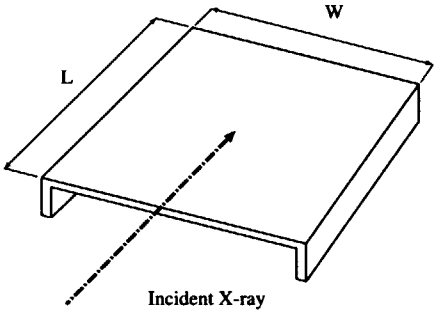

Fig. 1 Design of the sagittal focusing crystal showing the thicker legs used to hold and bend the crystal and the thin diffracting portion cut in the golden aspect ratio.

3. Results

The horizontal beam size was 36.5 mm at the screen position for the maximum bent radius. At the optimal focusing (R = 4 m), the horizontal sizes of the beam approached 4.0 mm. Then, the bending radius was tuned to minimize the horizontal beam size. After the horizontal fine focusing was obtained, the longitudinal beam size was focused to 0.5 mm with mirror. The double focused beam image at the sample position was measured by scanning the slit, as shown in Fig. 2.

The 2D sub-millimeter focusing was tested by using DCM and mirrors those are designed for the SPring-8 standard beamlines. The flux density of the focusing X-ray beam was increased by 70 times compared with that using flat-flat double crystals.

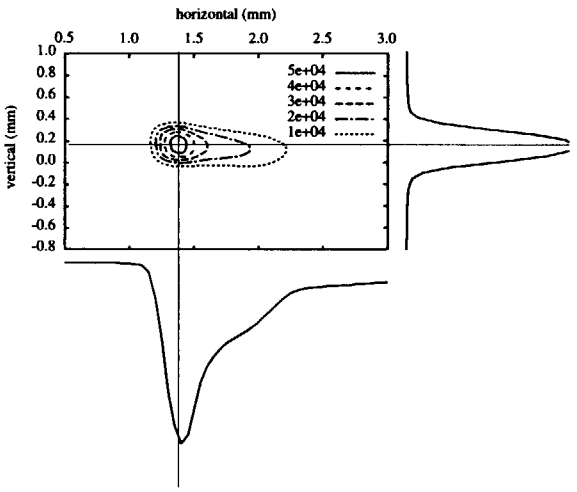

Fig. 2 2D beam profiles with the sagittally focusing crystal and longitudinal focusing mirror measured by translating a 500×500-μm slit on a sample.

References

1) Kushnir, V. I., Quitana, J. P., and Geogopoulos, P., Nucl. Instrum. Methods A **328**, 588, 1993.

5.4 Surface Chemistry Research

Surface Chemistry Research Group
Yuji BABA

Surface of solid is "active field" where various chemical reactions easily happen, because there exist lots of dangling bonds compared with inside of the solid. Also low-dimensional materials such as one-dimensional wires and two-dimensional ultrathin films have many interesting chemical properties because they have relatively large active surfaces compared with bulk materials. Such active properties of solid surface and low-dimensional materials are applied to many kinds of functional devices such as adsorbent, gas sensor and catalysis. In order to contribute to the development of new surface functional devices, it is of great importance to elucidate the dynamics of surface chemical reaction as well as to clarify the electronic structures of solid surface and low-dimensional materials in mono-layer and mono-atomic scale. Also the precise control of chemical reaction at semiconductor surfaces is one of the key techniques for the fabrication of next-generation semiconductor devices in nanotechnology field.

The main objectives of Surface Chemistry Research Group are, 1) to clarify the dynamics of gas-solid reaction in mono-layer and mono-atomic scale using synchrotron radiation, and 2) to search new low-dimensional materials and elucidate their electronic and geometrical structures. Another objective of this group is to control surface chemical reaction using synchrotron radiation as a driving force of chemical reaction. Using energy-tunability and polarization of synchrotron radiation in soft X-ray region, we found that we can cut chemical bond at a specific site and at a specific direction even in multi-element materials like using "scissors". The photochemical reaction induced by X-ray irradiation is also important in the field of radiation biology. Living things exposed to high-energy radiation result in serious transformations such as canceration and mutation due to the radiation-induced decomposition of the fundamental biomolecules such and DNA, amino acids, and bases. In order to know the mechanism of the radiation-induced transformations at molecular level, we installed an electron paramagnetic resonance (EPR) in the BL-23SU of the SPring-8 to detect radiolysis products in biological molecules in-situ.

In this chapter, four recent results from the above topics are presented. First one is concerning the dynamics of chemical reaction at semiconductor surfaces. The oxidation reactions at silicon surface can be precisely controlled by changing the translational kinetic energy of the incident oxygen molecules. The result as well as a series of the results obtained by supersonic molecular beams will surely contribute to the field of nanotechnology. The second and third reports are related to the specific chemical reaction induced by soft X-ray irradiation. In the second report, we succeeded in causing fragmentation for the molecules only at a specific direction in randomly oriented condensed system. The third report describes the specific fragmentation in biological molecules induced by soft X-ray irradiation. We found that the core-to-valence resonant excitation induces the specific fragmentation not only in simple molecules but also in relatively large, and bulky biological molecules. The fourth report deals with the observation on the short-lived radicals which are produced by the soft X-ray irradiation. A clear difference in the yields between X-ray absorption and radical production was observed. The results will certainly shed light on the elucidation of the mechanism of photo-fragmentation in biomolecules by X-ray irradiation.

5.4.1 Control of O_2 adsorption and SiO desorption by incident energy of O_2 molecules in the O_2/Si(001) surface reaction system

Yuden TERAOKA and Akitaka YOSHIGOE

1. Introduction

Since the translational kinetic energy (E_t) of incident O_2 molecules affects the passive oxidation (oxide-layers formation) and the active oxidation (SiO desorption) of the Si(001) surface, the study of surface chemical reactions for the O_2/Si(001) system is interesting from a viewpoint of chemical reaction dynamics. In the passive oxidation at room temperature, we have already reported the E_t dependence of initial adsorption probability and saturated oxygen amount on the clean and the H_2O-adsorbed surface.[1] Incident energy effects for the active oxidation was investigated by detecting $Si^{18}O$ molecules during irradiation of $^{18}O_2$ beams. Furthermore, they were studied from a standpoint of oxygen uptake by applying real-time in-situ photoemission spectroscopy.[2] We found the incident-energy-dependent coexistence of the passive and the active oxidation.[3]

2. Experimental

All experiments were performed at the surface chemistry experimental station (SUREAC2000), installed at the soft X-ray beamline (BL23SU) in the SPring-8. The incident energy of O_2 molecules was controlled by supersonic seeded molecular beam techniques. The maximum energy was estimated to be 3.0 eV (3.3 eV for $^{18}O_2$). The typical O_2-molecular-beam flux density is $3x10^{14}$ molecules cm^{-2} s^{-1}. The base pressure of the vacuum chamber was achieved to be $5x10^{-9}$ Pa. The $Si^{18}O$ desorption yield was measured by using a differentially-pumped quadrupole mass analyzer. The monochromatic synchrotron radiation of 830 eV was used in the real-time in-situ O-1s photoemission spectroscopy.

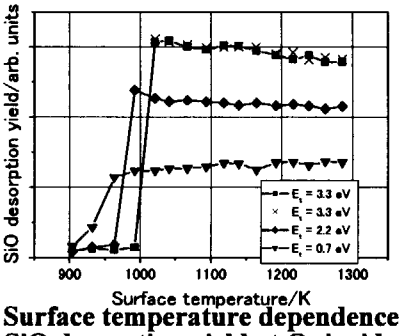

Fig. 1 Surface temperature dependence of SiO desorption yield at O_2 incident energies of 0.7 eV (▼), 2.2 eV (□) and 3.3 eV (■ and ×), respectively The net SiO signal intensity was normalized by the incident O_2-molecular-beam flux density.

3. Results

The $Si^{18}O$ desorption yields are shown in Fig. 1 at the $^{18}O_2$ incident energies of 0.7 eV, 2.2 eV and 3.3 eV, respectively. The $Si^{18}O$ desorption yield increased with increasing incident energy in a higher temperature region than 1000 K. The critical temperatures, at which the $Si^{18}O$ desorption took place suddenly, shifted toward a high temperature side with increasing incident energy, and in turn the $Si^{18}O$ desorption yield decreased with increasing incident energy in a lower temperature region than about 1000 K. In order to make clear SiO desorption mechanisms, oxygen uptake curves were measured at 945 K by applying the real-time in-situ O-1s photoemission spectroscopy. The uptake curves are shown in Fig. 2. The surface was clean during O_2 irradiation at 0.8 eV. This indicates that all O_2 molecules adsorbed desorb "immediately" as the SiO molecules. On the other hand, the oxygen uptakes at higher E_t than 1.5 eV showed a Langmuir-type character, indicating the random adsorption. Contrary to that, a strange uptake at 1.2 eV seems to be an auto-catalytic character. Although the coexistence of the passive and the active oxidation has been already discussed in the gas oxidation case, the new point of this work is that the adsorption kinetics is controllable by the incident energy.

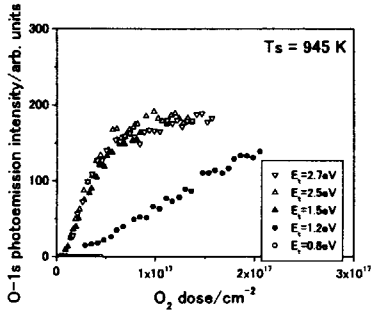

Fig. 2 Oxygen uptake curves at 945 K at various incident energies of the supersonic O_2 molecular beams

References

1) Y. Teraoka and A. Yoshigoe, Jpn. J. Appl. Phys. **41**, 4253, 2002
2) A. Yoshigoe and Y. Teraoka, Surf. Interface Anal. **34**, 432, 2002
3) Y. Teraoka, K. Moritani and A. Yoshigoe, Appl. Surf. Sci. **216**, 8, 2003

5.4.2 Direct and indirect photo-fragmentation processes of condensed molecules as studied by orientation-selective excitation

Tetsuhiro SEKIGUCHI, Yuji BABA, Iwao SHIMOYAMA, Krishna G. NATH

1. Introduction

One of the most intriguing topics in photo-fragmentation using soft X-rays from synchrotron radiation (SR) would be "atomic-site specific" fragmentation. If two or more different kinds of atom can be selectively excited by tuning the photon energy to each resonance of an atom's 1s orbital, the rapture of a chemical bond is expected to occur in the vicinity of an activated atom site. So far, some examples of site-specific fragmentation have been reported in the gas phase. However, if a molecule is coupled to surroundings in a condensed phase, this interaction extremely modifies the core-hole decays, bond-scissions, and desorption processes. The most significant feature of the fragmentation pathways in condensed phases compared with that in isolated systems is that indirect mechanism called XESD (X-ray-induced electron-stimulated-desorption) exists. In the indirect process, secondary electrons generated through inelastic scattering cause bond-breaking. If the XESD governs over the direct photo-dissociation processes, the site-selective reaction will never be seen. Therefore, it is essential to know how much the indirect process occurs. To distinguish the two mechanisms, we used polarized SR. The linearly polarized light can excite molecules with a bond axis pointing to a given direction that is defined by angles of polarization and symmetries of resonant excitation. It can be assumed that the fragment yields produced by the direct mechanism depend on the polarization angle, but the indirect ones do not.

2. Experimental

We developed the rotatable time-of-flight mass-spectrometer[1] to detect the polarization-dependent photo-fragment yields. The sample reported here are condensed formic acid (HCOOH) and fluorobenzene (C_6H_5F) grown on the cleaned Si(100) and gold substrate, respectively.

3. Results and discussion

C-H bonds are preferentially broken and H^+-fragments are efficiently desorbed following the C 1s→$\sigma^*_{C\text{-}H}$ resonant excitation of condensed formic acid[2]. For the $\sigma^*_{C\text{-}H}$ resonance shown in Fig. 1-(c), H^+-desrption probability in parallel polarization (θ=90°: the electric field vector of the light is parallel to the surface) is one-third of that in perpendicular (θ=10°). Re-neutralization of ions causes the polarization dependence. The directly produced fragments are mostly re-neutralized and cannot desorb as an ion when the direction of excited bonds is parallel to the surface. For fluorobenzene, H^+-yields (Fig.1-(a)) and F^+-yields (Fig.1-(b)) are proportional to C-H and C-F breakings, respectively. H^+-yields do not depend on the polarization angle, while F^+-yields depend on it for the F1s→$\sigma^*_{C\text{-}F}$ resonance. Note that the C-H site to be broken is far from the C-F site where a core-hole is created. We found the trend in which the fragmentation occurring at the sites far from the core-hole-site depended scarcely on the polarization: i.e., XESD was mostly 100%. Also the fragmentation occurring at the core-hole site depended well on the polarization[3,4].

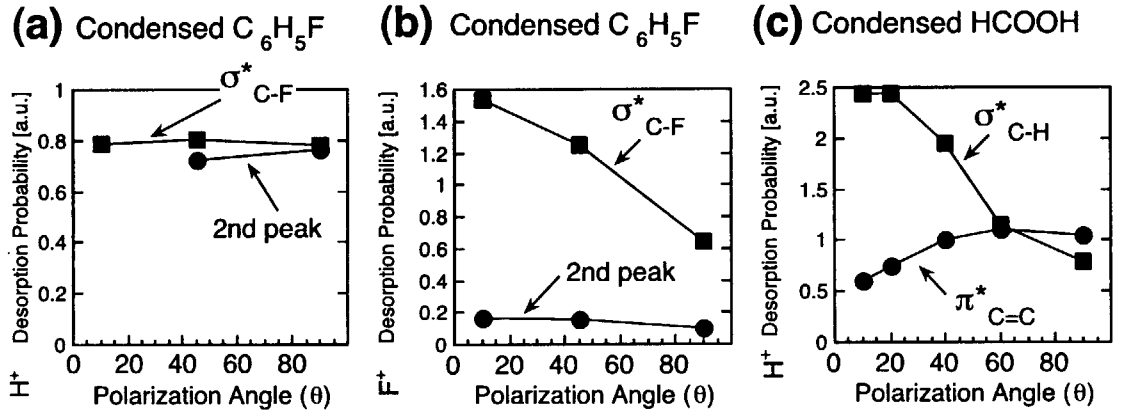

Fig. 1 Polarization-angle dependence of the desorption probabilities of fragment ions. (a) H^+ by F 1s excitation of C_6H_5F, (b) F^+ by F 1s excitation of C_6H_5F, (c) H^+ by C 1s excitation of HCOOH.

References

1) T. Sekiguchi et al., Applied Surface Science **169-170**, 286 (2001).
2) T. Sekiguchi et al., Surface Science, **482-485**, 279 (2001).
3) T. Sekiguchi et al., Surface Science, **532-535**, 1079 (2003); ibid **528**, 242 (2003).
4) S. Wada and T. Sekiguchi et al., Nucl. Instr. Meth. Phys. Res., **B199**, 361(2003).

5.4.3 Photon-stimulated ion desorption from sulfur-containing amino acids following sulfur K-edge excitation

Yuji BABA, Tetsuhiro SEKIGUCHI, Iwao SHIMOYAMA, Krishna G. NATH

1. Introduction

Irradiation of ultraviolet light or soft X-ray on a solid induces chemical-bond scission triggered by the excitation or ionization of core electrons. When the photon energy is tuned at the inner-shell ionization threshold, a chemical-bond scission around a specific atom is expected, because a core-level is localized at the atomic site even in a multi-element material. Such kind of specific bond scission by core-level photoexcitation was firstly found in gas-phase molecules[1], and then it was successfully applied to the adsorbed molecules[2]. For example, we succeeded in desorbing specific fragment-ions from adsorbed molecules following the resonant photoexcitation from core to valence unoccupied state[2]. For bulk material, this is not necessarily the case because secondary electrons produced after core excitation would also induce non-specific reaction. In order to elucidate whether or not such specific bond scission happens in bulk material, we present the results for the photon-stimulated ion desorption from some of biological molecules following the irradiation of monochromatized synchrotron soft X-rays around the core-level ionization thresholds.

2. Experimental

Experiments were performed at the BL-27A station of the Photon Factory in the High Energy Accelerator Research Organization. The molecules investigated were sulfur-containing amino acids such as L-cystine, L-cysteine and L-methionine. The samples were pressed into pellets at a pressure of 1 ton/cm^2. The desorbed ions were detected by a quadrupole mass spectrometer operating in a pulse counting mode. X-ray absorption spectra were measured by total electron yield (TEY) which was monitored by sample drain current.

3. Results and discussion

Figure 1 shows the mass spectra of the desorbed ions from L-cystine. The upper spectrum was taken by the irradiation of 14 eV electrons, and the lower one was obtained by the irradiation of 2472.8 eV photons which corresponds to the resonant excitation from the S 1s to unoccupied σ^* orbitals. For the electron-irradiated spectrum, we can see various fragment-ions, representing the ionic fragments by the valence excitation. While, the irradiation of 2472.8 eV photons induces only S^+-ion desorption. The clear difference shows that the core-level excitation localized at the sulfur atom is followed by the bond scission only around the excited sulfur atom.

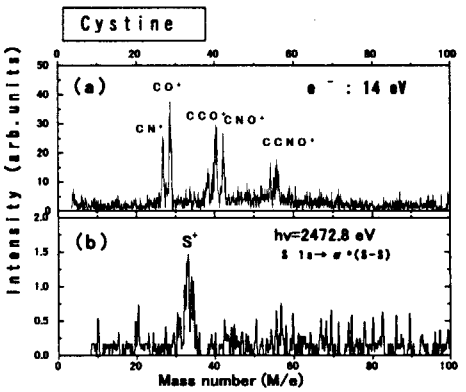

Fig. 1 Mass spectra of desorbed ions from cystine. (a) Irradiated by 14 eV electrons, (b) Irradiated by 2472.8 eV photons

Figure 2 shows the photon-energy dependencies of TEY and S^+ ion yield for L-cystine. When we compare the jump ratio (I_{on}/I_{off}) defined as the intensity ratio between off-resonance and on-resonance energies, the I_{on}/I_{off} ratio for the TEY curve is 1.5, but the value for the S^+ yield curve exceeds 20. The results clearly show that the S^+ desorption is caused not by the secondary electrons produced following the Auger decays but by the direct core-to-valence resonant excitation localized at the sulfur atom. The present results suggest that the core-to-valence resonant photoexcitation induces specific bond scission even in biological molecules where many of secondary electrons are produced after core-level excitation.

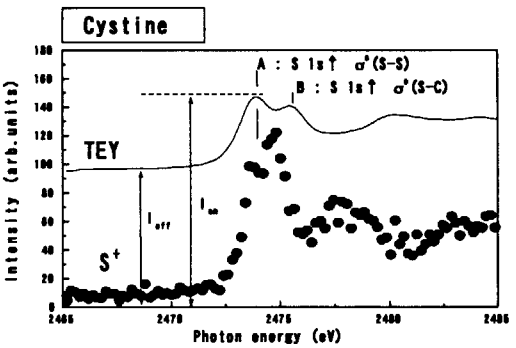

Fig. 2 Photon-energy dependencies of the TEY and S^+ yield around S *K*-edge for cystine

References

1) W. Eberhardt et al., Phys. Rev. Lett. **50**, 1038 (1983).
2) Y. Baba, K. Yoshii and T.A. Sasaki, Surf. Sci. **341**, 190 (1995).

5.4.4 Guanine radical induced by K- resonance photoexcitation at oxygen and nitrogen

Akinari YOKOYA, Ken AKAMATSU[a)] and Kentaro FUJII
[a)] Japan Society for the Promotion Science

1. Introduction

To understand the mechanism of the oxidative base lesion in DNA molecule, we have studied guanine radical using an *in situ* EPR method installed in a soft X-rays under beamline in SPring-8. In our previous study, the appearance of short-lived radicals in the guanine sample has been reported. These radicals are only observed during beam irradiation[1)]. In the present study, we further examined the radical yield of guanine around the oxygen and nitrogen *K*-edge.

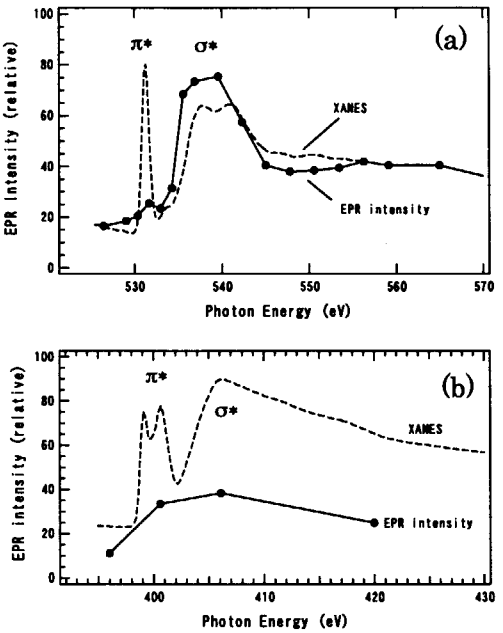

Fig. 1 EPR spectra of guanine pellet irradiated at oxygen (a) and nitrogen K-resonance energy (b) at 77 K XANES spectra of guanine are also shown by s dotted line for comparison.

2. Experimental

EPR signal of guanine was measured using a X-band electron paramagnetic resonance device (SLEEPRS: Synchrotron Light Excited Electron Paramagnetic Resonance Spectrometer) installed in a JAERI soft X-ray beamline (BL23SU) in SPring-8. The sample pellet was irradiated with soft X-ray photons at a microwave cavity in a vacuum chamber ($<10^{-6}$ Pa). A closed-cycle cryogenic system was used to control the sample temperature from 77 K to room temperature. Relatively low microwave power ranging 0.1 to 1 mW was used to avoid power saturation of EPR signals. Based on a XANES spectrum of guanine film reported in our previous paper[3)], several photon energies were chosen for irradiation. Resolution power, $E/\Delta E \sim 1{,}000$ at the Oxygen and nitrogen K-edge (0.4 - 0.5 keV) region, and a photon flux of the order of 10^{11} (photons/sec/100 mA ring current/0.02 % band width) were realized at the sample position.

3. Results and discussion

As shown in Fig. 1 (a), the EPR signal intensity at the energy of the oxygen K-resonance excitation (539 eV) was strongly enhanced to over five times that obtained on the lower energy side (525 eV). On the other hand, as shown in Fig. 1 (b), the enhancement was insignificant above and below the nitrogen K-edge (401 eV).

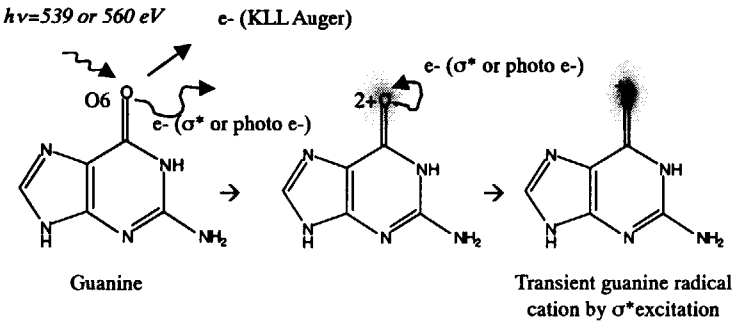

Fig. 2 Proposed physical process of the guanine radical formation

The short-lived radical species that we observed were mainly induced as a result of the final state of the resonant Auger process on oxygen atoms existing solely in the carbonyl group in guanine (Fig.2). Auger events at the other atoms in guanine (namely, carbon and nitrogen) do not induce this radical process to any great extent, even though the abundance of these atoms (i.e. the sum of their photoabsorption cross sections) is dominant in the guanine molecule.

References

1) A. Yokoya, K. Akamatsu and K. Fujii, *Nucl. Instr. Meth B*, 199 (2003), 366-369.
2) K. Fujii, K. Akamatsu and A. Yokoya, *Nucl. Instr. Meth B*, 199 (2003), 249-254..

5.5 Heavy Atom Science

Heavy Atom Science Group
Group Leader
Youichi MURAKAMI

The strong correlation between electrons in solids makes a great variety of phenomena, for example, high Tc superconductivity, colossal magnetoresitance, and heavy fermion characteristics and so on. This wide diversity of electric states in these systems is driven by a small change of the external condition such as a doping level, temperature and magnetic field. Actually, some different kinds of order coexist or are close each other in their phase diagram. The order-parameters in these phases are characterized by multi-degrees of freedom, namely, charge-, spin-, orbital- of an electron and the lattice-degrees of freedom. The orderings of these degrees of freedom sometimes appear simultaneously and sometimes compete with each other. The electric and magnetic properties of the strongly correlated electron systems are determined by the orderings of these degrees of freedom. One of our goals is to construct physics of these electric degrees of freedom in order to understand many novel properties from the strong electron correlation in heavy element compounds. We are also developing the experimental technique of synchrotron radiation to aim for the physics. In particular we have studied the resonant x-ray scattering technique and the diffraction technique in the extreme condition, for example, experiments under high pressure or high magnetic field in low temperature.

In this chapter, we will show our recent with regard to a electric excitation from the hole doped manganite $La_{0.8}Sr_{0.2}MnO_3$ and the high-pressure structure of charge-lattice-spin coupled vanadate NaV_2O_5. We also show the recent status of scanning type synchrotron radiation Mossbauer microscope.

5.5.1 Electronic excitation of $La_{0.8}Sr_{0.2}MnO_3$ studied by resonant inelastic x-ray scattering

Kenji ISHII, Toshiya INAMI, Kenji OHWADA, Kaori KUZUSHITA, Youichi MURAKAMI, Jun'ichiro MIZUKI, Yasuo ENDOH [a], Sumio ISHIHARA [b], Hiroshi KONDO [a], Sadamichi MAEKAWA [a], and Kazuma HIROTA [c]

a) IMR, Tohoku Univ., b) Dept. of Physics, Tohoku Univ., c) ISSP University of Tokyo

1. Introduction

Resonant inelastic x-ray scattering (RIXS) in hard x-ray regime is a new technique to investigate the electronic excitations, and it has been developed recently by utilizing the high brilliance of x-rays from the third generation synchrotron radiation. It can measure electron dynamics with momentum resolution by tuning the energy of incident x-ray near an absorption edge. One of the most suitable materials studied by RIXS is the strongly correlated electron system, which shows an interesting phenomenon, such as high-T_C superconductivity in cuprates and colossal magnetoresistance (CMR) in manganites. These phenomena occur in the vicinity of metal-insulator transition by carrier doping to Mott insulators, in which a band splits into occupied lower Hubbard band (LHB) and unoccupied upper Hubbard band (UHB) by the strong electron correlation (Coulomb interaction). The effect of carrier doping in a Mott insulator is much more complicated than that in a band insulator, and the electronic structure strongly reflects the underlying correlation effect. Here we report a RIXS study on $La_{0.8}Sr_{0.2}MnO_3$ which shows CMR near the metal-insulator and ferromagnetic transition at 309K[1], focusing on the temperature dependence of the electronic excitation spectra.

2. Experimental

The RIXS spectra of $La_{0.8}Sr_{0.2}MnO_3$ were measured at beamline BL11XU at SPring-8. A spectrometer for RIXS was installed in this beam line. The energy of the incident x-ray was 6.556 keV, and the energy resolution was 500 meV in the experiments.

3. Results and Discussion

We observed resonantly enhanced peak at 2 eV in the RIXS spectra of $La_{0.8}Sr_{0.2}MnO_3$, and it is identified as the excitation between LHB and UHB by comparing with $LaMnO_3$[2]. In Fig. 1, we show the spectra of low energy region at some temperatures. The scattering vectors are **Q** = (2.7,0,0) and (2.2,2.2,0) in *Pbnm* orthorhombic setting. It is clearly seen that the intensity at 2-4 eV increases with decreasing temperature at **Q** = (2.7,0,0), while the intensity does not depend on temperature at **Q** = (2.2,2.2,0). The temperature dependence of scattering intensity depends on the direction of scattering vector. The change of intensity is gradual rather than abrupt at the transition temperature. It is interesting to compare the temperature dependence of RIXS intensity with that of optical conductivity[3], which is considered as an electronic excitation at **Q** = 0. Surprisingly, the RIXS intensity at **Q** = (2.7,0,0) shows opposite temperature dependence to optical conductivity. Around 2 eV, the spectral weight of the optical conductivity decreases with decreasing temperature, while the RIXS intensity at **Q** = (2.7,0,0) increases. Moreover the scattering intensity at **Q** = (2.2,2.2,0) does not depend on temperature. The strong Hund's coupling between conduction and localized electrons and fully spin-polarized conduction band in ferromagnetic metallic phase explain the temperature dependence of optical conductivity[4], but this simple picture cannot be applied to our results. The anisotropic ferromagnetic exchange interaction which originates from orbital degrees of freedom may interpret the different temperature dependence.

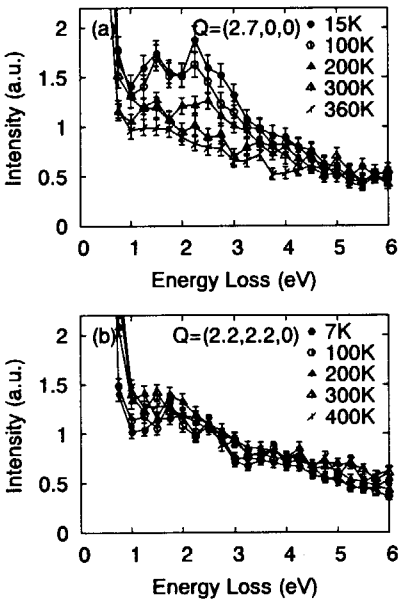

Fig. 1 RIXS spectra of $La_{0.8}Sr_{0.2}MnO_3$

Our experiments demonstrate that RIXS can be a powerful technique to the study the electronic excitation, especially in an anisotropic system, because of the advantage of the momentum resolution.

References

1) Y. Tokura *et al.*, J. Phys. Soc. Jpn. **63**, 3931, 1994.
2) T. Inami *et al.*, Phys. Rev. B **67**, 045108, 2003.
3) E. Saitoh *et al.*, J. Phys. Soc. Jpn. **69**, 3614, 2000.
4) Y. Okimoto *et al.*, Phys. Rev. B **55**, 4206, 1997.

5.5.2 Recent status of scanning type synchrotron radiation Mössbauer microscope at BL11XU (JAERI) of SPring-8

Takaya MITSUI and Makoto SETO [a)]
a) Research Reactor Institute, Kyoto University, Noda, Kumatori-cho, Sennan-gun, Osaka 590-0494, Japan

1. Introduction

The third generation synchrotron radiation (SR) makes enable us to perform the Mössbauer spectroscopy using a focusing X-ray. The remarkable beam properties (ultra high brilliance, pulse structure and linear polarization) hold promise to produce new tools for the solid material physics researches not accessible in "classical" Mössbauer spectroscopy with radioactive source. Recently, we have developed a scanning type synchrotron radiation Mössbauer microscope (SSRMM) for ^{57}Fe nucleus using X-ray focusing beam. In this report, we report on the current status of SSRMM at the BL11XU of SPring-8.

2. Optics and mechanics of SSRMM

As is shown in Fig. 1, SSRMM system is composed of an undulator source, a C(111) pre-monochromator, a high-resolution monochromator (HRM), a multi-layer X-ray focusing mirror (MXFM), a pinhole slit, a precision stage and a fast detector (APD). The incident X-rays are monochromatized at 14.4keV with Δ E=2.5meV by a pre-monochromator [1)] and a high-resolution monochromator [2)]. The multi-layer X-ray focusing mirror (MXFM) coated with 50 layers of [W(13Å) /Si(39.5Å)] on SiO_2 base is placed after HRM. As the result, incident X-rays are focused with a size of 300x35μm^2 at the sample position. A point-like focused Mössbauer probe beam (FMPB) is obtained by using a φ20μm pinhole slit. Precision sample stage consists of a coarse moving stage and a piezoelectric transducer driven fine moving stage, whose minimum spatial resolution is 10nm. Here, the beam size of FMPB was 16μm in vertical direction and 20μm in horizontal direction and the typical photon flux after pinhole slit was about 3.6x10^8 photons/sec at storage ring current of 98mA.

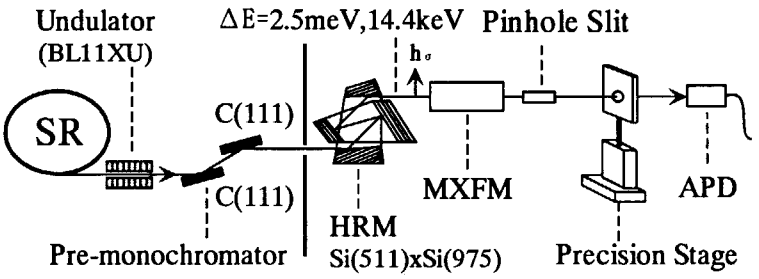

Fig. 1 Optics and mechanics of SSRMM

3. Results and Discussion

As for an example experiment, time spectra of the multi-domain state of a 2μm thick a-Fe foil enriched to 95% ^{57}Fe were measured with a line scanning of the sample. The irradiation position of FMPB was changed with step of 60μm. As is shown in Fig. 2, the measured time spectra revealed some different quantum beat patterns in accordance with the irradiation positions of the sample "clearly". Our results show that the most advantages of SSRMM are seen with special clarity in the research of the sample whose hyperfine fields don't have a uniform distribution. We expect that SSRMM system will be a very powerful tool for wide variety of the science research areas.

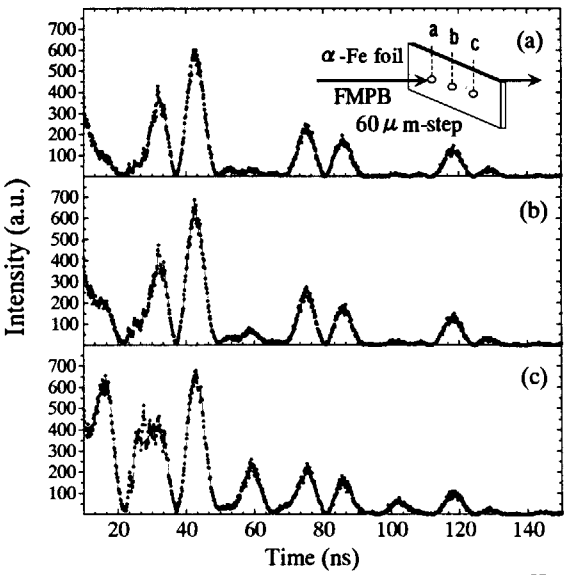

Fig. 2 Time spectra at local positions of an ^{57}Fe foil

References

1) M.Marushita et al., Nucl. Instr. and Meth. A. **467-468**(2001)392.
2) T. Mitsui et al., Nucl. Instr. and Meth. A. **467-468**(2001)1105.

5.5.3 X-ray diffraction study of the 2×2×1 structure of NaV_2O_5 under low temperature and high pressure

Kenji OHWADA[a)], Yasuhiko FUJII[b)], Hironori NAKAO[c)], Youichi MURAKAMI[a,c)], Yukio NODA[c)], Naoshi IKEDA[d)], Hiroyuki OHSUMI[d)], Masahiko ISOBE[b)] and Yutaka UEDA[b)]

a) JAERI/SPring-8, b) ISSP/University of Tokyo, c) Tohoku University, d) JASRI/SPring-8

Devil's flower has been perfectly reproduced in the Temperature-Pressure phase diagram of charge-lattice-spin coupled system NaV_2O_5[1]. All of experimentally observed phases have $2a \times 2b \times Zc$ type superstructures and the corresponding wave number q_c (= 1/Z, Cq_c-phase) sequences at several temperature and pressure ranges are well understood as the devil's staircase type sequence theoretically obtained from the Axial Next Nearest Neighbor Ising (ANNNI) model[2]. It is essentially important that there are only two stable ground states as T → 0, i.e., ↑↑↑↑•••••• (ferro, all up configuration, q_c = 0) state and ↑↑↓↓↑↑↓↓••••• (up-up-down-down configuration, q_c = 1/4) state[2] (Both ↑ and ↓ are Ising spins).

We focus our attention on the ground state of NaV_2O_5 under high pressure. Sawa *et al.* have determined the atomic shifts and the charge arrangements corresponding to the Ising spin ↑ (or ↓) from the structural analysis of $C_{1/4}$-phase (= ground state at low pressure) at ambient pressure[3]. However, there remains a question that "can the structure of C_0-phases (= ground state at high pressure) be simply explained by the one layer extracted from the $C_{1/4}$-phase?"

To solve the problem, single crystal x-ray diffraction experiments were performed under low temperature and high pressure at BL02B1/SPring-8. Intensity vs. Q(*hkl*) ($Å^{-1}$) data were collected for structural analysis. Pressure was generated in a DAC using 1:1 mixture of *n*-pentane:*i*-pentane pressure transmitting media. Pressure was determined by the lattice constant of the NaCl single crystal.

Figure 1 shows the analytical result, observed intensity $I_{obs.}$ vs. calculated intensity $I_{cal.}$. The structure of C_0 phase is well described by the one layer which is extracted from the $C_{1/4}$-phase. The space group of the C_0-phase is determined as P_{112}, which is one of the subgroups of A_{112} (the space group of the $C_{1/4}$-phase). It is estimated that the amount of the atomic shifts at 1.6 GPa is 27 % of the ones at ambient pressure.

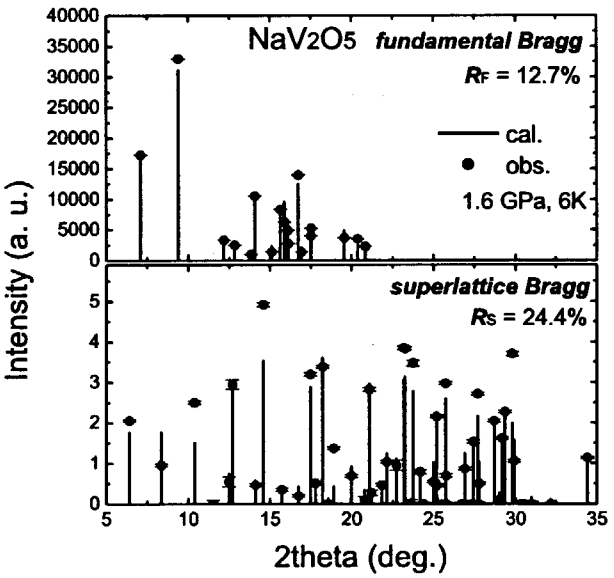

Fig. 1 Analytical result, $I_{obs.}$ vs. $I_{cal.}$ The space group of the C_0-phase is P_{112}.

References

1) K. Ohwada *et al.* Phys. Rev. Lett. **87**, 086402 (2001).; K. Ohwada *et al.* J. Phys. Soc. Jpn., **69**, 639 (2000).

2) P. Bak *et al.* Phys. Rev. B **21**, 5297 (1980).

3) H. Sawa *et al.* J. Phys. Soc. Jpn. **71**, 385 (2001).

5.6 Electronic Material Science

Yasuji MURAMATSU

The electronic material science group has constructed a soft x-ray beam line (BL23SU), in collaboration with the surface chemistry research group dating to 1997. We have developed a novel control system for the double-array APPLE-2 undulator (ID23) and a high-resolution optical system which is mainly composed of a varied-line-spacing plane grating (VLSPG) monochromator. Two experimental stations have been installed in the RI (radioisotope) experimental hall, which is located downstream of the BL23SU. These stations perform research on actinide materials, strongly correlated electron systems and various functional materials using high-resolution photoelectron spectroscopy (PES) and soft x-ray magnetic circular dichroism (MCD) spectroscopy. Figure 1 shows the PES and MCD apparatus in the RI experimental hall.

In 2002, we have prepared for the handling of uranium compounds in the RI experimental hall. We have successfully measured the PES and MCD spectra of US, USe, UTe, and U*T*Ga5 (*T*=Rh, Ir), and have observed some unique electronic structures in these compounds. Spectral analysis is now underway. The electronic structure of Fe_xNbS_2, in which Fe atoms form an ordered superlattice structure, has been studied by PES. The magnetic structures of $SrFe_{1-x}Co_xO_3$ and of Fe in the dysprosium iron garnet family have also been studied by MCD. In addition, the chemical bonding states of light-element functional materials have been studied using the Advanced Light Source (ALS) at Lawrence Berkeley National Laboratory (LBNL). The nanostructure of carbon films on Japanese smoked roof tile "Ibushi Kawara" has also been analyzed by soft x-ray emission and absorption spectroscopic measurements using the ALS.

For the nanotechnology support project of MEXT (Ministry of Education, Culture, Sports and Technology), a pulsed laser deposition (PLD) system was installed in the RI experimental hall for fabrication of nano-structured thin films. Adjustments the PLD system are currently underway.

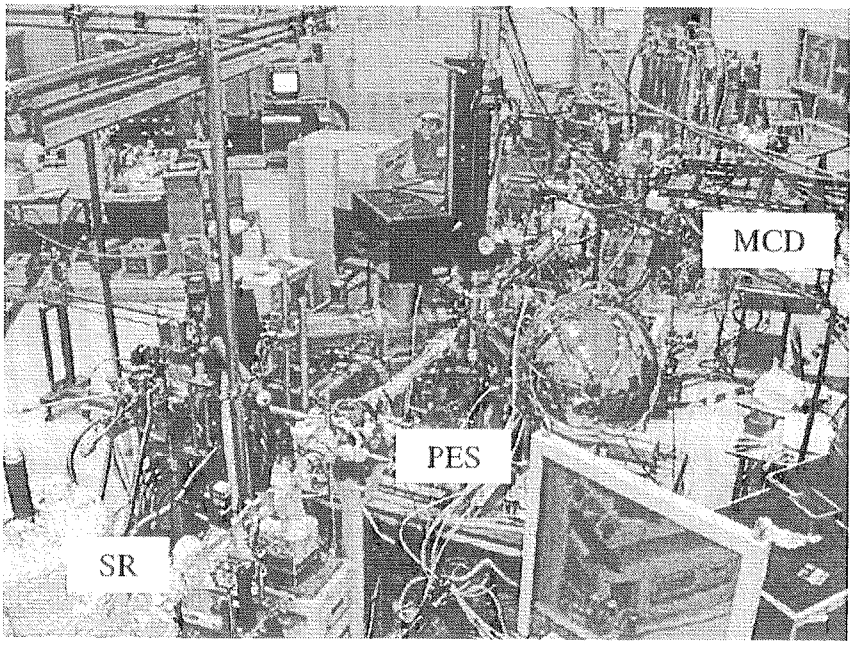

Fig. 1 PES and MCD systems installed in RI experimental hall of BL23SU

5.6.1 X-ray magnetic circular dichroism at the U $N_{4,5}$ edges of uranium monochalcogenides

Tetsuo OKANE, Jun OKAMOTO, Kazutoshi MAMIYA, Shin-ichi FUJIMORI, Yuji SAITOH, Yasuji MURAMATSU, Atsushi FUJIMORI[a], Akira OCHIAI[b]
a) Department of Complexity Science and Engineering, University of Tokyo
b) Center for Low Temperature Science, Tohoku University

1. Introduction

Uranium monochalcogenides US, USe and UTe crystallize in the NaCl structure and order ferromagnetically below the Curie temperatures T_c of 177, 160 and 104 K, respectively[1]. The magnetic moment deduced from neutron diffraction experiments becomes larger in the order US, USe, UTe[1]. It is important to evaluate experimentally the orbital moment μ_L and the spin moment μ_S separately atom in order to properly describe the mechanism of 5*f* electron magnetism in uranium compounds. X-ray absorption magnetic circular dichroism (MCD) measurement is a powerful experimental technique to obtain μ_L and μ_S separately for a given electronic shell of a specific element. We have performed the MCD measurement at the U $N_{4,5}$ ($4d \rightarrow 5f$) edges of US, USe and UTe.

2. Experimental

Single crystalline samples of US, USe and UTe were grown by the Bridgman method. The MCD measurements were performed at beamline BL23SU of the SPring-8, which is specially designed for the soft x-ray experiments of radioactive materials. In the measurements, the circularly polarized x-rays irradiated the sample along the [001] direction. The helicity of the x-rays was fixed, and the magnetic field of 2 T was induced in parallel and antiparallel to the incident x-rays. The sample temperature was fixed at 50 K. Clean sample surface was obtained by *in situ* cleaving along the (100) plane.

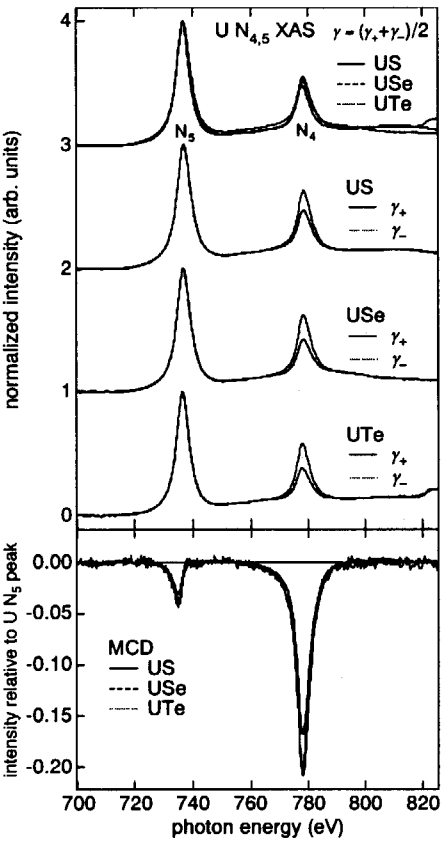

Fig. 1 XAS and MCD spectra of US, USe and UTe

3. Results

The upper panel of Fig.1 shows the XAS spectra of US, USe, and UTe measured at the U $N_{4,5}$ edges under the magnetization of two directions, denoted as γ_+ and γ_-. The MCD spectra obtained as $\Delta\gamma = \gamma_+ - \gamma_-$ are shown in the lower panel of Fig. 1 The magnitude of the MCD signals becomes clearly larger in going from US to USe, and remains almost the same or slightly decreases from USe to UTe, while the line shape is not significantly changed. Therefore, it appears that the magnetic nature of the uranium monochalcogenides is different between US and the other compounds. The values of μ_L and μ_S can be obtained by applying the sum rules[2,3] to the integrated intensity of the MCD and XAS spectra. The obtained values are summarized elsewhere[4]. Both the values of μ_L and μ_S are significantly enhanced in going from US to USe, reflecting a localization of 5*f* electrons. However, they are reduced in going from USe to UTe, although the total moment increases[1]. The increase of the total moments from USe to UTe is mainly caused by the decrease in μ_S.

References

1) J.M. Fournier and R. Troc, *Handbook on the Physics and Chemistry of Actinides*, North-Holland, 1985.
2) B.T. Thole *et al.*, Phys. Rev. Lett. **68**, 1943, 1992.
3) P. Carra *et al.*, Phys. Rev. Lett. **70**, 694, 1993.
4) T. Okane *al.*, to be published in Physica B.

5.6.2 Magnetic circular x-ray dichroism study of $SrFe_{1-x}Co_xO_3$

Jun OKAMOTO, Kazutoshi MAMIYA, Shinichi FUJIMORI, Tetsuo OKANE, Yuji SAITOH, Yasuji MURAMATSU, Atsushi FUJIMORI[a)], Miguel ABBATE[b)], Tsuneharu KOIDE[c)], Shintaro ISHIWATA[d)], Shuuji KAWASAKI[d)], and Mikio TAKANO[d)]
a) Univ. of Tokyo, b) Univ. of Parana, c) KEK-PF, d) ICR

Perovskite $SrFe_{1-x}Co_xO_3$ ($0 \leqq x \leqq 0.5$) shows a helical anti-ferromagnetic transition (T_N = 134 K) at Fe end (x =0) but its magnetic moment increases as Co dopant x increases and $SrFe_{1-x}Co_xO_3$ becomes ferromagnetic at $x \geqq 0.2$.[1)] Magnetic circular x-ray dichroism (MCXD) in the core-level soft x-ray absorption is a powerful method to obtain information about electronic structures related with magnetic properties and gives the orbital[2)] and spin[3)] magnetic moments on each atom that composes the measured magnetic compound with use of the magneto-optical sum rules. Electronic structures of Fe 3*d* and Co 3*d* states have been studied across the anti-ferromagnetic to ferromagnetic transition by using MCXD measurements. MCXD measuring system at BL23SU mainly consists of a superconducting magnet and a sample chamber. The base pressure of the chamber is 4×10^{-8} Pa at RT. Samples were cooled down to 30 K with use of a liquid He flow cryostat. The sample surface was cleaned by *in situ* scraping before each measurement. Magnetic field of 2 T was applied parallel and anti-parallel to the propagation vector of the incident circularly polarized light on the sample.

Figure 1 and Figure 2 show orbital, spin and total magnetic moments estimated by applying MCXD sum rules to Fe 2*p* and Co 2*p* MCXD spectra of $SrFe_{1-x}Co_xO_3$, respectively. Before ferromagnetic transition ($x \leqq 0.2$), as Co dopant x increases, spin and total magnetic moments of both Fe 3*d* and Co 3*d* states increases. After ferromagnetic transition ($x \geqq 0.2$), however, magnetic moments of Fe 3*d* and Co 3*d* states show different behavior. Although the spin and total magnetic moments of the Fe 3*d* states increases monotonically, those of the Co 3*d* states show complicated decrease and increase around x = 0.3. From this results, it is shown that the low spin (LS) state (d^6:$t_{2g\uparrow}{}^3 t_{2g\downarrow}{}^3$) and intermediate spin (IS) state (d^6:$t_{2g\uparrow}{}^3 t_{2g\downarrow}{}^2 e_{g\uparrow}{}^1$) mixes in the spin state of Co 3*d* states and that the mixing ratio of LS and IS states may change in the ferromagnetic region ($x \geqq 0.2$).

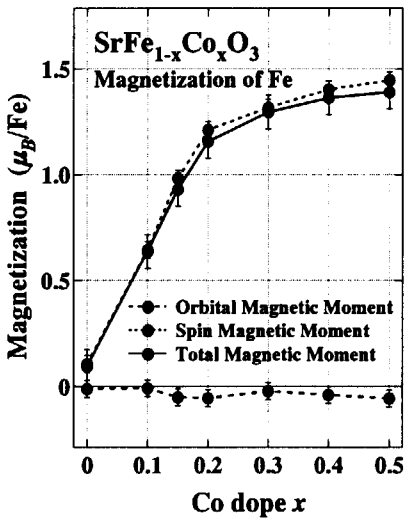

Fig. 1 Orbital, spin and total magnetic moments of Fe 3*d* states estimated by Fe 2*p* MCXD spectra

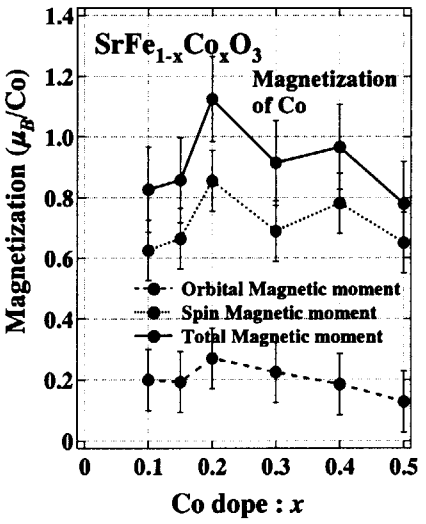

Fig. 2 Orbital, spin and total magnetic moments of Co 3*d* states estimated by Co 2*p* MCXD spectra

References

1) S. Kawasaki *et al.*, J. Solid State Chem. **121**, 174, 1996.
2) B. T. Thole *et al.*, Phys. Rev. Lett. **68**, 1943, 1992.
3) P. Carra *et al.*, Phys. Rev. Lett., **70**, 152, 1995.

5.6.3 Substitution effect of Fe on the MCD spectra of the Dysprosium Iron Garnet family

Akane AGUI, Masaichiro MIZUMAKI[a)], Tomohiro MATSUSHITA[a)], Naomi KAWAMURA[a)], Takeshi NAKATANI

a) Japan Synchrotron Radiation Research Institute

1. Introduction

Dysprosium iron garnet ($Dy_3Fe_5O_{12}$: DyIG) belongs to the rare earth iron garnet (RIG) family, which is a typical ferri-magnet composed of Rare earth element (=R) and iron. The iron and rare earth valences are both positive trivelent, while oxygen is negative divalent.

RIG has a crystal structure called "garnet structure", in which, an Fe^{3+} ion is surrounded by O^{2-} ions and has O_h symmetry or the T_d symmetry[1)]. $Dy_3Fe_{4.25}In_{0.75}O_{12}$ is made by site-selectively replacing 37.5 % of the Fe ions in the O_h symmetry sites in $Dy_3Fe_5O_{12}$ with In ions, on the other hand replacing 25 % of Fe ions in the T_d sites in $Dy_3Fe_5O_{12}$ with Ga ions makes $Dy_3Fe_{4.25}Ga_{0.75}O_{12}$. In this study, the substitution effect of Fe on the MCD spectra in this DyIG family at the Fe $L_{2,3}$-edges and the Dy $M_{4,5}$-edges was measured to investigate the magnetic properties of Fe in the T_d and the O_h symmetry site.

2. Experimental

MCD and XAS spectra at the Fe $L_{2,3}$ and the Dy $M_{4,5}$-edges for $Dy_3Fe_5O_{12}$, $Dy_3Fe_{4.25}Ga_{0.75}O_{12}$ and $Dy_3Fe_{4.25}In_{0.75}O_{12}$ compound were measured using synchrotron radiation at soft X-ray beamline BL23SU. During MCD measurements, the undulator and the monochromator was synchronously controlled, *i.e.*, photon helicity was switched at each photon energy point[2)]. The powder samples of DyIG were uniformly pasted on a sample holder using carbon tape. A static magnetic field of 0.4 Tesla was applied to the sample at room temperature (~300 K). The magnetic moment of DyIG was saturated at H=0.4 Tesla. The incident angle of the photon beam was set parallel to the magnetic field.

3. Results

Figure 1 shows the Fe L-edge and the Dy M-edge MCD spectra of DyIG[3)]. The MCD signal signs are the same for $Dy_3Fe_5O_{12}$ and $Dy_3Fe_{4.25}In_{0.75}O_{12}$ but $Dy_3Fe_{4.25}In_{0.75}O_{12}$ has the opposite. This means that the majority spin moment in $Dy_3Fe_{4.25}Ga_{0.75}O_{12}$ is changed from that in $Dy_3Fe_5O_{12}$ by Fe substitution site-selectively. The Fe ion in the T_d symmetry site plays an important role to the direction of magnetization of DyIG.

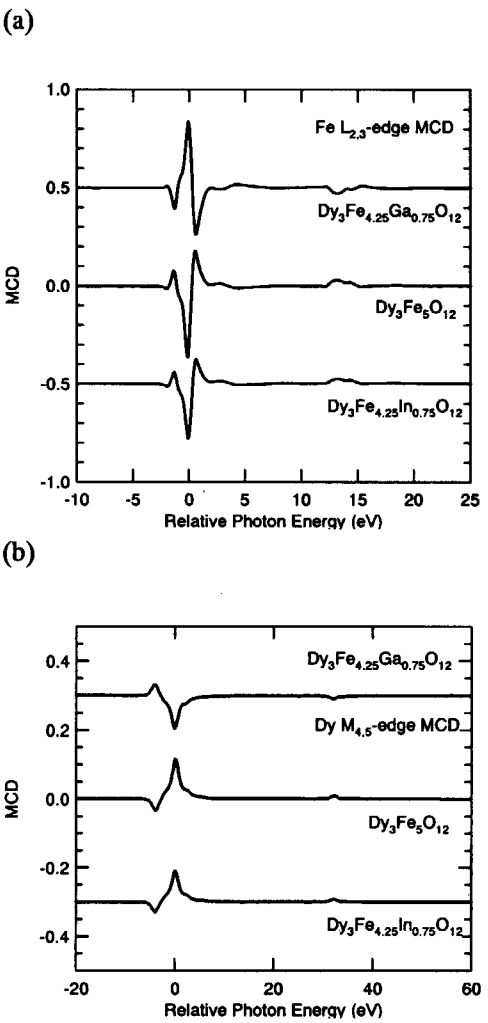

Fig. 1 (a) Fe $L_{2,3}$- and (b) Dy $M_{4,5}$- and MCD spectra of $Dy_3Fe_{4.25}Ga_{0.75}O_{12}$, $Dy_3Fe_5O_{12}$, $Dy_3Fe_{4.25}In_{0.75}O_{12}$ The photon energy of Fe L_3 and Dy M_5 peak are namely set to 0 eV.

References

1) E. P. Wolfarth, Ferro Magnetic Materials vol. 2 p.1-54.
2) A. Agui, *et. al.*, Rev. Sci. Inst, 72, 3191, 2001.
3) A. Agui *et. al.* to be published in Pyscia scripta.

5.6.4 Photoemission study of $UTGa_5$ (T=Rh, Ir)

Shin-ichi FUJIMORI, Tetsuo OKANE, Jun OKAMOTO, Kazutoshi MAMIYA, Yasuji MURAMATSU, Atsushi FUJIMORI[a)], Hiroshi YAMAGAMI[b)], Yoshifumi TOKIWA[c)], Shugo IKEDA[c)], Tatsuma MATSUDA[c)], Yoshinori HAGA[d)], Etuji YAMAMOTO[d)], and Yoshichika ONUKI[c,d)]

a) Department of Complexity Science and Engineering, University of Tokyo, b) Department of Physics, Faculty of Science, Kyoto Sangyo University, c) Department of Physics, Graduate School of Science, Osaka University, d) Advanced Science Research Center, Japan Atomic Energy Research Institute

1. Introduction

Photoelectron spectroscopy is a powerful tool to investigate the electronic structure of strongly correlated materials. Especially, high-resolution photoelectron spectroscopy with soft x-ray synchrotron radiation has been attracted much attention in recent years due to its bulk-sensitivity. However, for uranium compounds, such experiments are very restricted due to the difficulties in treating unsealed RI materials in the synchrotron radiation facilities. In SPring-8, the actinide science beamline BL23SU is constructed, and photoelectron spectroscopies for the uranium compounds in the soft x-ray regime can be performed. We have carried out the bulk-sensitive photoelectron spectroscopy with the soft x-ray synchrotron radiation ($h\nu$=800 eV) on the layered uranium compounds $UTGa_5$ (T=Pt and Fe) to understand their electronic structures. The $UTGa_5$ compounds crystallize in the tetragonal $HoCoGa_5$-type structure, and are isostructual to the heavy fermion superconductors $CeIrIn_5$ or $PuCoGa_5$. $UFeGa_5$ is paramagnetic and $UPtGa_5$ is antiferromagnetic with T_N=26 K.

2. Results

Figure 1 shows the valence band spectra of $UTGa_5$. The energy resolution was 130 meV. The prominent feature located at E_B~5 eV in the spectrum of $UPtGa_5$ is contribution from Pt 5*d* states. Meanwhile, in the spectra of $UFeGa_5$, the Fe 3*d* derived states are located at E_B~1.5 eV. In both spectra, the contributions from U 5*f* states are located at near the Fermi level (E_F). To observe these features more clearly, we have measured the near E_F part of these spectra. Figure 2 shows the near E_F part of the valence band spectra of $UTGa_5$. These features mainly consist from U 5*f* states. In the spectrum of $UPtGa_5$, the sharp structure is observed just below E_F. On the other hand, this structure is broad in the spectrum of $UFeGa_5$. These indicate that the width of the U 5*f*-derived band is narrow in $UPtGa_5$ compared with that of $UFeGa_5$. In these spectra, the satellite structures are observed at E_B~0.4 eV, and their positions and intensities are different in each compounds. These satellite structures have been observed in the valence band spectra of other uranium-based compounds also, and are considered to be originated with the correlation effect of U 5*f* electrons.

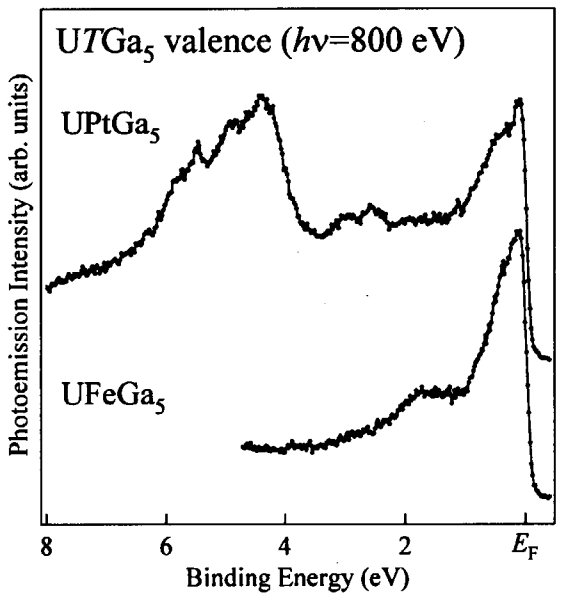

Fig. 1 Valence band spectra of $UTGa_5$

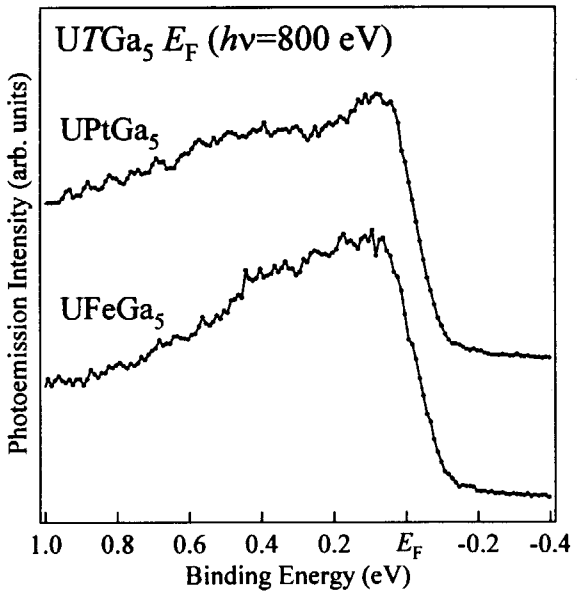

Fig. 2 Near E_F part of the valence band spectra of $UTGa_5$

5.6.5 Soft x-ray photoemission study of Fe_xNbS_2

Yuji SAITOH, Keisuke KOBAYASHI[a)], Atushi FUJIMORI[b)], Tomohiro MATSUSHITA[a)], Takehito NAKANO[a)], Takanori WAKITA[a)], Yasuhisa YAMAMURA[c)], Toshihide TSUJI[c)], Mikio KOYANO[c)] and Shin-ichi KATAYAMA[c)]

a) Japan Synchrotron Radiation Research Institute, b) University of Tokyo, c) Japan Advanced Institute of Science and Technology

1. Introduction

NbS_2 belongs to the class of transition-metal dichalcogenides with a layered structure. One remarkable property of many layered solids is the possibility to intercalate various atoms or molecules between the layers[1)].

The present work is done on the $2H$-NbS_2 and its intercalates with magnetic Fe atoms-Fe_xNbS_2, where $x \approx 1/4$ and 1/3. At these concentrations, the Fe atoms form an ordered superlattice with lattice parameters $a'=2a$ ($\sqrt{3}\,a$), where a is the host lattice parameter. We have measured photoemission spectra for polycrystalline $2H$-NbS_2 and single crystals of Fe_xNbS_2 (x= 0.239 and 0.325) for a systematic investigation of these compounds.

2. Experimental

Experiments were performed with a hemispherical analyzer (Gammadata-Scienta SES 200) at the twin-helical undulator beamline BL25SU for soft x-ray spectroscopy of solids[2)]. The samples were cleaved *in situ* parallel to the layers by knocking off a Cu plate glued on top of the samples. Cleavage and measurements were performed at a base pressure better than 4×10^{-8} Pa, and at low temperatures ~20 K in order to suppress thermal broadening of spectral features. The surfaces of the single crystals (x= 0.239 and 0.325) were examined by low energy electron diffraction (LEED), which in all cases showed a regular hexagonal spot pattern corresponding to the host lattice, together with the weaker intercalant superlattice spots. Angle-resolved photoemission spectra (ARPES) for x= 0.239 and 0.325 were measured along the ΓM (AL) and ΓK (AH) directions of the host $2H$-NbS_2 Brillouin zone.

3. Results

Figure 1 shows the ARPES spectra of $Fe_{0.325}NbS_2$ measured simultaneously over an angular range of ~12° at a photon energy ($h\nu$) of 620 eV. The peaks in the spectra move in energy as a function of the collection angle, reflecting the band dispersion in the Brillouin zone. The binding energies

The comparison of ARPES spectra for x=0.239 and 0.325 indicates some notable changes in the band structure upon intercalation.

In order to obtain information on the band structure from the ARPES spectra we utilize the fact that in photoemission process the wave-vector component parallel to the surface $k_{\parallel}$ is conserved. Further analysis is going on.

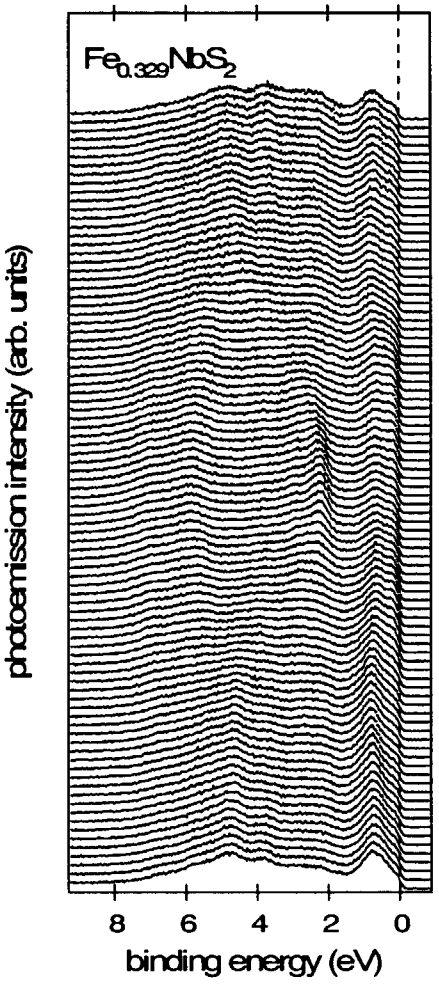

Fig. 1 Angle-resolved photoemission spectra of $Fe_{0.325}NbS_2$ measured at 20K with 620-eV photons at various polar emission angles.

4. References

1) R. H. Friend and A. D. Yoffe, Adv. Phys. **36**, 1,1987
2) Y. Saitoh *et al.*, Rev. Sci. Instrum. **71**, 3254, 2000

5.6.6 Application of PC based off-the-shelf measurement system

Takeshi NAKATANI, Naoyasu HOSODA[a)], Takemasa MASUDA[a)], Toru FUKUI[a)], Hitoshi TANAKA[a)] and Ryotaro TANAKA[a)]

a) Japan Synchrotron Radiation Research Institute (JASRI)

1. Introduction

In third generation light source, SPring-8, many experimental users are performing various kinds of experiments by using fine tuned synchrotron radiation light. In order to produce the brilliant and stable light, fluctuation of electron beam orbits in the storage ring should be controlled below the submicron level. We started a project to stabilize the electron beams in 2000. It was necessary to find a high-resolution digitizer system measuring many channels of beam position monitors (BPMs) simultaneously. Also, the outputs from various devices needed to be digitized to take the correlation between the insertion device (ID) operations and orbit fluctuation. Because the accelerator devices were distributed widely over the SPring-8 site, a remote control communication via Ethernet was one of the essential features of the system.

In the past years, we had to use storage oscilloscopes for digitizing many signals in DC ~ several kHz frequency ranges. Those measurement devices provided very limited functionality because the device was stand alone, time consuming for data analyses, and signal data transfer was in off-line. An interface of data transfer was not fast enough because the GP-IB bus was chosen in the most of cases. On the other hand, the fancy measurement system such as VXI is fast enough but it is expensive and too heavy to adopt for the quick measurements. It was a long waiting to have an inexpensive measurement system to fit our purpose.

We selected a PC based off-the-shelf measurement system, WE7000, made by Yokogawa Electric Corporation[1)]. This system supports many kinds of modules for control and measurement. The features of the system are summarized as follows. (1) Each module has a shielded case in consideration of noise resistance. (2) It is not necessary to configure the address setting or install driver software by "Plug and Play" feature. (3) The station has trigger signals and clock line on the back plane to synchronize modules. (4) The system has a 100Base-T Ethernet interface that communicates with UDP/IP. (5) The high-resolution isolated digitizer module is available.

2. Software

The system has a Windows-base graphics toolkit to support the rapid development in its standard package. We can develop prototype control programs by using this toolkit. The vender also provides a network communication library for Linux OS with the open source license. We can control any module with the same function call and command syntax. The software framework of SPring-8 control system[2)] (MADOCA) adopts the client/server structure with message-driven middleware running on HP-UX and Linux[3)]. In our control scheme, an equipment manager (EM) programs are running on front-end systems to control devices. It is necessarily to incorporate the WE7000 communication functions into our software framework. We easily developed the equivalent software working as an EM on PC-Linux by using the provided API library. The API library connects WE7000 system with EM by the socket like communication with UDP protocol. We can get data in the form of binary array and save it to a local ASCII file on a PC.

3. Application for measurement of orbit distortion with ID operation

An ID installed in the JAERI soft X-ray beamline (BL23SU) in SPring-8 is an APPLE-2 type undulator[4)]. This ID can generate either a linearly (in horizontal and vertical plane), an elliptically or a circularly polarized light by phase shift of the magnet rows. The periodic phase shift is about 0.1Hz. A closed orbit distortion (COD) of electron beams caused by the phase shift is corrected by steering magnets (STMs) installed upstream and downstream of the ID23. The STMs are operated according to the COD correction table at the period of 30 milliseconds. We make the table for feed-forward correction. The orbit fluctuation is measured with eight BPMs and 4 X-ray BPMs. We measure output voltage from the BPMs by using 4-CH 100kS/s isolated 16bit digitizer module (WE7272) at 100Hz sampling rate through the ~50Hz filters. Total 24 points of the measuring signals are translated to the horizontal and vertical beam position with the submicron precision. We synchronously acquire the ID phase shift and the orbit

fluctuation data. Correlation of the phase shift and the orbit fluctuation becomes very clear as shown in Fig. 1. We have been able to correct the orbit fluctuation by the STMs according to the high accuracy correction table.

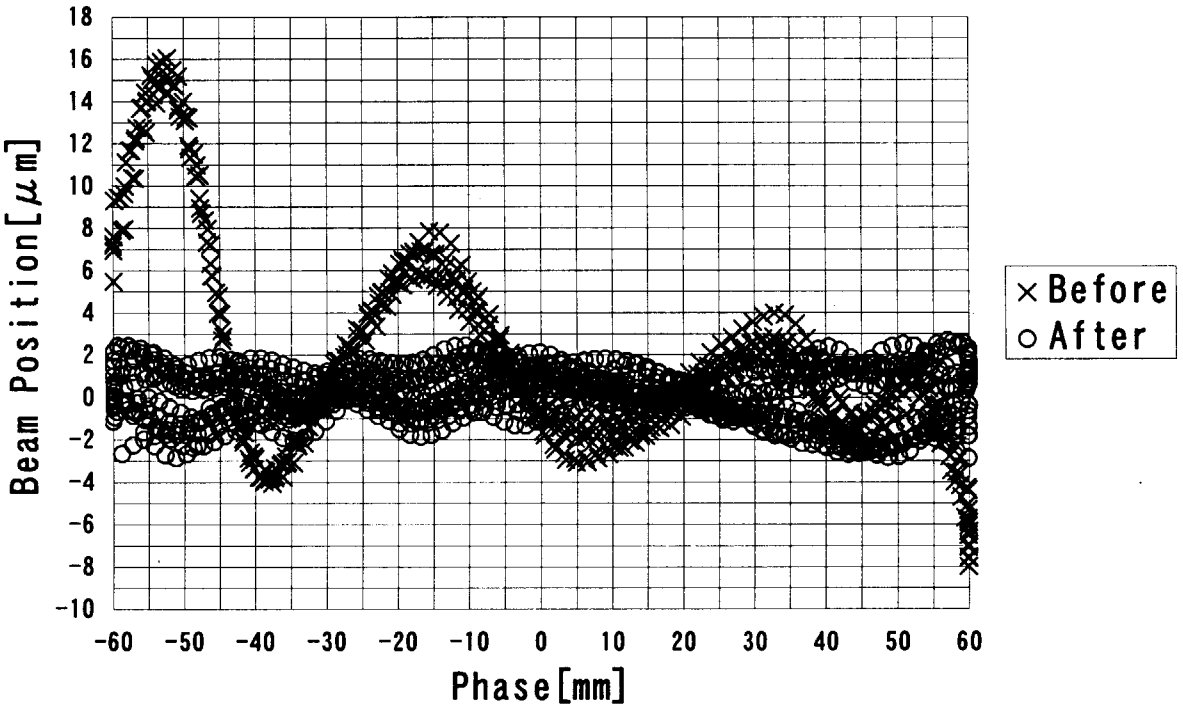

Fig. 1 Improvement of the horizontal orbit fluctuation with phase shift
The crosses are before correction and the circles are after.

4. Summary

We introduced a PC based off-the-shelf measurement system, WE7000, to our control system. The system is portable, reliable, networked and powerful to diagnose accelerator devices with enough precision. We have been working with this system non-trouble for two months.

References

1) http://www.yokogawa.com/tm/Bu/WE7000/
2) R. Tanaka *et al.*, "Control System of the SPring-8 Storage Ring", Proc. of ICALEPCS '95, Chicago, USA, 201, 1995
3) T. Masuda *et al.*, "Development of PC Based Field Controller with Linux", PCaPAC'99, 1999.
4) S. Sasaki *et al.*, Jpn. J. Appl. Phys. **31,** 1794 (1992).

5.6.7 Characterization of carbon films on the Japanese smoked roof tile "Ibushi-Kawara" by high-resolution soft x-ray spectroscopy

Yasuji MURAMATSU, Muneyuki MOTOYAMA[a)], Jonathan D. DENLINGER[b)], Eric M. GULLIKSON[b)] and Rupert C. C. PERERA[b)]
a) Hyogo Prefectural Institute of Technology, b) Lawrence Berkeley National Laboratory

1. Introduction

The smoked Japanese roof tile "Ibushi-Kawara" is generally made from sintered clay with carbon coating by smoking which can be regarded as the chemical vapor deposition (CVD) of hydrocarbons. The Ibushi-Kawara is a metallic oxidized-silver-colored tile and is very durable. In 1978, carbon films on the Ibushi-Kawara were characterized by Motoyama[1)] using electron probe microanalysis (EPMA), small-angle x-ray scattering, and transmission electron microscopy (TEM). This study revealed that the carbon films consisted of plane, spherical, and fibrous carbons. The plane carbon had a graphite-like layer structure, while both the spherical and fibrous carbons had carbon-black-like structures. Since then, few x-ray spectroscopic studies have focused on the carbon films of Ibushi-Kawara. To confirm the chemical bonding states and microstructure of the carbon films using advanced x-ray analysis methods, we characterized the carbon films by high-resolution soft x-ray emission and absorption spectroscopy using synchrotron radiation.

2. Experiments

Sample pieces of Ibushi-Kawara (hereafter "Kawara") were quarried from the surface portion of commercially available Kawara for spectroscopic measurements. Spectroscopic measurements of the soft x-ray emission and absorption in the C*K* region were performed at the Advanced Light Source (ALS). X-ray emission spectra were measured using a grating x-ray spectrometer installed in the undulator beamline, BL-8.0.1. Total electron yield (TEY) x-ray absorption spectra were measured in a bending-magnet beamline, BL-6.3.2, by monitoring the sample photocurrent. In both BL-8.0.1 and BL-6.3.2, the samples were rotated around the vertical axis to measure their angle-resolved x-ray emission and absorption spectra.

3. Results and Discussion

Figure 1 shows the take-off-angle-dependent C*K* x-ray emission spectra of Kawara and reference compounds. The peak intensities of the high-energy shoulders, which are assigned to the πpeaks, in Kawara and HOPG increase as the take-off angle increases. This take-off-angle dependence can be explained by the anistropy of the σ and π orbitals of the sp^2 carbon atoms in the oriented layer structure. From the take-off-angle dependence of the π/σ peak intensity ratio in the x-ray emission spectra of Kawara and HOPG, the orientation of the carbon films on Kawara is estimated to be 50% of HOPG. It has been concluded that half of the carbon atoms in Kawara form layer-structured clusters which give the metallic oxidized-silver color and the rest of the carbon atoms form random-structured clusters which make it durable.

We thank Dr. Takao Nomizu of Nomizu Kawara Sangyo Corporation for the sample preparation.

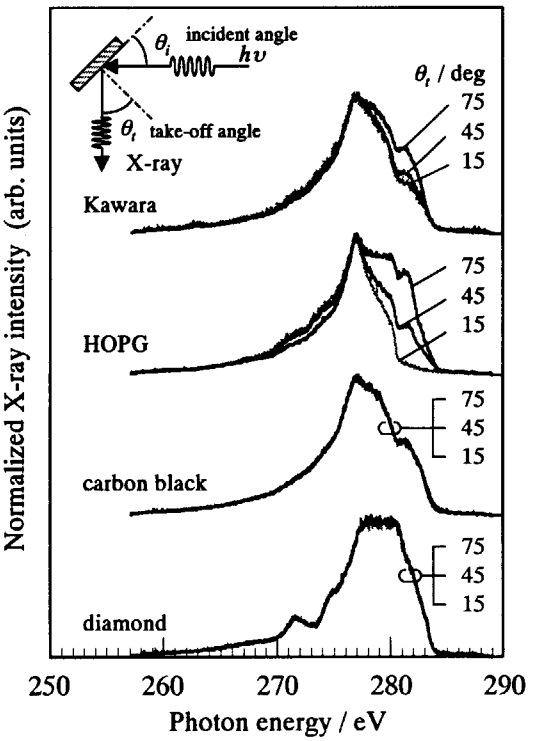

Fig. 1 Take-off-angle-resolved C*K* x-ray emission spectra of Kawara and the reference compounds

References

1) M. Motoyama, M. Tanaka, K. Ishima and G. Hashizume: Yogyo-Kyokai-Shi, **86** (1978) 13.
2) Y. Muramatsu, M. Motoyama, J. D. Denlinger, E. M. Gullikson, and R. C. C. Perera, Jpn. J. Appl. Phys. (in press).

5.7 Synchrotron Radiation Simulation Research

5.7.1 Theory of resonant x-ray scattering in $KCuF_3$

Jun-ichi IGARASHI, Manabu USUDA, and Manabu TAKAHASHI[a)]
a) Faculty of Engineering, Gunma Univ., Kiryu 376-8515

1.Introduction

Resonant x-ray scattering (RXS) has attracted much attention, since RXS signals on orbital and magnetic superlattice spots provide us useful information on ordered phase[1,2)] For the K edge in transition-metal compounds, RXS intensities arise from the modulation of 4p states in the intermediate states of the resonant process. Since 4p states are not the states of orbital or magnetic ordering, this causes complications on the interpretation of RXS. Two mechanisms have been proposed for the modulation of 4p states concerning orbital superlattice spots: (1)coupling to orbitally polarized 3d states through the anisotropic terms of the 3d-4p Coulomb interaction, and (2)coupling to electronic states at neighboring sites through the Jahn-Teller distortion (JTD). In addition, the mechanism concerning magnetic superlattice spots is also unclear. The purpose of our study is to clarify the mechanism of RXS in transition-metal compounds. We have chosen $KCuF_3$ as a typical example showing both orbital and magnetic orders[3)].

2.Results

We have calculated the RXS spectra by using the full-potential linealized augumented plane wave method within the LDA+U scheme. Figure 1 shows the spectra as a function of photon energy at the Cu-K edge. The left panel is for a orbital superlattice spot (331). The calculated curve reproduces well the experimental one (dotted line)[2)]. The spectra are nearly independent of whether the system is in the antiferromagnetic phase (thick-solid line) or the ferromagnetic phase (dotted line). They remain nearly the same even in a nonmagnetic state where the orbital order of the 3d states is much smaller (thin-solid line). In addition, the spectra are found to increase with increasing JTD. This strongly suggests that mechanism (2) is the main origin of the RXS. The right panel is for a magnetic superlattice spot (001). We also obtain the spectra in good agreement with the experiment[2)]. The intensity is found to arise from the orbital (not spin) polarization in the 4p band, which is induced through the spin-orbit interaction.

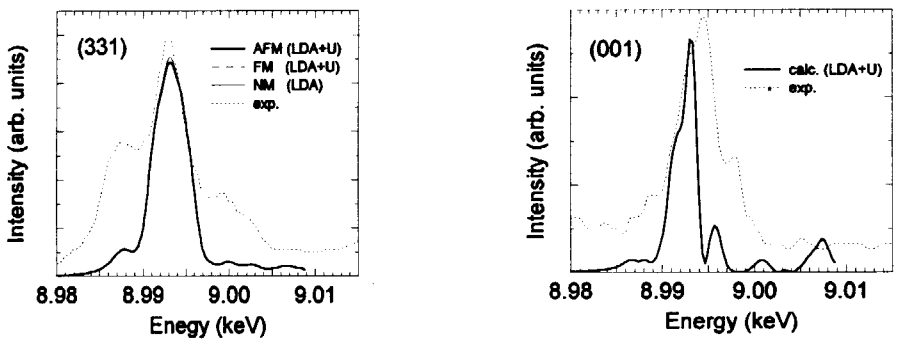

Fig. 1 RXS spectra at Cu-K edge as a function of photon energy

3. Summary

We have studied the RXS spectra on orbital and magnetic superlattice spots at the Cu-K edge in $KCuF_3$ on the basis of an ab initio calculation. Since the 4p states are well delocalized in space, they are sensitive to electronic structures at neighboring sites. The band structure calculation works well in reproducing the experimental spectra.. It is clarified that the JTD is the main origin to RXS intensities on orbital superlattice spots.

References

1) Y. Murakami *et al.*, Phys. Rev. Lett. **81**, 582, 1998
2) R. Caciuffo *et al.*, Phys. Rev. B **65**, 174425, 2002
3) M. Takahashi, M. Usuda, and J. Igarashi, Phys. Rev. B **67**, 064425, 2003

6. List of publications

6.1 List of publications on Advanced Photon Research Center

High Peak Power Laser Development (Laser System Development Group)

1. Journals

1) Generation of a 0.55-PW, 33-fs laser pulse from a Ti:sapphire laser system
K.Yamakawa, M. Aoyama, Y. Akahane, J. MA, N. Inoue, H. Ueda, and H. Kiriyama
The Review of Laser Engineering, Vol. 30, No. 12 (2002)

2) Optical field ionization of rare gas atoms by $>1019W/cm^2$, 10-Hz laser pulses
K. Yamakawa, Y. Akahane, Y. Fukuda, M. Aoyama, N. Inoue, H. Ueda
The Review of Laser Engineering, Vol. 30, No.12 (2002)

3) Ultrahigh peak power lasers
K. Yamakawa
KOGAKU, Vol. 31, pp. 287-289 (2002) (in Japanese)

4) Improved high-field laser characteristics of a diode-pumped Yb:LiYF4 crystal at low temperature
J. Kawanaka, K. Yamakawa, H. Nishioka and K. Ueda
Opt. Exp. Vol.10, pp. 455-460 (2002)

5) High efficiency frequency doubling of Nd:YAG laser in a two-pass quadrature frequency High energy second-harmonic generation of Nd:glass laser radiation with large aperture $CsLiB_6O_{10}$ crystals
H. Kiriyama, N. Inoue and K. Yamakawa
Opt. Exp. Vol.10, pp. 1028-1032 (2002).

6) High-efficiency frequency doubling of a Nd:YAG laser in a two-pass quadrature frequency-conversion schcme using $CsLiB_6O_{10}$ crystals
H. Kiriyama, N. Inoue and K. Yamakawa
Journal of the Optical Society of America B, Vol.19, pp. 1857-1864 (2002).

7) Large-aperture $CsLiB_6O_{10}$ frequency doubler for high-energy Nd:glass laser
H. Kiriyama, N. Inoue and K. Yamakawa
Proc. SPIE, 4914, pp. 6-13 (2002)

2. Proceedings

1) Diode-pumped Q-switched Yb:$LiYF_4$ laser at low temperature for chirped pulse regenerative amplification
J. Kawanaka, K. Yamakawa, H. Nishioka, and K. Ueda
Advanced Solid-State Lasers (Seventeenth Topical Meeting and Tabletop Exhibit, OSA and IEEE), WB7 (2002)

2) Q-switching operation with a diode-pumped cooled Yb:$LiYF_4$ for chirped pulse regenerative amplifier
J. Kawanaka, H. Nishioka, K. Yamakawa and K. Ueda
Technical Digest of Conference on Lasers and Electro-Optics (CLEO) 2002 (OSA),pp. 404 (2002)

3) 24-mJ, diode-pumped, chirped-pulse regenerative amplifier with a cooled Yb:$LiYF_4$
J. Kawanaka, H. Nishioka, K. Yamakawa and K. Ueda
Postdeadline papers of Conference on Lasers and Electro-Optics (CLEO) 2002 (OSA), CPDC8-1, 8-3 (2002)

4) A 20-mJ, diode-pumped, chirped-pulse regenerative amplifier with a cooled Yb:$LiYF_4$
J. Kawanaka, H. Nishioka, K. Yamakawa and K. Ueda
The XIII International Symposium on Gas Flow & Chemical Lasers and High Power Laser Conference (GCL/HPL, SPIE), pp. OR35 (2002)

5) Q-switching operation with a cooled Yb:$LiYF_4$ for diode-pumped chirped-pulse regenerative amplification
J. Kawanaka, K. Yamakawa, H. Nishioka and K. Ueda
Proceedings of the third symposium on advanced photon research (JAERI-Conf 2002-008), pp. 50-52 (2002)

6) Spectral control of diode-pumped Yb:$LiYF_4$ chirped-pulse regenerative amplifier
J. Kawanaka, K. Yamakawa, H. Nishioka and K. Ueda
Conference on Lasers and Electro-Optics Europe (CLEO/Europe) 2003 (EPS, IEEE, OSA), CH3T (2003)

7) Oscillation characteristics of the discharge-pumped vacuum ultraviolet Kr2* laser oscillation
S. Kubodera, T. Shirai, T. Higashiguchi, W. Sasaki, J. Kawanaka and T. Igarashi
Technical Digest of Conference on Lasers and Electro-Optics (CLEO) 2002 (OSA), pp. 443 (2002)

8) Oscillation characteristics of discharge pumped VUV Krypton excimer laser
T. Shirai, T. Higashiguchi, S. Kubodera, W. Sasaki, J. Kawanaka, and T. Igarashi
Proceedings of the XIII International Symposium on Gas Flow & Chemical Lasers and High Power Laser Conference (GCL/HPL, SPIE), pp. OR23 (2002)

9) Discharge pumped krypton excimer laser in the vacuum ultraviolet spectral region
(Invited) T. Shirai, T. Higashiguchi, S. Kubodera, W. Sasaki, J. Kawanaka, and T. Igarashi
International Quantum Electronics Conference 2002 (IQEC2002) and Conference on Lasers, Applications, and Technologies 2002 (LAT2002), QThC2 (2002)

10) Oscillation characteristics of the discharge pumped vacuum ultraviolet laser
T. Shirai, S. Mokuo, T. Higashiguchi, S. Kubodera, W. Sasaki, J. Kawanaka, and T. Igarashi
The Third Asian Pacific Laser Symposium (APLS 2002), WePB1 (2002)

11) 25-J green-beam generation with large aperture $CsLiB_6O_{10}$ crystals
H. Kiriyama, F. Nakano and K. Yamakawa
Conference on Lasers and Electro-Optics 2002 (CLEO 2002), Postdeadline Papers CPDC6-1 (2002)

12) Multiple ionization of rare gas atoms in relativistic intensity regime
Y. Akahane, Y. Fukuda, M. Aoyama, N. Inoue, H. Ueda, T. Utsumi, and K. Yamakawa
Abstracts, International Workshop on Photoionization (IWP2002) SE02 (2002)

13) Generation of a 0.55-PW, 33-fs laser Pulse from a Ti:sapphire laser system
M. Aoyama, Y. Akahane, J. Ma, N. Inoue, H. Ueda, H. Kiriyama, K. Yokoyama and K.Yamakawa (POSTDEAD LINE PAPER)
Proceedings of OSA Annual Meeting & Exhibition 2002, laser Science XVII, Florida, USA, September (2002)

14) Development of a petawatt Ti:sapphire laser system
M. Aoyama, J. Ma, Y. Akahane, N. Inoue, H. Ueda, H. Kiriyama and K.Yamakawa
Proceedings of CLEO2002, California, USA, May (2002)

15) Design and performance of a petawatt Ti:spphire laser system
M. Aoyama, J. Ma, Y. Akahane, N. Inoue, H. Ueda, H. Kiriyama, K. Yokoyama and K.Yamakawa
Proceedings of the 9th International workshop On Femtosecond Technology, Tsukuba, Japan, June (2002)

3. Report

1) Kerr-lens mode-locked oscillation with cooled Yb:YLF and Yb:glass
J. Kawanaka, K. Yamakawa, H. Nishioka and K. Ueda
JAERI-Review 2001-046 Annual Report of KANSAI Research Establishment 2000, pp. 9 (2002)

2) High efficiency, high energy second-harmonic generation of Nd:glass laser radiation in large aperture CsLiB6O10 crystals
H. Kiriyama, N. Inoue and K. Yamakawa
JAERI-Research 2002-020 (2002)

X-ray Laser Development (X-ray Laser Research Group)

1. Journals

1) Picosecond snapshot of the speckles from ferroelectric $BaTiO_3$ by means of x-ray lasers
R. Z. Tai, K. Namikawa, M. Kishimoto, M. Tanaka, K. Sukegawa, N. Hasegawa, T. Kawachi, M. Kado, P. Lu, K. Nagashima, H. Daido, H. Maruyama, A. Sawada, M. Ando and Y. Kato
Phys. Lev. Lett. 89, 257602 (2002)

2) Gain saturation of nickel-like silver and tin x-ray lasers by use of a table-top pumping laser system
T. Kawachi, M. Kado, M. Tanaka, A. Sasaki, N. Hasegawa, A. V. Kilpio, S. Namba, K. Nagashima, P. Lu, K. Takahashi, H. Tang, R. Z. Tai, M. Kishimoto, M. Koike, H. Daido, Y. Kato
Phys. Rev. A 66, 033815, 1-7 (2002)

3) Near field imaging of the transient collisional excitation Ni-like Ag x-ray laser
M. Tanaka, T. Kawachi, M. Kado, N. Hasegawa, K. Sukegawa, P. Lu, K. Nagashima, Y. Kato, H. Takenaka,
Surface Review and Letters 9, 641-644 (2002)

4) Demonstration of a Transient High Gain Soft X-Ray Laser for Neon-Like Argon
P. Lu, T. Kawachi, M. Suzuki, K. Sukegawa, S. Namba, M. Tanaka, N. Hasegawa, K. Nagashima, H. Daido, T. Arisawa, Y. Kato, H. Fiedorowicz
Jpn. J. App. Phys., 41, Pt. 2A, L133-135 (2002)

5) Demonstration of a transient-gain nickel-like xenon-ion x-ray laser
P. Lu, T. Kawachi, M. Kishimoto, K. Sukegawa, M. Tanaka, N. Hasegawa, M. Suzuki, R. Tai, M. Kado, K. Nagashima, H. Daido, Y. Kato, H. Fiedorowicz, A Bartnik
Opt. Lett. 27, 1911-1913 (2002)

6) Development of x-ray laser by transient collisional excitation
K. Nagashima, T. Kawachi, M. Kado, M. Tanaka, N. Hasegawa, K. Sukegawa, S. Namba, H. Tang, H. Daido, Y. Kato
Journal of plasma and fusion research, vol.78, No.3, 248-255 (2002)

7) Relativistic laser-plasma interaction (1)
K. Nagashima
Journal of plasma and fusion research, vol.78, No.5, 419-426 (2002)

2. Proceedings

1) Development of Soft X-ray Microscopy System Using X-ray Laser in JAERI Kansai
M. Kishimoto, M. Tanaka, R. Tai, K. Sukegawa, M. Kado, N. Hasegawa, H. Tang, T. Kawachi, P. Lu, K. Nagashima, H. Daido, Y. Kato, K. Nagai, H. Takenaka
VII International conference on X-ray microscopy (2002, France, Grenoble), Proc. pp.33 (2002)

2) Observation of strong amplification at 8.8 nm in the TCE scheme by a table-top pumping system
T. Kawachi, M. Tanaka, A. Sasaki, M. Kishimoto, M. Nishiuchi, K. Yasuike, N. Hasegawa, A. V. Kilpio, P. Lu, R. Tai, H. tang, M. Kado, K. Nagashima, M. Koike, H. Daido and Y. Kato
Proc. on 8th Int. Conf. on X-ray Laers (8th ICXRL), AIP-conf. Proc. 641, pp.40 (2002)

3) Picosecond Fourier holography using a Llyoyd's mirror and an X-ray laser at 13.9nm
B. Rus, H. Daido, H. Tang, M. Nishiuchi, M. Kishimoto, M. Tanaka, T. Kawachi, N. Hasegawa, K. Nagashima, T. Arisawa and Y. kato
Proc. on 8th Int. Conf. on X-ray Laers (8th ICXRL), AIP-conf. Proc. 641, pp.522 (2002)

4) Measurement of wavelength and linewidth of transient collisional x-ray lasers
T. Kawachi, N. Hasegawa, Y. Ochi, A. Sasaki, T. Utsumi, M. Tanaka, I. Uschmann, E. Foerster, E. Yanase, M. Suzuki, M. Nishiuchi, K. Nagashima and H. Daido
Proc. on 16th International Conf. on Spectral Line Shapes (ICSLS XVI), AIP-conf. Proc. 645, pp.457 (2002)

5) X-ray Laser Research in JAERI-Kansai
T. Kawachi, N. Hasegawa, M. Tanaka, Y. Ochi, M. Nishikino, P. Lu, R. Tai, K. Sukegawa, A. Sasaki, M. Kado, M. Kishimoto, K. Nagashima, H. Daido and Y. Kato
Proc. on 5th Asian International Semiinar on Atom and Molecular physics (AISAMP5), pp.38 (2002)

6) Measurement of the Instantaneous Speckles from $BaTiO_3$ Ferroelectrics by 13.9 nm Soft X-ray Laser
R.Z. Tai, K. Namikawa, M. Kishimoto, M. Tanaka, K. Sukegawa, N. Hasegawa, T. Kawachi, P. Lu, M. Kado, K. Nagashima, H. Daido, A. Sawada, H. Maruyama, M. Ando and Y. Kato
The Physical Society of Japan, Annual Meeting Abstract Vol. 57, Issue 2, Part 4, pp.788 (2002)

7) Development of the short wavelength x-ray laser with the short pulse laser
N. Hasegawa, T. Kawachi, K. Nagashima, M. Tanaka, M. Kishimoto, K. Sukegawa, P. Lu, H. Tang, R.Z. Tai, H. Daido

Annual meeting of Japan Society of Applied Physics, Abstract 1077, pp.36 (2002)
8) Design Study of High Repetition Rate X-ray Laser Driver
M. Kato, J. Mizui, S. Ishii, Y. Oda, K. Nagashima, M. Kishimoto, M. Tanaka
Proc.4th Symposium on Advanced Photon Research, JAERI-Conf 2003-008, pp.83
9) High Precision Measurement of the Ni-like Silver X-ray Laser Wavelength
N. Hasegawa, K. Murai, T. Kawachi, T. Utsumi, K. Nagashima
Proc.4th Symposium on Advanced Photon Research, JAERI-Conf 2003-008, pp.86
10) Observation of Biological Sell with Ultra-short Pulsed X-ray Lasers
M. Kado, M. Kishimoto, M. Tanaka, Y. Kinjou, M. Nishikino, K. Sukegawa, K. Nagashima, T. Kawachi, Y. Ochi, N. Hasegawa, P. Lu, R. Tai, K. Shinohara
Proc.4th Symposium on Advanced Photon Research, JAERI-Conf 2003-008, pp.157
11) Study of Plasma Polarization Spectroscopy
A. Iwamae, T. Fujimoto, T. Kawachi, N. Hasegawa
Proc.4th Symposium on Advanced Photon Research, JAERI-Conf 2003-008, pp.161
12) Charge Exchange Recombination in a Non-equilibrium Plasma Due to an Interaction of Ultrashort Pulse Laser and Cluster
S. Namba, N. Hasegawa, T. Kawachi, M. Kishimoto, K. Sukegawa, K. Nagashima, K. Takiyama
Proc.4th Symposium on Advanced Photon Research, JAERI-Conf 2003-008, pp.190
13) Spatial Coherence of X-ray Laser Beam After Double-target Amplification
M. Nishikino, M. Tanaka, M. Kishimoto, M. Kado, T. Kawachi, K. Sukegawa, N. Hasegawa, Y. Ochi, K. Nagashima
Proc.4th Symposium on Advanced Photon Research, JAERI-Conf 2003-008, pp.207
14) The Study of X-ray Lasers in a Shorter Wavelength Region
T. Kawachi, M. Tanaka, A. Sasaki, M. Kishimoto, M. Nishiuchi, K. Yasuike, N. Hasegawa, A. V. Kilpio, P. Lu, R. Tai, H. Tang, M. Kado, K. Nagashima, M. Koike, H. Daido, Y. Kato
Proc.4th Symposium on Advanced Photon Research, JAERI-Conf 2003-008, pp.211
15) Picosecond X-ray Speckles Diffracted from Ferroelectrics $BaTiO_3$
R. Z. Tai, K. Namikawa, M. Kishimoto, M. Tanaka, K. Sukegawa, N. Hasegawa, T. Kawachi , M. Kado, P. Lu, K. Nagashima, H. Daido, A. Sawada, H. Maruyama, M. Ando, Y. Kato
Proc.4th Symposium on Advanced Photon Research, JAERI-Conf 2003-008, pp.223
16) X-ray Laser Amplification with Double Target
M. Tanaka, M. Nishikino, T. Kawachi, N. Hasegawa, M. Kado, M. Kishimoto, K. Nagashima, Y. Kato
Proc.4th Symposium on Advanced Photon Research, JAERI-Conf 2003-008, pp.229
17) Demonstration of a Transient High Gain Nickel-like Xenon Ion X-ray Laser
P. Lu, T. Kawachi, M. Kishimoto, K. Sukegawa, M. Tanaka, N. Hasegawa, M. Suzuki, R. Tai, M. Kado, Y. Ochi, M. Nishikino, K. Nagashima, H. Daido, Y. Kato, H. Fiedorowicz, A. Bartnik
Proc.4th Symposium on Advanced Photon Research, JAERI-Conf 2003-008, pp.264

Free Electron Laser Development (Free Electron Laser Research Group)

1. Journals

1) High-K negative parity states in ^{184}Os
T. Shizuma, Paul D. Stevenson, Phil M. Walker, Y. Tou, T. Hayakawa, M. Oshima, K. Furuno, T. Komatsubara
Physical Review C, Vol. 65, p.64310_1-64310_12 (2002)
2) Tunneling in High-K isomeric decays
T. Shizuma, Y. Shimizu, T. Hayakawa
Journal of Nuclear Science and Technology, Vol.39, No.11, pp.1137-1141 (2002)
3) Improved Confinement of Neon Plama inside a High-Tc Superconducting Tube
T. Yamauchi, H. Matsuzawa, K. Mikami, J. Ishikawa
Jpn. J. Appl. Phys., Vol.41Part1 No9, pp.5799-5800 (2002)
4) Universal scalings between s- and p-process elements, and new ^{176}Lu- ^{176}Hf- ^{174}Hf cosmochronometer
T. Hayakawa, T. Shizuma, T. Kajino
Nature

5) Projectile Coulomb excitation of ^{78}Se
T. Hayakawa, Y. Tou, M. Oshima, A. Osa, M. Koizumi, Y. Hatsukawa, Y. Utsuno, J. Katakura, M. Matsuda, T. Morikawa, M. Sugawara, H. Kusakari, T. Czosnyka
Physical Review C 67, 064310, p.1-6 (2003)

6) A rotaional alignment of the h11/2 band with high-O in ^{157}Dy
T. Hayakawa, Y. Tou, M. Oshima, M. Matsuda, Y. Hatsukawa, J. Katakura, H. Iimura, T. Shizuma, S. Mitarai, M. Sugawara , H. Kusakari, Y. H. Zhang
European Physical Journal A 15, p.299-302 (2002)

7) Electric-dipole transition probabilities between yrast bands in ^{157}Gd
T. Hayakawa, Y. Tou, M. Oshima, M. Matsuda, Y. Hatsukawa, N. Shinohara, H. Iimura, T. Shizuma, M. Sugawara, H. Kusakari, Y. H. Zhang
Physics Letters B 551, p.79-85 (2003)

8) Neutron capture cross section to the ^{186}Re isomeric state
T. Hayakawa, T. Shizuma, T. Yamauchi, E. Minehara, T. Arisawa
Nuclear Physics A 718, p.665-667 (2003)

9) Octupole bands in ^{158}Dv
T. Hayakawa, Y. Tou, M. Oshima, M. Matsuda, Y. Hatsukawa, T. Shizuma, J. Katakura, H. Iimura, S. Mitarai, Y. H. Zhang, M. Sugawara, H. Kusakari
European Physical Journal A

10) Inelastic excitation of ^{187}Re
T. Shizuma, Y. Tou, M. Oshima, M. Sugawara, M. Matsuda, T. Hayakawa, M. Koizumi, A. Osa, Y. Zhang, Z. Lui
European Physical Journal A17, p.159-165 (2003)

2. Proceedings

1) A few hundred femtosecond FEL with a few kW average and one GW peak power for academic and industrial applications
E. Minehara, R. Hajima, M. Sawamura, R. Nagai, N. Nishimori, N. Kikuzawa, M. Sugimoto, T. Yamauchi, T. Hayakawa, T. Shizuma
Proceedings of International Congress On Laser Advanced Materials Processing

2) Recent results and future plans of the JAERI Energy-Recovery Linac
R. Hajima, T. Shizuma, M. Sawamura, R. Nagai, N. Kikuzawa, N. Nishimori, E. Minehara
Proceedings of ICFA 24th Beam Dynamics Workshop on Future Light Sources

3) Commissioning of JAERI Energy Recovery Linac
N. Nishimori, R. Hajima, R. Nagai, M. Sawamura, N. Kikuzawa, T. Shizuma
Proceedings of the 8th European Particle Accelerator Conference

4) A 2MV DC electron Gun and Injector for High Power FELs with a Depressed Geometry
E. Minehara, M. Sawamura, R. Hajima, R. Nagai, N. Kikuzawa, N. Nishimori, T. Shizuma
Nuclear Instruments and Methods in Physical Research A

5) Current Status and Future Plans for the JAERI Superconducting rf linac-based FEL Facility
E. Minehara, M. Sawamura, R. Hajima, R. Nagai, N. Kikuzawa, N. Nishimori, T. Shizuma, T. Yamauchi
Nuclear Instruments and Methods in Physical Research A

6) Recent Progress and Future Plans of the JAERI Superconducting rf Linac-based FEL Facility
E. Minehara, T. Yamauchi, M. Sugimoto, M. Sawamura, R. Hajima, R. Nagai, N. Kikuzawa, N. Nishimori, T. Shizuma
Proceedings of the 27th Linear Accelerator Meeting in Japan, p.21-23 (2002)

7) First demonstration of energy-recovery operation and 10kW upgrade at JAERI-FEL
R. Hajima, T. Shizuma, M. Sawamura, R. Nagai, N. Kikuzawa, N. Nishimori, E. Minehara
Proceedings of the 27th Linear Accelerator Meeting in Japan, p.97-99 (2002)

8) A full-DC injector for future ERL light sources
R. Hajima, E. Minehara
Proceedings of the 27th Linear Accelerator Meeting in Japan, p.169-171 (2002)

9) Systematics between s-, r- and p-processes in solar system by model independent analysis and proposal of new nuclear cosomchronometer of the p-process
T. Hayakawa, T. Shizuma, T. Kajino

Proceedings of the Physical Society of Japan 2002 Autumn Meeting
10) Neutron capture cross section to the ^{186}Re isomeric state
T. Hayakawa, T. Shizuma, T. Yamauchi, E. Minehara, T. Arisawa
Proceedings of the Seventh International Symposium on Nuclei in the Cosmos
11) View of the p-process study by supernovac
T. Hayakawa
Proceedings of Workshop of nucleosynthesis and unstable nuclei
12) Properties of HOM in Energy Recover FEL
M. Sawamura, R. Hajima, Y. Iwashita, R. Nagai, N. Nishimori, N. Kikuzawa, E. Minehara
Proceedings of the 27th Linear Accelerator Meeting in Japan, p.275-277 (2002)
13) Chirp estimation of an ulrtashort free-electron laser pulse
R. Nagai, R. Hajima, M. Sawamura, N. Nishimori, N. Kikuzawa, E. Minehara
Proceedings of the 27th Linear Accelerator Meeting in Japan, p.264-266 (2002)
14) A new nuclear cosmochronometer of the p-process
T. Hayakawa, T. Shizuma, T. Kajino
Proceedings of Workshop on "Light-to-heavy elements in cosmology and Galactic evolution"
15) First demonstration of energy-recovery operation in the JAERI superconducting linac for a high-power free-electron laser
R. Hajima, T. Shizuma, M. Sawamura, R. Nagai, N. Nishimori, N. Kikuzawa, E. Minehara
Nuclear Instruments and Methods in Physics Research A
16) Energy-Recovery Linac for the next generation light sources
R. Hajima
Proceedings of the Physical Society of Japan 2002
17) Electron beam dynamics through a return-arc and a deceleration path of the JAERI Energy-Recovery Linac
R. Hajima, E. Minehara
Nuclear Instruments and Methods in Physics Research A
18) Second Harmanic Generation in CdTe and Te Crystals by Free Electron Laser
T. Yamauchi, N. Kikuzawa, E. Minehara
Proceedings of the Third Asian Pacific Laser Symposium (APLS2002)
19) Behaviour of neon plasma inside a high-Tc superconducting tube
T. Yamauchi, H. Matsuzawa, T. Morita
Proceedings of the 19th JSPF Annual Meeting
20) Lethargy Effect in FEL Oscillators zt Zero Detuning of an Optical Carvity
N. Nishimori, R. Hajima, R. Nagai, E. Minehara
Nuclear Instruments and Methods in Physics Research A
21) Energy-recovery linac-based high power and highly efficient Industrial FELs
E. Minehara, R. Hajima, M. Sawamura, R. Nagai, N. Nishimori, N. Kikuzawa, T. Yamauchi
Proceedings of the 3rd Asian Pacific Laser Symposium (APLS2002)
22) Energy Recovery Linacs
E. Minehara, R. Hajima
Proceedings of the International Workshop on Photoionization 2002 (IWP2002)
23) JAERI FEL Facility at Tokai
E. Minehara, M. Sawamura
Proceedings of Atomic Energy Society of Japan 2002
24) The JAERI Energy-Recovery Linac for Free-Electron Lasers
E. Minehara, R. Hajima, M. Sawamura, R. Nagai, N. Nishimori, N. Kikuzawa, M. Sugimoto, T. Yamauchi, T. Hayakawa, T. Shizuma
Proceedings of the 21st International Linac Conference
25) A 100kW Average Power, and Highly-Efficient FEL with Femtosecond Pulses driven by the JAERI Compact Energy Recovery Superconducting rf Linac and its Industrial Applisations
E. Minehara
Proceedings of The 21st Century Interdisciplinary Symposium on Science and Technology, and Human beings
26) The JAERI Energy-Recovery Linac-based FEL sources and their applications
E. Minehara

Proceedings of the Japanese French Workshop on FELs (Workshop Franco-Japonais Surle Lel)

27) Chirp characteristic of a high intensity ultrashort pulse FEL
R. Nagai, R. Hajima, M. Sawamura, N. Nishimori, N. Kikuzawa, E. Minehara
Proceedings of the 11th Topical Meeting on FEL and Its Applications

28) Status of Energy-Recovery Linac light sources and possible applications to infrared wavelength region
R. Hajima
Proceedings of IMS Symposium "Status and perspectives of infrared radiation sources"

29) JAERI ERL plan for light source protorype and UV FELs
R. Hajima
Proceedings of the Japanese French Workshop on FELs (Workshop Franco-Japonais Surle Lel)

30) Studies on nuclear isomers by photo-nuclear excitation
T. Shizuma
Proceedings of Investigative Committee on Trend for Basic Studies of Nuclear Energy Science Technology

31) A design study of an ERL light source (1)
E. Minehara, R. Hajima, M. Sawamura, R. Nagai, N. Kikuzawa, N. Nishimori
Proceedings of the 16th Annual meeting of the Japanese Society for Synchrotron Radiation Research

32) A design study of an ERL light source (2)
R. Hajima, E. Minehara, M. Sawamura, R. Nagai, N. Kikuzawa, N. Nishimori
Proceedings of the 16th Annual meeting of the Japanese Society for Synchrotron Radiation Research

33) A next-generation infra-red light source using an energy-recovery linac
R. Hajima, T. Takahashi, S. Kimura
Proceedings of the 16th Annual meeting of the Japanese Society for Synchrotron Radiation Research

34) Development of a High-Power and High-Efficiency FEL based on Energy-Recovery-Linac
R. Nagai, R. Hajima, M. Sawamura, N. Nishimori, N. Kikuzawa, E. Minehara
Proceedings of The Japan Society of Applied Physics

35) Optimization for the Industrial Free-Electron Laser driven by the Energy Recovery Superconducting rf Linac
E. Minehara, T. Yamauchi, R. Hajima, M. Sawamura, T. Shizuma, T. Hayakawa, N. Nishimori, N. Kikuzawa, R. Nagai
Proceedings of the 23th Annual Meeting of The Laser Society of Japan

36) High-K isomers at the A=180 region and the K-mixing
T. Shizuma, T. Hayakawa, T. Morikawa , S. Mitarai, Y. Shimizu
Proceedings of the Physical Society of Japan 2003

37) Proposal for photo-nuclear experiments on ^{176}Lu and ^{180}Ta isomers using gamma-ray beams at a 1MeV region
T. Shizuma, T. Hayakawa
Proceedings of Generation of high energy synchrotron radiation by super conducting wiggler and its application

38) Loop design of the ERL light source in JAERI
N. Kikuzawa, R. Hajima, M. Sawamura, R. Nagai, N. Nishimori, E. Minehara
Proceedings of Atomic Energy Society of Japan 2003

39) HOM Instability Measurement of the JAERI ER-FEL
M. Sawamura, R. Nagai, R. Hajima, N. Kikuzawa, N. Nishimori, E. Minehara
Proceedings of Atomic Energy Society of Japan 2003

40) JAERI Superconducting rf Linac-based FEL for Industrial Application
E. Minehara, M. Sawamura, R. Hajima, R. Nagai, N. Kikuzawa, N. Nishimori, T. Shizuma, T. Yamauchi
Proceedings of Atomic Energy Society of Japan 2003

41) Formation of an FEL field with uniform phase at dL=0 lasing
N. Nishimori, R. Hajima, R. Nagai
Proceedings of the Physical Society of Japan 2003

42) Photo-induced reaction and p-process nucleosynthesis
T. Hayakawa
Proceedings of the Physical Society of Japan 2003
43) R&D challenges at the JAERI Free-Electron Laser
R. Hajima
Proceedings of ESFRI FEL Workshop "R&D challenges of 2nd Generation FELs"
44) Free-Electron Lasers for Isotope Separation and gamma-ray generation
R. Hajima, E. Minehara
Proceedings of Workshop on Science and Technology of LEPS in the Medium High Energy Region
45) Status and Perspectives of The Energy-Recovery Linac
R. Hajima
Proceedings of the 20th Photon Factory Symposium

Optics Research and Development (Novel Optics Research Group)

1. Journals

1) Optimization of the silicon oxide layer thicknesses inserted in the Mo/Si multilayer interfaces for high heat stability and high reflectivity
M. Ishino and O. Yoda
J. Appl. Phys. 92, 4952-4958, (2002)
2) Improved cooling performance of ytterbium-doped glass combined with sapphire
A. Nishimura, A. Sugiyama, T. Usami, and K.Ohara
J of Materials Science: Materials in Electronics, 14, 1-3, (2003)
3) Performance of laminar-type holographic grating for a soft X-ray flat field spectrograph in the 0.7-6 nm region
M. Koike, K. Sano, E. Gullikson, Y. Harada, H. Kumata
Rev. Sci. Instrum., 74,1156-1158, (2003)

2. Proceedings

1) Nd:YVO_4 and YVO_4 laser crystals integration by a direct bonding technique valuations of bonded region in a direct bonded Ti:sapphire laser crystal
A. Sugiyama, H. Fukuyama, M. Katsumata, and Y. Okada
Proc. SPIE, 4944, 46, (2002)
2) Heat stability of Mo/Si multilayers inserted with silicon oxide layers
M. Ishino, O. Yoda, K. Sano, and M. Koike,
Proc. SPIE 4782, 277-284, (2002)
3) New Type of Monk-Gillieson Monochromator Capable of Covering a 0.7-25nm Range
M. Koike, K. Sano, Y. Harada, O. Yoda, M. Ishino, K. Tamura, K. Yamashita, N.Moriya, H. Sasai, M. Jinno, T. Namioka,
Proc. SPIE, 4782, 300-307, (2002)

3. Patents

1) Method of laser pulse shortening by a Lead Molibdate Crystal
A. Sugiyama, K. Deki, Y. Anzai, M. Katsurayama and Y. Matsumoto
Japan patent application number 2002-107776 Apr 10, (2002)
2) Laser crystal bonding method using an ion beam etching process
A. Sugiyama and M. Katsumata
Japan patent application number 2002-215082 Jul 24, (2002)
3) Conical diffraction grazing incidence spectrometer and diffraction grating for use in the spectrometer
M. Koike, K. Sano, Y. Harada
US patent application number 10/191,993, Jul 10, (2002)

Laser Driven Particle Acceleration Development (Laser Acceleration Research Group)

1. Journal

1) Direct measurement of coherent ultrahigh wakefields excited by intense ultrashort laser pulses in a gas-jet plasma
H. Kotaki, M. Kando, T. Oketa, S. Masuda, J. K. Koga, S. Kondo, S. Kanazawa, T. Yokoyama, T. Matoba, and K. Nakajima
Phys. Plasmas, vol.9, 1392-1400 (2002)
2) High energy laser wakefield acceleration
H. Kotaki, M. Kando, T. Hosokai, S. Kondo, S. Masuda, S. Kanazawa, T. Yokoyama, T. Matoba, and K. Nakajima
International Journal of Applied Electromagnetics and Mechanics, vol.14, pp255-262 (2001/2002).
3) Effect of a laser prepulse on a narrow-cone ejection of MeV electrons from a gas jet irradiated by an ultrashort laser pulse
Tomonao Hosokai, Kenichi Kinoshita, Alexei Zhidkov, Kei Nakamura, Takahiro Watanabe, Toru Ueda, Hideyuki Kotaki, Masaki Kando, Kazuhisa Nakajima, and Mitsuru Uesaka
Phys. Rev. E 67, 036407 (2003)

2. Proceeding

1) High energy, high quality laser-plasma particle accelerator development at JAERI-APR
Masaki Kando, Hideyuki Kotaki, Shin'ichi Masuda, Shuji Kondo, Shuhei Kanazawa, Takayuki Homma and Kazuhisa Nakajima
Advanced Accelerator Concepts workshop 2002, Oxnard, USA, 24 June 2002.
2) Generation of high quality electron beam by laser-plasma interaction
H. Kotaki, S. Masuda, M. Kando, S. Kondo, S. Kanazawa, T. Homma, and K. Nakajima,
QUANTUM ASPECTS OF BEAM PHYSICS and Other Critical Issues of Beams in Physics and Astrophysics, Hiroshima University, Higashi-Hiroshima, Japan, January 7-11, (2003)
3) 1D PIC Simulation of Plasma Cathode
S. Masuda H. Kotaki, M.Kando, S.Kanazawa, S.Kondo, T.Honma, I.V.Smetanin, and K.Nakajima,
QUANTUM ASPECTS OF BEAM PHYSICS and Other Critical Issues of Beams in Physics and Astrophysics, Hiroshima University, Higashi-Hiroshima, Japan, January 7-11, (2003)
4) Improvement of quantum efficiency of RF gun for photo cathode
M. Kando, H. Kotaki, S. Kondo, S. Kanazawa, S. Masuda, R. Homma, K. Nakajima
Proceedings of the 27th Linear Accelerator Meeting in Japan,
7-9 August 2002, Kyoto, Japan.

Advanced Photon Simulation Research (Simulation Group for Advanced Photon Science)

1. Journals

1) Radiation damping effects on the interaction of ultra-intense laser pulses with an overdense plasma
A. Zhidkov, J. Koga, A. Sasaki, M. Uesaka
Phys. Rev. Lett., Vol. 88, No. 18, pp.185002-1 - 185002-4 (2002)
2) Extended description for electron capture in ion-atom collisions: Application of model potentials within the framework of the continuum-distorted-wave theory
L. Gulyas, P.D. Fainstein, T. Shirai
Phys. Rev. A, Vol. 65, No. 5, pp. 052720-1 – 052720-9 (2002)
3) A kinetic model for the one-dimensional electromagnetic solitons in an isothermal plasma
M. Lontano, S.V. Bulanov, J. Koga, M. Passoni, T. Tajima
Phys. Plasmas, Vol. 9, No. 6, pp. 2562-2568 (2002)
4) Effect of plasma inhomogeneity on ion acceleration when an ultra-intense laser pulse interacts with a foil target
A.A. Andreev, A.G. Zhidkov, A. Sasaki, K. Yu. Platonov
Plasma Physics Controlled Fusion, Vol. 44, No. 7, pp. 1243-1251 (2002)
5) Plasma wakefield acceleration for ultra high-energy cosmic rays
P. Chen, T. Tajima, Y. Takahashi
Phys. Rev. Lett., Vol. 89, No. 16, pp. 161101-1-4 (2002)
6) Generation of high-quality charged particle beams during the acceleration of ions by high-power

laser radiation
S.V. Bulanov, T.Zh. Esirkepov, F.F. Kamenets, Y. Kato, A.V. Kuznetsov, K. Nishihara, F. Pegoraro, T. Tajima, V.S. Khoroshkov
Plasma Physica Reports, Vol. 28, No. 12, pp. 975-991 (2002)

7) Proposed double-layer target for the generation of high-quality laser-accelerated ion beams
T.Zh. Esirkepov, S.V. Bulanov, H. Daido, Y. Kato, V.S. Khoroshkov, Y. Kitagawa, K. Mima, K. Nagai, K. Nishihara, S. Sakabe, F. Pegoraro, T. Tajima
Phys. Rev. Lett., Vol. 89, No. 17, pp. 175003-1 - 4 (2002)

8) Accurate numerical method for the solutions of the Schrodinger equation and the radial integrals based on the CIP method
T. Utsumi, J. Koga
Comput. Phys. Commun., Vol. 148, pp. 267-280 (2002)

9) New numerical method for the solutions of the MCDF equations based on the CIP method
T. Utsumi, J. Koga
Comput. Phys. Commun., Vol. 148, pp. 281-290 (2002)

10) Ion acceleration in a solitary wave by an intense picosecond laser pulse
A. Zhidkov, M. Uesaka, A. Sasaki, H. Daido
Phys. Rev. Lett., Vol. 89, No. 21, pp. 215002-1 – 4 (2002)

11) Improvement of Accuracy and Stability in Numerically Solving Hyperbolic Equations by IDO (Interporated Differential Operator) Scheme with Runge-Kutta Time Integration
H. Yoshida, T. Aoki, T. Utsumi
The Transactions of the Institute of Electronics, Information and Communication Engineers A, Vol. J86-A, No. 3, pp. 223-231 (2003)

2. Proceedings

1) Relativistic self-focusing of ultraintense laser pulses and ion acceleration
J. Koga, K. Nakajima, K. Nakagawa
SuperStrong Fields in Plasmas, AIP Conference Proceedings, Vol. 611, pp. 126-137 (2002)
Proc. 2nd Int. Conf. Superstrong Fields in Plasmas (Varenna, 2001.08)

2) Relativistic electromagnetic solitons in a high temperature plasma
M. Lontano, S.V. Bulanov, J. Koga
SuperStrong Fields in Plasmas, AIP Conference Proceedings, Vol. 611, pp. 157-163 (2002)
Proc. 2nd Int. Conf. Superstrong Fields in Plasmas (Varenna, 2001.08)

3) Short wavelength x-ray emission from inner-shell excited states generated by high intensity laser irradiation on Kr, Xe clusters
K. Moribayashi, A. Zhidkov, A. Sasaki, K. Suto, S. Suzuki
Inertial Fusion Science and Application 2001 (Kyoto, 2001.09) , pp. 1182-1185 (2002)

4) Charge transfer processes in ion-ion collisions
S. Suzuki, T. Shirai, A. Sasaki, K. Moribayashi, S. Nanba, T. Kawachi, N. Shimakura
Inertial Fusion Science and Application 2001 (Kyoto, 2001.09) , pp. 1174-1177

5) Quantum simulation of hot dense plasmas
H. Totsuji, Y. Nishii, C. Totsuji, K. Tsuruta, I. Fukumoto, J. Chihara, M. Yamagiwa, T. Tajima
Inertial Fusion Sciences and Applications 2001 (Kyoto, 2001.09) , pp. 952-956 (2002)

6) Handling technology and viewer for 3-dimensional large data
Y. Ueshima,
Proceeding of the Third Symposium of Large Data Management for Creative Research (Kyoto, 2001.10) JAERI-Conf 2002-006, pp. 60-64 (2002)

7) An Example of Large Data Management and Distributed System - Ion Acceraration with Laser Matter Interaction -
Y. Ueshima
Proceeding of PSE workshop 2002, pp. 1-8 (2002)

8) Acceleration of proton beams by relativistically self-focused intense laser pulses
J. Koga, K. Nakajima, M. Yamagiwa, A. Zhidkov
AIP Conference Proceedings 634, pp. 50-57 (2002)

9) Review and comparison of Particle-in-Cell and Vlasov simulation methods with application to

relativistic self-focusing
James Koga
AIP Conference Proceedings 634, pp. 388-397 (2002)

10) Kinetic simulation of laser-induced high-energy phenomena
M. Yamagiwa, J. Koga, Y. Ueshima, Simulation Group for Advanced Photon Science
Proceedings of the 3rd Symposium on Advanced Photon Research (Kyoto, 2001.12) JAERI-Conf 2002-008, pp. 42-45 (2002)

11) Development of the Web oriented hierarchical atomic model (WHIAM)
A. Sasaki
Proceedings of the 3rd Symposium on Advanced Photon Research (Kyoto, 2001.12) JAERI-Conf 2002-008, pp. 244-247 (2002)

12) Scientific visualization with Java for atomic process simulation
A. Sasaki, H. Yokota, K. Suto
Proceedings of the 3rd Symposium on Advanced Photon Research (Kyoto, 2001.12) JAERI-Conf 2002-008, pp. 248-251 (2002)

13) Simulation of atomic processes for high intensity laser irradiation on clusters
K. Moribayashi
Proceedings of the 3rd Symposium on Advanced Photon Research (Kyoto, 2001.12) JAERI-Conf 2002-008, pp. 232-235 (2002)

14) Development of the computer code for the atomic structure and the radiative and collisional atomic process
T. Utsumi, J. Koga
Proceedings of the 3rd Symposium on Advanced Photon Research (Kyoto, 2001.12) JAERI-Conf 2002-008, pp. 228-231 (2002)

15) Spectrum analysis of Al ions produced by high intensity laser irradiation
K. Suto, A. Sasaki, K. Moribayashi, K. Takahashi, M. Suzuki, E. Yanase, T. Oketa, H. Daido, T. Kagawa
Proceedings of the 3rd Symposium on Advanced Photon Research (Kyoto, 2001.12) JAERI-Conf 2002-008, pp. 72-75 (2002)

16) The charge exchange reactions in collisions between N^7+ ions and He atoms
S. Suzuki, T. Shirai, N. Shimakura
Proceedings of the 3rd Symposium on Advanced Photon Research (Kyoto, 2001.12) JAERI-Conf 2002-008, pp. 141-145 (2002)

17) Distributed system supporting large-scale-research and remote-research
Y. Ueshima
Proceedings of the 3rd Symposium on Advanced Photon Research (Kyoto, 2001.12) JAERI-Conf 2002-008, pp. 259-262 (2002)

18) ITBL as Production Computing Enviroment for Researchers
H. Ihara, M. Fukuda, Y. Ueshima, M. Kannari, Y. Takeda, K. Isogai, A. Sasaki
Proceedings of the 3rd Symposium on Advanced Photon Research (Kyoto, 2001.12) JAERI-Conf 2002-008, pp. 252-255 (2002)

19) The SHD display sysytem: revealing beauty in plasma motion as well as ancient glass
A. Sasaki, Y. Ueshima, J. Koga, A. Nishimura
Proceedings of the 3rd Symposium on Advanced Photon Research (Kyoto, 2001.12) JAERI-Conf 2002-008, pp. 263-266 (2002)

High Peak Power Laser Application (Applied Photon Research Group)

1. Journal

1) Photodissociation of Acetaldehyde, $CH_3CHO \rightarrow CH_3 + HCO$: Direct Ab Initio Molecular Dynamics Study
Y. Kurosaki and K. Yokoyama
Chem. Phys. Lett. 371, 568-575 (2003).

2) Global Ab Initio Potential Energy Surfaces for the Lowest Three Doublet States (12A, 22A, and 12A") of the BrH_2 system
Y. Kurosaki and T. Takayanagi

J. Chem. Phys. 119, 7838-7856 (2003).

3) Control of photodissociation branching using the complete reflection phenomenon : Application of HI molecules
H. Fujisaki, Y. Teranishi, and H. Nakamura
J. Theo. Comp. Chem. 1, 245 (2002).

4) New way of controlling molecular processes by a sequence of linearly chirped pulses
K. Nagaya, Y. Teranishi, and H. Nakamura
J. Chem. Phys. 117, 9588 (2002).

5) Review of soft x-ray laser development (Invited paper)
H. Daido
Rep. Prog. Phys. 65 1513-1576(2002).

2. Proceedings

1) Ion Generation via Interaction between Intense Ultra-short Laser Pulse and Solid Target for Application to Cancer Therapy
Koji Matsukado, Kenichi Kinoshita, Zhong Li, Hiroyuki Daido, Yukio Hayashi, Satoshi Orimo, Mitsuru Uesaka, Koji Yoshii, Takahiro Watanabe, Tomonao Hosokai, Alexei Zhidkov, Akira Noda, Yoshihisa Iwashita, Toshiyuki Shirai, Shu Nakamura, Atsushi Yamazaki, Akio Morita, Atsushi Ogata, Yoshio Wada, Tetsuo Kubota, Fuminori Soga, and Satoru Yamada
Proceedings of ADVANCED ACCELERATOR CONCEPTS: Tenth Workshop, Mandalay Beach, California (USA) 22-28 June 2002, pp. 265-268

2) High Energy Ion generation from Laser Plasma for a Compact Cancer Therapy Accelerator
Koji Matsukado, Hiroyuki Daido, Zhong Li, Atsushi Fukumi, Takeshi Takeuchi, Yukio Hayashi, Satoshi Orimo, Sergei Bulanov, Mitsuru Uesaka, Koji Yoshii, Takahiro Watanabe, Tomonao Hosokai, Ken-ichi Kinoshita, Alexei Zhidkov, Akira Noda, Yoshihisa Iwashita, Toshiyuki Shirai, Shu Nakamura, Atsushi Yamazaki, Akio Morita, Atsushi Ogata, Yoshio Wada, Tetsuo Kubota, Fuminori Soga, Satoru Yamada, Timur Esirkepov , Katsunori Nishihara
Proceedings of The Third Asian Pacific Laser Symposium(APLS2002) 17-20 September 2002, pp. 143-146

3) Laser Driven High Energy Ion Generation for A Compact Cancer Therapy Accelerator
Koji Matsukado, Hiroyuki Daido, Zhong Li, Atsushi Fukumi, Yukio Hayashi, Satoshi Orimo, Sergei Bulanov, Mitsuru Uesaka, Koji Yoshii, Takahiro Watanabe, Tomonao Hosokai, Ken-ichi Kinoshita, Alexei Zhidkov, Akira Noda, Yoshihisa Iwashita, Toshiyuki Shirai, Shu Nakamura, Atsushi Yamazaki, Akio Morita, Takeshi Takeuchi, Atsushi Ogata, Yoshio Wada, Tetsuo Kubota, Fuminori Soga, Satoru Yamada, Timur Esirkepov, Katsunori Nishihara
Proceedings of XXVII European Conference on Laser Interaction with Matter (ECLIM) 7-11 October 2002 (to be published)

6.2 List of publications on Synchrotron Radiation Research Center

Experimental facilities development (Experimental Facilities Development Group)

1. Journals

1) A Report of the 2nd International Workshop on Radiation Safety at Synchrotron Radiation Sources
Asano Yoshihiro
Nippon Hoshako Gakkai-shi,16,2,120-122,(2003/03)

2. Proceedings

1) Comparison of synchrotron radiation calculation between EGS4, FLUKA, PHOTON and STAC8
Asano Yoshihiro, Liu J.
KEK Proceedings 2002-18,48-54,(2003/01)

High pressure science (High Pressure Science Group)

1. Journals

1) Viscosity change and structural transition of molten Fe at 5 GPa
Terasaki Hidenori, Kato Takumi, Urakawa Satoru, Funakoshi Kenichi, Sato Kiminori, Suzuki Akio, Okada Taku
Geophysical Research Letters,29,8,68_1-68_3,(2002/05)
2) XAFS under extreme conditions
Katayama Yoshinori
X-sen Kyushu Bunko Ho; XAFS To Sono Oyo,162-169,(2002/06)
3) *In situ* X-ray observations of the decomposition of brucite and the graphite-diamond conversion in aqueous fluid at high pressure and temperature
Okada Taku, Utsumi Wataru, Kaneko Hiroshi, Yamakata Masaaki, Shimomura Osamu
Physics and Chemistry of Minerals,29,7,439-445,(2002/08)
4) Phase relations of AgI under high pressure and high temperature
Otaka Osamu, Takebe Hitoshi, Yoshiasa Akira, Fukui Hiroshi, Katayama Yoshinori
Solid State Communications,123,5,213-216,(2002/08)
5) *In situ* EXAFS study on GeS_2 glass under high-pressure
Miyauchi Koichi, Qiu J., Shojiya Masanori, Kawamoto Yoji, Kitamura Naouki, Fukumi Kohei, Katayama Yoshinori, Nishihata Yasuo
Solid State Communications,124,5-6,189-193,(2002/10)
6) Size-selective extended X-ray absorption fine structure spectroscopy of free selenium clusters
Nagaya Kiyonobu, Yao Makoto, Hayakawa Tetsuichiro, Omasa Yoshinori, Kajihara Yukio, Masashi Ishii, Katayama Yoshinori
Physical Review Letters,89,24,243401_1-243401_4,(2002/12)

2. Proceedings

1) *In situ* observation of a first-order liquid-liquid transition in phosphorus
Katayama Yoshinori
Journal of Non-Crystalline Solids,312-314,8-14,(2002/10)
2) *In situ* X-ray observations of the diamond formation process in the C-H_2O-MgO system
Okada Taku, Utsumi Wataru, Shimomura Osamu
Journal of Physics: Condensed Matter,14,44,11331-11335,(2002/11)
3) Synchrotron radiation studies on pressure-induced structural changes in liquids and glasses
Katayama Yoshinori, Inamura Yasuhiro
Journal of Physics: Condensed Matter,15,1,S343-S350,(2003/01)
4) *In situ* observation of a liquid-liquid transition in phosphorus
Katayama Yoshinori
Proceedings of the NATO Advances Research Workshop on New Kinds of Phase Transitions; Transformations in Disordered Substances,179-185,(2002)

Structural physics research (Structural Physics Research Group)

1. Journals

1) Magnetic properties of $LnMnO_3$ (Ln=Ho, Er, Tm, Yb and Lu)
Yoshii Kenji, Abe Hideki
Journal of Solid State Chemistry,165,1,131-135,(2002/04)

2) Structure and electrical transport property of a silicopnictide ZrCuSiP
Abe Hideki, Yoshii Kenji
Journal of Solid State Chemistry,165,2,372-374,(2002/05)

3) Electrochemical synthesis of superconductive boride MgB_2 from molten salts
Abe Hideki, Yoshii Kenji
Japanese Journal of Applied Physics, Part 2,41,6B,L685-L687,(2002/06)

4) Single-crystal growth of silver-lead oxide $Ag_5 Pb_2 O_6$ from fused nitrates
Abe Hideki, Ye J., Imai Motoharu, Yoshii Kenji, Matsushita Akiyuki, Kitazawa Hideaki
Journal of Crystal Growth,241,3,347-351,(2002/06)

5) Periodic hole structure in a spin-chain ladder material $Sr_{14} Cu_{24} O_{41}$
Fukuda Tatsuo, Mizuki Junichiro, Matsuda Masaaki
Physical Review B,66,1,012104_1-012104_4,(2002/07)

6) Self-regeneration of a Pd-perovskite catalyst for automotive emissions control
Nishihata Yasuo, Mizuki Junichiro, Akao Takahiro, Tanaka Hirohisa, Uenishi Mari, Kimura Mareo, Okamoto Tokuhiko, Hamada Noriaki
Nature,418,6894,164-167,(2002/07)

7) A Novel spectroelectrochemical cell for in situ surface X-ray scattering measurements of single crystal disk electrodes
Kondo Toshihiro, Tamura Kazuhisa, Takahashi Masamitsu, Mizuki Junichiro, Uosaki Kohei
Electrochimica Acta,47,19,3075-3080,(2002/07)

8) X-ray reflectivity and diffraction studies on lipid and lipopolymer Langmuir-Blodgett films under controlled humidity
Bolze J., Takahashi Masamitsu, Mizuki Junichiro, Baumgart T., Knoll W.
Journal of the American Chemical Society,124,32,9412-9421,(2002/08)

9) Magnetic behavior of $CeTi_1 Vx O_3$
Yoshii Kenji, Abe Hideki
Journal of Alloys and Compounds,343,1-2,199-203,(2002/09)

10) Electrical transport properties of bulk MgB_2 materials synthesized by electrolysis on fused mixtures of $MgCl_2$, NaCl, KCl and $MgB_2 O_4$
Yoshii Kenji, Abe Hideki
Superconductor Science and Technology,15,10,L25-L27,(2002/10)

11) The Structures of alkylimidazolium fluorohydrogenate molten salts studied by high-energy X-ray diffraction
Hagiwara Rika, Matsumoto Kazuhiko, Tsuda Tetsuya, Ito Yasuhiko, Kohara Shinji, Suzuya Kentaro, Matsumoto Hajime, Miyazaki Yoshinori
Journal of Non-Crystalline Solids,312-314,414-418,(2002/10)

12) X-Ray diffractometer for studies on molecular-beam-epitaxy growth of III-V semiconductors
Takahashi Masamitsu, Yoneda Yasuhiro, Inoue Hirotane, Yamamoto Naomasa, Mizuki Junichiro
Japanese Journal of Applied Physics, Part 1,41,10,6247-6251,(2002/10)

13) Structural physics with synchrotron radiation; Focus on a use of resonant effect
Mizuki Junichiro
Bussei Kenkyu,79,3,481-490,(2002/12)

14) Structure, magnetism and transport of La_2NiRuO_6
Yoshii Kenji, Abe Hideki, Mizumaki Masaichiro, Tanida Hajime, Kawamura Naomi
Journal of Alloys and Compounds,348,1-2,236-240,(2003/01)

15) Structural analysis of 1-ethyl-3-methylimidazolium bifluoride melt
Matsumoto Kazuhiko, Hagiwara Rika, Ito Yasuhiko, Kohara Shinji, Suzuya Kentaro
Nuclear Instruments and Methods in Physics Research B,199,29-33,(2003/01)

16) High-energy X-ray diffraction studies of disordered materials

Kohara Shinji, Suzuya Kentaro
Nuclear Instruments and Methods in Physics Research B,199,23-28,(2003/01)

17) Defect-induced phase separation in relaxor $Pb(In_{1/2}Nb_{1/2})O_3$ crystals
Yoneda Yasuhiro, Matsumoto Norimasa, Terauchi Hikaru,
Journal of Physics: Condensed Matter,15,3,467-474,(2003/01)

18) Neutron diffraction study of field-cooling effects on the relaxor ferroelectric $Pb[(Zn_{1/3}Nb_{2/3})_{0.92}Ti_{0.08}]O_3$
Owada Kenji, Hirota Kazuma, Rehrig P. W., Fujii Yasuhiko, Shirane Gen
Physical Review B,67,9,094111_1-094111_8,(2003/03)

19) Neutron diffraction measurements of the structure of an orthosilicate glass: Mg_2SiO_4
Weber J. K. R., Tangeman J. A., Key T. S., Loong C.-K., Takeuchi Ken, Suzuya Kentaro
Physics and Chemistry of Glasses, Vol. 43C 2002,68-70,(2002)

20) Intermediate range order of vitreous silica studied by high energy X-ray diffraction, neutron diffraction and reverse Monte Carlo modelling
Kohara Shinji, Suzuya Kentaro
Physics and Chemistry of Glasses, Vol. 43C 2002,51-54,(2002)

21) Automotive catalysts with self-regeneration
Tanaka Hirohisa, Nishihata Yasuo
Kogyo Zairyo,50,13,35-38,(2002/12)

22) Immortal catalytic activity for cleaning up automotive emissions; Intelligent catalyst
Nishihata Yasuo, Tanaka Hirohisa
SPring-8 Riyosha Joho,7,6,359-363,(2002/11)

23) Superconductivity of $M_I(M_{II0.5},Si_{0.5})_2$ (M_I=Sr and Ba, M_{II}=Al and Ga), ternary silicides with the AlB_2-type structure
Imai Motoharu, Nishida Kenji, Kimura Takashi, Kitazawa Hideaki, Abe Hideki, Kito Hijiri, Yoshii Kenji
Physica C,382,4,361-366,(2002/11)

24) Doping effects of Ru in $L_{0.5}Sr_{0.5}CoO_3$ (L=La, Pr, Nd, Sm, and Eu)
Yoshii Kenji, Abe Hideki
Physical Review B,67,9,094408_1-094408_8,(2003/03)

25) Structural and electronic investigation of TbPdAl by means of EXAFS and XANES measurements
Mizumaki Masaichiro, Yoshii Kenji, Kitazawa Hideaki, Tanida Hajime
Journal of Solid State Chemistry,171,1-2,291-294,(2003/02)

26) Magnetic properties of some transition metal perovskite oxide systems; Transition metal = Ti, Cr, and Co
Yoshii Kenji, Nakamura Akio
Recent Research Developments in Physics, 3,758-776,(2002)

2. Proceedings

1) Structure and magnetism of $Eu_{1-x}Dy_xTiO_3$
Yoshii Kenji, Mizumaki Masaichiro, Nakamura Akio, Abe Hideki
Journal of Solid State Chemistry,171,1-2,345-348,(2003/02)

2) Structural study of semiconductive CdTe-ZnTe alloy by high-energy X-ray diffraction
Yoneda Yasuhiro, Matsumoto Norimasa, Suzuya Kentaro, Kohara Shinji, Mizuki Junichiro
Ferroelectrics,268,277-282,(2002)

Surface chemistry research (Surface Chemistry Research Group)

1. Journals

1) Translational-kinetic-energy-induced surface reactions; Manifestation of their potential energy barriers in O_2/Si(001) system
Teraoka Yuden, Yoshigoe Akitaka
OMICRON Nanotechnology Newsletter,6,1,4-6,(2002/04)

2) Local electronic and geometric structures of silicon atoms implanted in graphite
Baba Yuji, Sekiguchi Tetsuhiro, Shimoyama Iwao
Nuclear Instruments and Methods in Physics Research B,194,1,41-46,(2002/07)

3) Local structure of the silicon implanted in a graphite single crystal

Baba Yuji, Shimoyama Iwao, Sekiguchi Tetsuhiro
Hyomen Kagaku,23,7,417-422,(2002/07)

4) Effect of hydration on the induction of strand breaks and base lesions in plasmid DNA films by γ -radiation
Yokoya Akinari, Cunniffe S. M. T., O'Neill P.
Journal of the American Chemical Society,124,30,8859-8866,(2002/07)

5) Influence of kinetic energy for initial adsorption probability of O_2 molecules on Si(001) surfaces and SiO desorption yield
Teraoka Yuden, Yoshigoe Akitaka
Hyomen Kagaku,23,8,519-523,(2002/08)

6) Reaction dynamics of Si(001) oxidation at room temperature induced by supersonic O_2 molecular beams
Teraoka Yuden, Yoshigoe Akitaka
Hyomen Kagaku,23,9,553-561,(2002/09)

7) In-situ photoemission spectroscopy for chemical reaction dynamics study of Si(001) oxidation by using high-energy-resolution synchrotron radiation
Teraoka Yuden, Yoshigoe Akitaka
Oyo Butsuri,71,2,1523-1527,(2002/12)

8) X-ray absorption near edge structure of DNA bases around oxygen and nitrogen K-edge
Fujii Kentaro, Akamatsu Ken, Muramatsu Yasuji, Yokoya Akinari
Nuclear Instruments and Methods in Physics Research B,199,249-254,(2003/01)

9) Electron paramagnetic resonance induced by K-shell resonance excitation in DNA bases in solid state
Yokoya Akinari, Akamatsu Ken, Fujii Kentaro
Nuclear Instruments and Methods in Physics Research B,199,366-369,(2003/01)

10) Active control of site specificity in ion desorption by core excitation
Wada Shinichi, Sako Erika, Sumii Ryohei, Waki Satoshi, Isari Koji,
Sekiguchi Tetsuhiro, Sekitani Tetsuji, Tanaka Kenichiro
Nuclear Instruments and Methods in Physics Research B,199,361-365,(2003/01)

11) Active control of chemical bond scission by site-specific core excitation
Wada Shinichi, Sumii Ryohei, Isari Koji, Waki Satoshi, Sako Erika,
Sekiguchi Tetsuhiro, Sekitani Tetsuji, Tanaka Kenichiro
Surface Science,528,1-3,242-248,(2003/03)

12) O_2 reaction dynamics with Si(001) surfaces as observed by synchrotron radiation photoemission spectroscopy
Teraoka Yuden, Yoshigoe Akitaka
Atomic Collision Research in Japan, No.28,97-99,(2002)

13) *In situ* analysis using high resolution synchrotron radiation photoemission spectrsocopy for initial oxidation of H_2O pre-adsorbed Si(001) surfaces induced by supersonic O_2 molecular beams at room temperature
Yoshigoe Akitaka, Teraoka Yuden
Atomic Collision Research in Japan, No.28,105-107,(2002)

2. Proceedings

1) Si 2p and O 1s photoemission from oxidized Si(001) surfaces depending on translational kinetic energy of incident O_2 molecules
Teraoka Yuden, Yoshigoe Akitaka
Applied Surface Science,190,1-4,75-79,(2002/05)

2) Photoemission spectroscopic study on influence of O_2 translational kinetic energy for Si(001) initial oxidation
Teraoka Yuden, Yoshigoe Akitaka
Surface Science,507-510,1-3,797-802,(2002/06)

3) Precise control of Si(001) initial oxidation by translational kinetic energy of O_2 molecules
Teraoka Yuden, Yoshigoe Akitaka
Japanese Journal of Applied Physics, Part 1,41,6B,4253-4260,(2002/06)

4) Initial oxidation prosesses of Si(001) surfaces by supersonic O_2 molecular beams; Different oxidation mechanisms for clean and partially-oxidized surfaces

Teraoka Yuden, Yoshigoe Akitaka
Shinku,45,7,604-608,(2002/07)

5) Nuclear resonant inelastic scattering of synchrotron radiation by icosahedral quasicrystal i-$Al_{62}Cu_{25.5}Fe_{12.5}$ and tetragonal crystal O-$Al_{70}Cu_{20}Fe_{10}$
Suzuya Kentaro, Shibata Kaoru, Seto Makoto, Kitao Shinji, Yoda Yoshitaka, Kashihara Yasuharu, Tsai A.
Journal of Non-Crystalline Solids,312-314,508-512,(2002/10)

6) Time-resolved photoelectron spectroscopy of oxidation on the Ti(0001) surface
Takakuwa Yuji, Ishizuka Shinji, Yoshigoe Akitaka, Teraoka Yuden, Mizuno Yoshiyuki, Tonda Hideki, Honma Teiichi
Nuclear Instruments and Methods in Physics Research B,200,376-381,(2003/01)

7) The Measurement of molecular fragments from DNA components using synchrotorn radiation
Fujii Kentaro, Akamatsu Ken, Yokoya Akinari
Surface Science,528,1-3,249-254,(2003/03)

3. Reports

1) Development of novel radiosensitizers for cancer therapy
Akamatsu Ken, Yokoya Akinari
JAERI-Research 2002-015,30,(2002/08)

Heavy atom science (Heavy Atom Science Research Group)

Journals

1) Symmetry breaking in the metal-insulator transition of $BaVS_3$
Inami Toshiya, Owada Kenji, Kimura Hiroyuki, Watanabe Masashi, Noda Yukio, Nakamura Hiroyuki, Yamasaki Tomoaki, Shiga Masayuki, Ikeda Naoshi, Murakami Yoichi
Physical Review B,66,7,073108_1-073108_4,(2002/08)

2) Orbital excitations in $LaMnO_3$ studied by resonant inelastic X-ray scattering
Inami Toshiya, Fukuda Tatsuo, Mizuki Junichiro, Ishihara Sumio, Kondo Hiroshi, Nakao Hironori, Matsumura Takeshi, Hirota Kazuma, Murakami Yoichi, Maekawa Sadamichi, Endo Yasuo
Physical Review B,67,4,045108_1-045108_6,(2003/01)

Electric material science (Electronic Material Science Group)

1. Journals

1) High-resolution resonance photoemission study of CeMX (M=Pt, Pd; X=P, As, Sb)
Iwasaki T., Sekiyama Akira, Yamasaki A., Okazaki Makoto, Kadono Koji, Utsunomiya Hiroshi, Imada Shin, Saito Yuji, Muro Takayuki, Matsushita Tomohiro, Harima Hisatomo, Yoshii Shunsuke, Kasaya Mitsuo, Ochiai Akira, Oguchi Tamio, Kato K., Niide Y., Takegahara K., Suga Shigemasa
Physical Review B,65,19,195109_1-195109_9,(2002/05)

2) Total-electron-yield X-ray standing-wave measurements of multilayer X-ray mirrors for interface structure evaluation
Muramatsu Yasuji, Takenaka Hisataka, Gullikson E. M., Perera R. C. C.
Japanese Journal of Applied Physics, Part 1,41,6B,4250-4252,(2002/06)

3) Angle-resolved photoemission study of the MX-chain compound $[Ni(chxn)_2Br]Br_2$; Spin-charge separation in hybridized *d-p* chains
Fujimori Shinichi, Ino Akihiro, Okane Tetsuo, Fujimori Atsushi, Okada Kozo, Manabe Toshio, Yamashita Masahiro, Kishida Hideo, Okamoto Hiroshi
Physical Review Letters,88,24,247601_1-247601_4,(2002/06)

4) Bulk-sensitive photoemission spectroscopy of A_2FeMoO_6 double perovskites (A=Sr, Ba)
Kang J.-S., Kim J. H., Sekiyama Akira, Kasai Shuichi, Suga Shigemasa, Han S. W., Kim K. H., Muro Takayuki, Saito Yuji, Hwang C., Olson C. G., Park B. J., Lee B. W., Shim J. H., Park J., Min B. I.
Physical Review B,66,11,113105_1-113105_4,(2002/09)

5) Coverage of the Cd underpotential deposited layer formed on an Au(111) substrate; Effect of the electrolytic condition
Kawamura Hiroyuki, Takahashi Masamitsu, Mizuki Junichiro
Journal of the Electrochemical Society,149,11,C586-C591,(2002/11)
6) Helicity switching of circularly polarized undulator radiation by local orbit bumps
Hara Toru, Shirasawa Katsutoshi, Takeuchi Masao, Seike Takamitsu, Saito Yuji, Muro Takayuki, Kitamura Hideo
Nuclear Instruments and Methods in Physics Research A,498,1-3,496-502,(2003/02)
7) Evaluation methods of interlayer-structure-distribution in multilayers by total-electron-yield X-ray standing wave measurements
Muramatsu Yasuji, Takenaka Hisataka, Gullikson E. M., Perera R. C. C.
X-sen Bunseki No Shimpo, 33,145-154,(2002)
8) Take-off/incident-angle-dependence of p/s peak intensity ratio in soft X-ray emission and absorption spectra of graphite and hexagonal boron nitride
Muramatsu Yasuji, Gullikson E. M., Perera R. C. C.
X-sen Bunseki No Shimpo, 34,153-163,(2003)
9) Angle-resolved photoemission study of quasi-two-dimensional heavy-fermion compounds $CeRhIn_5$ and $CeIrIn_5$
Fujimori Shinichi, Ino Akihiro, Okane Tetsuo, Fujimori, Atsushi, Harima Hisatomo, Aoki Dai, Ikeda Shugo, Shishido Hiroaki, Haga Yoshinori, Tokiwa Yoshifumi, Onuki Yoshichika
Physica B: Condensed Matter,312-313,,132-133,(2002/03)

2. Proceedings

1) High energy resolution magnetic circular dichroism measurement of the ferrite family
Agui Akane, Saito Yuji, Yoshigoe Akitaka, Nakatani Takeshi, Matsushita Tomohiro, Mizumaki Masaichiro
Surface Review and Letters,9,2,843-848,(2002/04)
2) Photoemission study of quasi-one-dimensional halogen-bridged compound $[Ni(chxn)_2Br]Br_2$
Fujimori Shinichi, Ino Akihiro, Okane Tetsuo, Fujimori Atsushi, Okada Kozo, Manabe Toshio, Yamashita Masahiro, Kishida Hideo, Okamoto Hiroshi
Surface Review and Letters,9,2,1065-1069,(2002/04)
3) High-resolution photoemission spectroscopy of $Yb_2Co_3X_9$(X=Ga and Al)
Okane Tetsuo, Fujimori Shinichi, Ino Akihiro, Fujimori Atsushi, Dhar S. K., Mitra C., Manfrinetti P., Palenzona A.
Physica B: Condensed Matter ,312-313,349-351,(2002)

3. Reports

1) Highlights of SPring-8 BL23SU in 2001
Agui Akane, Yoshigoe Akitaka, Nakatani Takeshi, Fujii Kentaro, Yokoya Akinari
JAERI-Tech 2002-064,57,(2002/08)

Synchrotron radiation simulation research (Simulation Group for Materials Science)

1. Journals

1) Lattice distortion and V K-edge resonant X-ray scattering in YVO_3
Takahashi Manabu, Igarashi Junichi
Physical Review B,65,20,205114_1-205114_7,(2002/05)
2) Resonant X-ray scattering from CeB_6
Igarashi Junichi, Nagao Tatsuya
Journal of the Physical Society of Japan,71,7,1771-1779,(2002/07)
3) All-electron GW calculation based on the LAPW method : Application to wurtzite ZnO
Usuda Manabu, Hamada Noriaki, Kotani Takao, Mark Van Schilfgaarde
Physical Review B,66,12,125101_1-125101_8,(2002/09)
4) Magnetic resonant X-ray scattering in $KCuF_3$
Takahashi Manabu, Usuda Manabu, Igarashi Junichi
Physical Review B,67,6,064425_1-064425_7,(2003/02)

2. Proceedings

1) Resonant X-ray scattering in $YTiO_3$ and YVO_3
   Takahashi Manabu, Igarashi Junichi
   Surface Review and Letters,9,2,1197-1201,(2002/04)
2) 5d states and resonant X-ray scattering from CeB_6
   Nagao Tatsuya, Igarashi Junichi
   Surface Review and Letters,9,2,1203-1207,(2002/04)

Appendix A Activities of the Research Committee

1. The research committee was organized in FY1996 to promote activities on advanced photon and synchrotron radiation research in Kansai Research Establishment, JAERI. There were three technical subcommittees for Laser System, Laser Utilization and Synchrotron Radiation Utilization, under the committee until FY2001. In FY2002 the technical subcommittees are re-organized to the two subcommittees.

1.1 Committee for Advanced Photon and Synchrotron Radiation Research

First meeting	March 21	1997	Tokyo
Second meeting	February 3	1998	Tokyo
Third meeting	March 9	1999	Tokyo
Fourth meeting	February 10	2000	Tokyo
Fifth meeting	March 2	2001	Kashiwa
Sixth meeting	March 11	2002	Kizu
Seventh meeting	February 18	2003	Kizu (Joint meeting*1)

Technical Subcommittee for Laser System

First meeting	December 8	1997	Tokyo
Second meeting	July 30	1998	Tokyo
Third meeting	December 13	1999	Tokyo
Fourth meeting	February 1	2001	Tokyo
Fifth meeting	February 12	2002	Kashiwa (Joint meeting*2)

Technical Subcommittee for Laser Utilization

First meeting	December 10	1997	Tokyo
Second meeting	December 3	1998	Tokyo
Third meeting	December 24	1999	Tokyo
Fourth meeting	February 15	2001	Kizu
Fifth meeting	February 12	2002	Kashiwa (Joint meeting*2)

↓ **Re-organized**

1.2 Technical Subcommittee for Advanced Photon Research

First meeting	February 18	2003	Kizu (Joint meeting*1)

Technical Subcommittee for Synchrotron Radiation Utilization

First meeting	December 9	1997	Tokyo
Second meeting	November 27	1998	Harima (SPring-8)
Third meeting	February 8	2000	Harima (SPring-8)
Fourth meeting	February 28	2001	Harima (SPring-8)
Fifth meeting	February 25	2002	Harima (SPring-8)

↓ **Re-organized**

1.3 Technical Subcommittee for Synchrotron Radiation Research

First meeting	February 18	2003	Kizu (Joint meeting*1)

2. The local organizing committee for the 25th International Free Electron Laser Conference was organized in FY2002 to prepare and organize the International Conference. There is a technical subcommittees for the Conference Program under the committee.

2.1 Local Organizing Committee for the 25th International Free Electron Laser Conference

First meeting	October 11	2002	Kashiwa

2.2 Technical Subcommittee for the Program of the 25th International Free Electron Laser Conference

3. The technical subcommittee for photon science under the committee for evaluation of JAERI research was organized in FY2001.

Technical Subcommittee for Photon Science under the Committee for Evaluation of JAERI Research

First meeting	June 21	2001	Kizu
Second meeting	November 26	2002	Kizu

4. Two technical subcommittees for advanced photon and synchrotron radiation under the committee for JAERI's Facility Use were organized in FY2000.

4.1 Technical Subcommittee for Advanced Photon under the Committee for JAERI's Facility Use

First meeting	December 19	2000	Kizu
Second meeting	January 18	2002	Kizu
Third meeting	January 20	2003	Kizu

4.2 Technical Subcommittee for Synchrotron Radiation under the Committee for JAERI's Facility Use

First meeting	January 22	2001	Harima (SPring-8)
Second meeting	January 21	2002	Harima (SPring-8)
Third meeting	January 24	2003	Harima (SPring-8)

Member of Committee

1.1 Committee for Advanced Photon and Synchrotron Radiation Research (FY2002)

Chair	Susumu	NAMBA	Professor, Technical Research Center, Nagasaki Institute of Applied Science
Vice-Chair	Seishi	KIKUTA	Executive Director, Deputy Director General, Synchrotron Radiation Research Laboratory, Japan Synchrotron Radiation Research Institute
	Shuntaro	WATANABE	Professor, Institute for Solid State Physics, University of Tokyo
	Katsunobu	AOYAGI	Professor, Interdisciplinary Graduate School of Science and Engineering, Tokyo Institute of Technology
	Nobutsugu	IMANISHI	Professor, Graduate School of Engineering, Kyoto University
	Kenichi	UEDA	Professor, Institute for Laser Science, University of Electro-Communications
	Naoki	SATO	Professor, Institute for Chemical Research, Kyoto University
	Hiroshi	TAKADA	Director, Harima Research Laboratory, Sumitomo Electric Industries, Ltd.
	Masaki	TANIGUCHI	Professor, Graduate School of Science, Hiroshima University
	Junji	MATSUI	Professor, Graduate School of Science, Himeji Institute of Technology
	Tadashi	MATSUSHITA	Deputy Director General, Institute of Materials Structure Science, High Energy Accelerator Research Organization
	Katsumi	MIDORIKAWA	Principal Scientist, Laser Technology Laboratory, Institute of Physical and Chemical Research
	Kazuyoshi	YAMADA	Professor, Institute for Chemical Research, Kyoto University
	Tatsuhiko	YAMANAKA	Director, Institute of Laser Engineering, Osaka University
	Makoto	WATANABE	Professor, Institute of Multidisciplinary Research for Advanced Materials, Tohoku University
	Mamoru	FUJIWARA	Assistant Professor, Research Center for Nuclear Physics, Osaka University Invited Researcher, Advanced Science Research Center, JAERI
	Kenji	NODA	Director, Office of Planning, JAERI
	Toshiki	TAJIMA	Director General, Kansai Research Establishment, JAERI
Subcommittee	Toyoaki	KIMURA	Director, Advanced Photon Research Center, JAERI
	Osamu	SHIMOMURA	Director, Synchrotron Radiation Research Center, JAERI
	Hiroyuki	DAIDO	Principal Scientist, Advanced Photon Research Center, JAERI
	Junichiro	MIZUKI	Deputy Director, Synchrotron Radiation Research Center, JAERI
Secretary	Haruyuki	KIMURA	Senior Staff, Office of Planning, JAERI
	Shunichi	KAWANISHI	Deputy Director, Advanced Photon Research Center, JAERI
	Noboru	TSUCHIDA	General Manager, Synchrotron Radiation Research Center, JAERI

1.2 Technical Subcommittee for Applied Photon Research (FY2002)

Chief	Shuntaro	WATANABE	Professor, Institute for Solid State Physics, University of Tokyo
	Shinichiro	AOSHIMA	Principal, Central Research Laboratory, Hamamatsu Photonics K.K.
	Akira	IWATA	Professor, Research Institute for Science and Technology Tokyo University of Science Technical Director, Kawasaki Heavy Industries, Ltd.
	Ichiro	KATAYAMA	Professor, Institute of Particle and Nuclear Studies, High Energy Accelerator Research Organization
	Yoneyoshi	KITAKAWA	Assistant Professor, Institute of Laser Engineering, Osaka University
	Hiroo	KINOSHITA	Professor, Laboratory of Advanced Science and Technology for Industry, Himeji Institute of Technology
	Takatomo	SASAKI	Professor, Graduate School of Engineering, Osaka University
	Seiichi	TAGAWA	Professor, Institute of Scientific and Industrial Research, Osaka University
	Toshihisa	TOMIE	Principal Scientist, Advanced Semiconductor Research Center, National Institute of Advanced Industrial Science and Technology
	Masahiro	NAKATSUKA	Professor, Institute of Laser Engineering, Osaka University
	Akira	NODA	Professor, Institute for Chemical Research, Kyoto University
	Takashi	FUJIMOTO	Professor, Graduate School of Engineering, Kyoto University
	Mihiro	YANAGIHARA	Assistant Professor, Institute of Multidisciplinary Research for Advanced Materials, Tohoku University
	Tetsuo	YAMAZAKI	Professor, Institute of Advanced Energy Laboratory, Kyoto University
	Kazuhisa	NAKAJIMA	Assistant Professor, Accelerator Laboratory, High Energy Accelerator Research Organization Invited Researcher, Advanced Photon Research Center, JAERI
	Toyoaki	KIMURA	Director, Advanced Photon Research Center, JAERI
	Hiroyuki	DAIDO	Principal Scientist, Advanced Photon Research Center, JAERI
Secretary	Shunichi	KAWANISHI	Deputy Director, Advanced Photon Research Center, JAERI
	Mitsuru	YAMAGIWA	Principal Scientist, Advanced Photon Research Center, JAERI
	Akihiko	NISHIMURA	Senior Scientist, Advanced Photon Research Center, JAERI
	Yuzuru	KUROSAKI	Senior Scientist, Advanced Photon Research Center, JAERI

1.3 Technical Subcommittee for Synchrotron Radiation Research (FY2002)

Chief	Seishi	KIKUTA	Executive Director, Deputy Director General, Synchrotron Radiation Research Laboratory, Japan Synchrotron Radiation Research Institute
	Tatsuo	UEKI	Director, Materials Science Division, Japan Synchrotron Radiation Research Institute
	Shik	SHIN	Professor, Institute for Solid State Physics, University of Tokyo
	Toshio	TAKAHASHI	Assistant Professor, Institute for Solid State Physics, University of Tokyo
	Kenichiro	TANAKA	Professor, Graduate School of Science, Hiroshima University
	Kazuhiko	TSUJI	Professor, Faculty of Science and Technology, Keio University
	Saburo	NASU	Professor, Graduate School of Engineering Science, Osaka University
	Kotaro	HIEDA	Professor, Faculty of Science, Rikkyo University
	Yoshichika	OHNUKI	Professor, Graduate School of Science, Osaka University Invited Researcher, Advanced Science Research Center, JAERI
	Yoichi	MURAKAMI	Professor, Graduate School of Science, Tohoku University Invited Researcher, Synchrotron Radiation Research Center, JAERI
	Osamu	SHIMOMURA	Director, Synchrotron Radiation Research Center, JAERI
	Junichiro	MIZUKI	Deputy Director, Synchrotron Radiation Research Center, JAERI
Secretary	Noboru	TSUCHIDA	General Manager, Synchrotron Radiation Research Center, JAERI

2.1 Local Organizing Committee for the 25th International Free Electron Laser Conference (FY2002)

Chair	Koichi	SHIMODA	Professor Emeritus, University of Tokyo
Vice-Chair	Tetsuo	YAMAZAKI	Professor, Institute of Advanced Energy, Kyoto University
Vice-Chair	Takio	TOMIMASU	Team Leader, Saga Prefectural Regional Industry Support Center
	Haruo	KURODA	Professor, Research Institute for Science and Technology, Science University of Tokyo
	Hiroyuki	HAMA	Professor, Graduate School of Science, Tohoku University
	Kazuo	IMASAKI	Principal Scientist, Laser Process Group, Institute for Laser Technology
	Kawakatsu	YAMADA	Prime Scientist, Photonics Research Institute, National Institute of Advanced Industrial Science and Technology
	Kunio	AWAZU	Professor, Graduate School of Engineering, Osaka University
	Yusuke	TOMITA	Director, Kansai Research Institute, JAERI
	Haruyuki	KIMURA	Senior Staff, Office of Planning, JAERI
	Toyoaki	KIMURA	Director, Advanced Photon Research Center, JAERI
	Taikan	HARAMI	Principal Scientist, Synchrotron Radiation Research Center, JAERI
Secretary	Shigeru	MORI	Administrative Manager, Advanced Photon Research Center, JAERI
	Eisuke	MINEHARA	Principal Scientist, Advanced Photon Research Center, JAERI
	Masaru	SAWAMURA	Senior Scientist, Advanced Photon Research Center, JAERI
	Ryoji	NAGAI	Senior Scientist, Advanced Photon Research Center, JAERI
	Ryoichi	HAJIMA	Senior Scientist, Advanced Photon Research Center, JAERI
	Shuichi	FUJITA	Cooperative Staff, Advanced Photon Research Center, JAERI

2.2 Technical Subcommittee for the Program of the 25th International Free Electron Laser Conference (FY2002)

Chief	Tetsuo	YAMAZAKI	Professor, Institute of Advanced Energy, Kyoto University
Committee	Kawakatsu	YAMADA	Prime Scientist, Photonics Research Institute, National Institute of Advanced Industrial Science and Technology
	Kunio	AWAZU	Professor, Graduate School of Engineering, Osaka University
Subcommittee	Kuniyoshi	YOKOO	Professor, Research Institute of Electrical Communication, Tohoku University
	Akira	IWATA	Professor, Research Institute for Science and Technology, Science University of Tokyo
	Ken	TAKAYAMA	Professor, Accelerator Laboratory, High Energy Accelerator Research Organization
	Hideo	KITAMURA	Principal Scientist, Harima Institute, Institute of Physical and Chemical Research
	Tsumoru	SHINTAKE	Principal Scientist, Harima Institute, Institute of Physical and Chemical Research
	Isamu	SATO	Professor, Institute of Quantum Science, Nihon University
	Masayuki	KAWAI	Special Advisor, Kawasaki Heavy Industries, Ltd.
	Natsuro	TSUBOUCHI	Professor, Graduate School of Engineering, Osaka University
	Makoto	ASAKAWA	Assistant Professor, Graduate School of Engineering, Osaka University
	Goro	ISOYAMA	Professor, Institute of Scientific and Industrial Research, Osaka University
	Ryuko	KATO	Assistant Professor, Institute of Scientific and Industrial Research, Osaka University
	Shuji	MIYAMOTO	Assistant Professor, Laboratory of Advanced Science and Technology for Industry, Himeji Institute of Technology
	Yoshiaki	TSUNAWAKI	Professor, Faculty of engineering, Osaka Sangyo University
	Masahito	HOSAKA	Assistant Researcher, Institute for Molecular Science, Okazaki National Research Institute
	Hideaki	OGAKI	Assistant Professor, Institute of Advanced Energy, Kyoto University
	Kai	MASUDA	Assistant Researcher, Institute of Advanced Energy, Kyoto University
	Hirobumi	SAITO	Professor, Research Division for Spacecraft Engineering, Institute of Space and Astronautical Science
	Takahide	MIZUNO	Assistant Professor, Center for Advanced Spacecraft Technology, Institute of Space and Astronautical Science
	Shigeru	YAMAMOTO	Professor, Institute of Material Structure Science, High Energy Accelerator Research Organization
	Shigenori	HIRAMATSU	Professor, Accelerator Laboratory, High Energy Accelerator Research Organization
	Ken	HAYAKAWA	Assistant Professor, Institute of Quantum Science, Nihon University
	Shuichi	OKUDA	Professor, Research Institute for Advanced Science and Technology, Osaka Prefecture University
	Norihiro	SEI	Principal Scientist, Collaboration Department, National Institute of Advanced Industrial Science and Technology
	Hironari	YAMADA	Professor, Faculty of Science and Engineering, Ritsumeikan University
	Hiroshi	HORIIKE	Professor, Graduate School of Engineering, Osaka University

3. Technical Subcommittee for Photon Science under the Committee for Evaluation of JAERI Research (FY2002)

Chief	Seishi	KIKUTA	Executive Director, Deputy Director General, Synchrotron Radiation Research Laboratory, Japan Synchrotron Radiation Research Institute
Subcommittee	Junzo	ISHIKAWA	Professor, Graduate School of Engineering, Kyoto University
	Tsuneo	URISU	Professor, Institute for Molecular Science, Okazaki National Research Institute
	Mikio	KATAOKA	Professor, Graduate School of Materials Science, Nara Institute of Science and Technology
	Takako	KATO	Professor, Data and Planning Center, National Institute for Fusion Science
	Shik	SHIN	Professor, Institute for Solid State Physics, University of Tokyo
	Kazuhiko	TSUJI	Professor, Faculty of Science and Technology, Keio University
	Yutaka	TSUCHIYA	Deputy Director General, Central Research Laboratory, Hamamatsu Photonics K.K.
	Kunioki	MIMA	Professor, Institute of Laser Engineering, Osaka University
	Kazuyoshi	YAMADA	Professor, Institute for Chemical Research, Kyoto University

4.1 Technical Subcommittee for Advanced Photon under the Committee for JAERI's Facility Use (FY2002)

Chief	Kunio	SHINOHARA	Professor, Graduate School of Medicine, University of Tokyo
Vice-chief	Takashi	FUJIMOTO	Professor, Graduate School of Engineering, Kyoto University
Subcommittee	Yoshihiko	KANAMITSU	Professor, Graduate School of Materials Science, Nara Institute of Science and Technology
	Hiroo	KINOSHITA	Professor, Laboratory of Advanced Science and Technology for Industry, Himeji Institute of Technology
	Yutaka	TSUCHIYA	Deputy Director General, Central Research Laboratory, Hamamatsu Photonics K.K.
	Katsunobu	NISHIHARA	Professor, Institute of Laser Engineering, Osaka University
	Akira	NODA	Professor, Institute for Chemical Research, Kyoto University
	Katsuichi	IIMORI	Director, Department of Materials Science, JAERI
	Hideki	NAMBA	Director, Department of Material Development, JAERI
	Toyoaki	KIMURA	Director, Advanced Photon Research Center, JAERI
	Toshiki	TAJIMA	Director General, Kansai Research Establishment, JAERI
	Shunichi	KAWANISHI	Deputy Director, Advanced Photon Research Center, JAERI
	Yuichi	SHIMIZU	Principal Scientist, Advanced Photon Research Center, JAERI

4.2 Technical Subcommittee for Synchrotron Radiation under the Committee for JAERI's Facility Use (FY2002)

Chief	Yoshichika	OHNUKI	Professor, Graduate School of Science, Osaka University Invited Researcher, Advanced Science Research Center, JAERI
Vice-chief	Haruki	KAWAMURA	Professor, Faculty of Science, Himeji Institute of Technology
Subcommittee	Yoichi	MURAKAMI	Professor, Graduate School of Science, Tohoku University Invited Researcher, Synchrotron Radiation Research Center, JAERI
	Makoto	SAKATA	Professor, Graduate School of Engineering, Nagoya University Invited Researcher, Synchrotron Radiation Research Center, JAERI
	Kenichiro	TANAKA	Professor, Graduate School of Science, Hiroshima University
	Jun	FUJIMORI	Professor, Graduate School of Frontier Sciences, University of Tokyo Invited Researcher, Synchrotron Radiation Research Center, JAERI
	Thoru	OGAWA	Deputy Director, Department of Materials Science, JAERI
	Osamu	SHIMOMURA	Director, Synchrotron Radiation Research Center, JAERI
	Junichiro	MIZUKI	Deputy Director, Synchrotron Radiation Research Center, JAERI
	Noboru	TSUCHIDA	General Manager, Synchrotron Radiation Research Center, JAERI

Appendix B Organization of Kansai Research Establishment
(April 1, 2002～March 31, 2003)

- **Kansai Research Establishment** (Director General: **Y.KATO**(until September) **T.TAJIMA**(from October))
  - **Department of Administrative Services** (Director: **Y.TOMITA**)
    - Administrative Services Division (G. M.: **T.SATO**)
    - Accounts Division (G. M.: **Y.YAMAMOTO**(until June) **H.TANAKA**(from July))
    - Utilities and Maintenance Division (G. M.: **T.KONNO**)
    - Safety Division (G. M.: **I.MANABE**)
  - **Advanced Photon Research Center** (Director: **T.KIMURA**)
    - Division of Advanced Photon Research Promotion (G. M.: **S.KAWANISHI**)
    - Laser System Development Group (G. L.: **H.DAIDO**)
    - X-ray Laser Research Group (G. L.: **K.NAGASHIMA**)
    - Novel Optics Research Group (G. L.: **M.KOIKE**)
    - Laser Acceleration Research Group (G. L.: **K.NAKAJIMA**)
    - Simulation Group for Advanced Photon Science (G. L.: **M.YAMAGIWA**)
    - Free Electron Laser Research Group (G. L.: **E.MINEHARA**)
    - Applied Photon Research Group (G. L.: **H.DAIDO**)
  - **Synchrotron Radiation Research Center** (Director: **O.SHIMOMURA**)
    - Synchrotron Radiation Administration Division (G. M.: **K.NAKAAKI**(until Sept.) **H.YOSHIDA**(from Oct.))
    - Experimental Facilities Development Group (G. L.: **T.HARAMI**)
    - High Pressure Science Group (G. L.: **N.HAMAYA**)
    - Structural Physics Research Group (G. L.: **J.MIZUKI**)
    - Surface Chemistry Research Group (G. L.: **Y.BABA**)
    - Heavy Atom Science Group (G. L.: **Y.MURAKAMI**)
    - Electronic Material Science Group (G. L.: **A.FUJIMORI**)
    - Simulation Group for Materials Science (G. L.: **J.IGARASHI**)

G. M.: General Manager G. L.: Group Leader

Appendix C Personnel

(April 1, 2002～March 31, 2003)

Personnel at Advanced Photon Research Center

Toyoaki KIMURA
Shunichi KAWANISHI
Norio OGIWARA
Osamu YAMASHITA
Shigeru MORI
Masaaki AKUTSU
Naohiko KAYORA(until September)
Kiyomi ENDOH
Rika SUMITANI
Masako SHIGENARI

Division of Advanced Photon Research Promotion
Shunichi KAWANISHI
Sayaka HARAYAMA
Shuichi FUJITA
Jun NAKAJIMA
Naoyuki SHINOHARA

Laser System Development Group
Hiroyuki DAIDO
Koichi YAMAKAWA
Akihiko NISHIMURA
Junji KAWANAKA
Hiromitsu KIRIYAMA
Yutaka AKAHANE
Keiichi YOKOYAMA
Kyoichi DEKI
Yoshimoto NAKAI
Fumiaki MATSUOKA
Norihiro INOUE
Makoto AOYAMA
Yuji FUKUDA
Toru NAGAI
Koichi WADA
Hidenao YAMADA
Shinji NISHIKAWA
Akihiro YABUSHITA
Kazuhiko SUMIMURA
Hideki UEDA
Koichi TSUJI

X-ray Laser Research Group
Keisuke NAGASHIMA
Maki KISHIMOTO
Masataka KADO
Yoji SUZUKI
Tetsuya KAWACHI
Noboru HASEGAWA
Momoko TANAKA
Yoshihiro OCHI
Kouta SUKEGAWA
Renzhong TAI
Akimoto NISHIKINO
Peixiang LU(until January)

Novel Optics Research Group
Masato KOIKE
Osamu YODA
Akira SUGIYAMA
Masahiko ISHINO
Kengo WADA

Applied Photon Research Group
Hiroyuki DAIDO
Yuichi SHIMIZU
Yuzuru KUROSAKI
Hiroshi MURAKAMI
Koichi OGURA
Akito SAGISAKA
Satoshi ORIMO
Mamiko NISHIUCHI
Yukio HAYASHI
Etsuya YANASE
Kazuhito YASUIKE
Yoshiaki TERANISHI
Keiko SUTO
Masayuki SUZUKI
Takatsugu OKETA
Shu NAKAMURA
Shinji NISHIKAWA
Koji MATSUKADO
Atsushi FUKUMI
Zhong LI

Laser Acceleration Research Group
Kazuhisa NAKAJIMA
Yuichi SHIMIZU
Shuhei KANAZAWA
Hideyuki KOTAKI
Shuji KONDO
Masaki KANDO
Takayuki HONMA
Shinichi MASUDA
Igor V. SNETANIN

Simulation Group for Advanced Photon Science
Mitsuru YAMAGIWA
Toshizo SHIRAI(until September)
Akira SASAKI
James KOGA
Kengo MORIBAYASHI
Yutaka UESHIMA
Takayuki UTSUMI
Takao KONDO
Nayu TSUJI
Shingo SUZUKI(until December)
Sergei V. BULANOV(until February)
Yasuaki KISHIMOTO
Hitoshi IHARA
Kentaro SUZUYA

Free Electron Laser Research Group
Eisuke MINEHARA
Toshihiko YAMAUCHI
Masaru SAWAMURA
Ryoichi HAJIMA
Ryoji NAGAI
Nobuhiro KIKUZAWA
Takehito HAYAKAWA
Nobuyuki NISHIMORI
Toshiyuki SHIZUMA

(April 1, 2002～March 31, 2003)

Personnel at Synchrotron Radiation Research Center

Osamu SHIMOMURA
Jun-ichiro MIZUKI
Nobuo NIIMURA(until March)
Hironobu OGAWA(until September)
Hitoshi IHARA(until March)
Noboru TSUCHIDA(from April)
Isao TAKARIKO(from October)
Teikichi SASAKI
Hiroko NISHIZAKI
Akiko SHIMAMURA(until August)
Sae TAMURA(from July)

Experimental Facilities Development Group
Taikan HARAMI
Hiroyuki KONISHI
Yoshihiro ASANO
Hideaki SHIWAKU
Haruhiko MOTOHASHI(until March)
Kazukiyo TOZAWA
Takahisa SHOBU

High Pressure Science Group
Nozomu HAMAYA
Katsutoshi AOKI(from March)
Makoto SAKATA
Wataru UTSUMI
Yoshinori KATAYAMA
Tetsu WATANUKI
Akihiko MACHIDA(from April)
Hiroshi KANEKO
Taku OKADA(until March)
Yasuhiro INAMURA
Tomohiro IKEDA

Structural Physics Research Group
Junichiro MIZUKI
Yasuo NISHIHATA
Kentaro SUZUYA
Norimasa MATSUMOTO
Kenji YOSHII
Masamitu TAKAHASI
Yasuhiro YONEDA
Tatsuo FUKUDA
Hiroyuki KAWAMURA(until March)
Kazuhisa TAMURA(from April)
Koji KIRIYAMA(from August)
Yuka OKAJIMA(from August)
Yusuke HIRAMITSU(until March)
Naomasa YAMAMOTO(until March)
Junichi TAGUCHI(until March)

Simulation Group for Materials and Science
Jun-ichi IGARASHI(from April)
Manabu USUDA(from April)

Surface Chemistry Research Group
Yuji BABA
Akinari YOKOYA
Yuden TERAOKA
Tetsuhiro SEKIGUCHI
Akitaka YOSHIGOE
Iwao SHIMOYAMA
Kentaro FUJII
Krishna G. NATH
Ken AKAMATSU(until August)
Kosuke MORITANI

Heavy Atom Science Group
Yoichi MURAKAMI
Makoto SETO
Toshiya INAMI
Takaya MITSUI
Kenji ISHII
Kenji OHWADA
Kaori KUZUSHITA(from April)

Electronic Material Science Group
Atsushi FUJIMORI
Yasuji MURAMATSU
Tetsuo OKANE
Yuji SAITOH
Akane AGUI
Shin'ichi FUJIMORI
Jun OKAMOTO
Kazutoshi MAMIYA
Kentoro KURAMOTO
Kana TOMIZAWA(until March)

Synchrotron Radiation Administration Division
Katsuhiko NAKAAKI(until September)
Hiroshi YOSHIDA(from October)
Hironobu OGAWA(until September)
Yukio SHINPO(from October)
Masahiko MATSUMOTO
Toshinori SUZUKI(from April)
Sachiko MITSUDERA
Junko MARUO(from August)
Kumi JIKKO(from August)

(April 1, 2002～March 31, 2003)

Personnel at Kansai Research Establishment

Yoshiaki KATO(until September)
Toshiki TAJIMA(from October)
Takashi ARISAWA

Personnel at Department of Administrative Services

Yusuke TOMITA
Hiroshi YOSHIDA

Administrative Services Division

Takashi SATO
Hiroshi YOSHIDA
Mamoru SUZUKI
Ken SASAKI
Daisuke USHIJIMA
Yuko HASEGAWA
Michiyo HASHIMOTO

Accounts Division

Yoshio YAMAMOTO(until June)
Hiroshi TANAKA(from July)
Shintaro EJIRI
Yuichi SUNAOSHI
Hitoshi YAMAGUCHI
Tatsuki SUKEGAWA
Junpei OGAKI
Shinobu KOIZUMI
Keiichi TSUKAMOTO
Reiko IYORI

Utilities and Maintenance Division

Toshio KONNO
Toshiaki KOBAYASHI(from October until February)
Ryuichi OI
Jun MATSUMOTO(until September)
Isao TAKARIKO(from October)
Tetsuya YAMAMOTO
Naoki NAKAGAWA
Kotomi WAKI

Safety Division

Iwao MANABE
Masayuki UENO
Masayuki KABUTOU(until September)
Tomio OHUCHI(from October)
Yaichi FUKUSHIMA
Isao TAKARIKO(until October)
Izumi TAMURA

Appendix D Symposia

FY1997

(1) The first JAERI-Kansai International Workshop on Ultrashort-pulse Ultrahigh-power Lasers and Simulation for Laser-plasma Interactions (held as "Joint ICFA/JAERI-Kansai International Workshop '97", organized by International Committee for Future Accelerators, hosted by Japan Atomic Energy Research Institute and High Energy Accelerator Research Organization)

July 14-18, **1997**, Kyoto, Japan

JAERI-Conf 98-004, "Proceedings of The first JAERI-Kansai International Workshop on Ultrashort-pulse Ultrahigh-power Lasers and Simulation for Laser-plasma Interactions, July 14-18, 1997, Kyoto Research Park, Kyoto, Japan", March 1998.

(2) The 6th International Conference on Synchrotron Radiation Instrumentation (cosponsored by Japan Atomic Energy Research Institute, Japanese Society for Synchrotron Radiation Research, RIKEN and Japan Synchrotron Radiation Research Institute)

August 4−8, **1997**, Himeji, Japan

J. Synchrotron Radiation, 5 part 3, "SRI'97 Proceedings", May 1998.

FY1998

(3) 6th International Conference on X-Ray Lasers (cosponsored by Japan Atomic Energy Research Institute and Osaka University)

August 31-September 4, **1998**, Kyoto, Japan

Institute of Physics Conference Series Number 159, "Proceedings of the 6th International Conference on X-Ray Lasers held in Kyoto, Japan, August 31-September 4, 1998"

(4) The Second International Conference on Synchrotron Radiation in Materials Science (cosponsored by Japan Atomic Energy Research Institute, RIKEN and Japan Synchrotron Radiation Research Institute)

October 31−November 3, **1998**, Kobe, Japan

Jpn. J. Appl. Phys. Suppl., 38-1, "Proceedings of the SRMS-2", June 1999.

FY1999

(5) The First Symposium on Advanced Photon Research

November 8-9, **1999**, Kyoto, Japan

JAERI-Conf 2000-006, "Proceedings of The First Symposium on Advanced Photon Research, November 8-9, 1999, Keihanna Plaza/Advanced Photon Research Center, Kyoto, Japan", March 2000.

(6) Workshop on Surface and Interface Using Synchrotron Radiation

March 16-17, **2000**, SPring-8, Japan

FY2000

(7) The Second Symposium on Advanced Photon Research

November 9-10, **2000**, Kyoto, Japan

JAERI-Conf 2001-011, "Proceedings of The Second Symposium on Advanced Photon Research, November 9-10, 2000, Advanced Photon Research Center, Kyoto, Japan", July 2001.

(8) 2nd UK-Japan International Seminar of Application Radiation to Studies of Nano-structured Materials

(cosponsored by institute of Molecular Science, Japan Atomic Energy research Institute, RIKEN and JASRI)

July 9-10, **2000**, SPring-8, Japan

(9) International Workshop on "Crystallography at High Pressure and High Temperature using X-ray and Neutrons"

(cosponsored by Synchrotron Radiation Research Center of JAERI, JASRI and International Union of Crystallography Commission on High Pressure)

September 30-October 3, **2000**, SPring-8, Japan

FY2001

(10) OECD Global Science Forum "Workshop on Compact High-Intensity Short-Pulse Lasers: Future Directions and Applications"
(cosponsored by OECD Global Science Forum and JAERI)
May 28-30, **2001**, Kansai Research Establishment, Kyoto, Japan
OECD Global Science Forum, "Final Report from the Workshop"

(11) The Third Symposium on Advanced Photon Research
December 13-14, **2001**, Kyoto, Japan
JAERI-Conf 2002-008, "Proceedings of The Third Symposium on Advanced Photon Research, December 13-14, 2001, Advanced Photon Research Center, Kyoto, Japan", July 2002.

(12) Korean-Japanese International workshop on Strongly Correlated Electron Systems
September 3-4, **2001**, SPring-8, Japan

FY2002

(13) International Workshop on Photoionization (IWP2002)
(hosted by Japan Synchrotron Radiation Research Institute (JASRI), RIKEN (The Institute of Physical and Chemical Research), Japan Atomic Energy Research Institute (JAERI), Hyogo Prefecture)
22-26 August, **2002**, SPring-8, Hyogo, JAPAN

(14) JAERI Symposium on Control of Lasers for Strong Field Phenomena
September 12-13, **2002**, Kyoto, Japan

(15) The 5th SRRTNet Workshop "Interface between theory, computation and experiments"
(Organized by Japan Atomic Energy Research Institute (JAERI), Research Institute of Chemical Sciences (RIKEN), High Energy Physics Research Organization (KEK-PF) and Japan Synchrotron Radiation Research Institute (JASRI))
15-16 October **2002**, SPring-8, Japan

(16) The Fourth Symposium on Advanced Photon Research
November 28-29, **2002**, Kyoto, Japan
JAERI-Conf 2003-008, "Proceedings of The Fourth Symposium on Advanced Photon Research, November 28-29, 2002, Advanced Photon Research Center, Kyoto, Japan", July 2003.

国際単位系 (SI) と換算表

表 1　SI 基本単位および補助単位

量	名称	記号
長さ	メートル	m
質量	キログラム	kg
時間	秒	s
電流	アンペア	A
熱力学温度	ケルビン	K
物質量	モル	mol
光度	カンデラ	cd
平面角	ラジアン	rad
立体角	ステラジアン	sr

表 2　SI と併用される単位

名称	記号
分，時，日	min，h，d
度，分，秒	°，′，″
リットル	l，L
トン	t
電子ボルト	eV
原子質量単位	u

1 eV = 1.60218 × 10^{-19} J

1 u = 1.66054 × 10^{-27} kg

表 5　SI 接頭語

倍数	接頭語	記号
10^{18}	エクサ	E
10^{15}	ペタ	P
10^{12}	テラ	T
10^{9}	ギガ	G
10^{6}	メガ	M
10^{3}	キロ	k
10^{2}	ヘクト	h
10^{1}	デカ	da
10^{-1}	デシ	d
10^{-2}	センチ	c
10^{-3}	ミリ	m
10^{-6}	マイクロ	μ
10^{-9}	ナノ	n
10^{-12}	ピコ	p
10^{-15}	フェムト	f
10^{-18}	アト	a

表 3　固有の名称をもつ SI 組立単位

量	名称	記号	他の SI 単位による表現
周波数	ヘルツ	Hz	s^{-1}
力	ニュートン	N	m·kg/s^2
圧力，応力	パスカル	Pa	N/m^2
エネルギー，仕事，熱量	ジュール	J	N·m
工率，放射束	ワット	W	J/s
電気量，電荷	クーロン	C	A·s
電位，電圧，起電力	ボルト	V	W/A
静電容量	ファラド	F	C/V
電気抵抗	オーム	Ω	V/A
コンダクタンス	ジーメンス	S	A/V
磁束	ウェーバ	Wb	V·s
磁束密度	テスラ	T	Wb/m^2
インダクタンス	ヘンリー	H	Wb/A
セルシウス温度	セルシウス度	℃	
光束	ルーメン	lm	cd·sr
照度	ルクス	lx	lm/m^2
放射能	ベクレル	Bq	s^{-1}
吸収線量	グレイ	Gy	J/kg
線量当量	シーベルト	Sv	J/kg

表 4　SI と共に暫定的に維持される単位

名称	記号
オングストローム	Å
バーン	b
バール	bar
ガル	Gal
キュリー	Ci
レントゲン	R
ラド	rad
レム	rem

1 Å = 0.1 nm = 10^{-10} m

1 b = 100 fm^2 = 10^{-28} m^2

1 bar = 0.1 MPa = 10^5 Pa

1 Gal = 1 cm/s^2 = 10^{-2} m/s^2

1 Ci = 3.7 × 10^{10} Bq

1 R = 2.58 × 10^{-4} C/kg

1 rad = 1 cGy = 10^{-2} Gy

1 rem = 1 cSv = 10^{-2} Sv

（注）

1. 表 1 − 5 は「国際単位系」第 5 版，国際度量衡局 1985 年刊行による。ただし，1 eV および 1 u の値は CODATA の 1986 年推奨値によった。
2. 表 4 には海里，ノット，アール，ヘクタールも含まれているが日常の単位なのでここでは省略した。
3. bar は，JIS では流体の圧力を表わす場合に限り表 2 のカテゴリーに分類されている。
4. EC 閣僚理事会指令では bar，barn および「血圧の単位」mmHg を表 2 のカテゴリーに入れている。

換　算　表

力	N(=10^5 dyn)	kgf	lbf
	1	0.101972	0.224809
	9.80665	1	2.20462
	4.44822	0.453592	1

粘　度　1 Pa·s(N·s/m^2) = 10 P(ポアズ)(g/(cm·s))

動粘度　1 m^2/s = 10^4 St(ストークス)(cm^2/s)

圧力	MPa(=10 bar)	kgf/cm^2	atm	mmHg(Torr)	lbf/in^2(psi)
	1	10.1972	9.86923	7.50062 × 10^3	145.038
	0.0980665	1	0.967841	735.559	14.2233
	0.101325	1.03323	1	760	14.6959
	1.33322 × 10^{-4}	1.35951 × 10^{-3}	1.31579 × 10^{-3}	1	1.93368 × 10^{-2}
	6.89476 × 10^{-3}	7.03070 × 10^{-2}	6.80460 × 10^{-2}	51.7149	1

エネルギー・仕事・熱量	J(=10^7 erg)	kgf·m	kW·h	cal(計量法)	Btu	ft·lbf	eV
	1	0.101972	2.77778 × 10^{-7}	0.238889	9.47813 × 10^{-4}	0.737562	6.24150 × 10^{18}
	9.80665	1	2.72407 × 10^{-6}	2.34270	9.29487 × 10^{-3}	7.23301	6.12082 × 10^{19}
	3.6 × 10^6	3.67098 × 10^5	1	8.59999 × 10^5	3412.13	2.65522 × 10^6	2.24694 × 10^{25}
	4.18605	0.426858	1.16279 × 10^{-6}	1	3.96759 × 10^{-3}	3.08747	2.61272 × 10^{19}
	1055.06	107.586	2.93072 × 10^{-4}	252.042	1	778.172	6.58515 × 10^{21}
	1.35582	0.138255	3.76616 × 10^{-7}	0.323890	1.28506 × 10^{-3}	1	8.46233 × 10^{18}
	1.60218 × 10^{-19}	1.63377 × 10^{-20}	4.45050 × 10^{-26}	3.82743 × 10^{-20}	1.51857 × 10^{-22}	1.18171 × 10^{-19}	1

1 cal = 4.18605 J (計量法)
= 4.184 J (熱化学)
= 4.1855 J (15 °C)
= 4.1868 J (国際蒸気表)

仕事率　1 PS (仏馬力)
= 75 kgf·m/s
= 735.499 W

放射能	Bq	Ci
	1	2.70270 × 10^{-11}
	3.7 × 10^{10}	1

吸収線量	Gy	rad
	1	100
	0.01	1

照射線量	C/kg	R
	1	3876
	2.58 × 10^{-4}	1

線量当量	Sv	rem
	1	100
	0.01	1

（86 年 12 月 26 日現在）

Annual Report of Kansai Research Establishment 2002 April 1,2002-March 31,2003